ELECTROCHEMICALLY INDUCED

ADDITION REACTIONS

Graeme S. Smith

Ph.D. Thesis

University of Edinburgh

1987

To my Mother and in memory
of my Father for his example
and devotion.

ACKNOWLEDGEMENTS

I am greatly indebted to Drs. G.A. Heath and A.J. Bellamy for their help, guidance and enthusiasm throughout the period of this study. I am also grateful to all my colleagues, particularly Dr. L.J. Yellowlees and Mr. M.R. Low, for their assistance during this project.

I would like to thank Dr. D. Reed, Mr. J. Millar and Mr. L. Bell for recording n.m.r. spectra, Mr. D. Thomas and Mr. A. Taylor for recording mass spectra, Miss E. Stevenson for recording GLC/mass spectra, and Mr. J. Grunbaum for performing microanalyses.

I also am grateful to the Science and Engineering Research Council for financial support and also to the University of Edinburgh for the provision of facilities.

I also thank my family and friends for their support and encouragement throughout the entire period of this study.

Finally, I would like to express my gratitude to Mrs. E. Glass and Mrs. A. Roper for their careful typing of this manuscript.

ABSTRACT

The thesis is divided into three parts:

Part A briefly outlines past and present electrochemical methodology with particular reference to the electroanalytical and electrosynthetic techniques subsequently used.

Part B is concerned with the reductive ethylation of aliphatic ketones in liquid ammonia/tetraalkylammonium salt solutions. The principles of electrochemistry in liquid ammonia and previous examples of electrochemically induced alkylations involving quaternary ammonium cations are discussed. Detailed examinations on the experimental conditions necessary for the reductive ethylation of pentan-2-one in NH_3/Et_4NBF_4 solutions shows the critical requirement of the electrochemical experiment in order that tertiary alcohol is formed. Further studies utilising a variety of different quaternary ammonium cations show that the chemical composition of the cation is crucial in the ethylation reaction which is proposed to occur via a radical-coupling mechanism.

Part C is concerned with electrochemical studies on some transition metal octaethylporphin and tetraphenylporphins. The redox and spectroscopic properties of porphyrins and known examples of redox-induced peripheral reactions of metalloporphyrins are outlined. Comprehensive voltammetric data for both d^8 metalloporphyrin series are listed and the trends in oxidation and reduction potential moving down the triad show the influence of $d\pi \rightarrow p\pi^*$ backbonding over the redox behaviour of these complexes. Spectroelectrochemical characterisation

of the first oxidation product of Pt(II)TPP shows that this process is localised on the metal-centre. Coulometry and e.s.r. spectroscopy confirm that a Pt(III) species is formed. The π-dicationic species generated from Pd(II)TPP and Pt(II)TPP are both unstable, undergoing a rapid and irreversible reaction with trace water. The product formed from the Pd parent was found to be stable, and spectroscopically identified as a dihydroxy complex with a novel pattern of peripheral substitution.

CONTENTS

List of Tables

List of Figures

Page

Part C

List of Schemes

Instrumentation

Electrochemical experiments were carried out in Part B using a Chemical Electronics 70 Potentiostat and in Part C with a Princeton Applied Research 170 General Electrochemical Instrument. N.m.r. spectra were recorded using Bruker WP80SY and WP200SY spectrometers. Infra-red spectra were recorded on a Perkin-Elmer 597 spectrometer. Electronic spectra were obtained from a Pye-Unicam SP8-400 uv/vis spectrometer. G.L.C.'s were performed with a Pye Unicam 4500 Chromatograph and preparative G.L.C. with a Carlo Erba Fractovap 2450. Mass spectra were recorded on a Kratos MS50TC and G.L.C./Mass spectra on a V.G. Micromass 12B. E.s.r. spectra were recorded on a Bruker ER200D spectrograph.

Postgraduate Courses Attended

Departmental Seminars and Colloquia, 1982 to 1985.

2nd International Conference on the Chemistry of the Platinum Group Metals, University of Edinburgh, 1984.

Inorganic Biochemistry Discussion Group Meeting, Birkbeck College, London, 1983.

"Electrochemistry in and out of Mothballs" - Dr. G.A. Heath (University of Edinburgh), 1983.

"Pulse sequences and their Application to n.m.r. Spectroscopy" - Dr. G.A. Morris (U.M.I.S.T.), 1983.

"Activation of Small Molecules" - Dr. M. Schröder (University of Edinburgh), 1984.

"Chemical Technology and Industrial Chemistry" - Drs. A.J. Nichol, L.H. Mustoe and R.S. Sinclair (Paisley College of Technology), 1985.

"History of the Chemistry Department" - Dr. W.P. Doyle (University of Edinburgh), 1983.

"The Chemistry of Photographic Processes" - Dr. L.A. Williams (Kodak Ltd.), 1983.

Abbreviations

CV	Cyclic Voltammetry
ACV	Alternating Current Voltammetry
N.H.E.	Normal Hydrogen Electrode
S.C.E.	Saturated Calomel Electrode
n.m.r.	Nuclear Magnetic Resonance
e.s.r.	Electron Spin Resonance
i-r	Infra-red
u-v	Ultra-violet
TPP	Tetraphenylporphin
OEP	Octaethylporphin
TMPP	Tetra-N-methylpyridylporphin
TBA	Tetra-n-butylammonium
DMF	Dimethylformamide
THF	Tetrahydrofuran
G.L.C.	Gas Liquid Chromatography
a.m.u.	Atomic Mass Units
TSPP	Tetra-p-sulphonatophenylporphin
EPT	Enhancement by Polarisation Transfer
DEPT.	Distortionless Enhancement by Polarisation Transfer
F.A.B.	Fast Atom Bombardment
DMSO	Dimethyl Sulphoxide
HMPA	Hexamethylphosphoramide
OMP	Octamethylporphin
OTS	Tosylate

PART A

ELECTROCHEMICAL TECHNIQUES

A.1 Introduction

The subject of electrochemistry encompasses the study of the processes associated with the transfer of electrons to, or from, a chemical substance via the surface of an electrode. The process of electron-transfer is induced when a potential is applied to the electrode, such that the energy difference between the electrons on the surface of the electrode and either of the frontier molecular orbitals of the substrate is large enough to promote electron-transfer. Electrochemical experiments, of various types, have been carried out for over one hundred years, but it is only in the last thirty years, with the development of modern instrumentation and techniques, that electrochemistry has become a readily used laboratory technique.

Electrochemical processes occur in the solution phase, and in the gaseous and molten states. The following discussion is concerned only with the electrochemistry of solutions, as it is with this sub-section of electrochemistry that this thesis is concerned.

In discussing the fundamentals of electrochemistry it is first worth noting that the energy required to initiate the oxidation or reduction of a substrate is a measure of the energy levels of the highest energy occupied molecular orbital (HOMO) and lowest energy unoccupied molecular orbital (LUMO) respectively. Thus, the results obtained by electrochemical methods can be used to outline the structure of a substrate's frontier molecular orbitals, and possibly carried further to define a set of parameters for a large scale electrolysis.

Consider the electrochemical cell shown on figure A.1, containing two separate compartments, or half-cells, each of which is filled with a conducting, or electrolyte, solution.

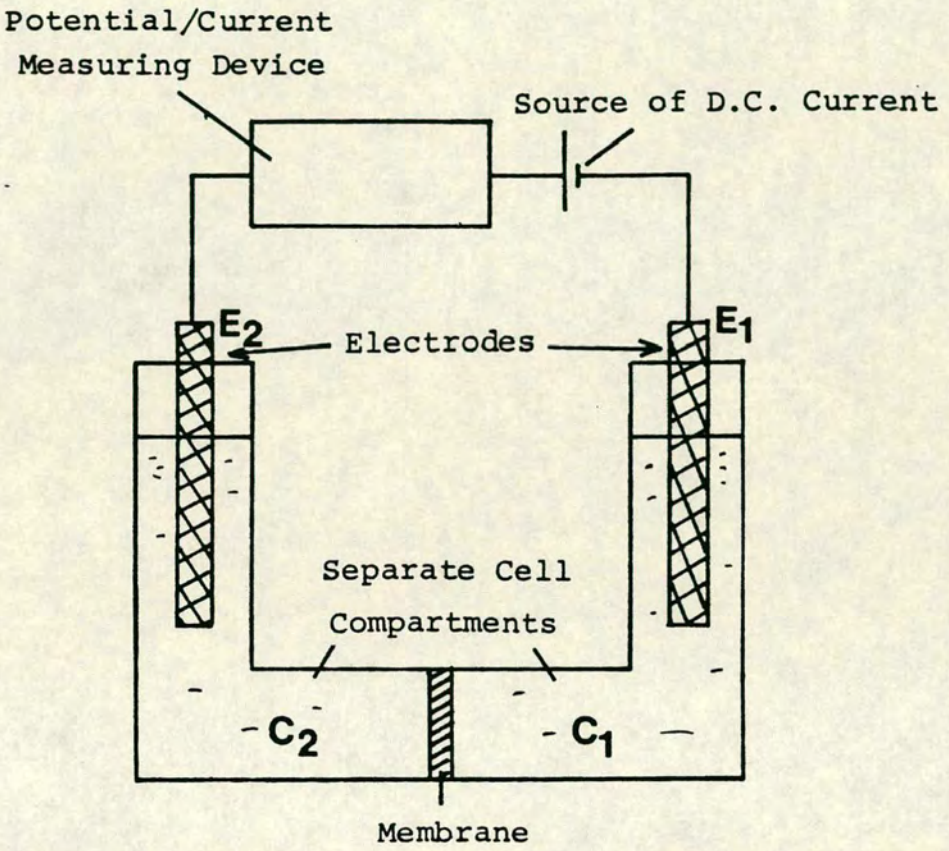

Figure A.1: Classical 2-compartment Electrochemical Cell

Compartment C_1 contains a solution of an electro-active substrate which is capable of existing in either an oxidised or reduced form. If these forms are labelled O and R, then the relationship between these species is shown in equation (1) where n is the number of electrons transferred to inter-convert O and R.

$$O + ne \underset{k_r}{\overset{k_f}{\rightleftharpoons}} R \qquad (1)$$

k_f and k_r represent the heterogeneous rate constants

for the forward and reverse electron-transfers between electrode surface and substrate. It thus follows that K_{eq}, the equilibrium constant for the electron-transfer reaction, is that shown in equation (2).

$$K_{eq} = \frac{k_f}{k_r} \qquad (2)$$

In order that nett reduction of substrate occurs, the potential of electrode E_1, the working electrode, has to be raised to a point where k_f is greater than k_r. As this is gradually done, there comes a particular potential at which equal amounts of O and R are present. At this potential, any cathodic adjustment results in excess R being present, while an anodic adjustment will produce excess O. In order to meaningfully measure this equilibrium potential it is necessary that the half-cell arrangement in compartment C_2 is of known potential. This half-cell is called the reference electrode compartment, the standard of which is the Normal Hydrogen Electrode (N.H.E.)[1] which has, by convention, a potential of 0V. The potential, vs N.H.E., at which equilibrium is achieved for a half-cell is called its Standard Electrode Potential, E°. This value is related to the free energy change for the electron-transfer reaction by the relationship shown in equation (3).

$$\Delta G^\circ = -nFE^\circ \qquad (3)$$

F = 1 Faraday≡Charge of 1 mole of electrons = 96,500 C.

As an electrode potential measurement is equivalent to a measure of the relative position of equilibrium of a system at any potential, it follows that there is a relationship between the potential of a half-cell, and the equilibrium concentrations of O and R. This relationship, known as the Nernst equation[2] is shown, in its modified concentration dependant form, in equation (4).

$$E = E^\circ - \frac{RT}{nF} \ln \frac{[R]}{[O]} \qquad (4)$$

It should be noted, however, that the preceding equations hold only when the system under study is fully reversible, i.e. both forms of the substrate are indefinitely stable in the test solution.

Thus, a system's electrode potential reveals an insight into the thermodynamics of the redox process being studied. In practice, however, electrode potentials are difficult to measure. This is due to techniques being time consuming, and also the fact that many redox processes produce species which are not stable in the time span of the electrode potential measurement.

Recently, though, there has been the development of electrochemical techniques which are capable of probing the redox character of substances without the need for setting up an equilibrium situation. These techniques operate on the principle of varying either the potential, or current, of the working electrode, while simultaneously measuring the response of the uncontrolled parameter. These techniques have the

general name, voltammetry. It is with the development of voltammetric techniques that the vast increase in the extent to which electrochemistry is used in laboratory investigations has arisen. The principles and requirements of voltammetry, with particular reference to the techniques used in this study, are described in the following section.

A.2 Voltammetry

There are over thirty different techniques of current/potential, perturbation/response measurements listed in the literature. Of these, only a small number have been extensively applied in practical situations. Amongst the most important of these techniques are polarography[3], which was the first fully developed voltammetric technique, cyclic voltammetry and alternating current voltammetry. The last two of these are the techniques utilised in this study, and are each fully discussed later. Before this is possible, it is necessary to outline the required layout and components of a modern voltammetric cell.

A.2-1 Voltammetric Cell Requirements

Voltammetry is conventionally carried out in a three-electrode cell driven by a potentiostat. In addition to the working and reference electrodes present in the previous cell, described in Section A.1, a third electrode is present. This electrode, called the secondary, or counter electrode, is responsible for the passage of cell current from the working electrode ensuring that current passed through the reference electrode is kept to a minimum. This is necessary because

the passage of current through the reference electrode affects its stability and hence the accuracy of any voltammetric data. Due to this current passing requirement, the secondary electrode should have a surface area at least ten times larger than the working electrode.

The working electrode of a voltammetric cell is normally small and symmetrically shaped to ensure even current flow from its surface. While polarography involves the use of a dropping mercury electrode, it is now more common to use stationary electrodes. The most widely used materials for these are mercury (hanging drops), platinum, gold and graphite (discs, wires etc.). As the working electrode area is small, and the time scale of voltammetric experiments generally fast (10^{-2}s to 10^{2} seconds typically), only negligible nett electrolysis of substrate occurs. This is as opposed to the large scale electrolysis required to set up the equilibrium systems necessary for the measurement of an electrode potential.

The choice of reference electrodes for voltammetry normally depends largely on the electrochemical solvent. While the N.H.E. remains the standard against which potential measurements are quoted, this electrode is not practicable for general laboratory use. There are however alternative reference electrodes, which are stable and readily reusable, and whose potentials vs N.H.E. are known. These include the saturated calomel electrode (S.C.E.), suitable for use in aqueous and organic systems, and the Ag/Ag^{+} and Ag/AgCl reference electrodes, used purely in organic solvents.

Thus, a voltammetric cell contains three electrodes. The reference electrode is normally kept in a separate compartment from the working and secondary electrodes in order to avoid contamination of the test solution. To minimise errors in potential readings caused by solution resistance between the working and reference electrodes most potentiostats contain positive feedback circuitry. This capability is normally referred to as "iR compensation".

While the values of standard electrode potentials are conventionally measured in aqueous solutions of unit activity, voltammetry can be carried out in either aqueous or organic solvents. In general, however, pure organic solvents do not conduct sufficiently for electrochemical purposes. This problem is surmounted by the addition of some salts to a level such that the resulting electrolytic solution has the desired conductivity. These salts, known as the supporting electrolyte, are typically present in a hundred-fold excess over the electroactive substrate. As well as lowering solution resistance, the supporting electrolyte ions carry the cell current through the solution, ensuring that mass transport of electroactive substrate to the working electrode does not occur by electrical migration.

The choice of an appropriate solvent for voltammetry depends upon many factors, including the solubility of the substrate and the reactivity of the solvent towards the substrate in its neutral and oxidised/reduced forms. For any electrolyte solution in a voltammetric cell there exists a "potential-window". This refers to the anodic and cathodic potential ranges which the cell can be exposed to without

oxidation or reduction of either the solvent, supporting electrolyte ions or the electrode material. It can be seen that each different cell set-up will have its own limiting cathodic and anodic potentials where one of these processes occurs. It is only between these limiting potentials that the redox properties of a substrate can be examined.

It can be seen from the preceding discussion that before commencing a voltammetric experiment it is necessary to consider fully all the desired cell components. This must be done with respect to the substrate's solubility and reactivity, and to the probable potential of the redox process being studied.

A.2-2 Cyclic Voltammetry [4]

One of the methods used most commonly for routine electrochemical studies is cyclic voltammetry (CV). In this technique the potential of the working electrode is linearly varied over a period of time until it reaches a switching potential, whereupon the potential is ramped back to its starting value. The potential waveform has the triangular shape illustrated in figure A.2.

During CV the cell solution is left unstirred, thus ensuring that all of the mass transport of substrate to the working electrode surface occurs by diffusion. This results in the cyclic voltammogram of a substrate that undergoes a reversible electron-transfer having the form shown in figure A.3. Cyclic voltammetry can be carried out over a range of potential scan rates, this generally being between 20 mVs^{-1} and $10Vs^{-1}$.

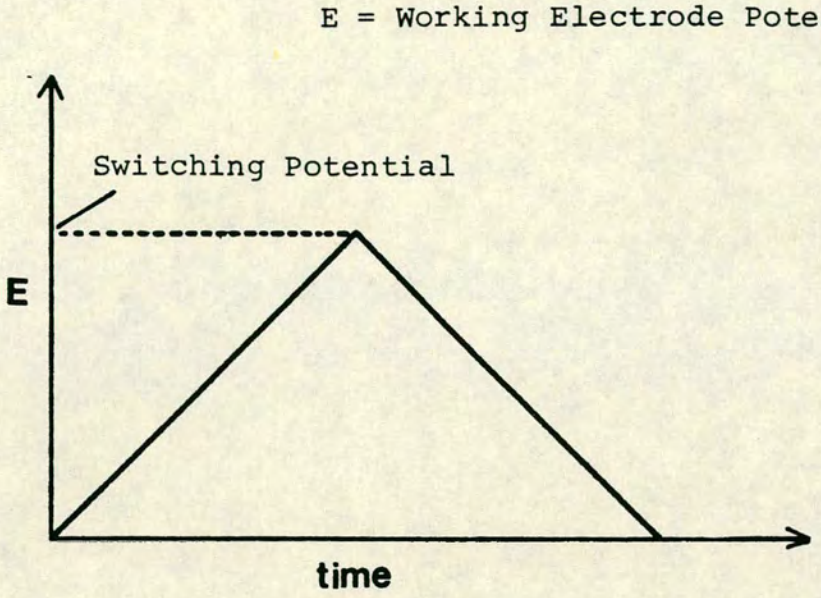

Figure A.2: Potential Waveform for Cyclic Voltammetry

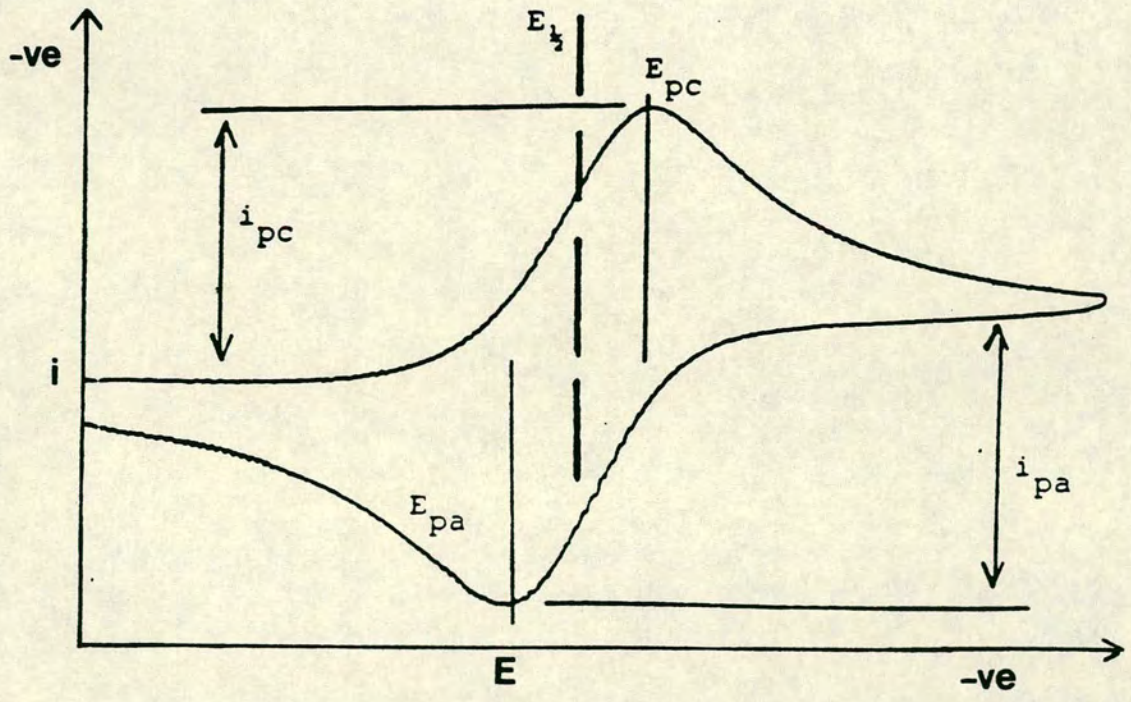

Figure A.3: Typical Reversible Cyclic Voltammogram

The figure shows a rise in current to a maximum, i_{pc}, at a potential E_{pc}, on the cathodic sweep, followed by a fall-off in current to a diffusion controlled limit. The reason for this shape is that at E_{pc} the amount of reduction occurring is related to the bulk concentration of the substrate. The region adjacent to the surface of the electrode, however, rapidly becomes depleted of substrate, due to its electrochemical reduction, and this can only be replaced by diffusion of substrate from the bulk of solution. The diffusion rate, however, cannot maintain the concentration of substrate, in the region adjacent to the electrode, at that of the bulk solution, hence the fall-off in current to a diffusion controlled level. A similar picture exists for the reverse sweep with the observation of an anodic peak current (i_{pa}) at E_{pa}, which falls off to a diffusion limited value. This process is due to reoxidation of the substrate reduced during the forward sweep.

The potential value normally quoted for redox processes studied by CV is $E_{\frac{1}{2}}$, which is the average of the peak cathodic and anodic potentials. $E_{\frac{1}{2}}$ can be considered to be an equivalent value to E° only when the process being studied is both chemically and kinetically reversible. The kinetic reversibility of a redox-couple depends on the rates of electron-transfer to and from the substrate being diffusion controlled. As the diffusion of a substrate is a process that has been mathematically modelled[5], then the kinetic reversibility of a redox process can be determined, at any temperature, by a set of criteria peculiar to the voltammetric technique being used. When a system obeys all these criteria it is said to follow Nernstian behaviour.

The reversibility criteria for cyclic voltammetry are listed in Table A.1 below.

Table A.1: Cyclic Voltammetry Reversibility Criteria

Measured Parameter	Condition for Reversibility
Potential	$E_{pa}-E_{pc} = \frac{59}{n}$ mV at 25°C E_p independant of ν ν = potential scan rate
Current	$i_{pa}/i_{pc} = 1$ i_p vs $\nu^{\frac{1}{2}}$-linear plot through origin

The shape of a cyclic voltammogram is affected when reduction/oxidation is immediately followed by chemical reaction of the substrate. Such a process is said to follow an EC (electrochemical, chemical) mechanism. Cyclic voltammograms of these processes are characterised by the absence of a return wave on the reverse sweep. In some instances the chemically altered substrate is itself redox-active in the observed voltammetric range. When this happens the redox process is said to follow an ECE mechanism. Typical cyclic voltammograms observed for EC and ECE processes are illustrated on figures A.4 and A.5 respectively.

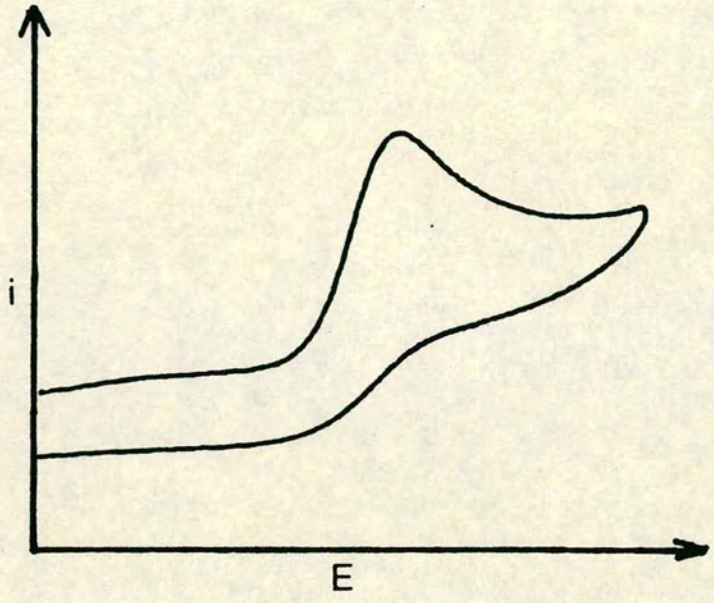

Figure A.4: Cyclic Voltammogram of an EC Process

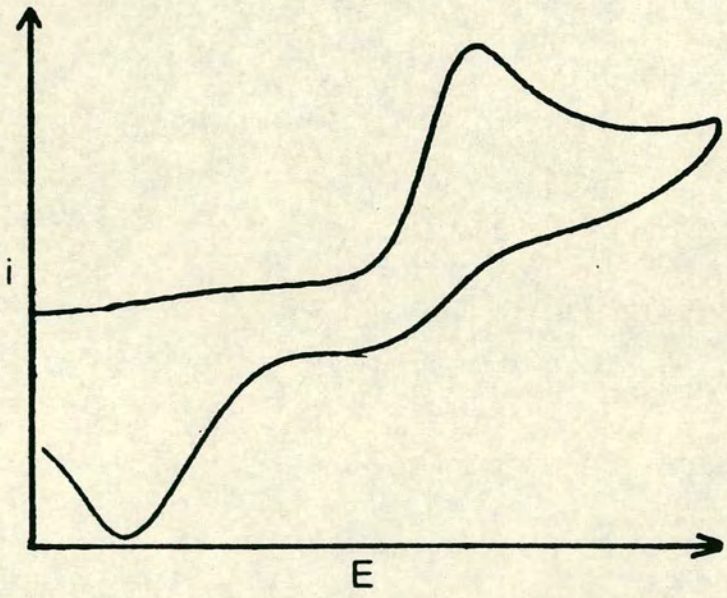

Figure A.5: Cyclic Voltammogram of an ECE Process

By carrying out cyclic voltammetry of a mechanically stirred solution, it is possible to gain additional information on the redox processes under study that cannot be elucidated from unstirred CV. Stirred CV reveals information about the type of electron-transfer processes under study, i.e. whether the voltammetric wave is due to oxidation or reduction of the substrate. This is necessary as the conventional cyclic voltammogram of a substrate is the same whether the substrate is present in its oxidised or reduced form; it is only by ensuring that the concentration of substrate close to the electrode surface is equal to the bulk concentration of substrate throughout the voltammetric sweep, that the nature of the redox process can be assigned. The relative position of the lines of peak current vs the zero current line for the cell reveals this information. This is illustrated on figure A.6 where the stirred cyclic voltammograms representing reduction and oxidation occurring for the same conventional cyclic voltammogram are shown.

The potential scan-rates employed during a stirred cyclic voltammogram are generally in the range 5 to 20 mVs^{-1}, somewhat slower than the scan rates used in conventional CV.

As well as revealing further insight into the redox properties of the substrate being studied, stirred CV is a particularly useful method for following the progress of an electrosynthesis. The technique is capable of determining when a substance has undergone 100% electrolysis.

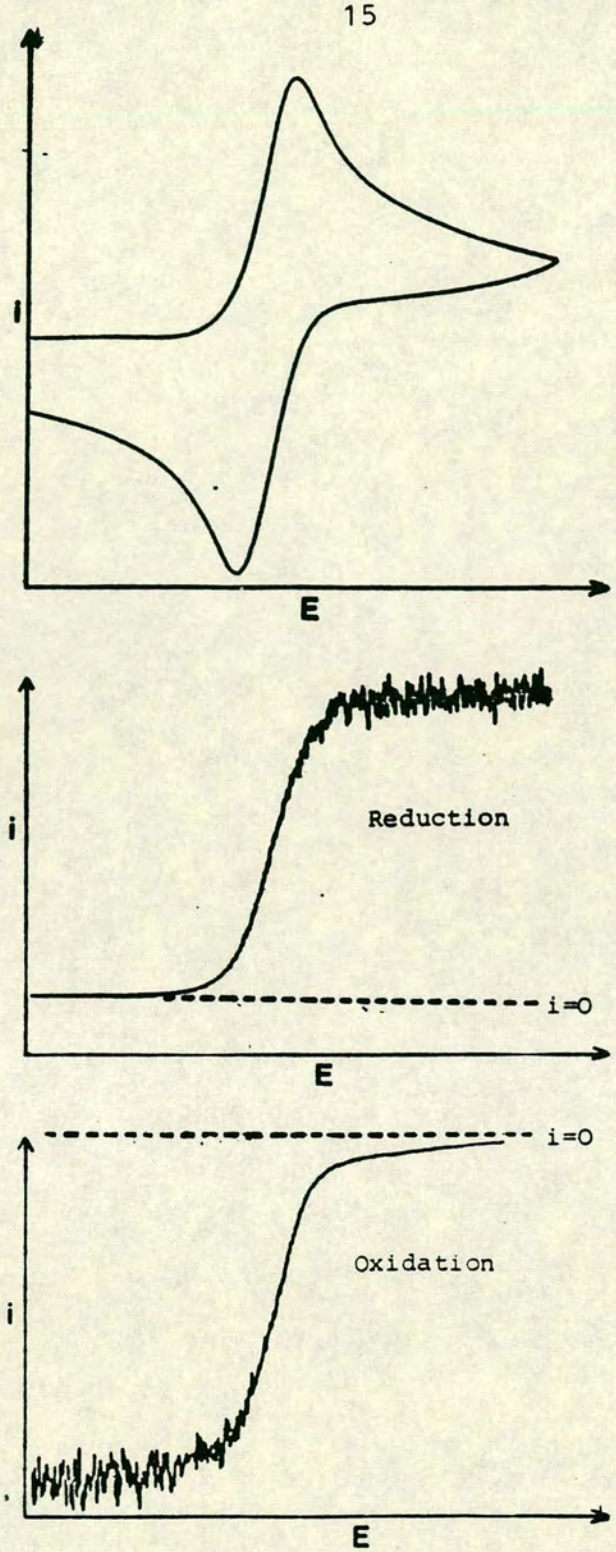

Figure A.6: Conventional and Stirred Cyclic Voltammograms for the same Redox Process

A.2-3 Alternating Current Voltammetry [6]

Alternating current voltammetry (ACV) follows a potential ramp similar to CV, but with a small alternating voltage (5 to 20 mV) superimposed on it. The waveform of the alternating voltage is normally sinusoidal, and has a frequency in the range 10 to 1000 Hz. A typical potential ramp for ACV is shown in figure A.7.

The component measured in ACV is the alternating current response of the cell. The signal obtained has the appearance of the single peak illustrated on figure A.8.

The value of E_p measured by AC voltammetry is similar to the $E_{\frac{1}{2}}$ value determined by CV. Typical scan rates for A C voltammetry lie in the range 2 to 20 mVs^{-1}. Due to the nature of this technique there are much higher resistances between the working and reference electrodes, ensuring that high amounts of iR compensation have to be employed.

As with CV, AC voltammetry has its own set of criteria to determine whether the electron-transfer process being studied is Nernstian. These criteria are listed on Table A.2.

Table A.2: AC Voltammetry Reversibility Criteria

Measured Parameter	Criteria
Potential	Width at ½ height of wave $= \frac{90}{n}$ mV at 25°C E_p independant of ω ω = AC frequency
Current	i_p vs $\omega^{\frac{1}{2}}$ - linear relationship passing through origin

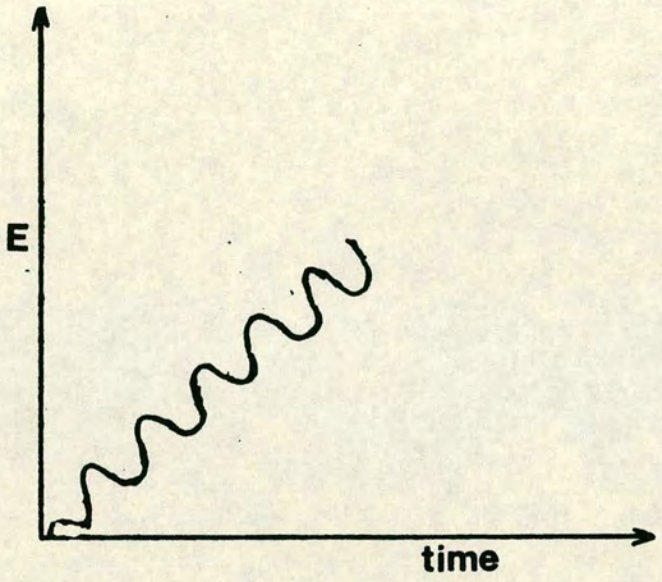

Figure A.7: Potential Ramp for Alternating Current Voltammetry

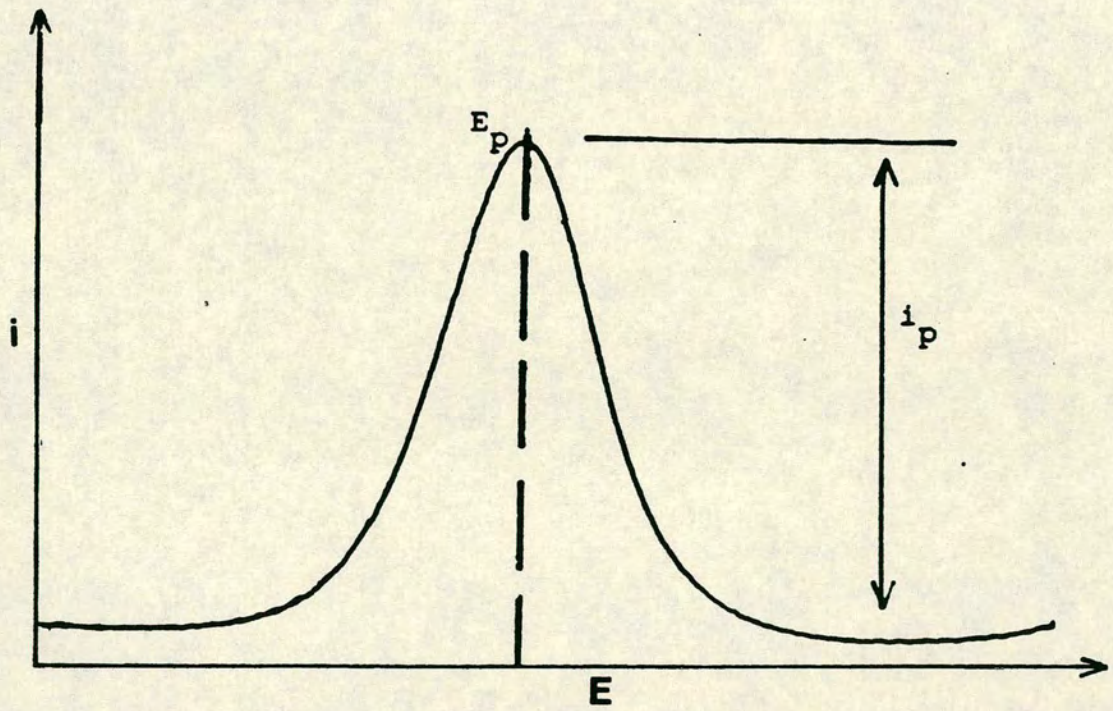

Figure A.8: Typical Alternating Current Voltammogram

AC voltammetry is a much more sensitive technique than CV. The anodic and cathodic limits observed for any cell system are generally 300 mV greater than those observed by CV. Additionally the quantitative assignment of peaks separated by only 80 mV is possible (c.f. 150 mV for CV), while qualitative separation of peaks is possible when these are separated by as little as 30 mV.

A.3 Electrosynthetic Methods

One of the most exciting areas of electrochemistry is that of large scale electrosynthesis. The study of chemical reactions induced by the electrolysis of substrates forms a large and important portion of this thesis.

Electrochemical methods can be utilised to carry out the complete oxidation/reduction of substrates, and while this may be all that is required to effect the desired synthesis, it is common for the electrolysed substrate to undergo further chemical reaction. This can either be an intramolecular reaction, or an intermolecular reaction with another substrate molecule, a component of the electrolyte solution, or an added reactant.

Electrochemical oxidation/reduction of substrates has an advantage over the equivalent chemical oxidation/reduction in that as the process is heterogeneous it does not require the presence of an extra, potentially contaminating, substance. Electrolysis can readily and precisely control the extent to which the substrate is reduced/oxidised. This factor is an

important advantage as it is often difficult to prevent the "over-oxidation" of a species during chemical oxidation.

In addition to its synthetic utility, the bulk electrosynthesis of a substrate forms a crucial part of the complete redox characterisation of the species. Voltammetry by itself cannot determine the number of electrons transferred during each redox process, and cannot reveal the chemical nature of the products of electron-transfer.

Characterisation of the chemical nature of the products of electrolysis can be best carried out by spectral examination. When the species produced is air-stable this is a simple process, but the examination of air-sensitive species has to be carried out in electrolysis cells that have been specially designed to sit in a spectrometer beam. These, in situ spectroelectrochemical cells are comparatively recent developments, having so far been designed for use in tandem with e.s.r., i.r. and electronic absorption[7,8] spectrometers.

Before discussing the different electrolysis techniques it is necessary to outline the special requirements that a bulk electrosynthesis cell has.

A.3-1 Electrolysis Cell Requirements

As the size of the current passing through a properly conducting and efficient electrochemical cell is determined largely by the surface area of the electrodes, it is necessary that both the working and secondary electrodes have a much larger surface area than the corresponding electrodes have in a voltammetric cell. Amongst the most common forms of working

electrodes for an electrosynthetic cell are the platinum basket and the mercury pool.

It is also necessary that the purity of the electrogenerated product is maintained by avoiding contamination with any species that may have been generated at the secondary electrode. To ensure this, it is normal that the secondary electrode of an electrogeneration cell is placed in a separate compartment. This ensures that an electrolysis cell consists of three separate compartments.

The large working electrodes used for bulk electrogenerations are generally inapplicable for voltammetry. It is normal practice that the working electrode compartment of an electrosynthesis cell contains an additional, voltammetric size, working electrode. This enables voltammetric scans to be carried out before, during and on completion of electrolysis, in particular stirred cyclic voltammograms.

A.3-2 Controlled Potential (Potentiostatic) Electrolysis

Controlled potential electrolysis involves carrying out electrosynthesis at a potential that is slightly (∿100 mV) in excess of the E_p value (determined by CV) for the desired electron-transfer. Electrolysis is then carried out until all the available substrate has been consumed. This can be determined by the stirred CV of the system, or by monitoring the exponential decay in cell-current with time until all substrate is electrolysed. A typical current-time curve for a potentiostatic electrolysis is illustrated on figure A.9.

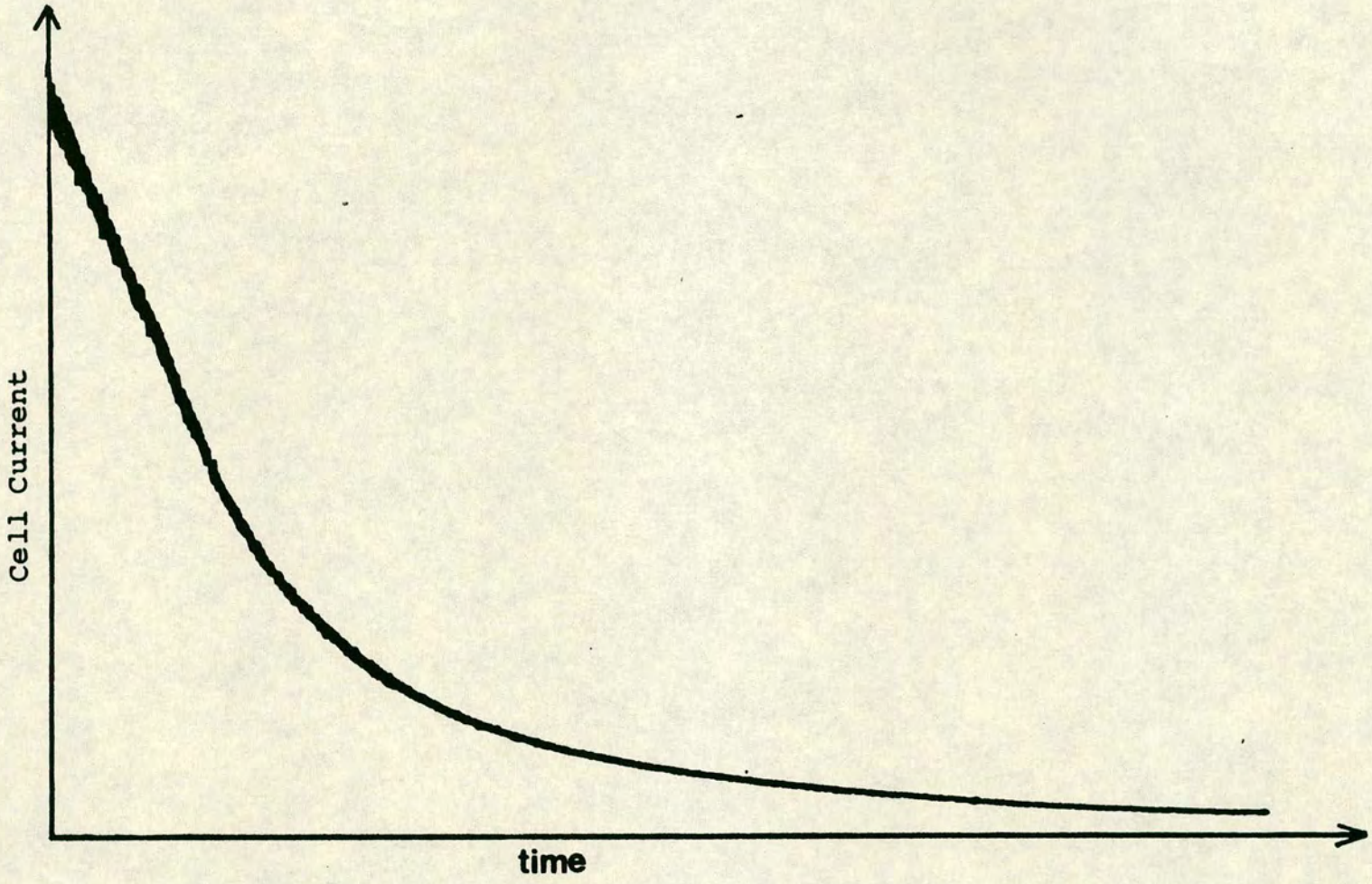

Figure A.9: Typical Current vs Time curve for Controlled Potential Electrolysis.

The area under the current-time graph represents the total charge that has passed during the electrolysis. The measurement of this is the basis of coulometry, where precise knowledge of the charge passed and amount of substrate present enables calculation of the number of Faradays passed per mole of substrate.

Potentiostatic electrolysis is a particularly good method whereby changes in the redox level of a substrate may be effected, whilst maintaining precise control over the extent to which electron-transfer is carried out. This method of electrolysis is the one employed for spectroelectrochemistry.

A.3-3 Controlled Current (Galvanostatic) Electrolysis

This method involves maintaining the current flow between the working and secondary electrodes at a constant level during electrolysis. As control of the potential of the working electrode is not required, a reference electrode is not necessary, and a two-compartment cell may be used.

This method is best used when prior knowledge of the desired number of Faradays to be passed to the substrate is available. When a substrate, that has two discrete reduction steps, is reduced using this method it is the first, easiest, reduction that occurs initially. Upon completion of this process the second reduction will commence and proceed to completion if the cell is left running. Continued cell operation after this process is complete will result in the limiting cathodic process occurring on the working electrode

surface. Thus it can be seen that galvanostatic electrolysis, while not exerting any overall control over which electron-transfer processes occur, is a useful method for carrying out an electrolysis that requires the transfer of a pre-determined number of Faradays.

Galvanostatic electrolysis, although not as selective as controlled potential electrolysis, is much easier to use in practice, particularly where a large quantity of substrate has to be electrolysed. This is due to the overall time of electrolysis being considerably shorter using this technique than with potentiostatic electrolysis.

References

1. D.J.G. Ives and G.J. Janz, 'Reference Electrodes', Academic, New York, 1961.
2. For full derivation of Nernst Equation see A.J. Fry, 'Synthetic Organic Electrochemistry', Harper and Row, New York, 1971, p. 22-24.
3. L. Heites, 'Polarographic Techniques', Wiley, New York, 1965.
4. J.E.B. Randles, Trans. Faraday Soc., 1948, 44, 327.
5. A. Fick, Pogg.Ann., 1855, 94, 59.
6. A.M. Bond, Anal.Chem., 1970, 42, 1169.
7. R.W. Murray, W.R. Heineman and G.W. O'Dom, Anal.Chem., 1967, 39, 1666.
8. G.A. Heath, L.J. Yellowlees and P.S. Braterman, J.Chem.Soc., Chem.Commun., 1981, 287.

PART B

SYNTHETIC AND MECHANISTIC STUDIES ON THE ELECTROCHEMICAL REDUCTIVE ALKYLATION OF ALIPHATIC KETONES IN LIQUID AMMONIA/ QUATERNARY AMMONIUM SALT SOLUTIONS

B.1 Introduction

B.1-1 Liquid Ammonia as an Electrochemical Solvent

Liquid ammonia as a solvent has been extensively used for synthetic organic chemistry. The most well-known organic reaction carried out in this solvent is the Birch Reduction[1] in which an unsaturated, often aromatic, organic compound is reduced by a solution of solvated electrons in liquid ammonia. The solvated electrons are supplied by dissolution of a metal, normally an alkali metal, in liquid ammonia. The low boiling point of liquid ammonia (-33.4°C) enables relatively easy work-up of reaction mixtures.

It is therefore surprising that this solvent has not been extensively used for electrochemical studies. Its aprotic properties (pKa $\sim$ 34) enable stabilisation of reactive intermediates, e.g. radical-anions and dianions, and its dielectric constant (ε = 23) is sufficiently high to enable electrochemical studies to be carried out in relatively low concentrations of supporting electrolyte (0.1M electrolyte required c.f. methylene chloride, ε = 8, 0.5M electrolyte required). The topic of electrode reactions in liquid ammonia was reviewed by Brown in 1974.[2] Major contributions in this area since then have come from Bard,[3] Brown[4] and Saveant.[5]

The properties of liquid ammonia pertinent to its use as an electrochemical solvent will be discussed briefly.

(a) Acid-Base Properties of Liquid Ammonia

Liquid ammonia undergoes auto-ionisation in a manner similar to water, as indicated below but to a lesser extent.

$$2NH_3 \rightleftharpoons NH_4^+ + NH_2^-$$

This process ensures that the ammonium and amide ions are respectively the strongest acids and bases that can occur in a liquid ammonia solution.

The acidity of a liquid ammonia solution can be controlled by addition of proton donors (HA). Reaction of the proton donor with solvent as shown below is generally slow.

$$NH_3 + HA \rightleftharpoons NH_4^+ + A^-$$

Reaction of the proton donor with solvent is increasingly suppressed as the concentration of the conjugate base A^- increases and reaction of the proton donor with, for example, an electrogenerated radical-anion in low flux will occur more readily.

(b) Solubilities of Ionic and Covalent Compounds in Liquid Ammonia

The properties of liquid ammonia relevant to its use as a solvent have been discussed by Hildebrand.[6] In general, the solubilities of ionic compounds are slightly lower than in water. Salts with polynegative anions are almost insoluble and salts with highly polarisable anions are generally more soluble in ammonia than they are in water. The reason for this behaviour is the higher polarisability of the ammonia molecule compared to water.

Covalent organic compounds are generally more soluble in liquid ammonia than they are in water, this being due to the greater dispersion energy of ammonia (caused again by the molecule's high polarisability). Substances that are capable of hydrogen bonding exhibit high solubilities in liquid ammonia. Many compounds, however, are relatively insoluble and as a consequence organic co-solvents have often to be used to enable sufficient quantities of substrate to dissolve in ammonia. For example, THF and diethyl ether have been used successfully in this way.

(c) Supporting Electrolytes Used in Liquid Ammonia

The earliest electrochemical studies in liquid ammonia[7] used tetrabutylammonium iodide as supporting electrolyte but the saturated concentration of this salt is only 0.0056M. More recent studies have utilised the more soluble salts; potassium bromide and iodide, tetraethylammonium bromide

and fluoroborate, tetrabutylammonium fluoroborate and trimethylbutylammonium fluoroborate and iodide.

(d) Limiting Cathodic and Anodic Processes in Liquid Ammonia/Electrolyte Solutions

The thermodynamically controlled potential range of liquid ammonia is only 0.04V, this being governed by the standard NH_3-N_2 and H_2-NH_3 couples. Both of these sluggish processes, however, show large overvoltages dependant on the electrode material used. The kinetically favoured limiting cathodic process can be either dissolution of solvated electrons, characterised by the formation of a blue solution, or reduction of the supporting electrolyte cation. When the electrode material is mercury, reduction of the supporting electrolyte cation results in the formation of an amalgam.

Depending on the circumstances, the limiting anodic process in liquid ammonia may be oxidation of the electrode material, oxidation of the supporting electrolyte anion or oxidation of the solvent itself. This last process results in the formation of nitrogen and ammonium ions according to the equations shown below:

$$NH_3 \longrightarrow \tfrac{1}{2}N_2 + 3H^+ + 3e^-$$

$$H^+ + NH_3 \longrightarrow NH_4^+$$

B.1-2 Electrochemical Reductive Alkylations Carried Out in Quaternary Ammonium Salt Solutions

There have been a number of recent reports concerning the electrochemical reductive alkylation, notably ethylation of organic compounds in aprotic solvent/quaternary ammonium salt solutions.

Abbot and Bellamy[8] studied the reduction of aliphatic ketones in liquid ammonia/tetraethylammonium fluoroborate solution. The initial study concerned the reduction of acetylcyclopropane (1), the objective being to ascertain the number of electrons transferred to (1) in the initial ring-opening step of the reduction for comparison with data for the conventional Birch reduction of this compound. Unfortunately, this compound, and all aliphatic ketones subsequently studied, proved to be electroinactive in the available voltammetric cathodic range. Investigation of these compounds was thus limited to galvanostatic reduction at a mercury pool cathode and analysis of product mixtures. The results of this study showed that no nett reduction of the ketone function occurs until the ring-opening step of the reaction is complete. The ring-opening step was found to be a two-electron reduction, as in the case of chemical reduction. After ring-opening is complete to give pentan-2-one (2), further reduction of the carbonyl group occurs but this gives as the major product not the expected secondary alcohol, pentan-2-ol (3)

(obtained in 25% yield), but the ethylated tertiary alcohol 3-methylhexan-3-ol (4) (obtained in 75% yield). The mechanism proposed for the ethylation step involved formation of the ketone dianion which then acted as a nucleophile, attacking the tetraethylammonium cation. The overall proposed reaction pathway is shown in Scheme B.1.

Two-electron reduction of pentan-2-one (2) under similar conditions gave the tertiary alcohol (4) but in a lower yield (34%) with the secondary alcohol (3) being the major product (66%).

As these reductions were being carried out beyond the cathodic limit there was the possibility that formation of a tetraethylammonium radical amalgam with mercury was playing a role in the alkylation reaction. The reductions were therefore repeated using platinum as the cathode material. When (1) was the starting material, the tertiary alcohol (4) was obtained but in lower yield (43%) than when mercury was the cathode material. The other products of the reduction were (3) pentan-2-ol (12%), and (2) pentan-2-one (45%). When (2) was the starting material the products obtained were the tertiary alcohol (22%), with pentan-2-ol (60%) and pentan-2-one (18%) also present. The overall current efficiency of these reactions was somewhat lower than when the reductions were performed with a mercury cathode. This is probably

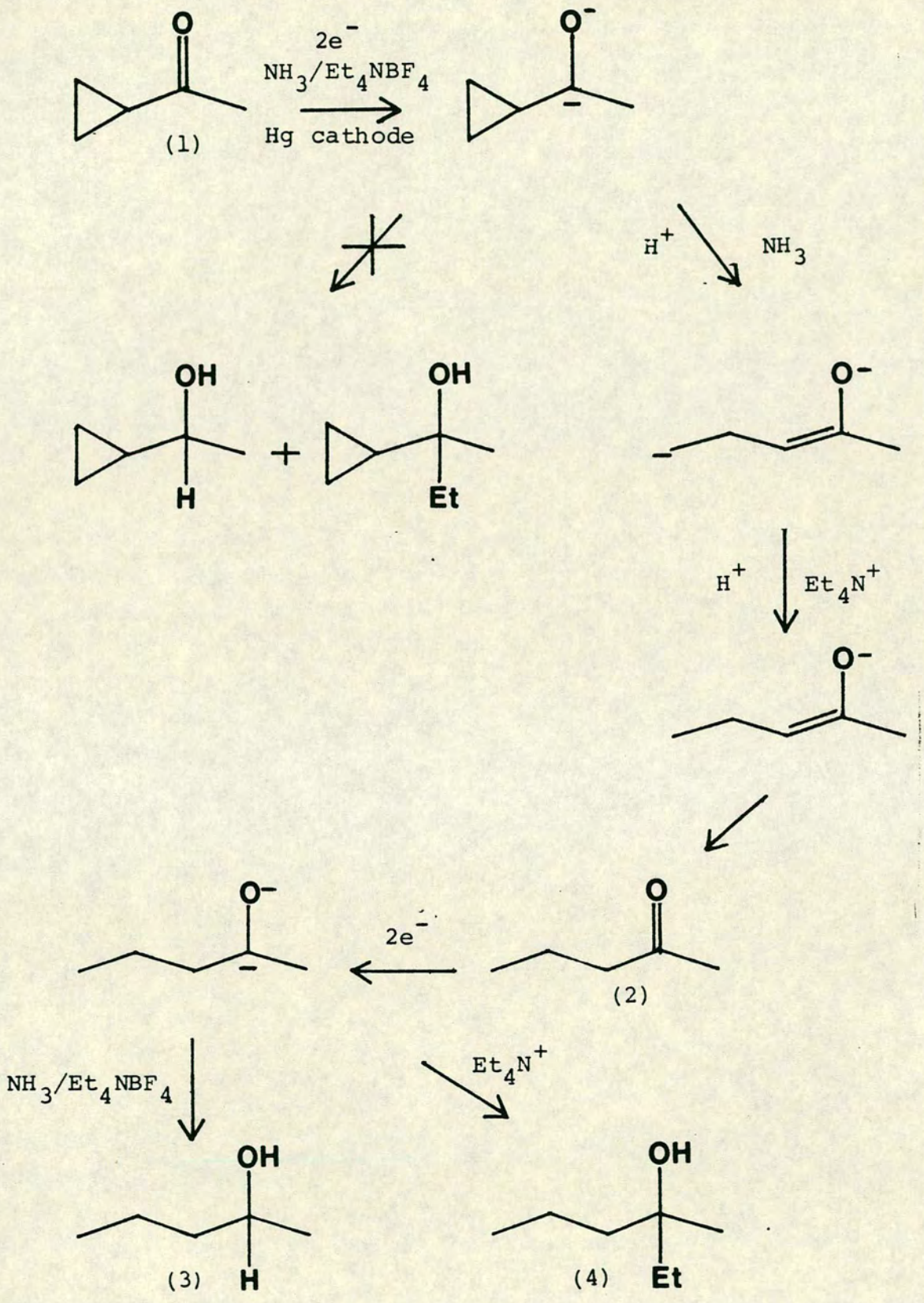

Scheme B.1: Electroreduction of Acetylcyclopropane(1) in Liquid Ammonia/Tetraethylammonium Fluoroborate

due to slow evolution of hydrogen on platinum which competes with electron dissolution as the limiting cathodic process on a platinum electrode.[9] There is no evidence of critical participation of $Et_4N\cdot/Hg$.

An important factor in the alkylation reaction appeared to be the presence of a stable solution of solvated electrons. When acetylcyclopropane was being reduced a blue solution of solvated electrons appeared after two-electron reduction of the substrate had occurred, indicating that during the time in which reduction of the carbonyl group and alkylation were occurring an excess of solvated electrons was present in solution. For pentan-2-one, however, the presence of a solution of solvated electrons was not observed until approximately 1F mol^{-1} had passed. In addition, the lower yield of tertiary alcohol obtained with pentan-2-one reduction led to the postulate that alkylation of substrate only occurs in the presence of a solution of solvated electrons. The lower yield of tertiary alcohol obtained in pentan-2-one reduction was explained as being due to the presence of protic impurities in the cell. The source of these impurities was thought to be the solvent/electrolyte system; typically their concentration is about $5 \times 10^{-4}M$ in a 'dry' conventional electrochemical cell. For acetylcyclopropane, these impurities would mainly be consumed in the initial ring-opening step, and reduction of the ketone function

would occur in the absence of proton donors. For pentan-2-one reduction, however, the protic impurities present would protonate the initially formed radical-anion which would then be further reduced to give a carbanion. The latter would protonate to give pentan-2-ol as shown in Scheme B-2.

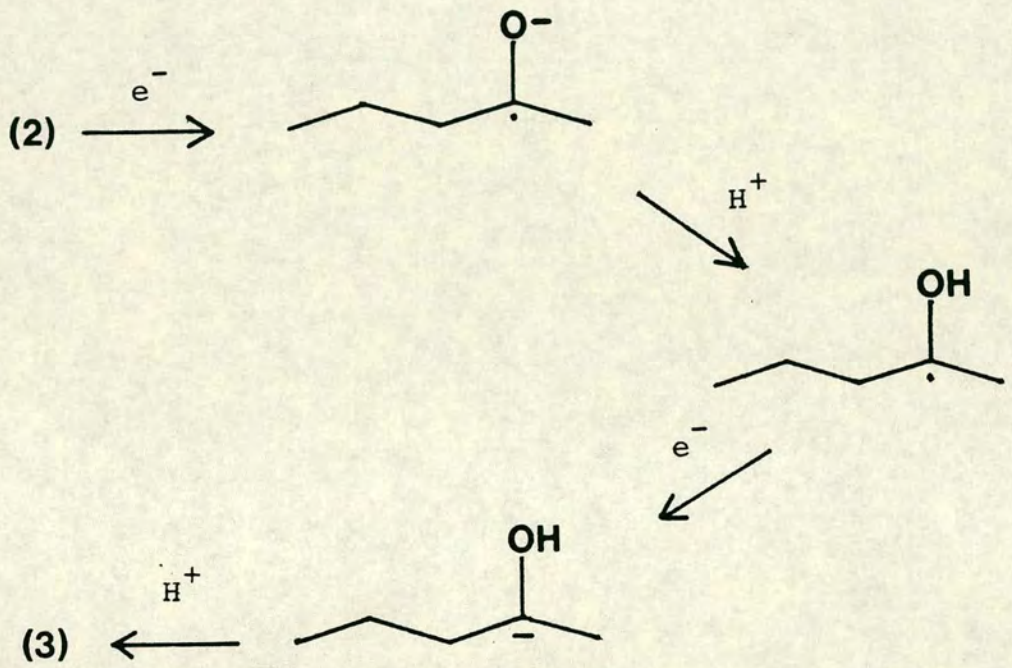

Scheme B-2 Formation of Pentan-2-ol (3) by Reaction of Pentan-2-one radical-anion with Protons.

It was found that when these reductions were carried out in the presence of an excess of proton donor (ethanol) the only product formed was the secondary alcohol (3).

A series of quaternary ammonium salts were prepared containing a variety of alkyl groups, including R_3EtN^+, $R_2Et_2N^+$ and REt_3N^+, and these were used as supporting

electrolytes in the reduction of acetylcyclopropane to see if any analogous alkylations would take place. All attempts were unsuccessful with the exception of tributylethylammonium salts which gave only the ethylated tertiary alcohol (4).

Electrochemical reductions of some other organic compounds (benzophenone, oct-4-yne) were carried out in liquid ammonia/tetraethylammonium fluoroborate solutions to see if any of these compounds underwent ethylation in a similar manner to that observed for aliphatic ketones, but no ethylation was observed with these substrates.

A study carried out by Shono[10] found similar types of reaction. Electroreduction of non-conjugated acetylenic ketones (5) in dimethylformamide (DMF), 0.1M tetra-ethylammonium tosylate at a graphite cathode was carried out in an attempt to prepare cyclised tertiary alcohols (6). These were in fact the major products of electro-reduction but the ethylated acetylenic tertiary alcohols (7) were obtained as minor products (Scheme B-3).

The cyclised alcohol (6) was obtained in 60% and 53% yield, and the ethylated alcohols (7) in 25% and 29% yield when the terminal group R on the starting ketone was methyl and ethyl respectively.

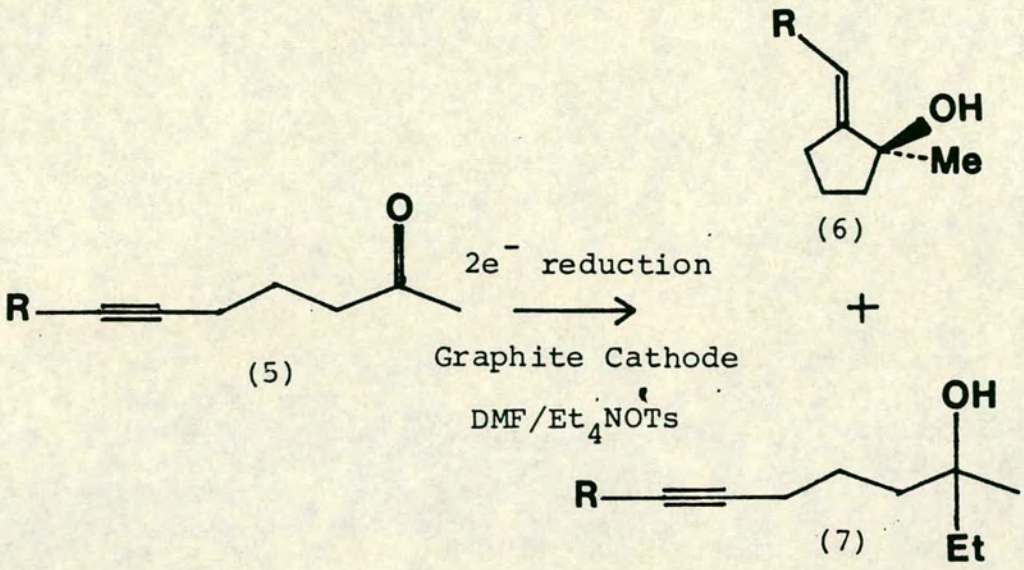

Scheme B-3 Electroreduction of Non-Conjugated Acetylenic Ketones (5) in DMF/Et_4NOTs (0.1M)

Shono observed similar behaviour in the reduction under the same conditions of non-conjugated olefinic ketones[11] (8) (Scheme B-4).

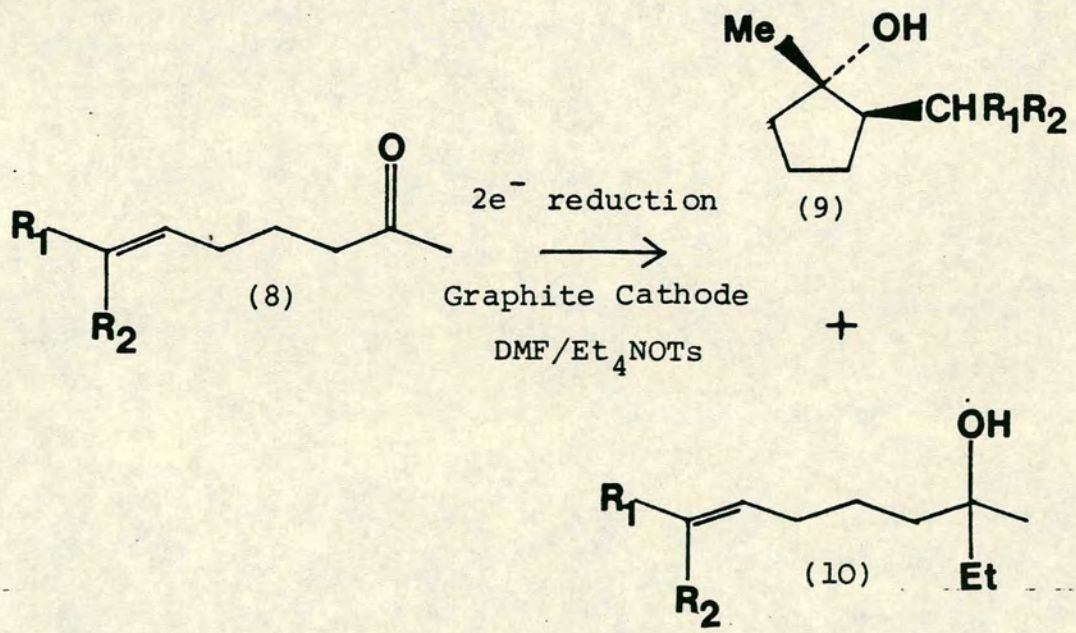

Scheme B-4 Electroreduction of Non-Conjugated Olefinic Ketones (8) in DMF/Et_4NOTs (0.1M)

The yields of cyclised (9) and ethylated tertiary (10) alcohols with various terminal groups on the starting ketone (8) are summarised in Table B-1.

Table B-1 Yields of (9) and (10) obtained by reduction of (8).

Terminal Group		Yield (9) %	Yield (10) %
R_1	R_2		
Me	H	77	0
Et	H	68	19
Pr-i	H	71	15
Me	Me	54	19
Et	Me	23	18
Pr-i	Me	26	37

The highest proportion of ethylated tertiary alcohol was obtained with two terminal alkyl groups on the olefin function. The mechanism of the ethylation step was suggested to involve direct nucleophilic attack of an anionic species on the tetraethylammonium cation.

A further study was then carried out on electro-reduction of a series of aliphatic and aromatic ketones (11) under the same conditions.[12] The results obtained gave a mixture of secondary (12) and tertiary (13) alcohols as shown in Scheme B-5. The results obtained are summarised in Table B-2.

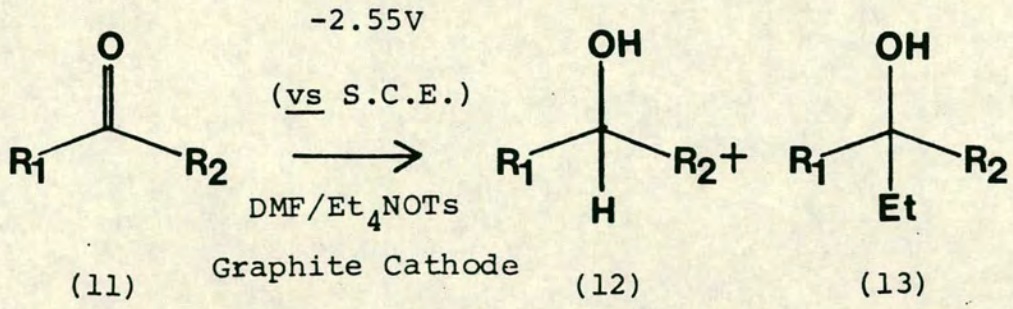

(11) (12) (13)

Scheme B-5 Electroreduction of Ketones (11) in DMF/Et_4NOTs (0.1M)

Table B-2 Yields of (12) and (13) obtained when (11) is reduced.

Terminal Group on (11)		% Yield (12)	% Yield (13)
R_1	R_2		
Me	Bu	9	58
Me	n-pentyl	9	55
$-(CH_2)_4-$	-	6	11
$-(CH_2)_5-$	-	14	51
Me	$PhCH_2CH_2$	7	42
Me	$CH_2=CHCH_2CH_2$	-	65
Ph	Ph	65	-

Thus, high yields of tertiary alcohol (13) are obtained when both the substituent groups R_1 and R_2 are alkyl. It is interesting to note that no ethylation was observed when both substituent groups were aromatic. It was noted that these reductions were only complete after $4F\ mol^{-1}$ had been consumed.

A further study[12] was carried out on the reduction of heptan-2-one under the same solvent/electrode regime but using Me_4N^+, $Pr^n_4N^+$ and $Bu^n_4N^+$ electrolytes, to see if any analogous alkylations occurred. Alkylation was only observed with tetrapropylammonium salts which gave ca. 12% yield of the propylated tertiary alcohol.

The reduction of anthracene (14) at a mercury cathode in molten tetra-n-butylammonium nitrate has been the subject of two studies. The first of these[13] stated that the major product of this reduction was 9-butyl-anthracene (15).

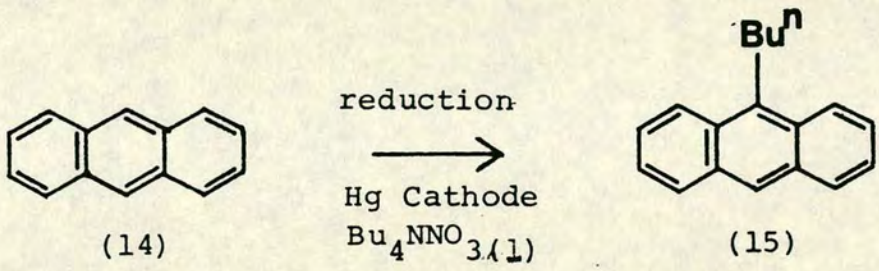

(14) (15)

A more recent study[14] of this reduction at both mercury and platinum cathodes showed, however, that the major product was in fact 9-butyl-9,10-dihydroanthracene (16) with small amounts of (15), and probably 1- and 2-butylanthracene also present as minor products. The proposed reaction mechanism is shown in Scheme B-6.

This same medium was then employed,[15] as well as molten tetraethylammonium nitrate, to see whether reduction of aliphatic ketones would result in formation of alkylated tertiary alcohols under these conditions. No alkylation was observed.

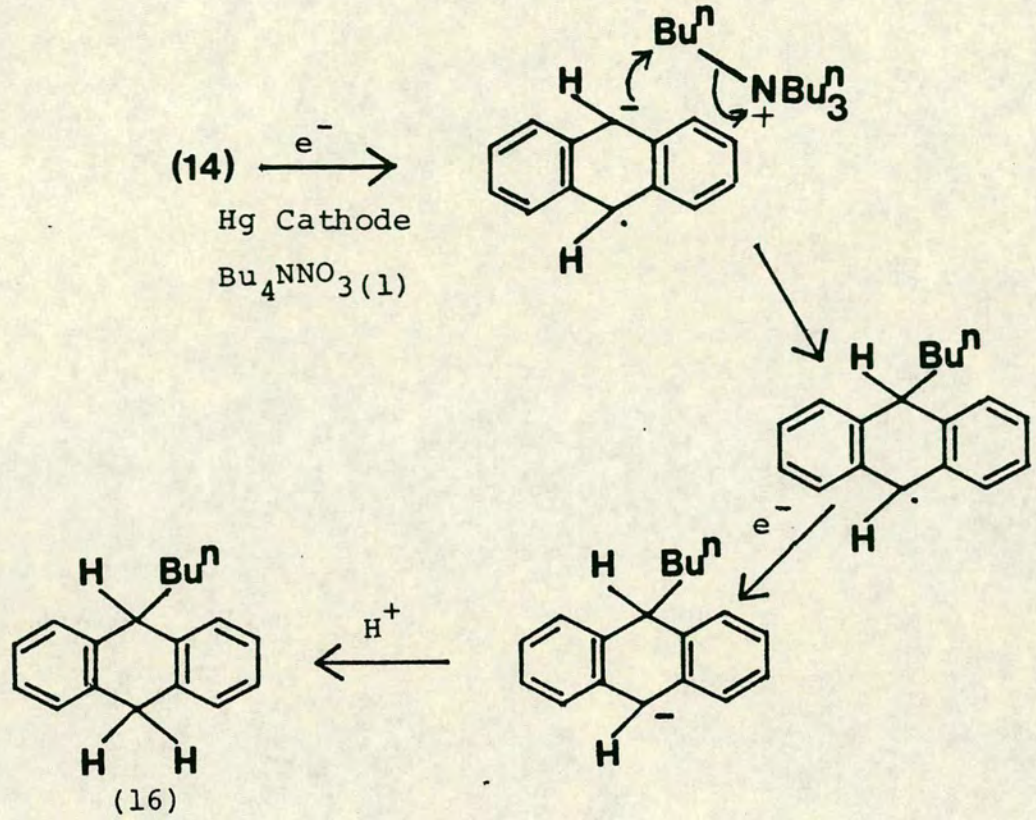

Scheme B-6 Electroreduction of Anthracene (14) in Molten Tetra-n-butylammonium Nitrate

The tertiary-butylation of naphthalene (17) has been reported[16] to occur during its electrochemical reduction in DMF with tetra-n-butylammonium iodide present as the supporting electrolyte together with added t-butyl-trimethylammonium iodide. The electrolysis was continued until 4F mol^{-1} had been consumed. The mechanism proposed for this reaction involves solution electron-transfer between the naphthalene radical-anion and the t-butyl-trimethylammonium cation, giving the quaternary ammonium radical. This decomposes to give the t-butyl radical

which then couples with the naphthalene radical-anion. The overall reaction scheme is shown in Scheme B-7.

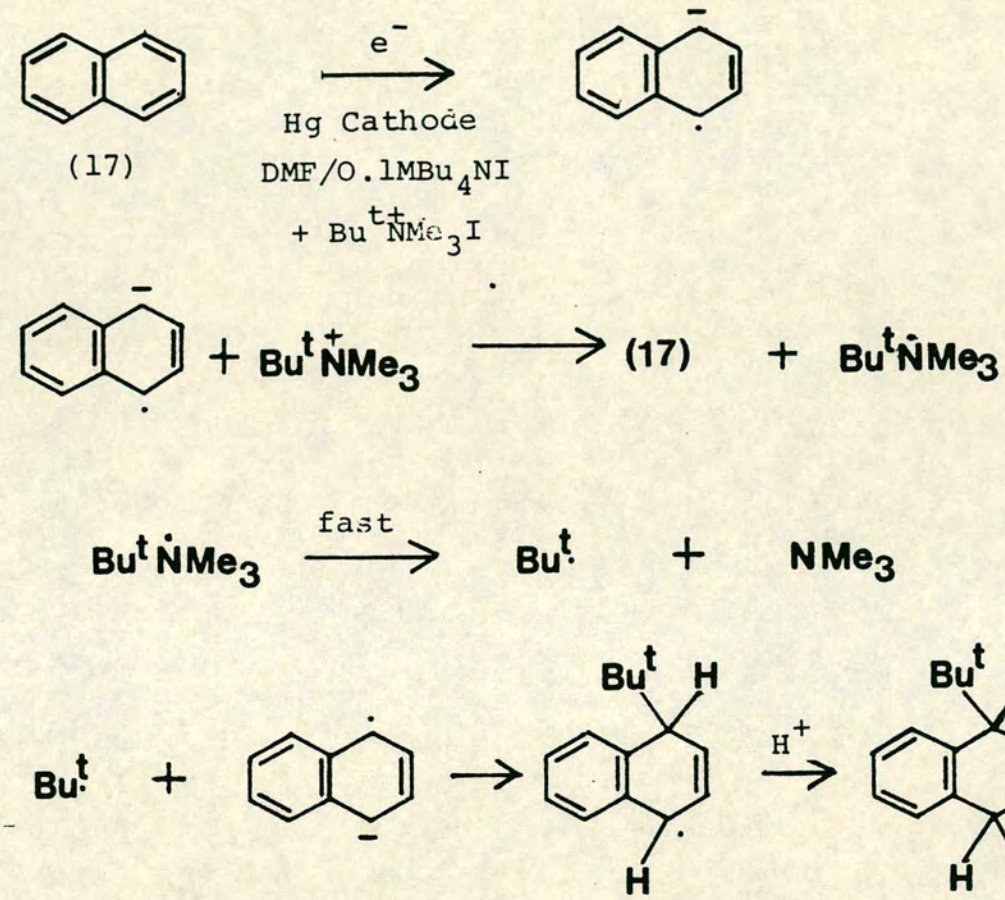

Further Reduction Gives The Final Products

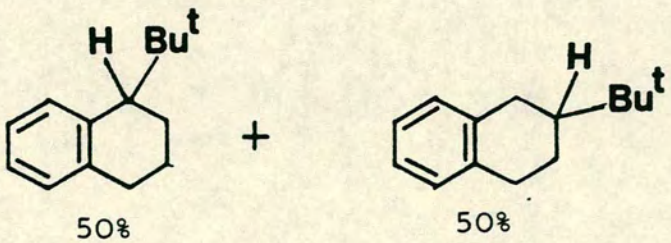

50% 50%

Scheme B-7 t-Butylation of Naphthalene by a Solution Electron-Transfer Mechanism

The preponderance of t-butylation over methylation in the product mixture was explained by the greater stability of the t-butyl radical. Evidence for the solution electron-transfer mechanism was also obtained from the increased peak current in the polarographic wave of naphthalene as the concentration of t-butyltrimethyl-ammonium iodide was increased.

B.2 Discussion

In the present work, the reductive alkylation of aliphatic ketones in liquid ammonia observed by Abbot and Bellamy[9] was re-examined in order to obtain further mechanistic information about this process. The electrolysis conditions were similar to those previously employed, i.e. galvanostatic reduction at a mercury cathode in a two-compartment cell. The experimental conditions and results are summarised in Table B.3 (see Appendix).

B.2-1 Reduction of Pentan-2-one in Liquid Ammonia/ Tetraethylammonium Fluoroborate at a Mercury Electrode with Mechanical Stirring

The general observations were as follows:

Reduction of pentan-2-one at a mercury pool in a mechanically stirred cell gave the secondary alcohol pentan-2-ol as the only alcohol formed. During the

reduction, large amounts of a black solid were generated at the constantly renewed electrode surface, and no solvated electrons were observed throughout the reduction. The black solid observed in such circumstances is the known tetraethylammonium/mercury amalgam. Before attempting to accommodate a possible role for a quaternary ammonium amalgam in the mechanistic sequence, it is first necessary to review some of the previous work with these amalgams.

They were first extensively studied by Littlehailes and Woodhall[17] who prepared a range of quaternary ammonium amalgams by electrolysis of a 0.1M solution of the appropriate salt at a mercury cathode in anhydrous DMF. The general reaction which occurs is:

$$R_4N^+ \xrightarrow[\text{Hg cathode}]{e^-} R_4N\cdot/(Hg)_n$$

DMF

The amalgams which were formed were found to consist of between 12 and 13 mercury atoms per quaternary ammonium radical. They were found to be stable at -10°C but, sensitive to heat, protons and oxygen. Slow thermal decomposition was observed at 25°C resulting in the formation of tertiary amines and products associated with the expulsion of an alkyl radical as shown below:

$$R_4N\cdot/Hg \xrightarrow{\Delta} Hg + R_3N + R\cdot \downarrow \text{Further products}$$

Decomposition of an amalgam by addition of proton donors results in the reformation of the cation and liberation of gaseous hydrogen:

$$H^+ + R_4N\cdot/Hg \longrightarrow Hg + R_4N^+ + \tfrac{1}{2}H_2$$

Quaternary ammonium amalgams, in common with alkali-metal amalgams, have reducing properties and are found to transfer electrons to organic substrates.

Kariv-Miller and Nanjundiah[18] carried out an electrochemical study on the quaternary ammonium amalgam generated by electrolysing a solution of N,N-dimethyl-pyrrolidinium iodide in DMF containing 0.1M tetrabutyl-ammonium iodide as the supporting electrolyte. The dimethylpyrrolidinium cation has a sufficiently less negative reduction potential than the tetrabutylammonium cation to enable voltammetric examination. This showed that the reduction was a one-electron, reversible step occurring with simultaneous precipitation of the amalgam, as shown by the presence of a cyclic voltammetric oxidation wave typical of a "stripping" reaction. Coulometry, however, showed that the nett charge transferred was somewhat greater than 1 $Fmol^{-1}$. This was attributed to a slow reaction between the amalgam and the DMF solvent, generating dimethylamine and formaldehyde, which could only be observed on the longer time scale of coulometry. This reaction illustrates the ability of quaternary

ammonium amalgams to transfer electrons even to substrates which are more difficult to reduce electrochemically than the quaternary ammonium cation itself.

In the present context, it is probable that the electrochemical process does entail the formation of the tetraethylammonium amalgam, as evidenced by the generation of large quantities of a black solid. In order to investigate whether this amalgam was capable of reducing pentan-2-one by itself, some of this material was generated in the absence of pentan-2-one, and the ketone was then added to the mixture without further electrolysis. This resulted in the formation of pentan-2-ol as the only alcohol, though in lower yields than before. Although the reaction conditions in the two reactions are not identical it can be concluded from the second case that the tetraethylammonium amalgam can reduce pentan-2-one to pentan-2-ol, but that no alkylation of the ketone occurs under these conditions. Thus, the process occurring at a continuously renewed mercury cathode surface during the electroreduction of pentan-2-one can be summarised as in Scheme B-8.

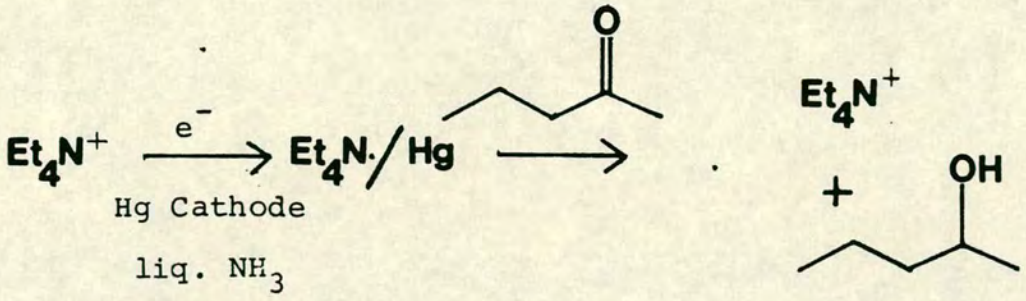

Scheme B-8 Mechanism for Reduction of Pentan-2-one in Liquid Ammonia/Tetraethylammonium Fluoroborate at a Continuously Renewed Mercury Cathode.

B.2-2 Reduction of Pentan-2-one in Liquid Ammonia/ Tetraethylammonium Fluoroborate at a Mercury Electrode with Stirring by Nitrogen Bubbles

This method of stirring, being the one previously employed,[9] resulted in the formation of both pentan-2-ol (67%) and 3-methylhexan-3-ol (33%). When the reduction was begun, the cathode surface immediately became tarnished with a thin layer of amalgam. Continued electrolysis gave a blue solution of solvated electrons after 1.2 $Fmol^{-1}$ had passed. Such solutions are well characterised for liquid ammonia, and their general properties and properties pertinent to liquid ammonia solutions of quaternary ammonium salts are summarised below.

Solvated Electrons in Liquid Ammonia and their Reactions with Tetraalkylammonium Cations

A solvated electron is defined as an electron existing in a weakly ionising or non-ionising solvent. Solvents that are known to support solutions of solvated electrons are ammonia, HMPA, low molecular weight amines and some ethers (e.g. THF).

The most common method of producing a solution of solvated electrons is by dissolution of an alkali metal in the particular solvent. The reason for the stability of these metal solutions is the existence of a potential well and a large activation barrier to be overcome for proton abstraction from the solvent. This is illustrated below in Figure B-1 for the contrasting examples of solutions created by the dissolution of sodium in liquid ammonia and in water.

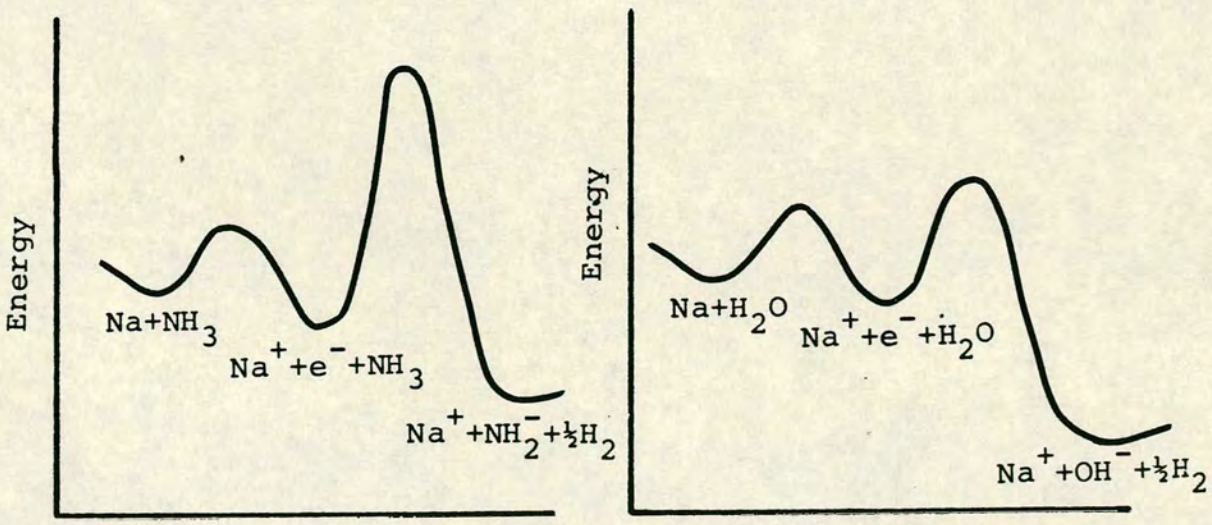

Figure B-1 Comparison of the Stability of Solvated Electrons in Sodium/Ammonia and Sodium/Water Systems.[19]

For the specific case of liquid ammonia solutions of solvated electrons, when prepared under rigorously pure conditions these are extremely stable, decomposing at rates of less than 0.1% per day.[20]

In liquid ammonia there are two distinct physical classes of solutions of solvated electrons. The first class exists at low concentrations of dissolved metal; in the case of sodium up to concentrations of 1.51 M. This type of solution is the well known intensely dark-blue coloured solution. The colour in this case is due to the low wavelength tail of an intense absorption band centred at 1440 nm. At higher concentrations, a remarkable liquid-liquid phase separation occurs, with a metallic bronze coloured liquid phase floating on top of the blue liquid. As the concentration of dissolved alkali metal is increased, the ratio of bronze to blue phases increases until, at a concentration of 3.91 M for sodium, the solution consists exclusively of the bronze coloured liquid.

The nature of these two phases is quite distinct. For extremely dilute solutions (<0.005 M) the solution can be considered as consisting of essentially independant solvated electrons and metal cations. As the concentration increases ion-pairing becomes important with a wide variety of species present, e.g. M^+e^-, $e^-M^+e^-$. At very high concentrations, i.e. in the metallic bronze phase

the nature of the solution is more akin to the metallic state with the metal cations loosely held together by solvated electrons.

From an electrochemical viewpoint, it is sometimes preferable to refer not to solvated electrons but to radical-anions of solvent molecules.[21] The stability of these can be related to similar factors as those for normal organic radical-anions. The conditions of an electrochemical experiment, where the concentration of substrates to be reduced is normally low, mean that a solution of solvated electrons is of the low-concentration type.

The nature of electrochemically generated solvated electrons in liquid ammonia has been studied by Quinn and Lagowski.[22] In their study, a wide range of quaternary ammonium salts were employed as supporting electrolytes with solvated electrons generated at a platinum cathode. The results showed that there was only a small variation in the position of the centre of the absorption band (1440 ± 4 nm) even though a wide range of cation sizes were employed.

Although it is possible to generate solvated electrons in liquid ammonia/quaternary ammonium salt solutions, the lifetime of these solutions is limited by reaction of the quaternary ammonium cations with solvated electrons.

This reaction was first observed[23] when it was noted that addition of potassium to a solution of tetramethylammonium iodide resulted in the formation of trimethylamine and a hydrocarbon gas identified as ethane. A separate study[24] of the reaction of a solution of tetraethylammonium chloride with potassium showed that triethylamine was formed but, that more gas was liberated from the solution than would correspond, by analogy, to exclusive formation of butane.

More recently these reactions have been extensively studied by Hazlehurst, Holliday and Pass.[25] Their experiments involved addition of potassium metal to a solution of the particular quaternary ammonium chloride in liquid ammonia. The reaction mixture would thus consist solely of solvated electrons and quaternary ammonium cations since the potassium ions would be precipitated out of solution in the form of insoluble potassium chloride. The direct cleavage of the tetraalkylammonium cation by solvated electrons was proposed to occur via the formation of the unstable quaternary ammonium radical which then spontaneously decomposes to give the alkyl radical and tertiary amine. The expelled alkyl radical undergoes further reactions, including eventual proton abstraction from the solvent, resulting in the formation of the amide ion. The latter is known[26] to attack quaternary ammonium cations possessing hydrogen

at the β carbon atom of an alkyl group, giving alkenes by a Hoffmann elimination reaction. The overall reactions occurring are summarised in Scheme B-9.

$$NR_4^+ + e^-_{(solv)} \longrightarrow [NR_4\cdot] \longrightarrow NR_3 + R\cdot$$

$$R\cdot + e^- \longrightarrow R^- \qquad R = \text{alkyl}$$

$$R^- + NH_3 \longrightarrow RH + NH_2^-$$

$$NH_2^- + NR_4^+ \longrightarrow NH_3 + NR_3 + \text{alkenes}$$

Scheme B-9 Direct Cleavage of Quaternary Ammonium Cations by Solvated Electrons.

Analysis of the reaction is, however, complicated by the slow solvolysis reaction of solvated electrons with ammonia, causing formation of amide ion which then attacks the quaternary ammonium cation as previously described. The rate of this reaction depends greatly on the presence of trace impurities, e.g. iron. The mechanism for the decomposition of tetraethylammonium cations is shown on Scheme B-10.

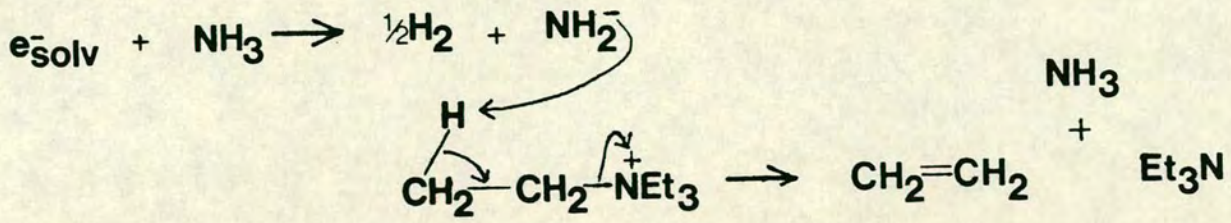

Scheme B-10 Decomposition of Tetraethylammonium Cation by Reaction with Amide Ion.

Hoffmann elimination is also the mechanism followed when tetraalkylammonium cations act as proton donors.

The results for the various tetraalkylammonium salts showed that the relative amounts of alkane and alkene formed were dependant upon the substrate. For the reaction of tetramethylammonium salts the results differed from the earlier work in that the major hydrocarbon detected was methane, with ethane being present only in small (ca. 1%) quantities. For tetraethylammonium cations almost equal amounts of ethane and ethene were detected, thus indicating that decomposition of the cation occurs exclusively by direct attack of solvated electrons on the cation. Similar elimination products were observed for other tetraalkylammonium salts, with the reaction rates decreasing in the order:

$$Pr^{n}_{4}N^{+} > Me_{4}N^{+} > Et_{4}N^{+}.$$

For quaternary ammonium cations containing a range of alkyl substituents, the alkyl group expelled appeared to be the one with the shortest chain length.

In a study by Grovenstein and Stevenson[27] on the cleavage of tetraalkylammonium halides by sodium in liquid ammonia similar cleavage products were obtained. The mechanism proposed for cleavage was essentially the same, although it was thought possible in some cases that cleavage occurred with simultaneous two-electron reduction of the cation, resulting in ejection of an alkyl carbanion rather than a radical. Amine formation from the cleavage reaction was thought to be of importance to the reaction rate. It was suggested that the rate of reaction depends upon the relief of steric strain in the cation. Thus, in general, bulkier cations tend to decompose faster. When different alkyl groups are present in the cation, the amine produced and alkyl group expelled depend upon the relative activation energies of the cleavage transition state rather than upon the relative steric crowding present in the amine product. The consequence of this is that shorter chain length alkyl groups tend to be preferentially expelled.

Mechanistic Conclusions

Previously (Scheme B-1) it had been suggested that the reductive alkylation of pentan-2-one takes place by formation of the ketone dianion, followed by nucleophilic attack of the dianion on the tetraethylammonium cation. The formation of dianions of aliphatic ketones in aprotic solvents is a rare process, and normally only occurs in the presence of small counter-ions, e.g. Li, when tight ion-pairs can be formed:

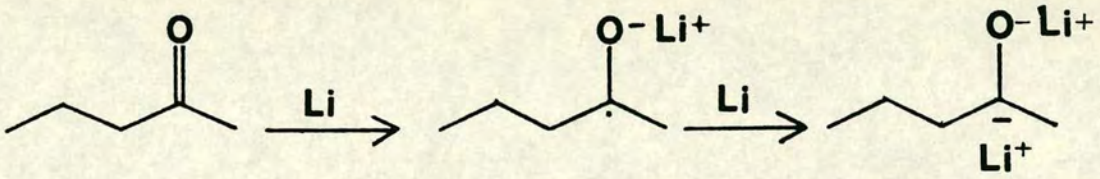

It is very unlikely that these conditions would prevail with the bulky cations used in the electrochemical experiments.

At the commencement of electrolysis, the mercury cathode becomes tarnished with tetraethylammonium amalgam but production of this ceases after thin layer coverage of the electrode is complete. Direct electron-transfer to the ketone then occurs on the cathode until just over 1 $Fmol^{-1}$ has passed. This could correspond to reduction of pentan-2-one to its radical-anion, a process known for aliphatic ketones in aprotic solvents. After this

stage a solution of solvated electrons appears. These electrons could react with tetraethylammonium cations to give triethylamine as detected and ethyl radicals. As these radicals are being formed in the presence of an excess of pentan-2-one radical-anions, a coupling reaction could occur according to the mechanism shown in Scheme B-11.

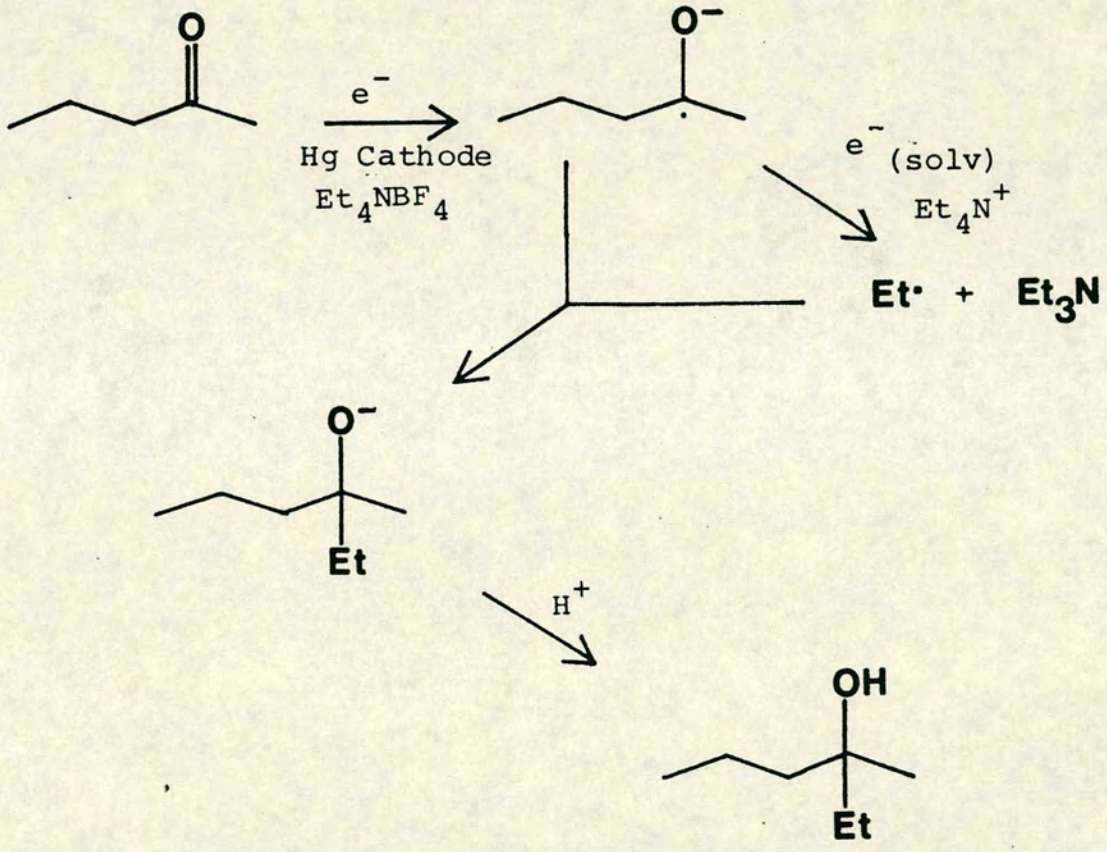

Scheme B-11 Proposed Mechanism for Reductive Alkylation of Pentan-2-one via Radical Coupling.

Formation of the secondary alcohol pentan-2-ol could occur by reaction of the radical-anion with protic impurities in the solution, and by proton abstraction from the tetraethylammonium cation by the Hoffmann elimination reaction shown in Scheme B-12.

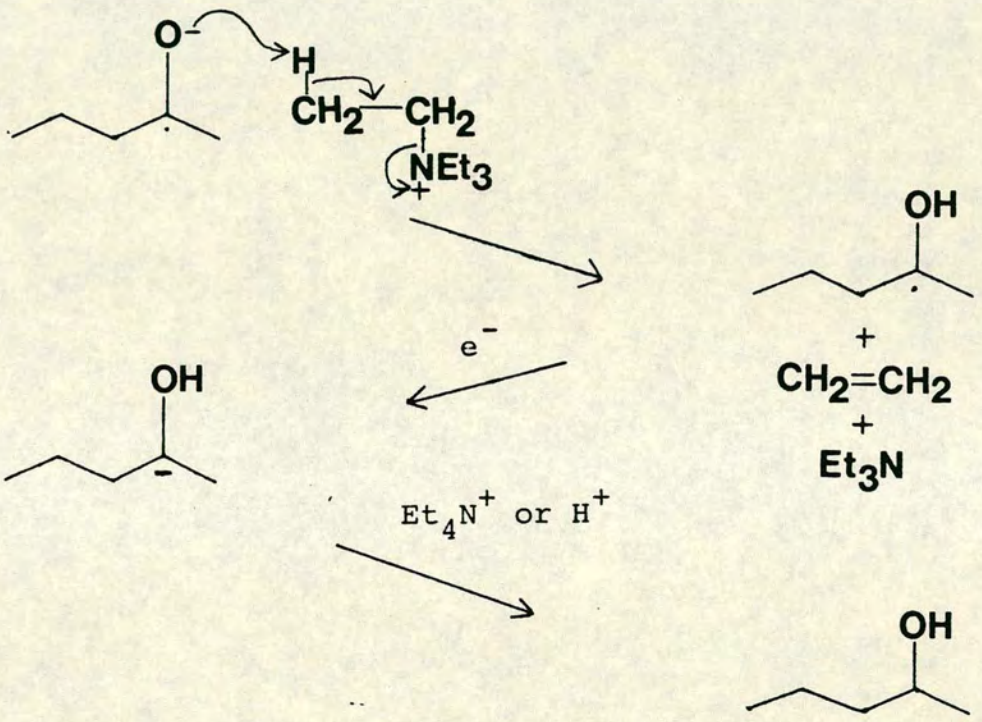

Scheme B-12 Mechanism for Formation of Pentan-2-ol by Proton Abstraction from Tetraethylammonium Cation.

Attempted alkylation of pentan-2-one using chemically generated solvated electrons in the presence of tetraethylammonium fluoroborate produced only pentan-2-ol.

This indicates that the conditions necessary for alkylation to occur must be unique to the electrochemical experiment. The conditions prevailing during chemical reduction are very inhomogeneous, with very large concentrations of solvated electrons being released into solution in a short time. This strongly suggests that one possible alkylation mechanism, resembling a Grignard reaction, and involving expulsion of an ethyl carbanion from the tetraethylammonium cation, followed by nucleophilic attack of this carbanion on pentan-2-one, suggested by Grovenstein and Stevenson[24], is not taking place.

B.2-3 Reduction of Pentan-2-one using Tributylethylammonium Iodide as Supporting Electrolyte

Galvanostatic reduction of pentan-2-one in a solution of tributylethylammonium iodide in liquid ammonia at a mercury cathode with stirring by nitrogen bubbles resulted in the formation of 3-methylhexan-3-ol (45%) and pentan-2-ol (55%). This is in agreement with the previously observed reductive ethylation of acetylcyclopropane in this medium. In addition to the products derived from the ketone, two previously unobserved compounds were detected. These were found to be tributylamine and dibutylethylamine.

Accurate quantitative analysis of these products proved difficult, but tributylamine was present in at least a 5-fold excess over dibutylethylamine. An excess of solvated electrons was present only after 1.1 $Fmol^{-1}$ had passed. Thus formation of these amines could have been by either direct cleavage of the cation by solvated electrons or attack on the protons attached to the β carbon atoms of the alkyl chains according to the previously described Hoffmann elimination mechanism.

Reduction of Pentan-2-one using Isotopically Labelled Tributyl-1,1-[$^2H_2$]-ethylammonium Iodide as Supporting Electrolyte

A further possible mechanism for the ethylation process is an indirect one, involving a nitrogen-ylide intermediate. Nitrogen-ylides are often invoked as intermediates when tetraalkylammonium cations are acting as alkylating agents,[28] and there is also a report[29] in which a nitrogen ylide was proposed as an intermediate in the electro-reduction of butylbromide in DMF/tetraethylammonium bromide in the presence of carbon dioxide, as shown in Scheme B-13.

The proposed mechanism by which pentan-2-one could be alkylated via a nitrogen-ylide intermediate is shown in Scheme B-14, where an epoxide is formed and cleaved electrochemically to give 3-methylhexan-3-ol. The

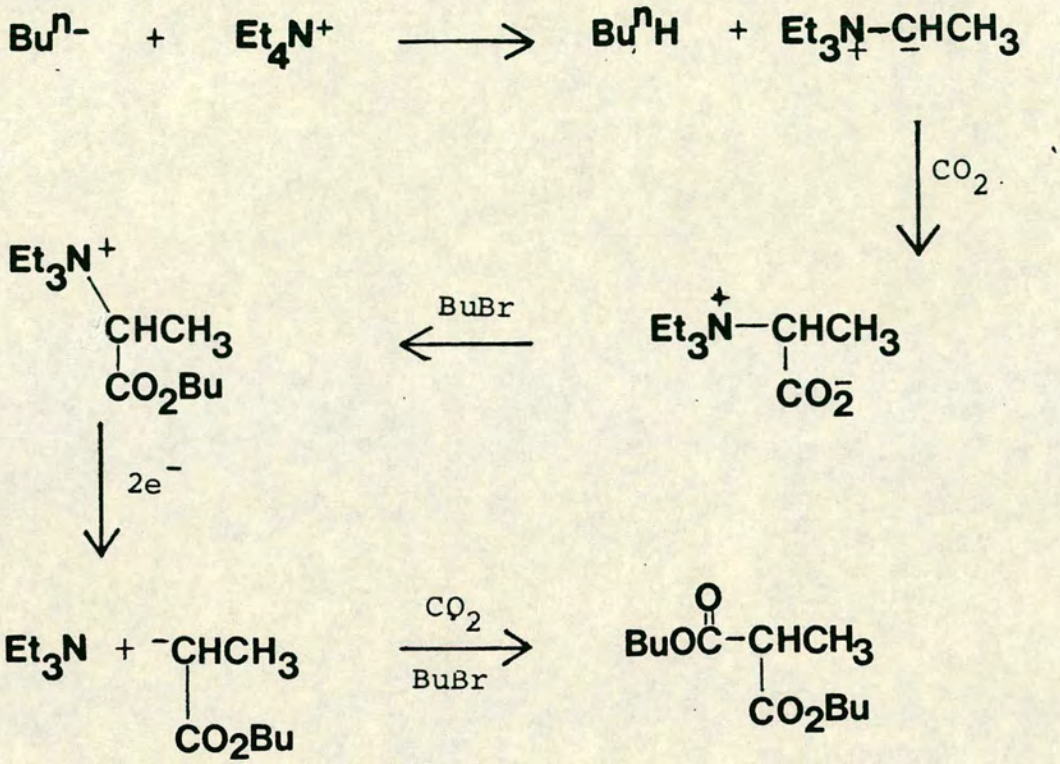

Scheme B-13 Intervention of a Nitrogen-Ylide in the Electroreduction of Butyl Bromide in the Presence of Carbon Dioxide.

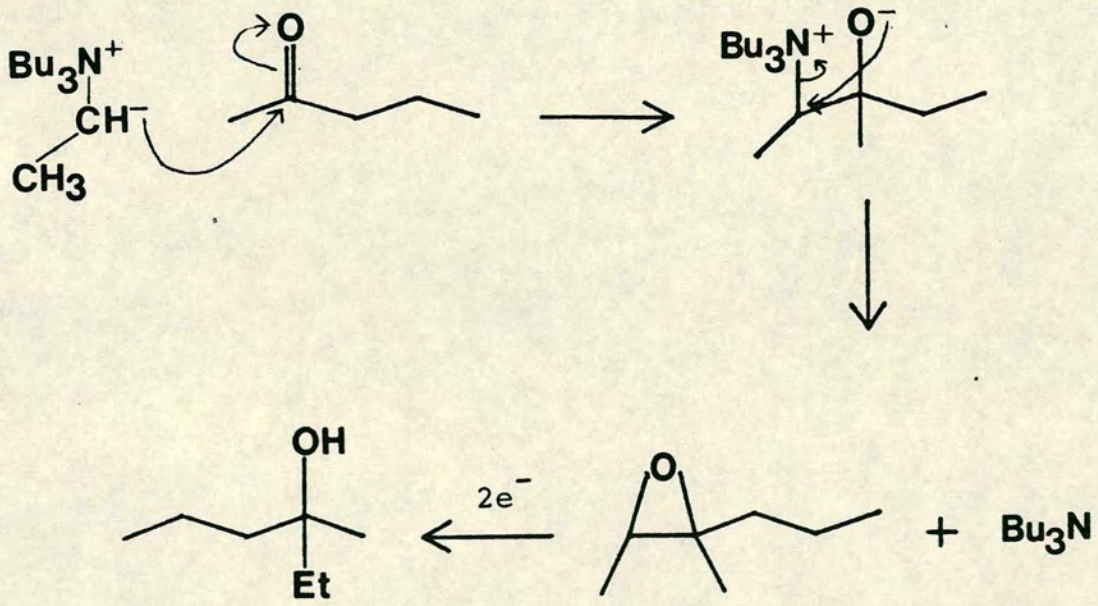

Scheme B-14 Mechanism for Indirect Alkylation of Pentan-2-one via an Ylide Intermediate.

regioselectivity of ring cleavage of epoxides ensures that tertiary alcohols are formed preferentially to secondary alcohols in these reactions.[30]

If the two α protons on the ethyl group of tributyl-ethylammonium iodide could be labelled with deuterium, it should be possible to ascertain whether or not this mechanism is operating. The operation of an ylide mechanism would lead to the incorporation of a maximum of one deuterium atom in the product tertiary alcohol. The route followed for the preparation of the isotopically labelled electrolyte is shown on Scheme B-15.

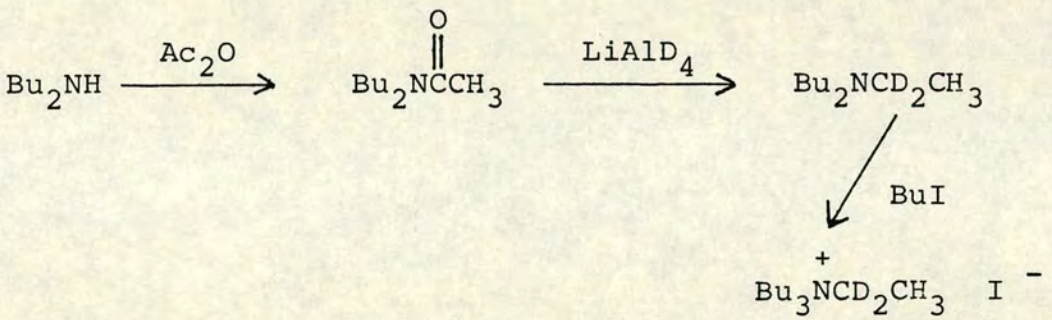

Scheme B-15 Synthesis of Isotopically Labelled Tributyl-1,1-[$^2H_2$]-ethylammonium Iodide.

Reduction of pentan-2-one in the presence of this electrolyte, and examination of the GLC/MS of the 3-methylhexan-3-ol product, showed that both deuterium atoms had been incorporated into the product. Hence the possibility of ethylation occurring via an ylide intermediate can be dismissed.

Mechanistic Conclusions

These experiments have shown that the mechanism of reductive ethylation does not involve an ylide intermediate. The amines formed, and the relative amounts of these present, show that although the ethyl group is preferentially lost from the quaternary ammonium cation, some butyl groups are also expelled. As no butylated tertiary alcohol is observed, this means either that loss of the butyl group only occurs when the quaternary ammonium cation is acting as a proton donor in the Hoffmann elimination mechanism, or that, if the previously proposed radical coupling mechanism is operating, the butyl radical is unreactive towards the ketone radical-anion.

B.2-4 Electrochemical Reduction of Pentan-2-one using Heterocyclic Equivalents of Tetraethylammonium Salts as Supporting Electrolyte.

Heterocyclic analogues of the tetraethylammonium cation were used as supporting electrolyte cations to see if they would transfer ethyl groups analogously during the reduction of pentan-2-one. N-ethylquinuclidinium (18) and N,N-diethylpiperidinium (19) iodides were prepared and used as electrolytes.

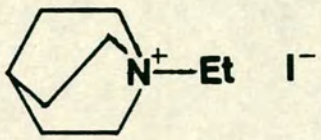

(18)

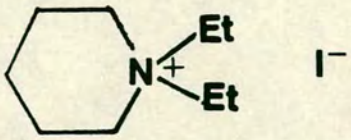

(19)

With (18), only pentan-2-ol was found along with some quinuclidine. Solvated electrons were observed in solution during the later stages of the electrolysis.

With (19), the main product was pentan-2-ol (93%), but 3-methylhexan-3-ol (7%) and N-ethylpiperidine were also present in the product mixture. A solution of solvated electrons was observed after 1.6 $Fmol^{-1}$ had passed.

Mechanistic Conclusions

In the case of N,N-diethylpiperidinium iodide, the yield of tertiary alcohol was significantly lower than that observed with the tetraethylammonium and tributyl-ethylammonium salts.

With N-ethylquinuclidinium iodide, no ethylation was observed even though solvated electrons were present during reduction and quinuclidine was observed in the products. This suggests that the only source of quinuclidine

was by the electrolyte acting as a proton donor, eliminating ethene, rather than via expulsion of an ethyl radical.

An explanation for the behaviour of these salts may lie in the proposal[27] that the rate of cleavage of quaternary ammonium salts is governed by the relief of steric strain on expulsion of an alkyl group. Compared with the conditions required for ethylation of tributylamine (Iodoethane/THF; reflux 48 h.), N-ethylpiperidine and quinuclidine form their ethylammonium salts very readily. Quinuclidine in fact reacts almost instantly at room temperature with ethyl iodide, while N-ethylpiperidine requires 24 h. at room temperature to react. Triethylamine will react slightly more readily than tributylamine due to the reduced steric crowding around the amine nitrogen caused by the shorter ethyl groups.

These experiments have thus shown that there appears to be a correlation between the ease of expulsion of the ethyl group from the quaternary ammonium cation and the relative amount of tertiary alcohol formed upon reduction of pentan-2-one. This evidence strongly supports the previously postulated mechanism (Scheme B-11) of alkylation in which the pentan-2-one radical-anion couples with an ethyl radical in solution. The presence of some quinuclidine in the product mixture when (18) is used as supporting electrolyte, very likely arises

through the supporting electrolyte acting as a proton donor by the Hoffmann elimination mechanism, since no tertiary alcohol is formed.

B.2-5 Reduction of Ketones other than Pentan-2-one in Liquid Ammonia/Tetraethylammonium Fluoroborate.

It was considered that valuable mechanistic information might be obtained by reducing 4-t-butylcyclohexanone (20). It was anticipated that the isomeric distribution of the ethylated tertiary alcohols, could be meaningfully compared with the ratios formed when (20) was reductively ethylated in a normal Grignard reduction.[31]

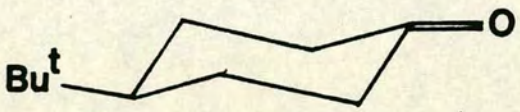

(20)

Unfortunately, (20) was insoluble in liquid ammonia and had to be introduced using THF as a co-solvent. Only the secondary alcohol, 4-t-butylcyclohexanol, was observed as a reduction product. In order to determine if the co-solvent has any influence upon the result, pentan-2-one was reduced in the same medium. This resulted in the tertiary alcohol being formed in a comparable yield to that obtained when THF was absent.

Since it was conceivable that cyclic ketones in general may not participate in the reductive alkylation reaction, cyclohexanone, which was partially miscible with ammonia, was reduced in a similar THF/ammonia system. This resulted in the formation of 1-ethylcyclohexanol (10%), a lower yield of tertiary alcohol than that obtained from pentan-2-one.

Mechanistic Conclusions

From the results obtained there appears to be a correlation between the yield of ethylated tertiary alcohol and the solubility of the various ketones in liquid ammonia. This suggests that the nature of the primary solvation shell of the ketone during reduction is important. For 4-t-butylcyclohexanone this will consist principally of THF molecules, and for pentan-2-one mainly ammonia molecules, while for cyclohexanone an intermediate situation will exist. Thus, it appears that an ammonia-rich solvation shell may be required to support the intermediates involved in the reductive alkylation.

B.2-6 Summary of Conclusions

The series of experiments carried out has illustrated the sensitivity of the electrochemically induced reductive ethylation of aliphatic ketones to changes in the nature of the electrode, solvent and electrolyte. The accuracy

of the yield determination in these instances has an absolute error of ca. ±3% in each measurement, as determined by the reproducibility of results.

It is apparent that in a system containing a mercury cathode, quaternary ammonium salt and pentan-2-one, the easiest cathodic process (least negative $E_{\frac{1}{2}}$) is amalgamation of a quaternary ammonium radical with mercury. When the cell conditions are appropriate for this reaction to occur, i.e. a continually renewed mercury cathode, reduction of the ketone occurs indirectly, via amalgam decomposition with no ethylation, as shown in Scheme B-8.

When amalgam formation is restricted, i.e. when the surface of the mercury pool cathode is left undisturbed, the lack of immediate formation of a solution of solvated electrons suggests that in this case an electron-transfer process is occurring on the electrode surface (now an amalgam electrode). As this continues for just over one electron equivalent for the pentan-2-one present, the most likely process occurring is direct formation of the pentan-2-one radical-anion. During the transfer of the second electron equivalent, a blue solution of solvated electrons appears. These can then react with the quaternary ammonium cation to form a tertiary amine and an alkyl radical. When the alkyl group expelled is Et· a radical-radical coupling occurs with the ketone radical-anion,

the latter being present in large excess following its prior generation. This efficient coupling reaction forms the tertiary alcohol. This complex set of conditions simply does not prevail during chemical reduction.

A mechanism also exists whereby the quaternary ammonium cation, by Hoffmann elimination of an alkene, can act as a proton donor to the radical-anion, forming the secondary alcohol. Formation of the secondary alcohol can also occur via reaction of the radical-anion with any protic impurities in solution.

The overall picture for the reduction of pentan-2-one in the presence of tetraethylammonium fluoroborate is shown in Scheme B-16.

The relative amounts of ethylation vary according to the particular quaternary ammonium cation. The behaviour of these cations in this respect appears to be linked to the relief of steric strain in the cation when the ethyl group is cleaved. For tributylethylammonium cations a high yield of tertiary alcohol is obtained since there is a considerable decrease in steric crowding on expulsion of the ethyl group, while for N-ethylquinuclidinium cations, no tertiary alcohol is obtained since very little or no steric strain will be relieved by expulsion of an ethyl group. The case of the N,N-diethylpiperidinium cation is intermediate between these two extremes.

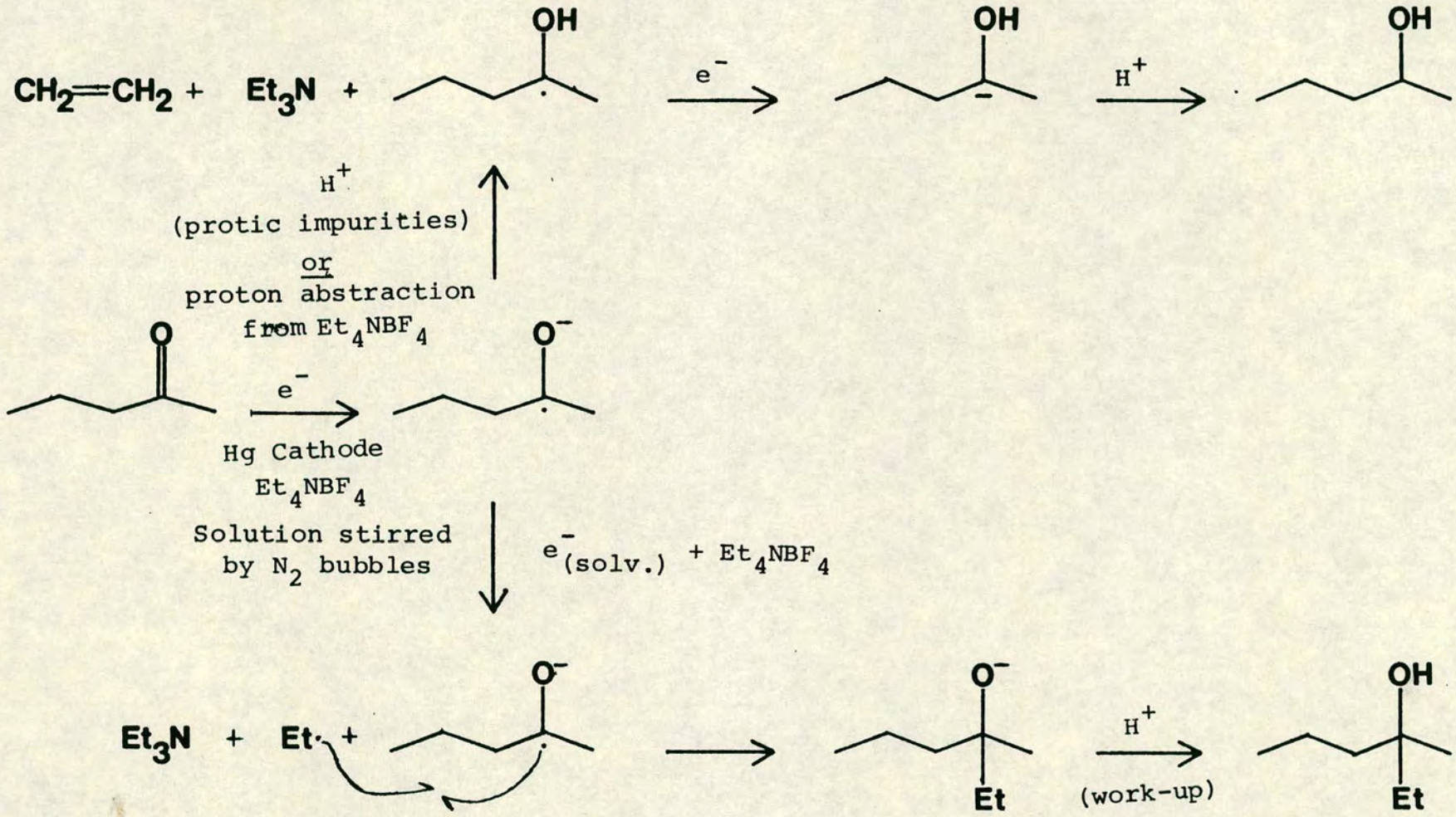

Scheme B.16: Summary of processes occurring on Electro-reduction of Pentan-2-one in Liquid Ammonia/Tetraethylammonium Fluoroborate

An anomaly exists in the behaviour of the tripropylethylammonium cation. Previous studies showed that this cation does not participate in the formation of tertiary alcohols.

Attempts to explore the reaction mechanism further, showed that reductive ethylation of the alternative substrate 4-t-butylcyclohexanone failed, due presumably to the insolubility of the compound in liquid ammonia and the consequent use of a co-solvent. This, however, implies the importance of the structure of the solvation shell in the alkylation process. It is possible that the alkylation of this substrate could ultimately be achieved by using a co-solvent that has the ability to stabilise the radical intermediates proposed here, which suggests a further line of enquiry.

B.3 Experimental

B.3-1 Practical Aspects of Performing Electrochemistry in Liquid Ammonia

(a) Solvent Collection and Purification (see Fig. B-2)

Liquid ammonia (200 ml) was added directly from the inverted cylinder into V_1, which contained a small, clean, freshly cut piece of sodium (1 cm^3). V_1 was then connected to the vacuum line via its B34 joint, T_2 was closed and the liquid ammonia was frozen by immersing V_1 in liquid nitrogen. When freezing was complete, taps T_1, T_2, T_3, a_1 and a_2 were opened, the line was evacuated and then filled with dry nitrogen gas. The line was evacuated and flushed with nitrogen 2 more times, then T_1 was closed and the liquid nitrogen removed from around V_1. The frozen ammonia in V_1 then proceeded to melt and boil. After 10 min., V_2 was immersed in liquid nitrogen and ammonia was distilled from V_1 to V_2. Distillation of 100 ml liquid ammonia took ca. 2 h., after which time T_2 was closed and the frozen, distilled ammonia was stored under dry nitrogen gas until required.

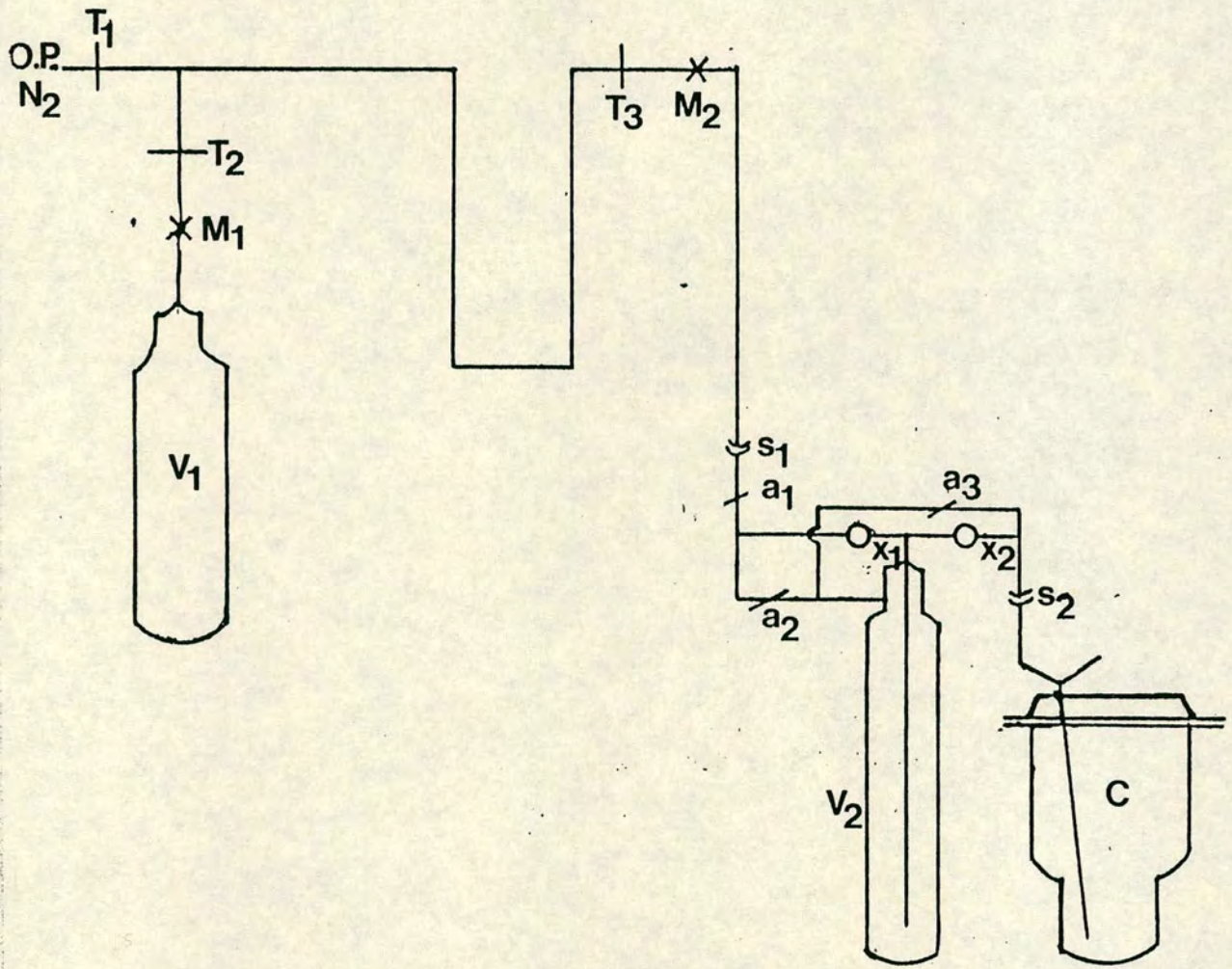

Key

a = Rotaflo tap

V = Liquid ammonia reservoir

T = High vacuum greased taps

M = Manometer

S = S_{13} ball and socket joint

X = Young's glass barrel taps ORT_4

C = Electrochemical cell

O.P. = Oil pump

N_2 = Source of dried nitrogen gas

Figure B.2: Vacuum Line for the Purification of Liquid Ammonia and its transfer to the Electrochemical Cell

(b) Cell Assembly (see Fig. B-3)

The electrochemical cell C was constructed from a flange flask (FG75) with the width of the bottom of the cell reduced. The cell was graduated at 25, 50 and 100 ml. The cell top (Fig. B-4) consisted of one SQ13 and four SQ18 screw thread joints. These accommodated the various cell components which were employed as follows:

(i) Inlet Tube (Fig. B-3)

This consisted of a narrow glass tube (o/d 5 mm) which divided at its top into two branches. One of these branches terminated in the socket joint S_2 and was used for connecting the cell to the vacuum line via V_2. The other branch terminated in a SQ13 screw thread joint which was normally covered with a suba-seal. This could be used as a port for injecting substrate into the electrochemical cell.

(ii) Outlet Tube

This was connected to a mercury bubbler allowing outflow of gas from the cell during operation.

(iii) Working Electrode Connection

The working electrode used in these studies was a mercury pool. Electrical connection to this was made via a thin platinum wire sealed in a soda glass tube (o/d = 10 mm).

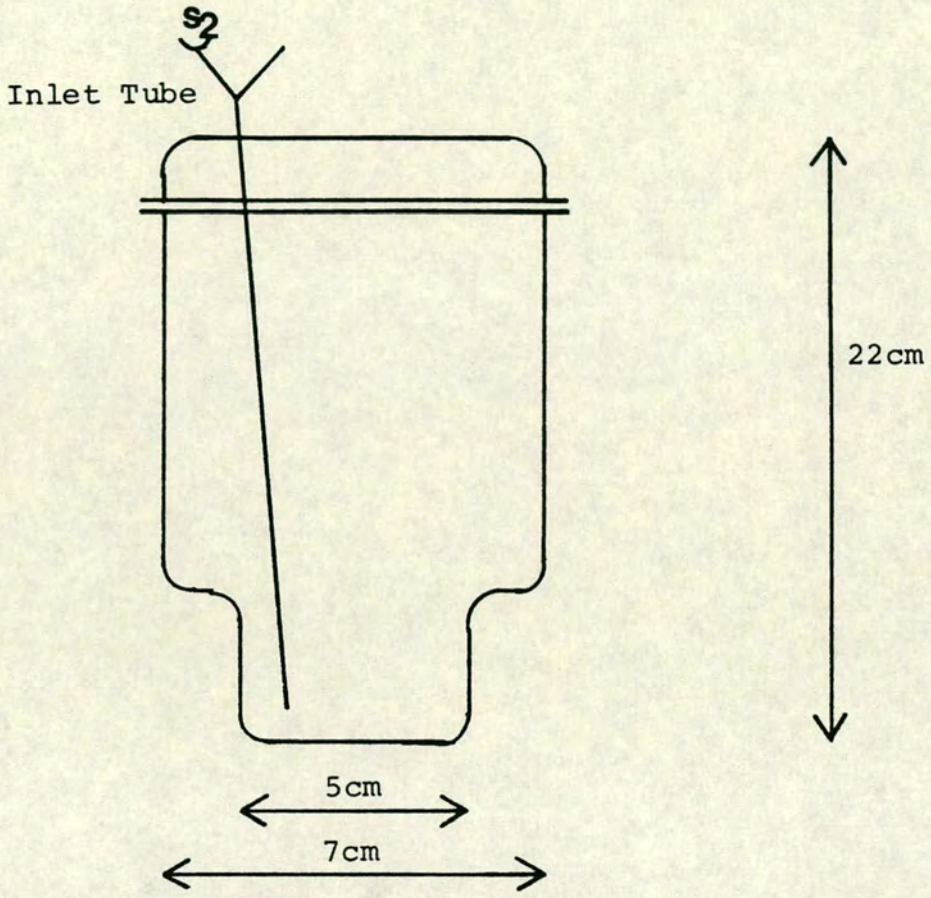

Figure B.3: Electrochemical cell for performing electrochemistry in liquid ammonia

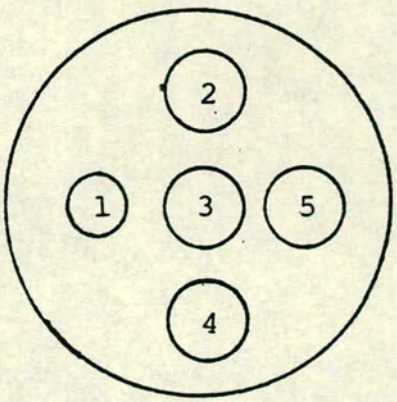

1 = SQ13 screw thread joint

2-5 = SQ18 screw thread joints

Figure B.4: Electrochemical Cell Top

(iv) Secondary Electrode Compartment (Fig. B-5)

This consisted of a widened glass cylinder (20 mm o/d) which terminated in a glass frit (porosity 4). The electrode itself consisted of a graphite rod (5 mm diameter) which was sealed with wax into a glass tube. Electrical connection was made through a thin copper wire sealed alongside the graphite rod.

(v) This SQ18 screw thread joint was normally covered by a suba-seal and used as a sample injection point but could also hold a reference electrode compartment in place, if required.

(c) Thermostatting of the Cell

During cell operation, the cell and liquid ammonia reservoir were immersed in an ethylene glycol/water (60/40, v:v) bath which was maintained at -36°C. The bath was contained in a large transparent Dewar vessel. A refrigeration unit (MGW Lauda, Type DLK 50) was attached to a peristaltic pump (Glen Creston, Type L25) which circulated cooled methanol from the refrigeration unit through a metal heat exchange coil in the base of the Dewar vessel. The bath was stirred mechanically and temperature control was maintained via an electronic temperature sensor. Heat gain from the atmosphere was minimised by covering the surface of the bath with small polypropylene spheres.

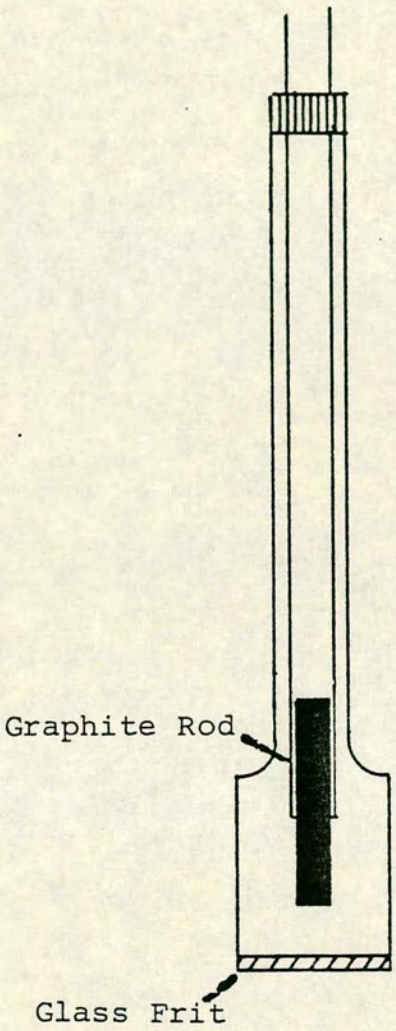

Figure B.5: Secondary Electrode Compartment

(d) Cell Operation

V_2, containing frozen distilled ammonia, was immersed in the cooled thermostat bath with taps T_1, T_3, a_1 and a_2 open. The cell, with the electrodes in position and containing dried supporting electrolyte, was lowered into the bath and connected to V_2 via the ball and socket joint S_2. When all the ammonia had melted, a_2 and X_2 were closed and X_1 and a_3 were opened and dry nitrogen gas was passed through the reservoir and cell for 10 min. Taps X_1 and a_3 were then closed and X_2 and a_2 opened carefully. Liquid ammonia was transferred from V_2 to the cell using gentle nitrogen pressure until the required cell volume of ammonia was achieved. Taps a_2 and X_2 were then closed, a_3 and X_1 were opened, and nitrogen was passed through the reservoir (still containing ammonia; thus the nitrogen was saturated with ammonia before entering the cell) and cell for 5 min. at which time cell operation commenced.

Addition of substrate was achieved by injecting neat substrate, or substrate dissolved in a co-solvent through the suba-seal contained in the cell head.

(e) Cell Stirring

Cell stirring could be achieved in two ways.

(i) By a stream of dry, ammonia saturated nitrogen bubbles. This method efficiently stirs the cell solution

whilst leaving the surface of the mercury pool working electrode undisturbed.

(ii) By using a magnetic stirring bar in the cell driven from below by a magnet connected to an air turbine. This method efficiently stirs the cell solution and also constantly renews the surface of the mercury pool working electrode.

B.3-2 Preparation of Supporting Electrolytes

(a) Tetraethylammonium Fluoroborate

Tetraethylammonium hydroxide (20% solution, 17.6 ml, 0.1 mol) was neutralised with fluoroboric acid (40% solution, ∿16.5 ml) and the solution was filtered. The filtrate was concentrated by rotary evaporation and the resulting solid was recrystallised twice from methanol to give the fluoroborate salt (17.9 g, 88% yield), m.p. >300°C.

(b) Tributylethylammonium Iodide

Tributylamine (18.5 g, 0.1 mol) was dissolved in THF (100 ml) and ethyl iodide (20 g, excess) was added to the solution, which was then refluxed for 48 h. Ether (50 ml) was added to the cooled solution, the resulting precipitate was filtered off and recrystallized from ethanol/ethyl acetate to give the quaternary ammonium iodide (28.4 g, 83%), m.p. 200-201°C lit.[32] 202-203°C.

(c) N-ethylquinuclidinium Iodide

Quinuclidine (11.11 g, 0.1 mol) was dissolved in THF (200 ml) and ethyl iodide (20 g, excess) was added to the solution, which was then allowed to stand at room temperature for 15 min. The resultant precipitate was filtered off and was recrystallised twice from ethanol/ethyl acetate to give the quaternary ammonium iodide (21.9 g, 82%), m.p. 281-283°C, lit.[33] 270-271°C.

(d) N,N-diethylpiperidinium Iodide

N-ethylpiperidine (11.3 g, 0.1 mol) was dissolved in THF (100 ml) and ethyl iodide (20 g, excess) added to the solution, which was then allowed to stand at room temperature for 24 h. The resulting precipitate was filtered off and was recrystallised twice from ethanol/ethyl acetate to give the quaternary ammonium iodide (16.9 g, 70%), m.p. 241-244°C, lit.[34] 242-243°C.

(e) Preparation of Tributyl-1,2-[$^2H_2$]ethylammonium Iodide

(i) N,N-dibutylacetamide: Di-n-butylamine (25.8 g, 0.2 mol) was added to a mixture of glacial acetic acid (12 g, 0.2 mol) and acetic anhydride (30.6 g, 0.3 mol) at such a rate that the temperature was held between 15 and 17°C. On completion of the addition the temperature was raised to 55°C for a further 30 min. Water (96 ml) was

then added and the mixture was stirred for a further 1 h to ensure that all of the acetic anhydride was hydrolysed. The organic layer was taken up in ether (75 ml) and the aqueous layer was extracted with ether (4 x 75 ml). The combined ethereal extracts were dried ($MgSO_4$) and the solution concentrated by evaporation. The product was purified by distillation, b.p. 118-120°C, 8 mm Hg (29.07 g, 85%).

$\delta_{^1H}$ ($CDCl_3$) 80 MHz: 0.6-0.95 (6H - 2 overlapping triplets), 1-1.7 (8H, m), 1.9 (3H, s), δ2.95-3.25 (4H - 2 overlapping triplets).

$\delta_{^{13}C}$ ($CDCl_3$) 50.6 MHz exhibited a quaternary carbon peak at 169.2 p.p.m.

ν_{max} (film) exhibited C=O acetamide stretch at 1640 cm^{-1}.

(ii) N,N-dibutyl-1,1-[$^2H_2$]-ethylamine: A solution of N,N-dibutylacetamide (3.42 g, 0.02 mol) in dry ether (20 ml) was added over a period of 1 h. to a suspension of lithium aluminium deuteride (%D = 99%+, 1.68 g, 0.04 mol) in ether. On completion of the addition the mixture was refluxed for 3 h. Ethanol was then added slowly to destroy the excess of deuteride. Sufficient 10M sodium hydroxide solution was added to convert all aluminium residues to aluminium hydroxide. The upper organic layer was separated and the aqueous layer was extracted with ether. The combined ethereal extracts were washed with

water, dried ($MgSO_4$) and concentrated. The product was purified by distillation, b.p. 88-90°C, 54 mm Hg (2.27 g, 71%).

$\delta_{^{13}C}$ ($CDCl_3$) 50.6 MHz exhibited five large peaks and one small multiplet at 46.7 p.p.m. associated with the deuterated carbon atom.

ν_{max} (film) exhibited no carbonyl absorption but peaks at 2250-2050 cm^{-1} (C-D stretch).

Analysis of the M:M+1 and M:M-1 peak ratios for the deuterated and corresponding undeuterated compounds showed that the deuterium uptake in the required position was ca. 100%.

(iii) Tributyl-1,1-[$^2H_2$]-ethylammonium iodide: Dibutyl-1,1-[$^2H_2$]-ethylamine (2.20 g, 0.014 mol) was dissolved in THF (20 ml) and n-butyl iodide (3.30 g, excess) was added to the solution which was then refluxed for 48 h. Ether (10 ml) was then added to the cooled solution, and the resulting precipitate was filtered off and recrystallised from ethanol/ethyl acetate to give the deuterated quaternary ammonium iodide (3.52 g, 76%).

Analysis of the product mass spectrum (FAB mass spectrum of cation) and comparison of the M:M+1 and M:M-1 ratios with those for the undeuterated compound showed that deuterium uptake in the required position was ca. 100%.

B.3-3 Electrochemical Reductions in Liquid Ammonia

(a) General Procedure

The cell was assembled as previously described. The working electrode was a mercury pool of volume 2 cm^3; this corresponded to a surface area of *ca.* 5 cm^2. Supporting electrolyte was also present in the cell at this stage, this having previously been vacuum dried at 100°C for 48 h. On completion of the electrolysis the secondary electrode compartment was removed from the cell and the contents of the working electrode compartment were quenched with solid ammonium chloride. Ether (50 ml) was then added to the cell and the liquid ammonia was allowed to evaporate. The resulting ether solution was washed with water, dried ($MgSO_4$) and concentrated to 2 ml by distillation at 50°C through a Vigreux column. When the supporting electrolyte anion was iodide, it was necessary to add a saturated aqueous solution of sodium sulphite to the secondary electrode compartment in order to destroy the explosive nitrogen tri-iodide that formed on the electrode.

Product identification was established by GLC using mixed injections with authentic samples to verify identifications, by GLC/MS, and by preparative GLC followed by examination by n.m.r. spectroscopy. In some cases the ether extract was further treated with 8N chromic acid and/or 8N sulphuric acid to yield further structural information.

Quantitative analysis of reaction mixtures was made by comparing GLC peak integrations, sensitivity corrections being made using mesitylene as an internal standard.

(b) Electrochemical Reduction of Pentan-2-one using Tetraethylammonium Fluoroborate as Supporting Electrolyte

A 0.1M solution of tetraethylammonium fluoroborate in liquid ammonia (50 ml) was prepared. Pentan-2-one (0.086 g, 0.001 mol) was added to the solution and a current of 100 mA was passed until 2 $Fmol^{-1}$ had passed. The mixture was then worked up and examined by GLC (5% carbowax, 70°C).

(i) Stirring by Nitrogen Bubbles: Pentan-2-one was subjected to 2 $Fmol^{-1}$ reduction. On commencement of the electrolysis the surface of the mercury pool became tarnished and covered by a layer of black powder. After 1.2 $Fmol^{-1}$ had passed the solution turned blue, indicating that a solution of solvated electrons was present. Product analysis showed that the reaction mixture consisted of pentan-2-ol (66%) and 3-methylhexan-3-ol (34%).

(ii) Magnetic Stirring: (i) was repeated but in this case the cell was stirred by means of a Teflon coated magnetic stirring bar. During electrolysis large amounts of a black solid were generated on the electrode surface

and at no time did the cell solution turn blue. The black solid decomposed on addition of ammonium chloride. Product analysis showed that the reaction mixture consisted of pentan-2-one (20%) and pentan-2-ol (80%).

(iii) Reduction of Pentan-2-one with Electrochemically Generated Tetraethylammonium Amalgam: (ii) was repeated except that pentan-2-one was not added until the end of the electrolysis. The mixture was then stirred for a further 30 min. when the reaction mixture was worked up. Product analysis showed that the reaction mixture consisted of pentan-2-one (84%) and pentan-2-ol (16%).

(iv) Chemical Reduction of Pentan-2-one: The reaction conditions for (i) were set up but the secondary electrode and compartment were omitted. Small, freshly cut pieces of sodium (0.23 g, 0.01 mol) were added to the solution which was then stirred by a stream of nitrogen bubbles for 30 min. A blue solution of solvated electrons was observed throughout the reaction. After work-up in the normal manner, product analysis showed that pentan-2-one (23%) and pentan-2-ol (77%) were present, together with a third more volatile product which was later identified as triethylamine.

(c) Electrochemical Reduction of Pentan-2-one Using Tributylethylammonium Iodide as Supporting Electrolyte

A 0.1M solution of tributylethylammonium iodide in liquid ammonia (50 ml) was prepared. Pentan-2-one was then added to the solution and a current of 100 mA was passed until 2 $Fmol^{-1}$ had been consumed. Stirring during the electrolysis was by means of a stream of nitrogen bubbles. After work-up the products were examined by GLC and GLC/MS (5% carbowax, 70°C), and by preparative GLC (5% carbowax, 80°C).

(i) Pentan-2-one (0.086 g, 0.001 mol) was subjected to two-electron reduction in this medium. The electrode surface became tarnished with black powder during the electrolysis and the solution turned blue due to the presence of solvated electrons after 1.1 $Fmol^{-1}$ had passed. GLC analysis of the isolated product mixture showed that the known products present were pentan-2-one (2%), pentan-2-ol (45%) and 3-methylhexan-3-ol (53%). In addition to these, two other products were observed, one of similar volatility to pentan-2-ol and the other less volatile than 3-methylhexan-3-ol. Treatment of the ethereal extract with 8N chromic acid resulted in the disappearance of these peaks; GLC analysis now indicated that pentan-2-one (45%) and 3-methylhexan-3-ol (55%)

only were present. Treatment of another portion of the ethereal extract with 8N sulphuric acid left only pentan-2-one (2%), pentan-2-ol (43%) and 3-methylhexan-3-ol (55%).

(ii) (i) was repeated using a larger quantity of pentan-2-one (0.344 g, 0.004 mol). Product analysis showed that the same products as obtained in (i) were present in similar ratios. Examination of the unknown products by GLC/MS showed that the more volatile unidentified product had M/E at 114 (48%), 72 (100%), 58 (22%), 44 (11%) and 42 (11%), while the less volatile unidentified product had major peaks at M/E 142 (68%), 100 (100%), 58 (38%), 44 (44%) and 41 (24%).

Preparative GLC of the ethereal extract and examination of the unknown compounds by n.m.r. spectroscopy showed:

More volatile product

$\delta^{1}H$ ($CDCl_3$) 80 MHz: broad spectrum with two areas δ0.8-1.5 and δ2.3-2.6 in the ratio 3:1.

$\delta^{13}C$ ($CDCl_3$) 50 MHz: 53.4 (CH_2), 47.5 (CH_2), 29.2 (CH_2), 20.7 (CH_2), 11.7 (2 x CH_3).

Less volatile product

$\delta^{1}H$ ($CDCl_3$) 80 MHz: showed three areas δ0.75-1, δ1.1-1.6 and δ2.2-2.5 in the ratio 3:4:2.

$\delta^{13}C$ ($CDCl_3$) 50.6 MHz: 54.0 (CH_2), 29.3 (CH_2), 20.7 (CH_2), 13.9 (CH_3).

Assignments of CH_2 and CH_3 carbon atoms in the ^{13}C n.m.r. spectra were made by running an EPT (PØ = $3\pi/4$) spectrum.

Identification of the unknown compounds as dibutylethylamine and tributylamine respectively was made by comparison of the observed GLC, GLC/MS and n.m.r. behaviour of these compounds with that of authentic samples.

(iii) Reduction of Pentan-2-one using Tributyl-1,1-[$^2H_2$]-ethylammonium iodide as supporting electrolyte: (i) was repeated using the deuterium labelled supporting electrolyte. Product analysis showed the same products present in the same ratios as for (i). Examination of the 3-methylhexan-3-ol fraction by GLC/MS showed major peaks at M/E 103 (11%), 87 (38%) and 75 (100%). Comparison with the GLC/MS of undeuterated 3-methylhexan-3-ol indicated that both deuterium atoms from the supporting electrolyte are incorporated in the tertiary alcohol.

(d) Electrochemical Reduction of Pentan-2-one using Other Supporting Electrolytes

A 0.1M solution of the electrolyte in liquid ammonia (50 ml) was prepared. Pentan-2-one (0.086 g, 0.001 mol) was then added and a current of 100 mA was passed until

2 $Fmol^{-1}$ had been consumed. A stream of nitrogen bubbles was used to stir the solution during electrolysis. The products were worked-up in the normal manner and examined by GLC and GLC/MS (5% carbowax, 70°C).

(i) N,N-diethylpiperidinium iodide: 2 $Fmol^{-1}$ reduction of pentan-2-one in this electrolyte system gave pentan-2-ol (94%), 3-methylhexan-3-ol (6%) and a third, previously unobserved, compound as products. The unknown compound was identified as N-ethylpiperidine by comparison of its GLC and GLC/MS (major peaks at M/E 113 (15%), 112 (16%), 98 (100%), 57 (16%) and 42 (45%)) behaviour with that of an authentic sample. The working electrode surface became tarnished with a black powder during electrolysis and a solution of solvated electrons appeared after 1.6 $Fmol^{-1}$ had passed.

(ii) N-ethylquinuclidinium iodide: 2 $Fmol^{-1}$ reduction of pentan-2-one in this electrolyte system gave pentan-2-ol and a small amount of quinuclidine as the only products. The electrode surface became tarnished with a black powder and a blue solution of solvated electrons appeared after 1.6 $Fmol^{-1}$ had passed.

(e) Electrochemical Reduction of Ketones other than Pentan-2-one in Liquid Ammonia/Tetraethylammonium Fluoroborate

In this series of reductions the ketone to be reduced (0.001 mol) was dissolved in dry ether (5 ml) before addition to the electrochemical cell containing 0.1M tetraethylammonium fluoroborate in liquid ammonia (50 ml). 2 $Fmol^{-1}$ reduction of the substrate was then performed with the solution being stirred by a stream of nitrogen bubbles. The products were worked-up in the normal manner and examined by GLC, and GLC/MS when appropriate.

(i) 4-t-butylcyclohexanone: 2 $Fmol^{-1}$ reduction of 4-t-butylcyclohexanone (0.154 g, 0.001 mol) in this solvent system was performed. The electrode surface became tarnished with black powder during electrolysis but no solution of solvated electrons was observed at any stage. The products were worked up and examined by GLC (5% carbowax, 130°C). The only product observed was 4-t-butylcyclohexanol.

(ii) Cyclohexanone: 2 $Fmol^{-1}$ reduction of cyclohexanone (0.098 g) in this solvent system was performed. The electrode surface became tarnished with black powder during electrolysis and a blue solution of solvated electrons appeared after 1.6 $Fmol^{-1}$ had passed. The products were worked-up and analysed by GLC (5% carbowax, 80°C). Products present were cyclohexanol (90%) and

1-ethylcyclohexanol (10%). Identification of the tertiary alcohol was made from its GLC/MS behaviour (major peaks at M/E, 99 (100%), 85 (81%), 81 (89%), 72 (33%) and 43 (61%)) and by comparison of its GLC behaviour with that of an authentic sample.

(iii) Pentan-2-one: 2 $Fmol^{-1}$ reduction of pentan-2-one (0.086 g) in this solvent system was performed. The electrode surface became tarnished with black powder during electrolysis and a blue solution of solvated electrons appeared after 1.2 $Fmol^{-1}$ had passed. The solution was worked-up and examined by GLC (5% carbowax, 70°C). Products present were pentan-2-ol (61%) and 3-methylhexan-3-ol (39%).

B.3-4 Related Chemical Syntheses

When authentic samples of compounds were not readily available for GLC comparison these compounds had to be synthesised:

(a) 4-Methyloctan-4-ol: Butyl bromide (2.5 g, 0.02 mol) in dry ether (10 ml) was added dropwise to dry magnesium turnings (0.45 g) covered with dry ether (5 ml). The mixture was stirred for one hour before pentan-2-one (1.58 g, 0.018 mol) in dry ether (15 ml) was added dropwise. Once the addition was complete, the mixture was heated under reflux for a further 1 h. The mixture was then

poured onto crushed ice (50 g) and neutralised with 0.1M hydrochloric acid. The ethereal layer was separated and the aqueous layer was extracted with ether (2 x 50 ml). The combined ethereal extracts were dried ($MgSO_4$) and concentrated by evaporation. The tertiary alcohol was purified by distillation, b.p. 88-90°C, 24 mmHg, lit.[35] 78.5-79.5°C, 15 mmHg.

δ^1H ($CDCl_3$) 80 MHz, broad spectrum between δ0.25 and 1.75 with peaks at 0.88, 1.11, 1.34 and 1.37.

$\delta^{13}C$ ($CDCl_3$) 50 MHz: 13.8, 14.5, 17.0, 23.1, 26.0, 26.7, 41.5, 44.2 and 72.6 (quaternary).

(b) Dibutylethylamine: Dibutylamine (1.28 g, 0.01 mol) and ethyl iodide (2.0 g, excess) were dissolved in THF (10 ml) and the mixture was left to stand at room temperature for 1 week. The mixture was then poured into aqueous 2M NaOH. The organic layer was extracted with ether (50 ml) and the ethereal extract was washed with water, dried ($MgSO_4$) and concentrated by evaporation. The tertiary amine was purified by distillation, b.p. 82-84°C, 11 mmHg.

$\delta^{13}C$ ($CDCl_3$), 50 MHz: 11.6, 13.7, 20.5, 29.3, 47.4, 53.2.

(c) 1-ethylcyclohexanol: Ethyl bromide (3.48 g, 0.032 mol) in dry ether (40 ml) was added dropwise to dry magnesium turnings (0.46 g) covered with ether (10 ml). After the addition was complete the solution was heated under reflux for a further 20 min. before cyclohexanone (0.79 g, 0.008 mol) in ether (20 ml) was slowly added. The mixture was heated under reflux for a further 1 h. and then saturated, aqueous ammonium chloride (100 ml) was added. The ethereal layer was separated and the aqueous layer was extracted with ether (100 ml). The combined ethereal extracts were washed with water, dried ($MgSO_4$) and concentrated by evaporation. The tertiary alcohol, which was a low-melting solid, was purified by distillation, b.p. 78-80°C, 24 mmHg.

APPENDIX 1

Table B-3 Summary of the Results of Reductive Alkylation of Aliphatic Ketones in Liquid Ammonia/Quaternary Ammonium Salt Solutions

No.	Ketone	Experimental Conditions	Reduction Products (Yields)	Other Products
(1)	PrCMe (O)	2F mol^{-1} reduction at Hg cathode, Et_4NBF_4, mechanical stirring	PrCMe (O) (20%) PrC(OH)H-Me (80%)	-
(2)	PrCMe (O)	As (1), except ketone added after 2F mol^{-1} equivalent passed	PrCMe (O) (84%) PrCMe(OH)H (16%)	-
(3)	PrCMe (O)	As (1), except cell stirred by N_2 bubbles	PrC(OH)HMe (66%) PrC(OH)(Et)-Me (34%)	Et_3N
(4)	PrCMe (O)	As (3), except reduction by addition of Na (10 equivalents)	PrCMe (O) (23%) PrCMe(OH)H (77%)	Et_3N

Table B-3 (Contd.)

No.	Ketone	Experimental Conditions	Reduction Products (Yields)	Other Products
(5)	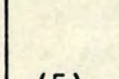	As (3), except Bu_3EtNI electrolyte	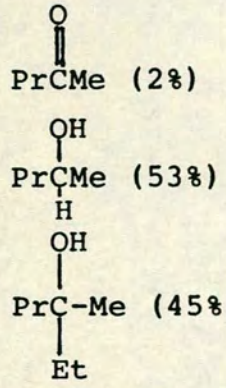	Bu_3N Bu_2EtN
(6)	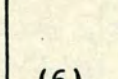	As (5), but $Bu_3\overset{+}{N}CD_2CH_3\ I^-$ used	As (5) with 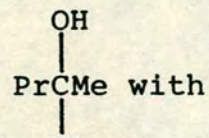 atoms in Et group	As (5)
(7)	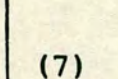	As (3) but electrolyte 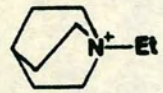 I^-	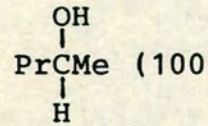	
(8)	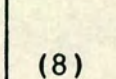	As (3) but electrolyte 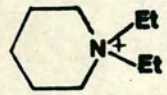 I^-	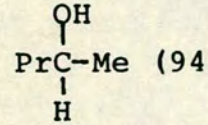	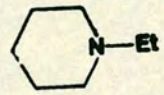

Table B-3 (contd.)

No.	Ketone	Experimental Conditions	Reduction Products (Yields)	Other Products
(9)		As (3), but ketone dissolved in THF prior to reduction	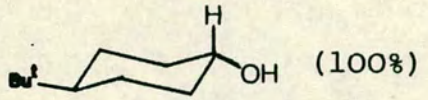 (100%)	Et_3N
(10)		As (9)	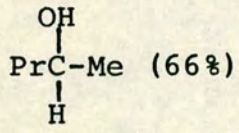 (66%) 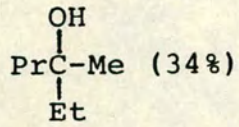 (34%)	Et_3N
(11)	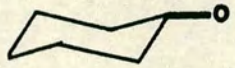	As (9)	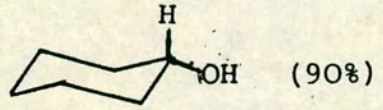 (90%) 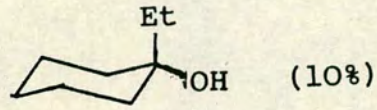 (10%)	Et_3N

References

1. A.J. Birch, Quart.Rev.Chem.Soc., 1950, 4, 69.
2. "Electrode Reactions in Liquid Ammonia", O.R. Brown, Chem.Soc., Specialist Periodical Reports, Electro-Chemistry, 1974, 4, 55.
3. A. Demortier and A.J. Bard, J.Am.Chem.Soc., 1973, 95, 3495.
4. O.R. Brown and R. Butterfield, Electrochim.Acta, 1982, 27, 321.
5. J.M. Saveant, Acc.Chem.Res., 1980, 13, 323.
6. J.M. Hildebrand, J.Chem.Educ., 1948, 25, 74.
7. H.A. Laitenen and C.J. Nyman, J.Am.Chem.Soc., 1948, 70, 2241.
8. E.M. Abbot and A.J. Bellamy, J.Chem.Soc., Perkin Trans. 2, 1978, 254.
9. E.M. Abbot, Ph.D. Thesis, University of Edinburgh, 1977.
10. T. Shono, I. Nishiguani and H. Omizu, Chem.Letts., 1976, 1233.
11. T. Shono, I. Nishiguani, H. Omizu and M.M. Tani, J.Am.Chem.Soc., 1978, 120, 545.
12. T. Shono, EUCHEM meeting 1977, Pitlochry, Scotland.
13. G.R. Davies and B.J. Woodhall, J.Appl.Electrochem., 1971, 1, 137.
14. W. Stewart, Chemistry Honours Project, University of Edinburgh, 1980.
15. S. Robertson, Chemistry Honours Project, University of Edinburgh, 1982.

16. R. Markgry and J. Simonet, J.Electroanal.Chem. Interfacial Electrochem., 1979, 101, 275.

17. J.D. Littlehailes and B.J. Woodhall, Faraday Discuss. Chem.Soc., 1968, 45, 187.

18. E. Kariv-Miller and C. Nanjundiah, J.Electroanal. Chem. Interfacial Electrochem., 1983, 147, 319.

19. D. Holton and P. Edwards, Chem.Br., 1985, 21, 1007.

20. W.L. Jolly, Prog.Inorg.Chem., 1959, 1, 235.

21. L. Eberson and K. Nydberg, Adv.Phys.Org.Chem., 1976, 12, 66.

22. R. Quinn and J. Lagowski, J.Phys.Chem., 1968, 72, 1374.

23. C. Thompson and J. Cundau, J.Chem.Soc., 1888, 53, 761.

24. H. Schlubach and F. Ballauf, Chem.Ber., 1921, 54, 2811.

25. D. Hazlehurst, A. Holliday and G. Pass, J.Chem.Soc., 1956, 4653.

26. W. Jolly, J.Am.Chem.Soc., 1955, 77, 4958.

27. E. Grovenstein and R. Stevenson, J.Am.Chem.Soc., 1959, 81, 4850.

28. J. Brewster and E. Eliel, Org.React.(N.Y.), 1953, 7, 99.

29. J. Wagenknecht, J.Electroanal.Chem. Interfacial Electrochem., 1974, 52, 489.

30. A.J. Birch, J.Proc.Roy.Soc., New South Wales, 1950, 83, 245.

31. E. Ashby and J. Laemmle, Chem.Rev., 1975, 75, 521.

32. W.A. Henderson and C.J. Schultz, J.Org.Chem., 1962, 27, 4643.

33. J. Meisenheimer, J. Neresheimer, O. Finn and W. Schneider, Justus Liebigs Ann.Chem., 1920, 420, 190.

34. K.F. Lampe and F.W. Scheiler, Acct.Intern. Pharmacodynamie, 1956, 105, 285.

35. J. Woodburn, J.Am.Chem.Soc., 1933, 55, 363.

PART C

ELECTROCHEMICAL STUDIES ON SOME

TRANSITION METAL METALLOPORPHYRIN SPECIES

C.1 Introduction

C.1-1 The Structure, Electronic Spectra and Redox Properties of Porphyrins and Metalloporphyrins

The porphyrins form a class of compounds of great natural importance, due to their forming the prosthetic groups of many biologically active compounds. Amongst these are haemoglobin, myoglobin, the cyctochromes and the peroxidases, whose biological roles involve respectively; transport of oxygen through the bloodstream and muscle tissue, electron transfer across cell membranes and decomposition of poisonous peroxides in living systems. The most well-known natural porphyrin is haem(1), an iron(II) complex present in both haemoglobin and myoglobin. This complex can reversibly bind dioxygen to the iron(II) centre when a histidine group is also axially bound to the metal. In the absence of this protein environment, haem loses this reversible dioxygen binding ability, except in aprotic media at temperatures lower than -40°C.[1]

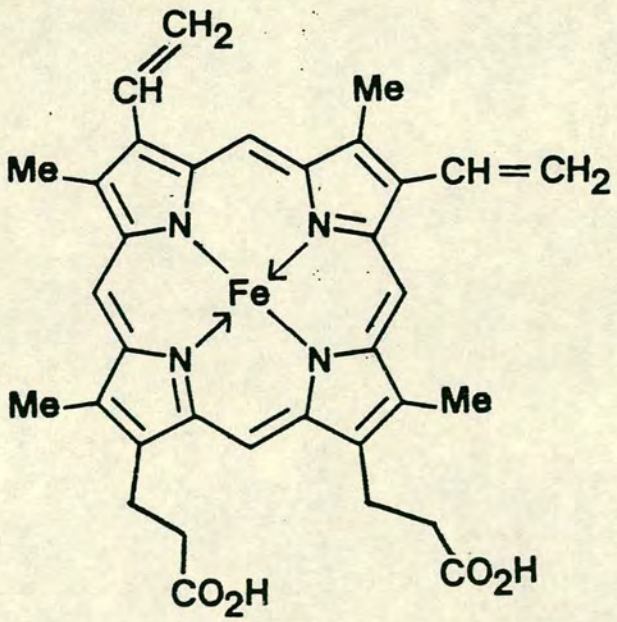

(1) Haem

Porphyrins are formally derived from the planar tetrapyrrolic macrocycle Porphin(2), with some or all of the positions on the macrocyclic periphery being substituted. Positions on the macrocycle are normally numbered as shown, with 1 to 20 representing the carbon atoms, and 21 to 24 the nitrogen atoms. In addition the pyrrole rings are labelled A to D, and the bridging methine carbon atoms often referred to as the meso carbon atoms.

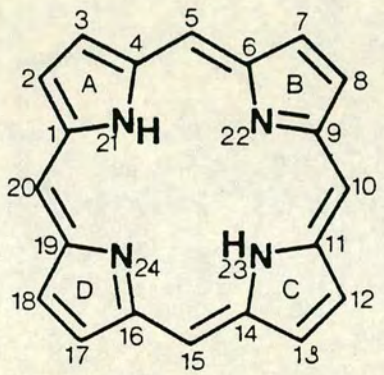

(2) Porphin (H_2P)

Porphyrins retaining the two N-H functions, with no coordinated metal present, are referred to as free-base porphyrins. In nature it is normal for porphyrins to exist as metallated complexes with the central metal ion coordinated to the doubly N-deprotonated porphyrin dianion. Iron, cobalt and manganese are amongst the more common metals found in natural systems.

All porphyrins are intensely coloured materials whose electronic absorption bands have very large extinction

coefficients. These bands arise from electronic transitions within the extended π-orbitals of the highly conjugated aromatic macrocycle. Although there are a total of 22 π electrons in porphin, only 18 of these can participate in the longest classical delocalisation pathway. The two 18π-electron, 16-membered rings, outlined below in Figure C.1 conform to the Hückel (4n+2)π electron rule for aromaticity. Both of the illustrated tautomeric forms contribute equally to the overall structure of porphin.

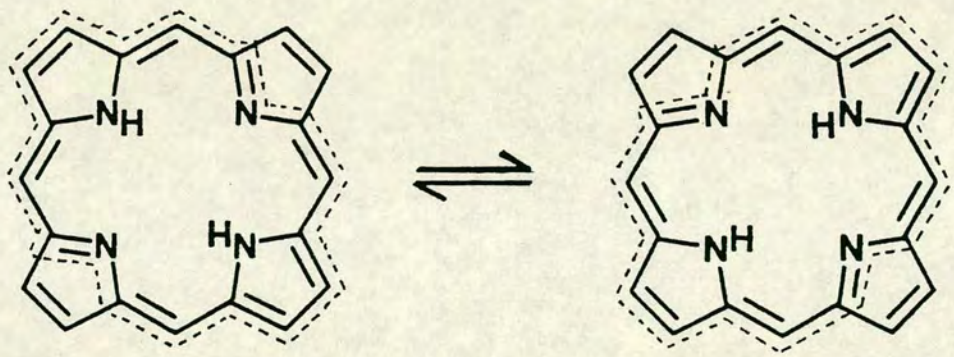

Figure C.1: Tautomeric Forms of Porphin with Classical 18π-Electron Delocalisation Pathways Illustrated

A tetrapyrrolic macrocycle related to porphin is its 17,18-dihydro derivative, chlorin(3). A magnesium chlorin complex forms the basic unit of the chlorophylls, which are the crucial photoreceptors responsible for the photosynthesis of green plants. Significantly, the 18π-electron delocalisation pathway present in the porphyrins is also found, undisturbed, in the chlorins.

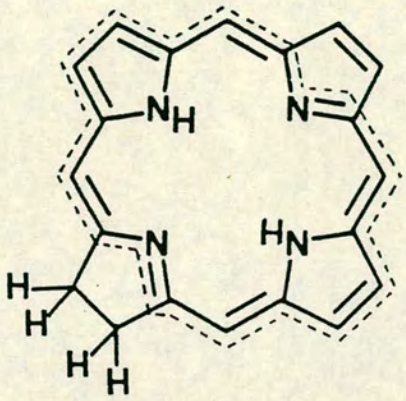

(3) Chlorin (H_2C): showing 18π electron delocalisation pathway.

A further related structure is that of bacteriochlorin(4), the 7,8,17,18-tetrahydro derivative of porphin. Magnesium derivatives of this macrocyclic unit control the respiration process in anaerobic bacteria. This structure again maintains the 18π electron delocalisation pathway present in the porphyrins and the chlorins.

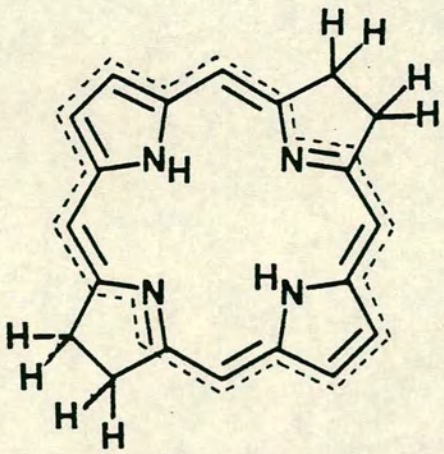

(4) Bacteriochlorin (H_2BC): showing 18π electron delocalisation pathway.

The tetrapyrrolic macrocycles described, and their metallated derivatives, form a group of great academic interest due to the natural functions of these compounds. Biological activity of these complexes appears always to be simultaneous with a change in either the overall redox state of the compound, or in the electronic configuration of the molecular frontier orbitals. It is not surprising, therefore, that these aspects of the chemistry of the tetrapyrrolic macrocycles have been the subject of a great deal of study.

Study of the natural porphyrin systems is generally severely constrained by the small amounts of material isolable from natural sources, and alternatively by difficulties in synthesising these in quantity. It is for this reason that many studies are carried out on synthetic model porphyrins which should have similar chemical properties to the natural systems. Model porphyrins are usually soluble, and can be fairly readily synthesised, making them particularly useful for studying trends in metalloporphyrin behaviour where a large series of metals is to be examined. In addition these compounds are often symmetrical, considerably simplifying many of their spectral properties. The model porphyrins most commonly used are 5,10,15,20-tetraphenylporphin(5) and 2,3,7,8,12,13,17,18-octaethylporphin(6).

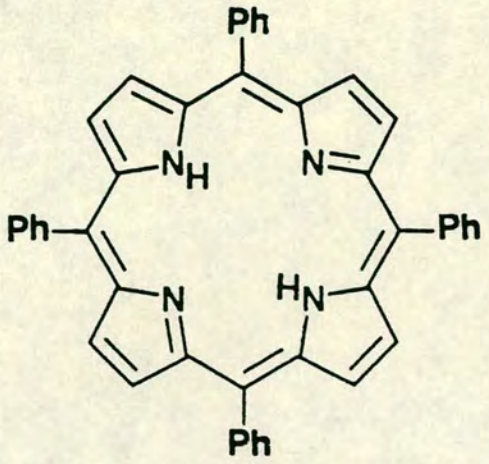

(5) H_2TPP

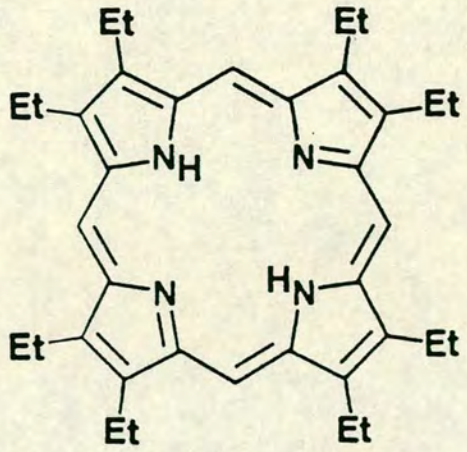

(6) H_2OEP

The range of diverse metals that have been successfully incorporated within porphyrins by chemical synthesis encompasses a broad spectrum of the Periodic Table. Porphyrin derivatives are known for all the alkali metals, all alkaline earth metals (except Be), and for all first, second and third row transition metals although complexities exist for the heavier transition elements. In addition to these, complexes of the Group IIIA, IVA below and including Silicon, VA below and including Arsenic, and some of the lanthanide and actinide elements have been synthesised.

The simplest types of metalloporphyrins are monometallic complexes. With divalent metal ions the charges on metal and macrocycle match, resulting in the formation of complexes of stoichiometry MP. For metals of valency greater than two, the excess charge on the metal is generally balanced by the presence of axially bound ligands leading to compounds of stoichiometry MPL and MPL_2, where L represents an axial

ligand. Examples of these simple monometallic metalloporphyrins are Cu(II)OEP(7), Fe(III)TPPCl(8) and $Sn(IV)TPP(OH)_2$(9).

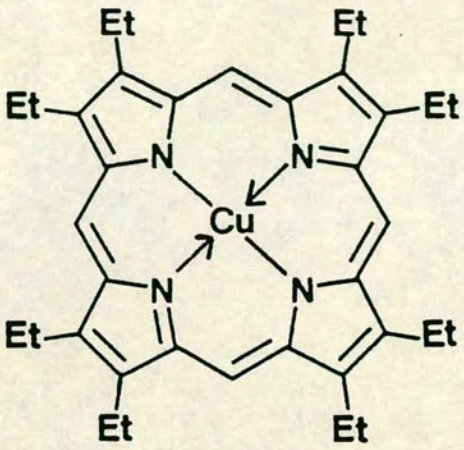

(7)

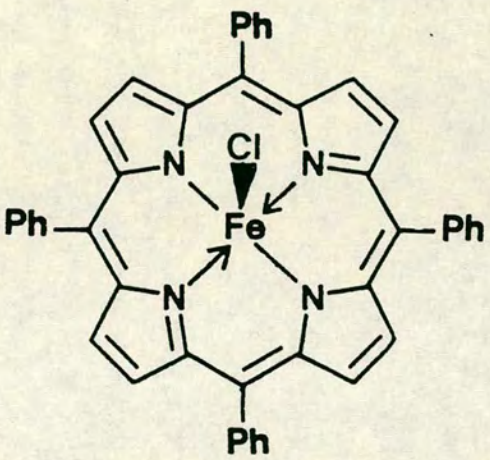

(8)

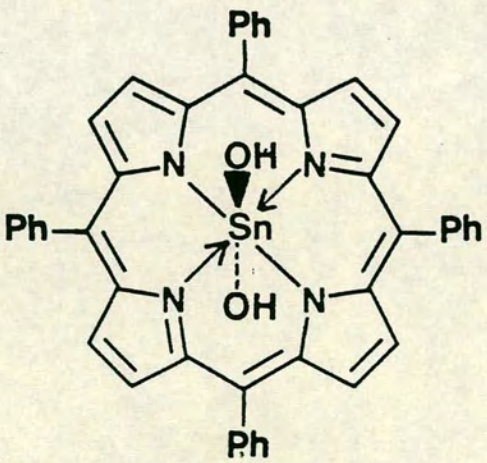

(9)

In addition to these systems, more complicated species with stoichiometries such as M_2P, $(MP)_2$, MP_2, $(MP)_2X$ and $(MPL)_2X$, where X is a bridging ligand, and many others are known to exist. These less common systems are particularly prevalent with complexes containing some of the heavier transition elements.

Electronic Spectroscopy of Porphyrins and Metalloporphyrins

As porphyrins are all intensely coloured, and their biological activity appears always to intimately involve changes in the electronic configuration of the frontier molecular orbital manifold, it is not surprising that the optical transitions between these levels have been extensively studied by optical spectroscopy for fully a century.

The electronic spectrum of a typical metalloporphyrin, in this case Zn(II)OEP, is shown on figure C.2. The spectrum evidently consists of two distinct principle regions. The visible region between 500 and 600 nm contains two bands. These generally have extinction coefficients in the range 0.5 to 4×10^4 $M^{-1}cm^{-1}$. In the near-uv region there is a further single intense absorption between 370 and 430 nm which has extinction coefficients in the range 1 to 4×10^5 $M^{-1}cm^{-1}$. This intense band is often referred to as the Soret band after its discoverer.[2] The Soret band is uniquely characteristic of tetrapyrrolic macrocycles containing the 18π electron system described previously. The presence, in this spectral region, of a band of this intensity in an unidentified complex is often taken to imply the presence of the unbroken 18π electron tetrapyrrolic conjugation.

These bands originate from transitions between the macrocyclic π and π* molecular orbitals of the 18π electron aromatic ring. It is now accepted that these transitions involve the two highest-energy filled macrocyclic π orbitals and the two lowest-energy unfilled π* orbitals. For a

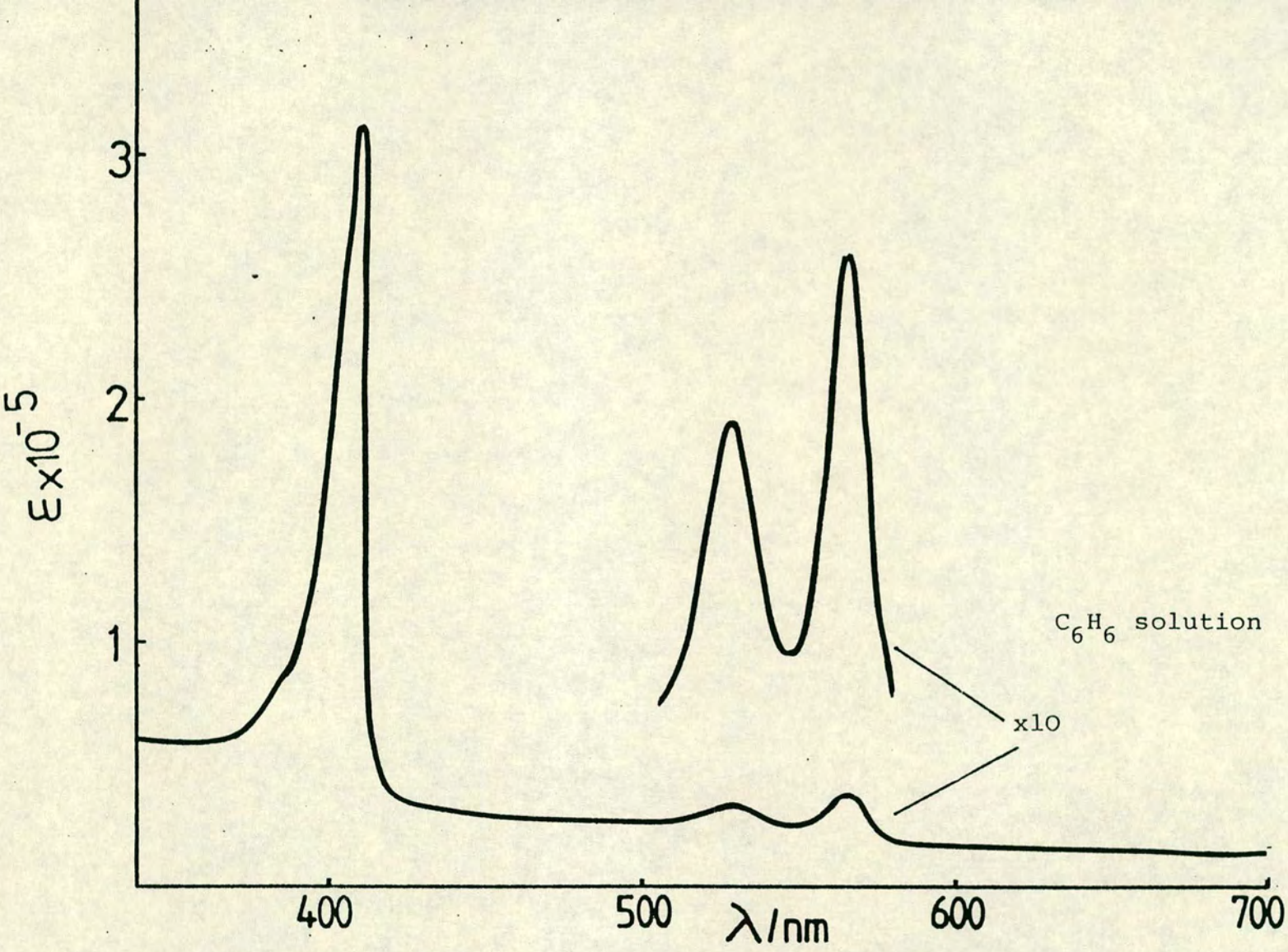

Figure C.2: Electronic Spectrum of Zn(II)OEP

metalloporphyrin of D_{4h} symmetry these consist of two energetically close orbitals of a_{1u} and a_{2u} symmetry, and a degenerate pair of orbitals of e_g symmetry as represented in figure C.3.

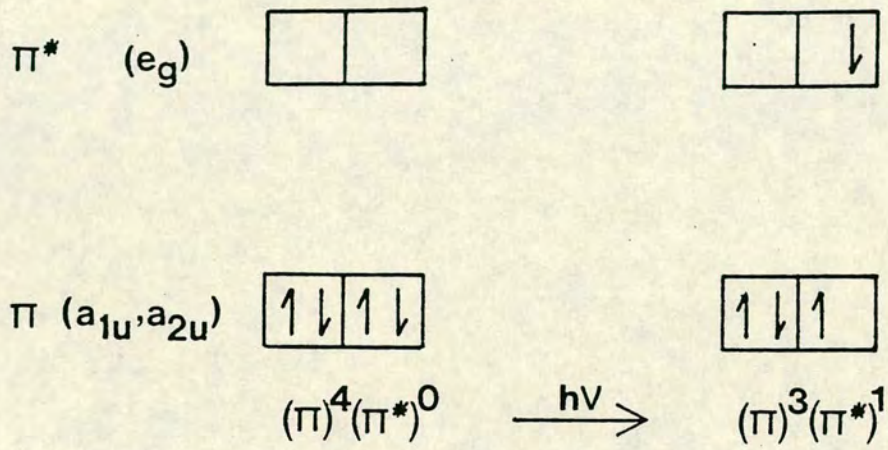

Figure C.3: The Frontier Orbital Transitions underlying Metalloporphyrin Electronic Spectra.

The electronic spectra of porphyrins and metalloporphyrins have been explained by the four-orbital theory developed by Gouterman et al.[3] This states that the principle regions of the electronic spectrum of porphyrins can be attributed essentially to one-electron excitations between the configurations shown in figure C.3. Electron-electron interactions make the two possible permutations of the $(\pi)^3(\pi^*)^1$ configuration differ in their energies and the symmetry allowedness of the excitation, and are therefore responsible for the emergence of the two band systems (uv and visible) of differing intensity.

Platt[4] has labelled the major features of the porphyrin electronic spectrum as the Q bands, which are the less-intense visible bands, and the B band, which is the Soret band. These labels refer to the extent of symmetry allowedness of the transitions, indicating quasi allowed and strongly allowed excitations. The higher energy band of the two Q bands is attributed to a vibronic overtone of the fundamental Q band giving these the labels Q(0,0) and Q(1,0).

There are additional, low intensity, $\pi \rightarrow \pi^*$ bands in the uv region of a metalloporphyrin spectrum at approximately 325, 280 and 215 nm which have been labelled N, L and M respectively. These arise from transition other than the HOMO → LUMO ones which are responsible for the two major features of metalloporphyrin electronic spectra.

When the central ion in a metalloporphyrin is a transition element containing an incomplete d-electron shell, the metal can affect the electronic spectrum in two ways. These contrasting effects both involve the metal $d\pi(d_{xz},d_{yz})$ orbitals which are of e_g symmetry, thus allowing them to overlap with the vertical macrocyclic $p\pi$ orbitals. For d^1 metal ions (eg. Sc^{2+}, Ti^{3+}), these orbitals and indeed the whole d-orbital manifold are of much higher energy than the highest filled macrocyclic π-orbitals (π_{a1u}^2, π_{a2u}^2 - see figure C.3), but on moving across the transition series the $d\pi$ levels descend in energy until approximate equivalence is reached for the d^8 metals where the d-orbital manifold may be spanned by the macrocyclic frontier orbitals. For later elements, the completed d^{10} subshells (e.g. Zn^{2+}, In^{3+}) descend into the subvalent core, well below the macrocyclic π-orbitals.

For transition metal ions containing between 1 and 5 d electrons, the dπ orbital sub-shell is only partially occupied. This permits optical ring to metal charge transfer to occur and spectral bands arising from these transitions are observed. These bands, however, are generally less intense than the macrocyclic $\pi \rightarrow \pi^*$ Q bands. For later transition metal ions, containing between 6 and 9 d electrons, the filled dπ orbital set tends to interact with the vacant macrocyclic π^* (e_g) orbitals. This corresponds to metal to ligand backbonding, familiar in transition metal coordination chemistry. This effect stabilises the metal dπ orbitals but raises the energy of the macrocyclic π^* orbitals, resulting in the macrocyclic $\pi \rightarrow \pi^*$ bands being shifted to slightly higher energies.

In the unmetallated free-base porphyrins (H_2P) the molecular symmetry changes from pseudo-D_{4h} to pseudo D_{2h}. The effect of this lower symmetry is that the two lowest unfilled molecular orbitals lose the strict degeneracy they possess in the metallated species. These become split into x and y symmetric orbitals, separated in energy by approximately 3000 cm^{-1}. This results in doubling up of the spectrum which now contains four bands between 500 and 650 nm. These are given the labels $Q_x(0,0)$, $Q_x(1,0)$, $Q_y(0,0)$ and $Q_y(1,0)$ in order of increasing energy. Similarly, in the uv region, the Soret band decreases in intensity but broadens distinctly. The electronic spectrum of a typical free-base porphyrin, Deuteroporphyrin IX, is shown on figure C.4 with both spectral regions illustrated.

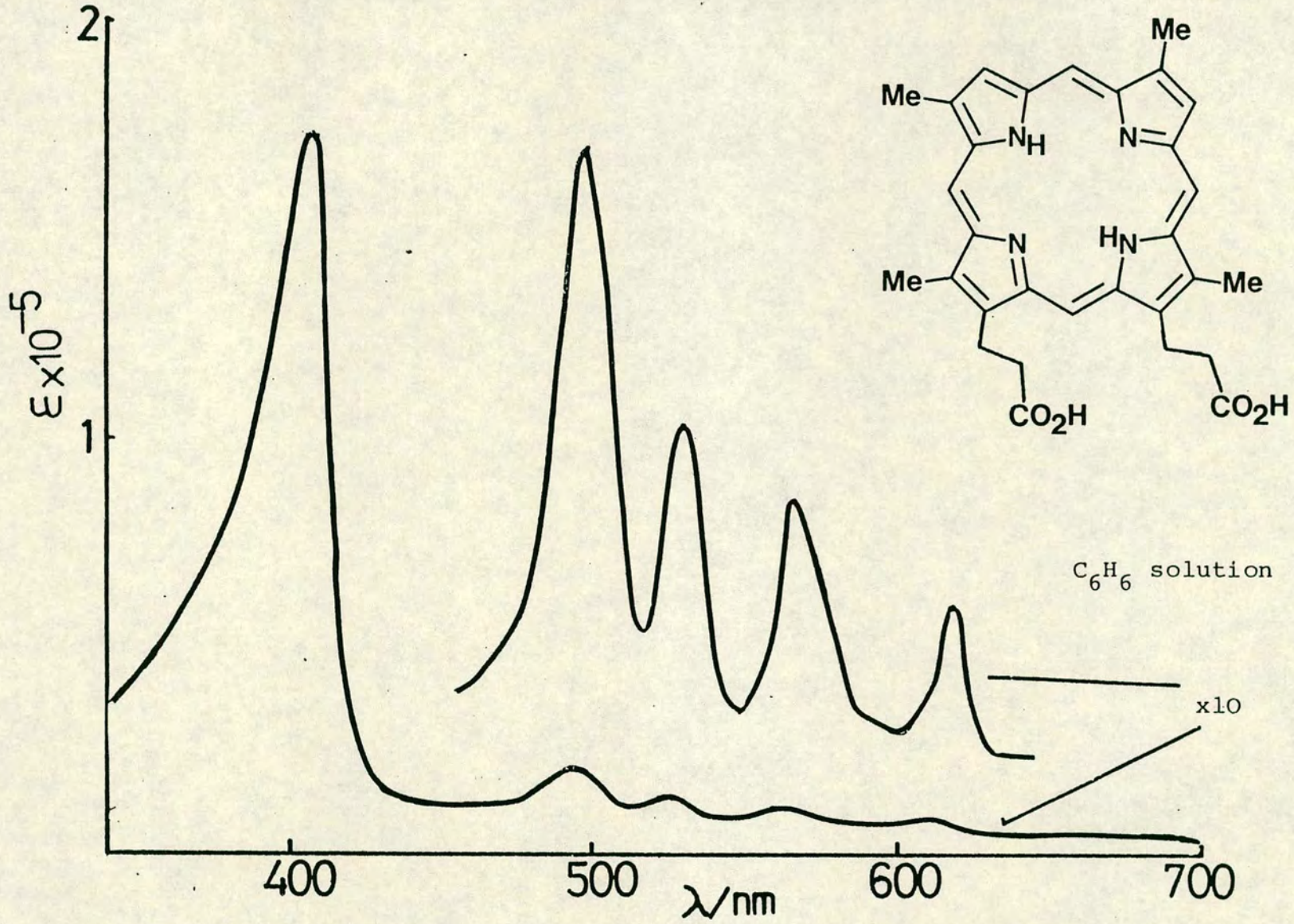

Figure C.4: Electronic Spectrum of Deuteroporphyrin IX

Electrochemistry and Spectroelectrochemistry of Porphyrins and Metalloporphyrins

In addition to electronic spectroscopy, the other common means of exploring frontier orbital levels is by the use of electrochemistry.

The redox properties of porphyrins have been studied for the past 50 years, and it is now recognised that the π-orbital manifold of the macrocycle is able to undergo two reversible one-electron oxidations and at least two reversible one-electron reductions. In some instances up to four one-electron reductions have been reported.[5] The species normally formed are the π-radical-cation, π-dication, π-radical-anion and π-dianion as illustrated in Scheme C.1.

$$H_2P^{2+} \underset{-e}{\rightleftharpoons} H_2P^{\cdot+} \underset{-e}{\rightleftharpoons} \underline{H_2P} \overset{+e}{\rightleftharpoons} H_2P^{\cdot-} \overset{+e}{\rightleftharpoons} H_2P^{2-}$$

Scheme C.1:- Normal Porphyrin Electrochemical Processes.

The first reported oxidation of a tetrapyrrole was when Rabinowitch and Weiss[6] chemically oxidised chlorophyll a with ferric chloride. This produced a green species which was almost certainly the π-radical-cation. Further studies[7] on the oxidation of copper porphyrins led to the postulate that the oxidised species produced had an unpaired electron delocalised throughout its π-orbital system. In 1963 Closs and Closs[8] became the first to isolate metalloporphyrin π-radical-anions and π-dianions when they chemically reduced Zn(II)TPP. In addition, the electronic spectra of these reduced species were reported, and polarography used to determine the appropriate reduction potentials.

This polarographic study was closely followed by one by Clack and Hush[5] in 1965, and since then porphyrins and metalloporphyrins have been frequently examined voltammetrically due to the growth in accessibility of electrochemical techniques.

The electrochemical behaviour of free-base porphyrins normally consists of two reversible oxidations and reductions as described previously. The cyclic and A.C. voltammograms of a typical example, H_2TPP, are illustrated on figure C.5.

In metalloporphyrins the central metal can change the electrochemical behaviour of the porphyrin in two ways:-

(1) The energy levels of the macrocyclic frontier orbitals will be altered by interactions between the metal and macrocycle. These interactions can be electrostatic, inductive, mesomeric or even steric in origin.

(2) Transition metal ions are intrinsically redox-active, and electron transfer may occur directly on the metal centre. The effect of this on any subsequent macrocyclic electron transfers will be to push their potentials to more extreme values than expected, due to a change in the polarising power of the central ion.

Thus the central metal changes the energy of the porphyrin π-orbital manifold from that of the free-base and one consequence of this is a change in the values of the reduction and oxidation potentials. There have been many studies that have tried to quantify and explain the metal-macrocycle interactions in such complexes. The first attempt by Felton et al.[9], led

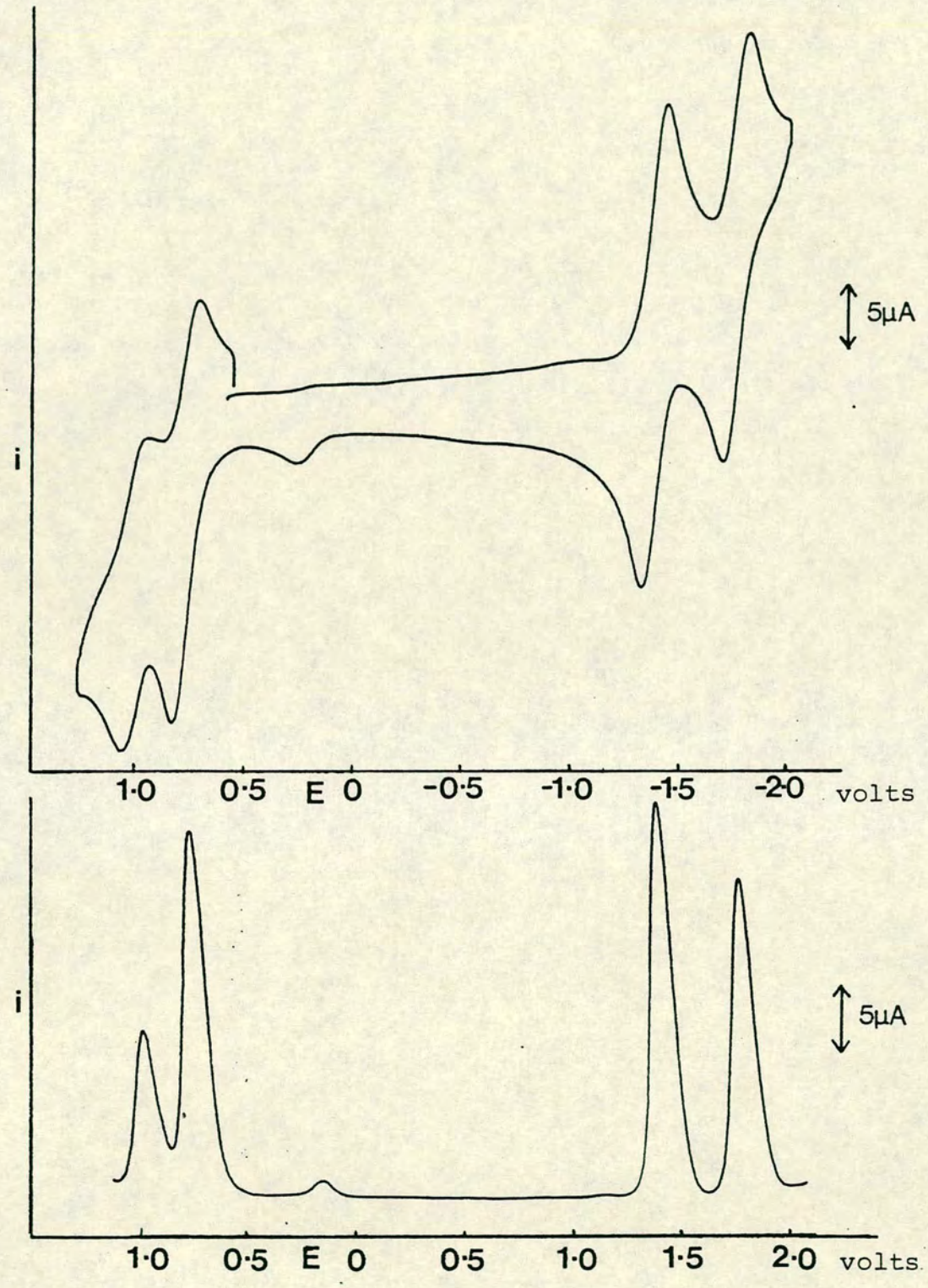

Figure C.5: Cyclic and A.C. Voltammograms of H_2TPP CH_2Cl_2/0.5M $TBABF_4$. E vs Ag/AgCl

to a correlation being proposed between reduction potential and metal electronegativity. A later study by Stanienda and Biebl [10] on some metallotetraphenylporphin oxidations led to consideration of the influences of metal ionisation energy and metal ion radius without any direct correlations being drawn. The most comprehensive study was by Fuhrop, Kadish and Davies[11] who examined 25 metallooctoethylporphins voltammetrically. The reductions of these complexes were studied in DMSO and the oxidations in butyronitrile. They observed that in the absence of any metal-based redox processes the separation between the first oxidation and first reduction potentials was 2.25 ± 0.15V. They also observed that the first and second macrocyclic based reductions were separated by 0.42 ± 0.05V and similar oxidations by 0.29 ± 0.05V. The almost constant separation between the oxidation and the reduction potentials for this series led to the belief that the metal ion exerts an inductive influence through the metal-nitrogen σ bonds whose effect is to raise or lower the energy of the π and π^* orbitals by the same amount, i.e. to shift the frontier orbital manifold bodily without narrowing or widening the HOMO/LUMO gap. A correlation was found, for the divalent metal ions, directly relating the electronegativity of the central metal ion with the first macrocyclic based oxidation and reduction potentials. This relationship was then inverted to calculate an inferred value, called the induction parameter, for metals in other valency states in order to quantify their inductive influence over the redox behaviour of porphyrins. The overall conclusion of this study was that a central metal in a metalloporphyrin influences the

macrocyclic redox behaviour by exerting an electrostatic influence through the metal-nitrogen σ bonds.

A later study[12] of this supposed correlation, which also compared the voltammetry of the structurally related metallophthalocyanines (10), questioned these conclusions and particularly the selection of electronegativity values used.

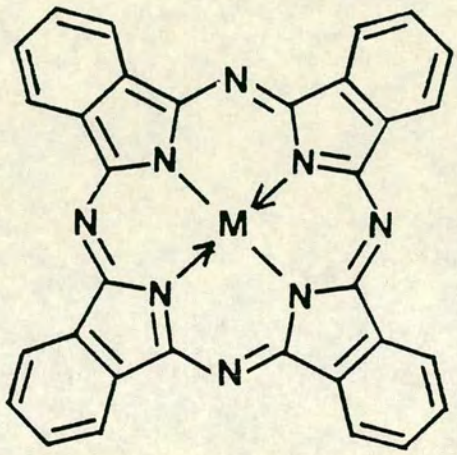

(10) Metallophthalocyanine (MPc)

This study showed that the linear relationship between oxidation and reduction potentials and central metal electronegativity was not as well fitting as previously stated. The study showed that the oxidation and reduction potentials for some of the metallated complexes were influenced by solvent and counter-ions and also found inversions in the $E_{\frac{1}{2}}$/metal ion order on moving to different tetrapyrrolic

macrocycles. The conclusion arrived at was that although electronegativity correlations were qualitatively helpful, it was misleading to say that a strict quantitative relationship existed between central ion electronegativity, or any other single metal parameter, and oxidation or reduction potential.

Recognition of the site of electron transfer on a metalloporphyrin as being either on the metal or the macrocycle is essential in interpreting the voltammetric behaviour of metalloporphyrins, and is particularly important for elucidating mechanisms of biological activity of natural systems. The most telling method of determining these processes is by examination of the electronic spectrum of the oxidised or reduced species. As previously stated the electronic spectra of metalloporphyrins are dominated by $\pi \rightarrow \pi^*$ transitions of the macrocycle in the near-uv and visible regions. Addition or removal of an electron from the π-orbital manifold results in major systematic changes in the electronic spectrum.

Formation of the π-radical-cation creates a hole in the HOMO, enabling transitions from lower lying levels to this orbital for the first time. The electronic spectrum of a metalloporphyrin π-radical-cation is now well documented and consists of two areas. There is a broad series of overlapping bands in the visible region from 500 to 700 nm, and also a broadening and decrease in intensity of the Soret band. Metalloporphyrin π-radical-cations can be formed by removal of an electron from either of the two highest energy occupied

molecular orbitals, these being of a_{1u} and a_{2u} symmetry in a square planar D_{4h} complex. The actual electronic structure of the π-radical-cation formed depends on which of these orbitals is singly occupied. This can vary with different metals, porphyrins, solvents and counter-ions, and as yet no satisfactory systematic explanation of this behaviour has been forthcoming. Although the overall electronic spectra of the two different types of π-radical-cation have similar patterns, the electronic configuration of these species can be precisely identified by detailed examination of the visible spectrum.[13]

When the electron is removed from an a_{1u} orbital the π-radical cation has a ground electronic state of $^2A_{1u}$. The visible spectrum of this ground state shows a large peak at ∿680 nm with a second smaller peak at ∿580 nm. An example of this spectral type, obtained in our laboratory, is that of the π-radical-cation $[Zn(II)OEP]^{\cdot+}$, whose electronic spectrum is shown on figure C.6.

In contrast, when the electron is removed from an a_{2u} orbital the π-radical-cation has a $^2A_{2u}$ ground state. The visible spectrum of this species shows four broad overlapping peaks of similar intensity in the 500 to 700 nm region. An example of this spectral type, also obtained in our laboratory is that of the π-radical-cation $[Zn(II)TPP]^{\cdot+}$, illustrated on figure C.7.

Electron spin resonance spectra of these contrasting ground states[14] has shown that the location of the unpaired

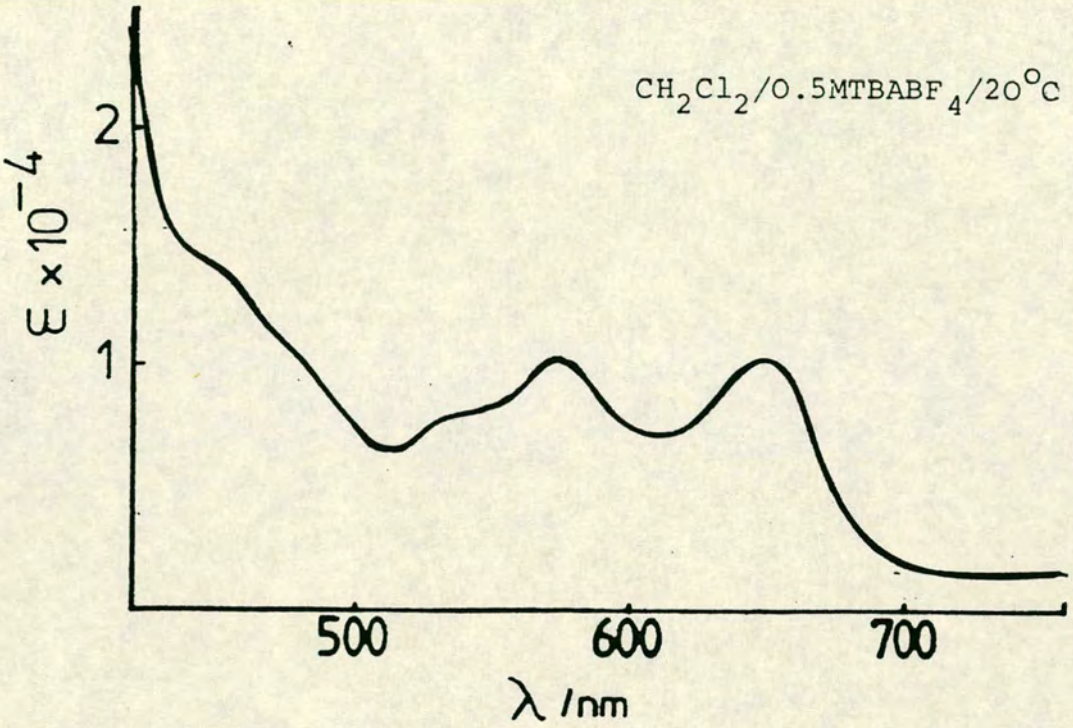

Figure C.6: Electronic Spectrum (visible region) of $[Zn(II)OEP]^{+\cdot}$

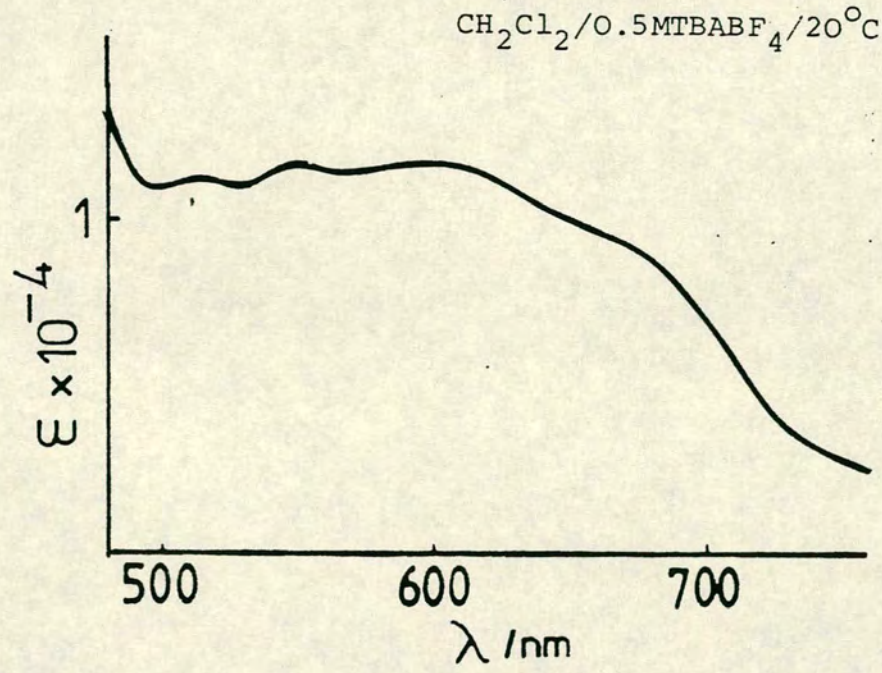

Figure C.7: Electronic Spectrum (visible region) of $[Zn(II)TPP]^{+\cdot}$

electron is indeed different for each case. For the $^2A_{1u}$ ground state the e.s.r. spectrum shows large spin densities on the meso carbon atoms, while the $^2A_{2u}$ systems show large spin densities on the four pyrrolic nitrogen atoms.

Removal of a further electron from the π-electron manifold results in π-dication formation and consequently further changes in the electronic spectrum. The electronic spectrum of a metalloporphyrin π-dication is dominated by a single absorption in the uv region at ∿320 nm and is almost featureless elsewhere. The second electron is removed from the second doubly occupied orbital of the pair of highest energy filled orbitals thus ensuring that the electronic configuration of all metalloporphyrin π-dications is the same, independent of the ground state of the preceding π-radical cation. In fact, spin-coupling occurs and the resultant electronic ground state of a metalloporphyrin π-dication is $^1A_{2g}$.[13] Electronic spectra of the π-dications $[Zn(II)OEP]^{2+}$ and $[Zn(II)TPP]^{2+}$ are illustrated on figures C.8 and C.9 respectively.

Addition of an electron to the 18 π-electron manifold of a metalloporphyrin results in π-radical-anion formation. The electron will enter one of the erstwhile unoccupied e_g orbitals thus drastically changing the electronic spectrum from that of the neutral complex. The Soret band collapses to about 50% of its original intensity and the visible bands in the spectrum are replaced by absorptions at ca. 700, 800 and 900 nm. These lower energy bands are attributed to mixing of the transitions from the newly occupied e_g orbital to even

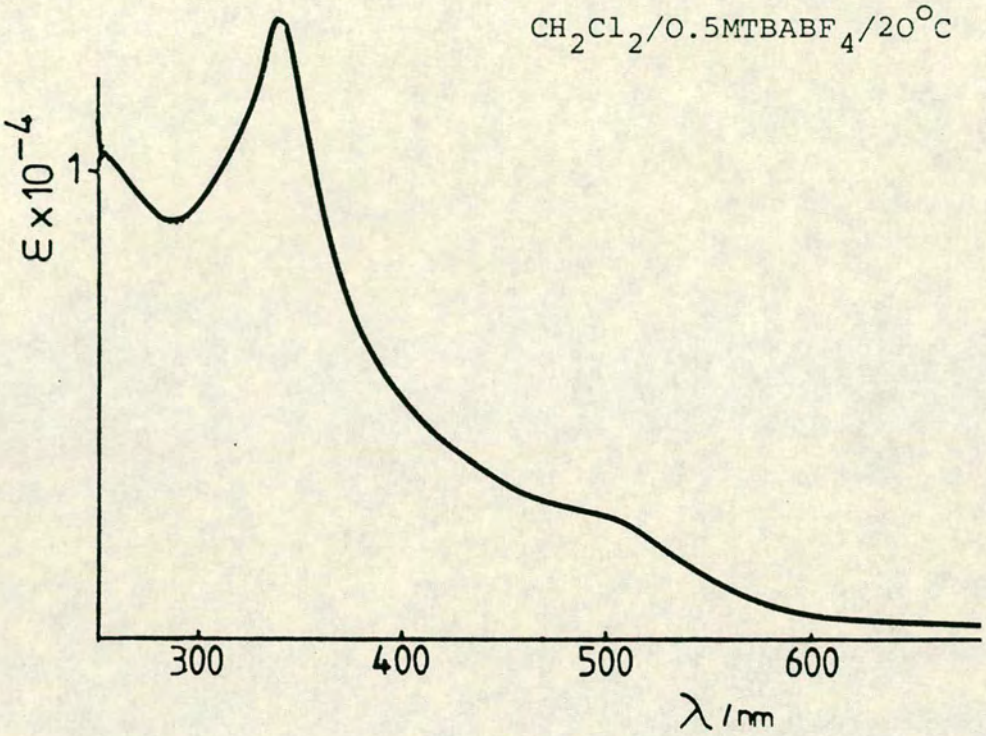

Figure C.8: Electronic Spectrum of $[Zn(II)OEP]^{2+}$

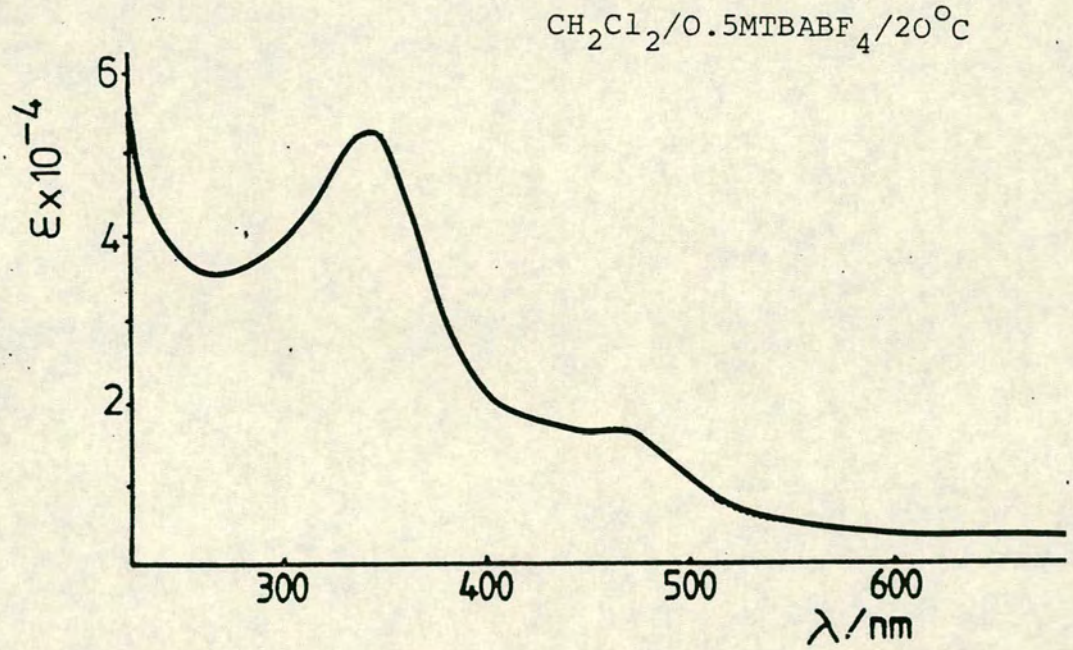

Figure C.9: Electronic Spectrum of $[Zn(II)TPP]^{2+}$

higher levels with the original Q transitions. A typical electronic spectrum of a metalloporphyrin π-radical-anion is that of $[Zn(II)TPP]^{-\cdot}$ shown on figure C.10.

Addition of a further electron results in the formation of a π-dianion. This electron enters the second e_g orbital of the degenerate pair of LUMO's. The electronic spectrum changes again with a further reduction in intensity of the Soret band and a growth of bands in the region 500 to 700 nm where the visible Q bands of the original neutral metalloporphyrin are located. For the π-dianion, there are normally three absorptions in this region, these being attributed to the fundamental and first two vibronic overtones of the lowest energy major band. A typical π-dianion electronic spectrum, that of $[Zn(II)TPP]^{2-}$, is illustrated on figure C.11.

In contrast to the dramatic spectral changes observed on electron transfer to and from the macrocycle, electron transfer to or from the metal centre of a metalloporphyrin results in little change in the dominant macrocycle-based $\pi \rightarrow \pi^*$ intense bands. The Soret band and two visible bands will still be observed, but will be shifted to higher or lower energy depending on the changing electronegativity of the metal. An illustrative example of this behaviour is provided by the spectra of the products of the first oxidation and first reduction of Co(II)TPP. The electronic spectra resulting from the complexes $[Co(III)TPP]^{+}$, Co(II)TPP and $[Co(I)TPP]^{-}$ are shown on figure C. 12.

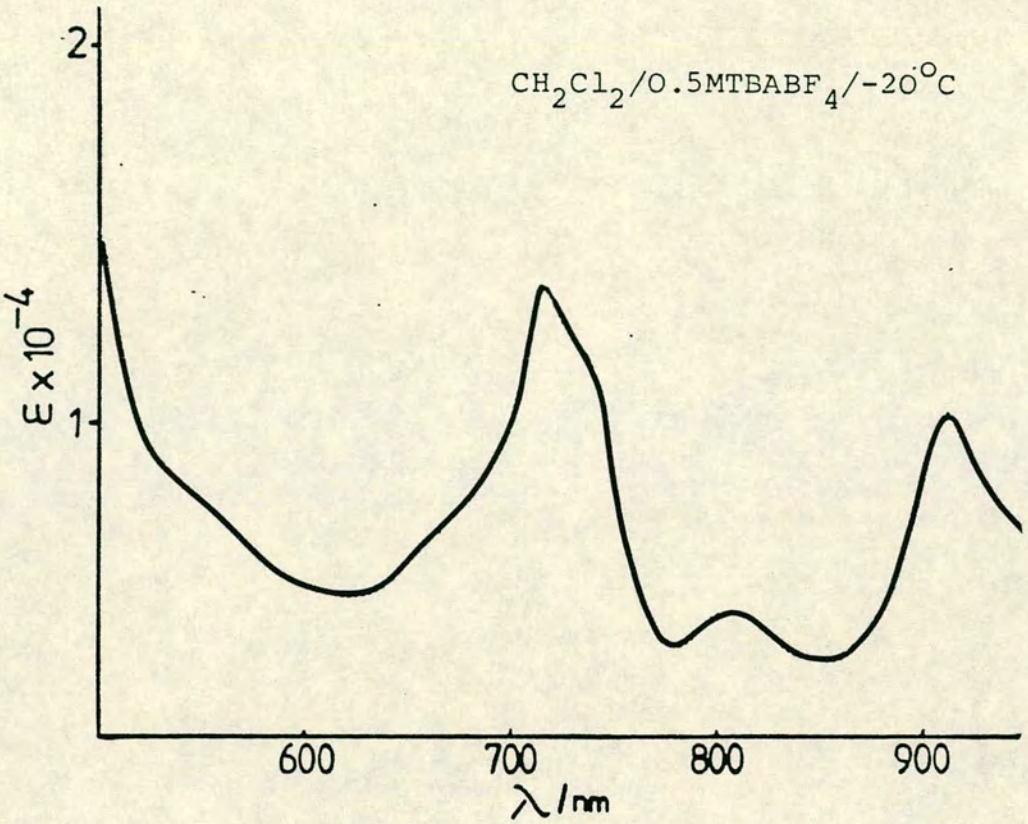

Figure C.10: Electronic Spectrum (visible region) of $[Zn(II)TPP]^-$

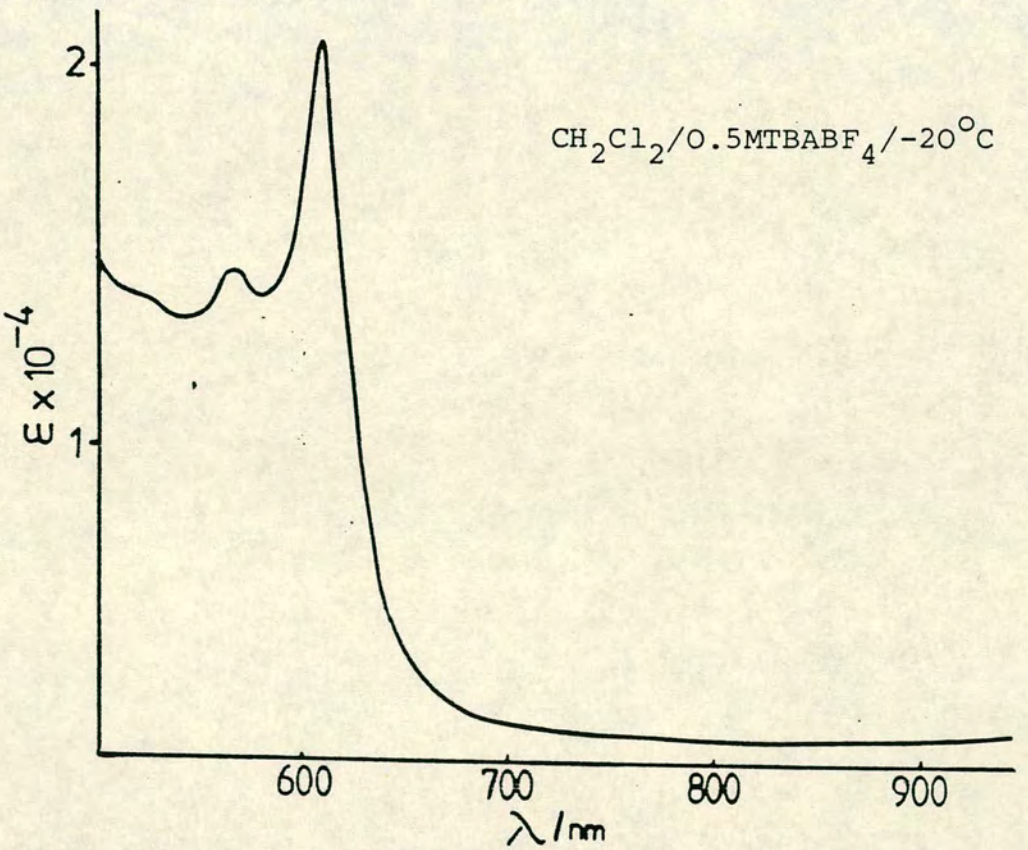

Figure C.11: Electronic Spectrum (visible region) of $[Zn(II)TPP]^{2-}$

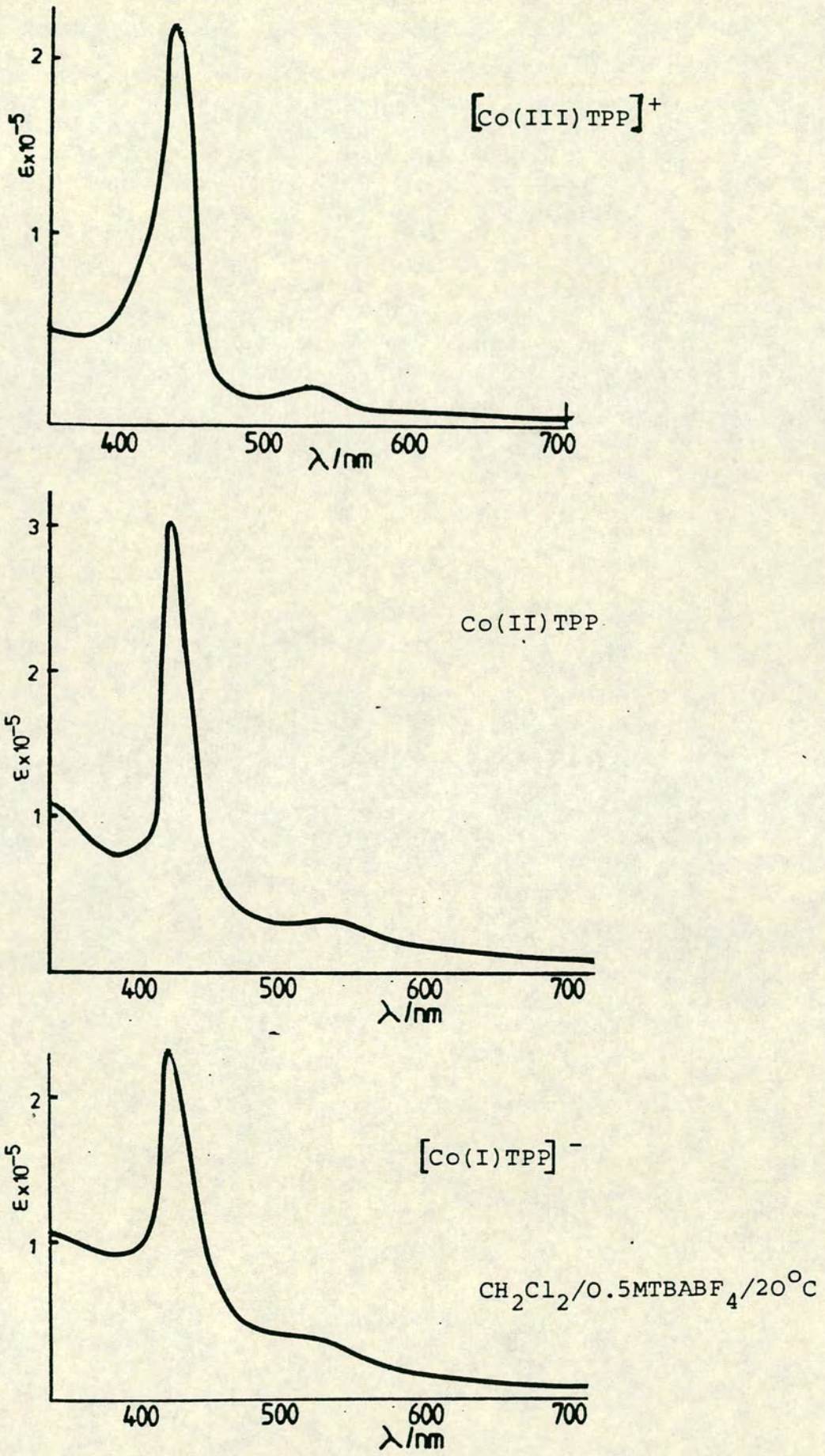

Figure C.12: Electronic Spectra of $[Co(III)TPP]^+$, Co(II)TPP and $[Co(I)TPP]^-$

There is to date one example of interchanging metal and macrocyclic based electron transfer products. Study of the first oxidation of Ni(II)TPP, initially using benzonitrile as solvent[15], led to the assignment of the first oxidation product as $[Ni(III)TPP]^+$. By contrast a later electrochemical study[16] on this compound, carried out in non-coordinating dichloromethane showed that, at room temperature, the first oxidised species was clearly a π-radical-cation. When the temperature was lowered to 77K, however, the electronic and e.s.r. spectra of the product showed the characteristics of a Ni(III) neutral porphyrin species. This thermally controlled valence isomerism is completely reversible and since then has been attributed[17] to reversible axial coordination of a perchlorate anion present in the supporting electrolyte. This is believed to stabilise the Ni(III) species at low temperature. The overall scheme is summarised on Scheme C.2.

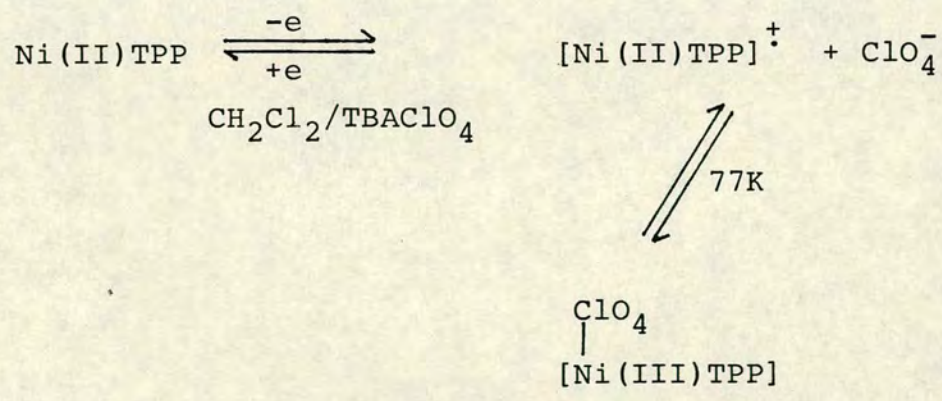

Scheme C.2:- Thermally Controlled Valence Isomerism of Oxidation Product of Ni(II)TPP

C.1-2 Redox-Induced Peripheral Reactions of Metalloporphyrins

The pyrrolic and bridging meso carbon atoms of a metalloporphyrin constitute its macrocyclic periphery. These positions are, by virtue of the aromatic stability present in porphyrins, resistant to chemical alteration unless reactions are carried out using potent reagents and under vigorous conditions.

Examples of these types of reactions include the meso-methylation of PdOEP (11).[18] Successful conversion, in 36% yield, to the meso-methyl porphyrin (12) has been reported by reaction with methyl fluorosulphonate in boiling chloroform.

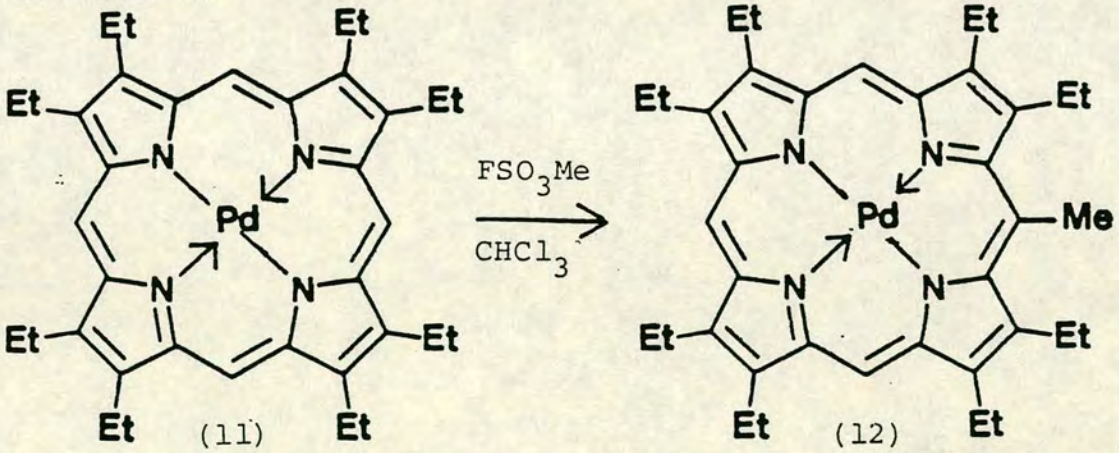

Similarly, introduction of the nitro function onto the meso position of copper octaethylporphin has been carried out using nitronium fluoroborate as the nitrating agent.[19]

Many of these reactions are of limited synthetic utility due to the strongly acidic conditions which prevail. These preclude the use of some of the commoner metals, such as magnesium and zinc, whose complexes demetallate in acidic media.

Recently, however, the scope of peripheral reactions of metalloporphyrins has widened considerably with the discovery of the enhanced peripheral reactivity of metalloporphyrin π-anions and π-cations. These species have been found to react under much milder circumstances than the corresponding neutral complexes. This has enabled peripheral reactions to be observed for all macrocyclic redox-active metalloporphyrins. Direct introduction of some functionalities onto the macrocyclic periphery, which hitherto have only been prepared by chemical modification of other peripheral substituents, has also been observed for the first time. These can be regarded as early evidence for a new general strategy whereby new reactivity patterns are conferred on porphyrins by deliberate manipulation of oxidation state, whether chemically or electrochemically.

Peripheral Reactivity of Metalloporphyrin π-anions

The first observed reaction of a metalloporphyrin π-anion arose in a study on the reductive behaviour of Zn(II)TPP by Closs and Closs. Chemical generation of a THF solution of the π-dianion, $ZnTPP^{2-}$, by addition of sodium anthracenide, followed by the addition of one molar equivalent of methanol, resulted in formation of the meso-protonated species (13), known as a phlorin. Helpfully, (13) possesses a characteristic, less intense, electronic spectrum with a broad absorption between 700 and 900 nm and its ^{1}H n.m.r. spectrum shows considerable upfield shift in the resonances of the pyrrolic protons compared with those of the starting material. This

indicates a decrease in ring current caused by a disruption of the 18π-electron aromatic system of the parent compound. Addition of excess methanol to (13) resulted in the slow formation of zinc tetraphenylchlorin (14). The reactions taking place are summarised in Scheme C.3.

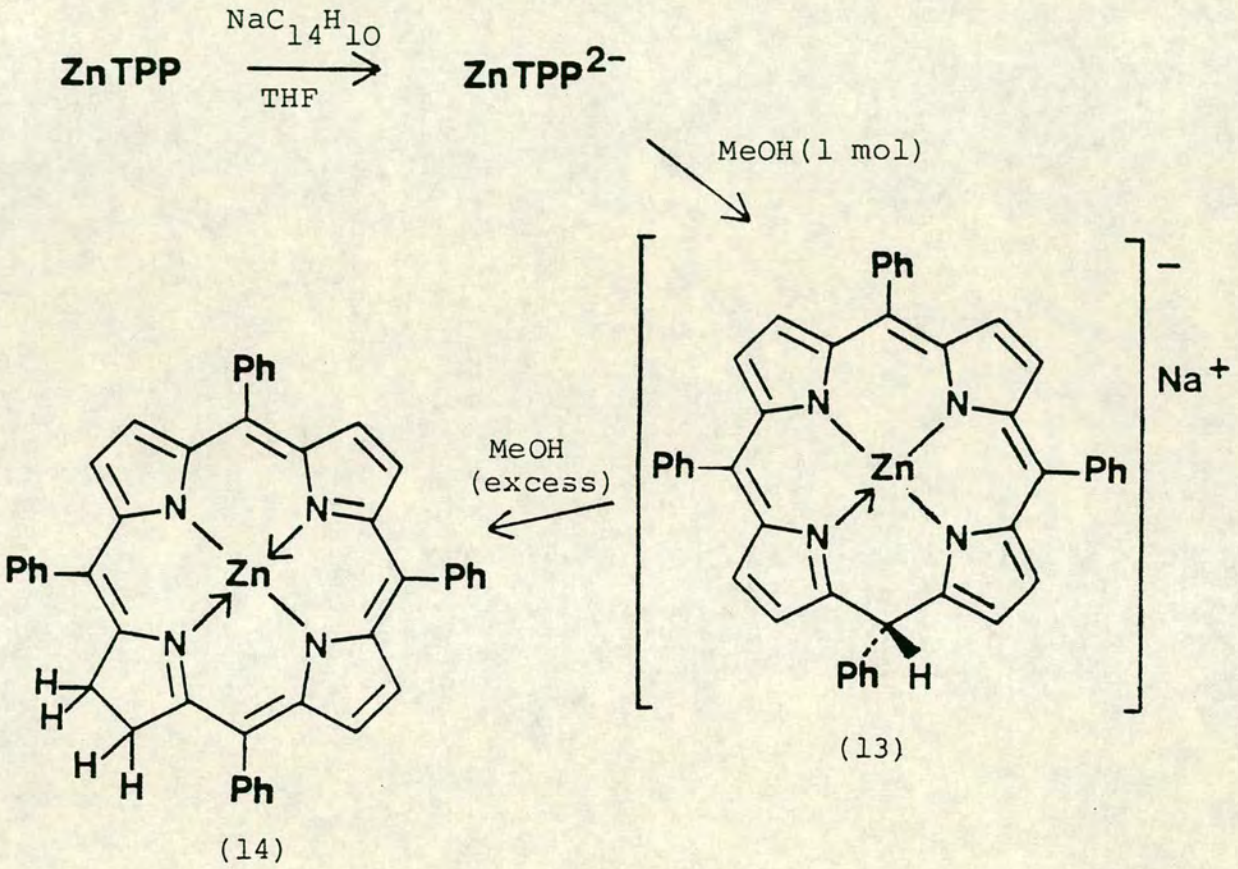

Scheme C.3:- Stepwise Reaction of the π-dianion, $ZnTPP^{2-}$, with Methanol

Extensive investigations on the reactivity of the π-dianions of a large series of metallooctaethylporphins have been conducted by the Buchler group. Initial study concerned the reaction of the chemically generated π-dianions, $MOEP^{2-}$, with excess methanol.[20] These reactions, when carried out in sealed tubes, gave orange-red species that were assigned as

the α,γ-dihydroxyporphyrins (15). These structures are commonly referred to as porphodimethenes. These species, which had electronic spectra with bands at ca. 460 and 580 nm, were air-labile, reverting to the parent metalloporphyrin on atmospheric exposure. The metalloporphodimethenes (15) in turn slowly converted to a mixture of cis and trans chlorins (16), and some tetrahydroporphyrins over a period of days. The reactions observed are summarised in Scheme C.4.

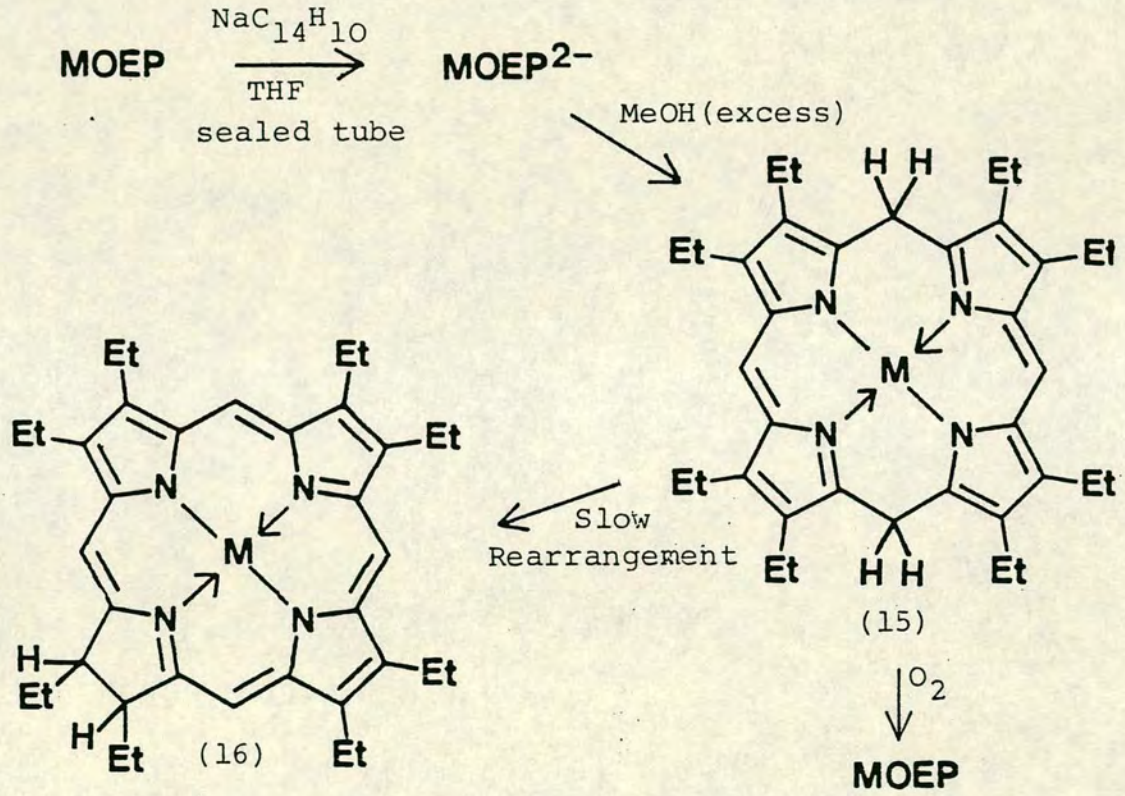

Scheme C.4:- General Reaction of $MOEP^{2-}$ with Methanol

In this study 17 different metals were used, 14 of which had complexes that successfully converted to (15). Only some of these, however, rearranged to the chlorin (16) and this rearrangement took place at vastly differing rates. A

study of this rearrangement at elevated temperatures showed that the zinc porphodimethene rearranged to the chlorin markedly faster than the other systems. In general, rearrangement was faster for divalent metal complexes than for systems containing metals in higher valence-states.

This work was extended to study the reaction of the π-dianion, $ZnOEP^{2-}$, with methyl iodide.[21] The product of this reaction has a similar electronic spectrum to the porphodimethene (15) previously observed, implying that an α,γ-dimethylporphodimethene (17) has been formed.

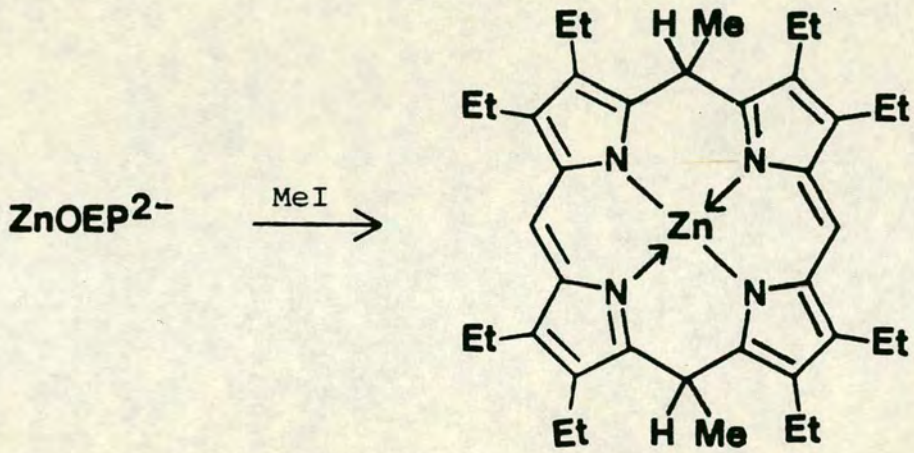

(17)

The structural confirmation of (17) was performed using ^{1}H and ^{13}C n.m.r., i.r. and mass spectroscopy on this air stable compound. (17) showed no tendency, even at elevated temperatures, to rearrange to a chlorin.

Demetallation of (17) was achieved using weak mineral acids, to give the free-base α,γ-dimethylporphodimethene. The free-base was unstable in air, losing H_2 and electrons to give the α,γ-dimethyl-octaethylporphin, but nonetheless was isolated and successfully complexed to nickel and copper.

A later study[22] reported direct formation of many of these metallo-dimethylporphodimethene complexes by addition of methyl iodide to the $MOEP^{2-}$ π-dianions. Yields varied for different metals but ranged from 5% for Pt(II) complexes, to ca. 40% for Ti=O and Zn complexes. No systematic explanation for the different yields obtained was offered. None of these complexes showed any tendency to rearrange to chlorins in contrast to the parent systems (15). An X-ray crystallographic study[23] on the nickel(II) dimethylporphodimethene showed that the conformation of the methyl groups in this complex is syn-axial. This finding was in agreement with the predictions based on the n.m.r. spectra of this daughter complex and the corresponding zinc complex (17).

Gurinovich and Sinyakov[24] have studied the reactivity of different alkyl halides with the π-dianions generated by the addition of sodium anthracenide to zinc etioporphyrin I (18) and zinc octamethylporphin (19).

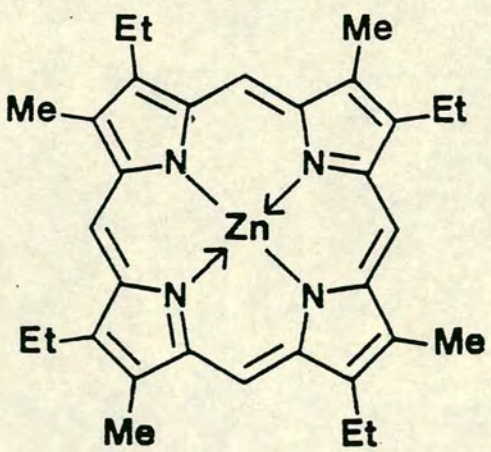

(18) Zn Etio(I)

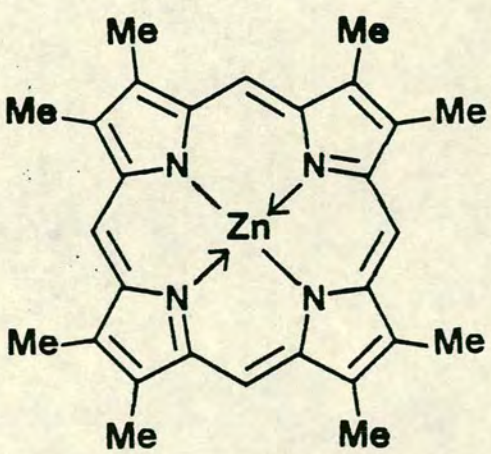

(19) ZnOMP

Reaction of these π-dianions with methyl iodide resulted, in each case, in the formation of α,γ-dimethylporphodimethenes. During purification, however, very small amounts (< 1%) of a species with an electronic spectrum similar to that of a metallochlorin were detected. Further reactions of the π-dianion, $ZnOMP^{2-}$, with ethyl iodide and propyl iodide led to detection of this by-product in 5-7% yield. Reaction of $ZnOMP^{2-}$ with ethyl bromide, however, yielded this metallochlorin-like complex as the major component of the product mixture. The ^{1}H n.m.r. spectrum of this complex showed the structure to be that of the zinc diethylchlorin (20).

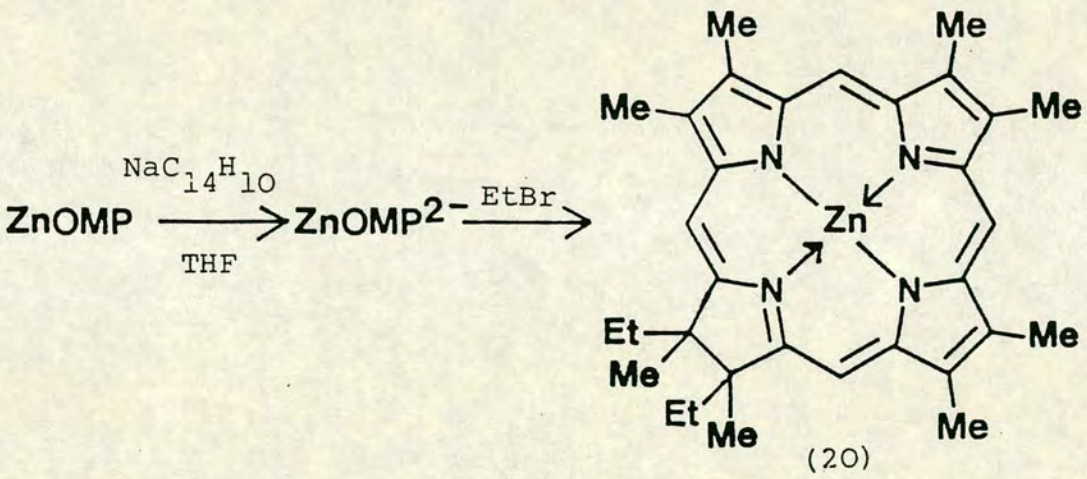

(20)

As attack of EtBr to form (20) happened considerably more slowly than the previously observed formation of dialkylporphodimethenes under similar conditions it was proposed that the mechanism of formation of (20) involved direct attack of the ethyl groups on the pyrrolic carbon atoms. This mechanism differs from the alternative one in which a diethylporphodimethene is formed initally, which then rearranges to give (20).

Reactions of Metalloporphyrin π-cations

Dolphin et al.[25] reported the first peripheral reaction of a metalloporphyrin π-cation. This involved the irreversible reaction of the electrochemically generated π-dication, $ZnTPP^{2+}$, with methanol. This reaction formed an olive-green solution of a stable compound that was identified by ^1H n.m.r., i.r. spectroscopy and electrophoresis as the metalloisoporphyrin salt (21).

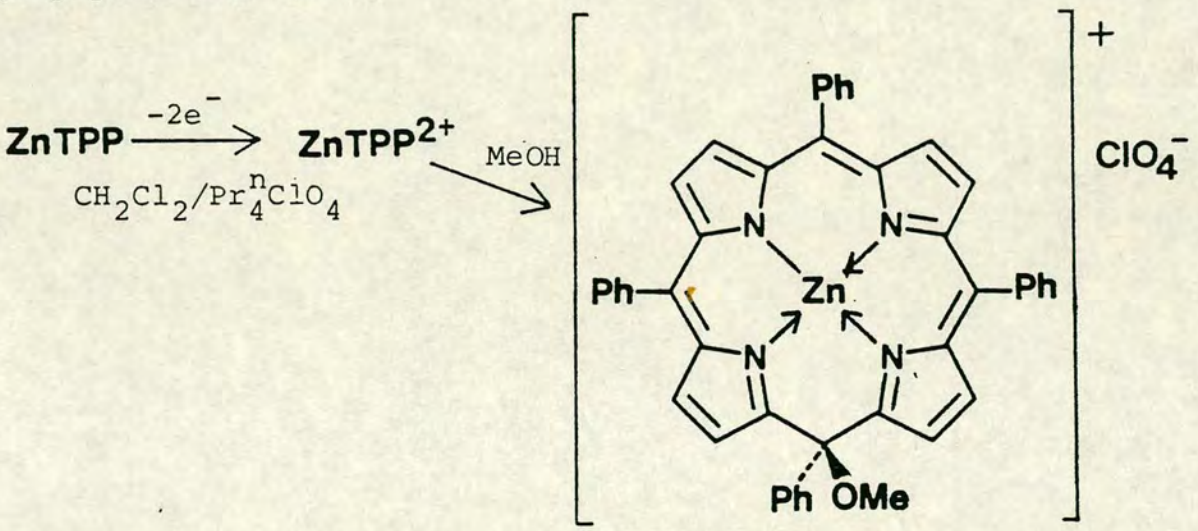

(21)

The electronic spectrum of (21) has two overlapping bands in the region between 700 and 900 nm and several more in the uv region. These all have extinction coefficients less than $4x10^4\ M^{-1}cm^{-1}$, indicating disruption of the 18 π electron aromatic pathway in the parent metalloporphyrin. This is supported by the ^1H n.m.r. spectrum which shows that the resonances of the pyrrolic protons consist of two AB multiplets at frequencies considerably upfield to those of the parent compound. (21) is stable in glacial acetic acid, but addition of potassium iodide to a solution of this type causes demetallation to occur.

There are several other instances where metalloisoporphyrin structures like (21) have been isolated. Guzinski and Felton[26] have reported that overall 2-electron electrooxidation of Fe(III)TPPCl in a 1% methanol in dichloromethane solution yields the ferric methoxyisoporphyrin (22). The proposed mechanism involved initial formation of an Fe(IV) species followed by internal electron-transfer to the macrocycle as outlined in Scheme C.5.

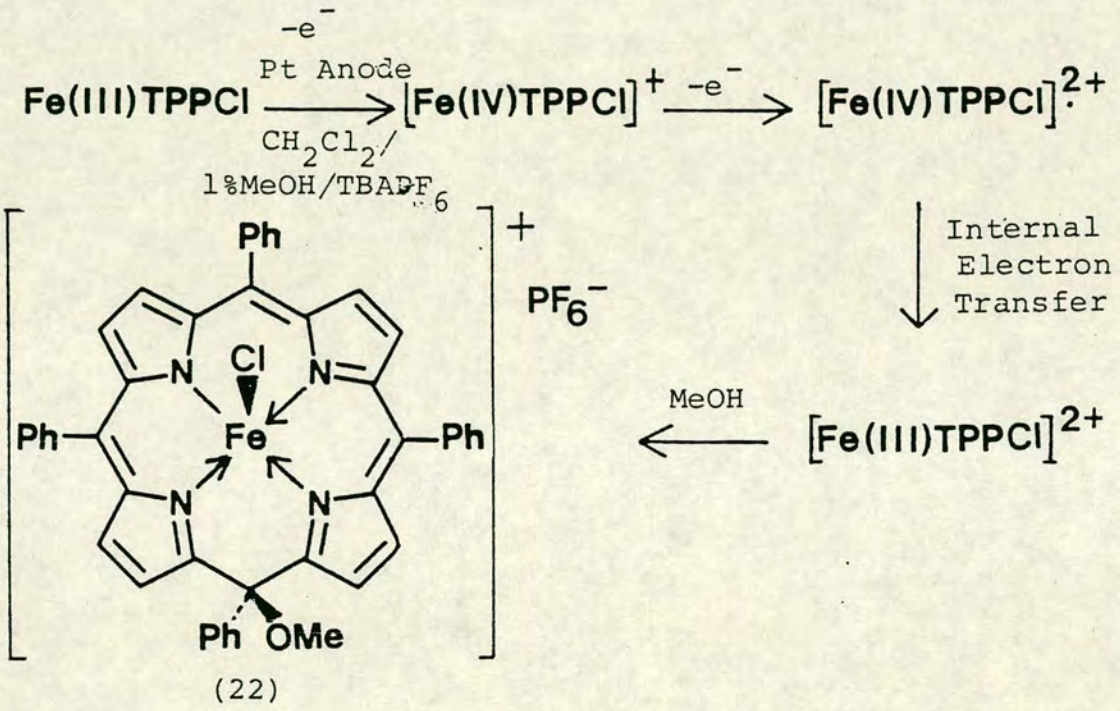

(22)

Scheme C.5: Electrooxidation of Fe(III)TPPCl in the presence of Methanol

In addition to the characteristic isoporphyrin electronic spectrum with broad absorbances in the near i.r. and uv regions, structural elucidation of (22) was aided by the use of deuterated methanol CD_3OD. The i.r. spectrum of the deuterated isoporphyrin remained unchanged on treatment with HCl, indicating that the methoxy group was attached to the porphyrin

periphery rather than axially bound to iron. Two-electron reduction of (22) in protic media (methanol) led to reformation of Fe(III)TPPCl.

Dolphin et al.[16] have invoked such an isoporphyrin complex in an electrochemical study of the oxidative behaviour of Ni(II)TPP. Addition of methanol to the product of two-electron oxidation led to the observation of a metalloisoporphyrin type electronic spectrum. This result was used to imply that this oxidation product was the π-dication $NiTPP^{2+}$.

The most recently reported isolation of a metalloisoporphyrin, by Gold et al.[27] involved chemical oxidation of iron(III) tetra(-4-methoxyphenyl)porphin chloride (23) by t-butyl hydroperoxide. The reaction involved oxidation of (23) to its π-dication followed by nucleophilic attack on this by the t-butylperoxy anion to give the isoporphyrin (24).

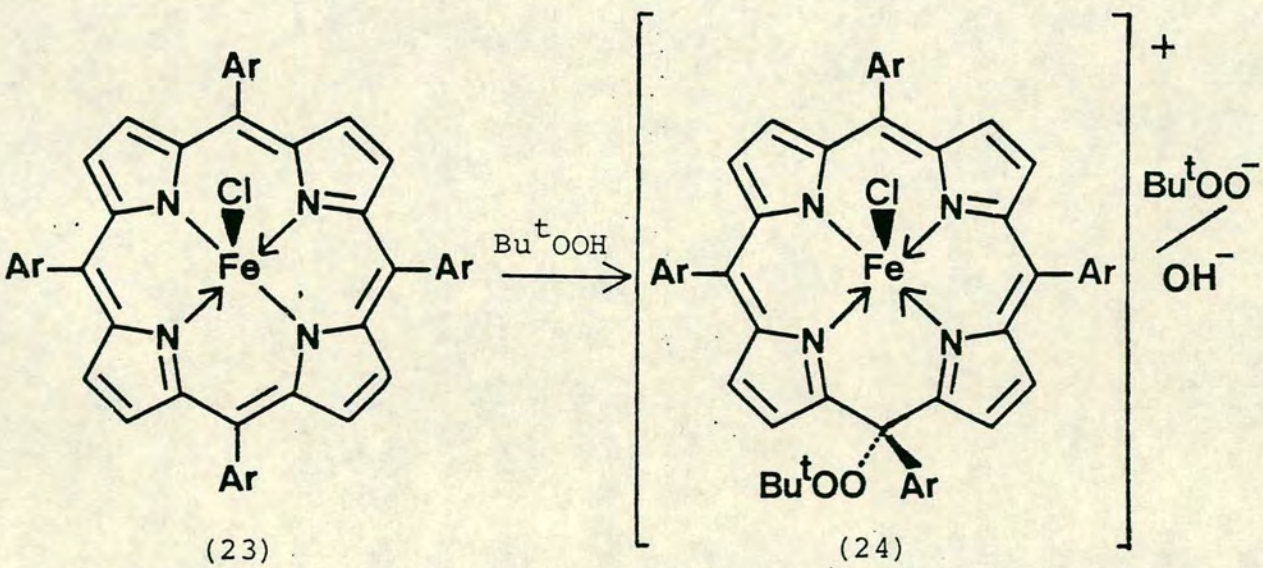

(23) (24)

Ar = 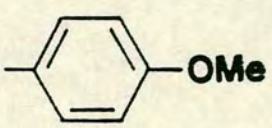

The counter-ion present in (24), as isolated, was stated to be a 50:50 mixture of hydroxy and t-butoxy anions. Structural characterisation of (24) was carried out using elemental analysis, ^{1}H n.m.r. and, critically, by a F.A.B. mass spectrum of the isoporphyrin cation. The F.A.B. ionisation method ensures that the mass spectra of cations and anions, unattainable using conventional electron impact ionisation techniques, can be readily recorded.

All reports of stable metalloisoporphyrins relate to meso-substituted porphyrin precursors. In contrast to these examples, reaction of Zn(II)OEP with thallium(III) trifluoroacetate[28] led to formation of the π-dication, $ZnOEP^{2+}$, followed by attack of the trifluoroacetyl anion to form an unstable isoporphyrin (25). (25) rapidly lost a proton to give the meso-trifluoroacetyl porphyrin (26) according to the mechanism shown in Scheme C.6.

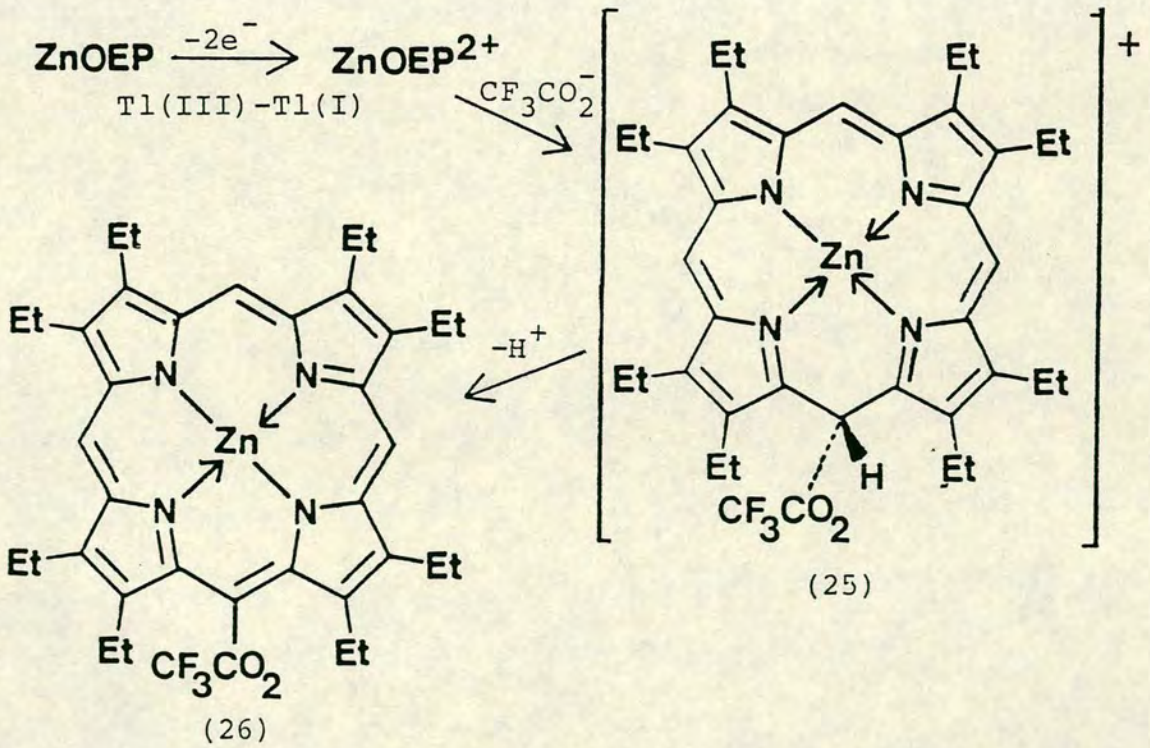

(25)

(26)

Scheme C.6: Formation of Trifluoroacetyl substituted Porphyrin (26) via the Isoporphyrin (25)

Thus it appears that nucleophilic attack on metalloporphyrin π-dications leads quite generally to formation of the respective isoporphyrins, but in the case where only protons are present on the meso positions these complexes rapidly undergo loss of protons to give the meso-substituted metalloporphyrin.

In contrast to the reactivity of metalloporphyrin π-dications described above, it was thought[29] that the less oxidised metalloporphyrin π-radical-cations were unreactive toward nucleophiles. Since 1975, however, there have been several reports of the reactivity of metalloporphyrin π-radical-cations toward a wide variety of nucleophiles.

Smith et al.[30-33] have reported the reaction of magnesium, zinc and cadmium octaethylporphin π-radical-cations with various nucleophiles. The successful reactions in this study have formed meso-substituted metalloporphyrins. The general procedure for these reactions involves initial generation of the π-radical-cation by addition of a chemical oxidant. Chemical oxidants used have included silver nitrite, iodine and 1-chlorobenzotriazole. Oxidation was then followed by addition of a methanolic solution of the nucleophile. A typical example of the type of reaction reported is the oxidation of MgOEP to its π-radical-cation with iodine followed by addition of sodium nitrite. This reaction resulted in the preparation of meso-nitro-MgOEP (27) in 84% yield.

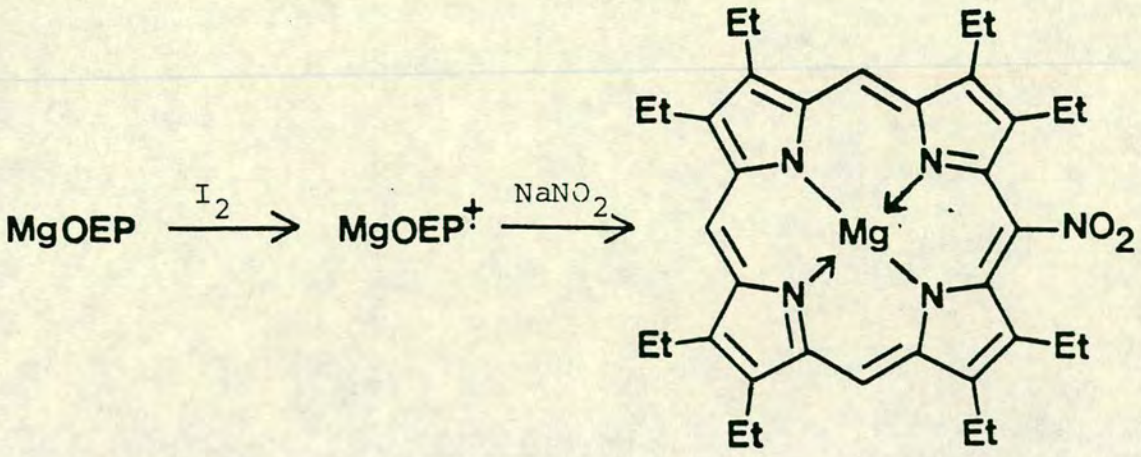

(27)

Cadmium, zinc and magnesium porphyrins were utilised in these studies because of their low oxidation potentials and their ease of demetallation. Facile demetallation enables coordination of the peripherally altered free-base porphyrin to a wide range of metals, broadening the synthetic scope of these reactions. The nucleophiles successfully introduced in these studies, were nitrite, chloride, pyridine, imidazole, acetoxyl, cyanide, triphenylphosphine and thiocyanate. In some cases, particularly those involving nitration, di-substitution was observed. This generally takes place on the meso position opposite to the one already substituted.

The mechanism proposed for these reactions involves the nucleophile coupling with the metalloporphyrin π-radical-cation to give a radical species. This is then subject to further oxidation, forming the isoporphyrin cation which itself loses a proton to give the meso substituted porphyrin as outlined in Scheme C.7.

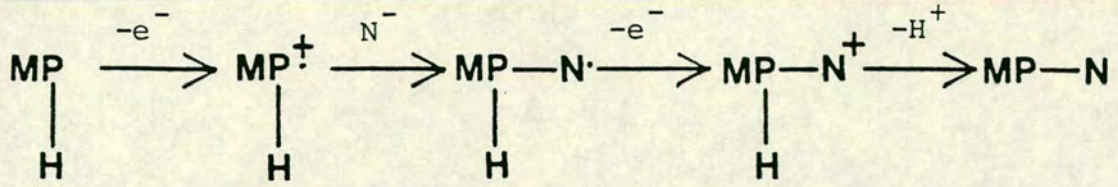

Scheme C.7: Reaction of nucleophile (N^-) with Metalloporphyrin (MP-H) π-radical-cation

Substitution at the outer pyrrolic carbon atoms of a metalloporphyrin was first reported by Shine, Padillo and Wu[34] for the reaction of pyridine with the chemically generated π-radical-cation, $ZnTPP^{+\cdot}$. Addition of pyridine formed the pyrrole-substituted pyridinium salt (28) in 36% yield.

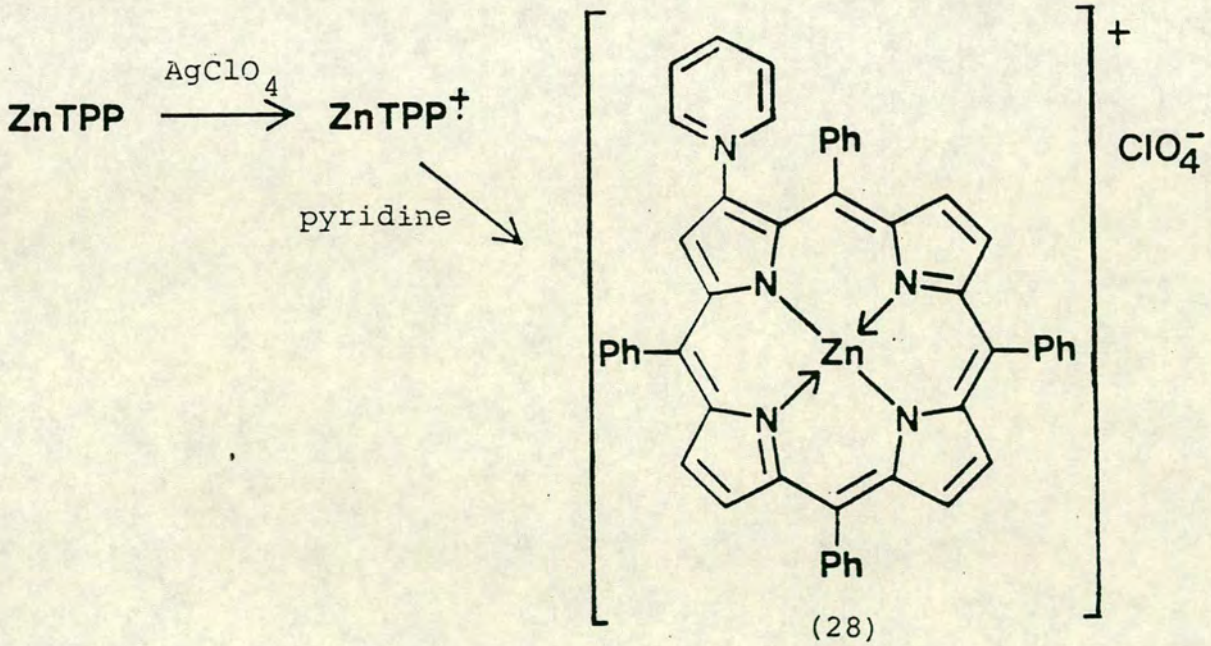

(28)

Baldwin and Crossley[35] have reported similar examples of pyrrole substitution of zinc meso-tetraaryl porphyrins. Reaction of the zinc "capped" porphyrin (29), with iodine gave its π-radical-cation which then reacted with silver

nitrite to give the pyrrole substituted nitro-porphyrin (30) in 98% yield.

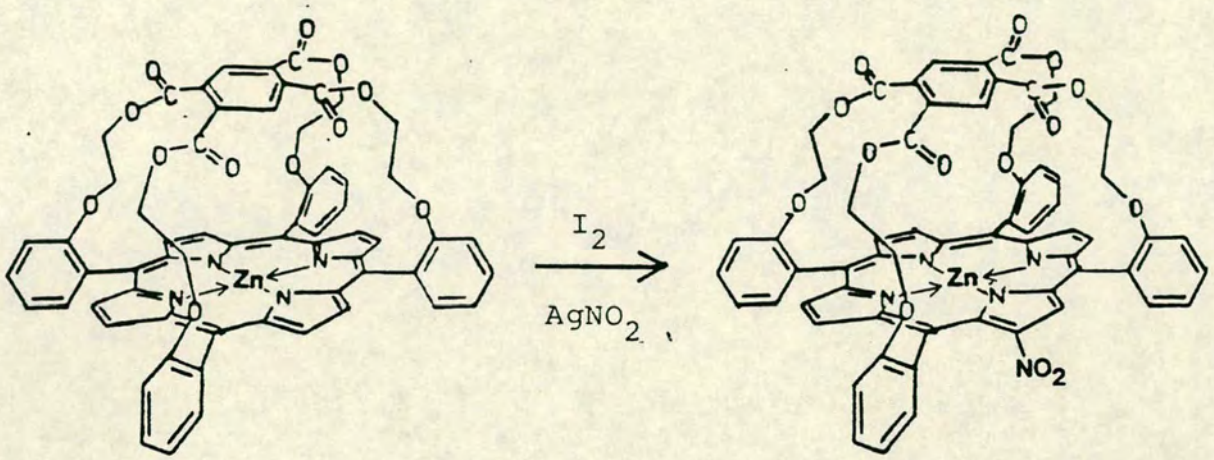

(29) (30)

Similar reaction, using Zn(II)TPP, led to formation of the pyrrole substituted nitro-porphyrin in 51% yield. The lower yield of nitrated product was attributed to the greater steric hindrance of the freely rotating phenyl groups in Zn(II)TPP compared to (29) where these are held rigid.

Further study showed that the reaction, under similar conditions, of a zinc "strapped" porphyrin (31), in which two of the meso carbon atoms are protonated and the other two are phenyl substituted, led to exclusive formation of the meso-nitrated porphyrin (32).

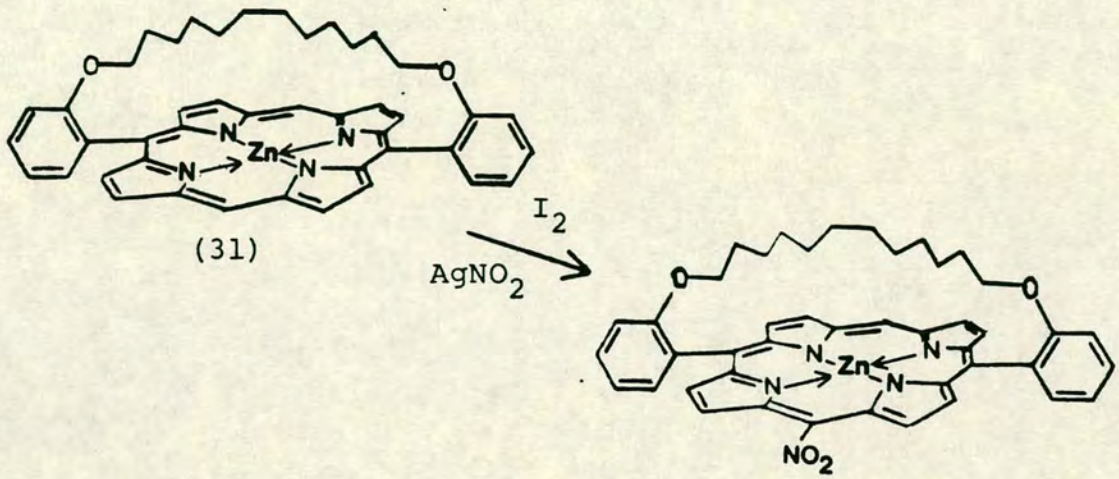

(31) (32)

This result led to the postulate that meso-substitution is the preferential reaction in the nucleophilic substitution of metalloporphyrin π-radical-cations, and that substitution of the outer pyrrolic carbon atoms only occurs when all the meso positions are apparently blocked.

A later study by Crossley[36] on the nitration of some metallotetraphenylporphin π-radical-cations attempted to elucidate the products obtained, and the yields of these, with the electronic ground states of the π-radical-cations. The reaction studied involved passing a stream of nitrogen-dioxide through a solution of the particular compound. NO_2 is both an oxidising agent and a nucleophile, although it was the radical species $NO_2\cdot$ that was said to attack the metalloporphyrin periphery. These reactions produced the pyrrole substituted nitro-porphyrin (33) and the ring-opened demetallated bilinone (34).

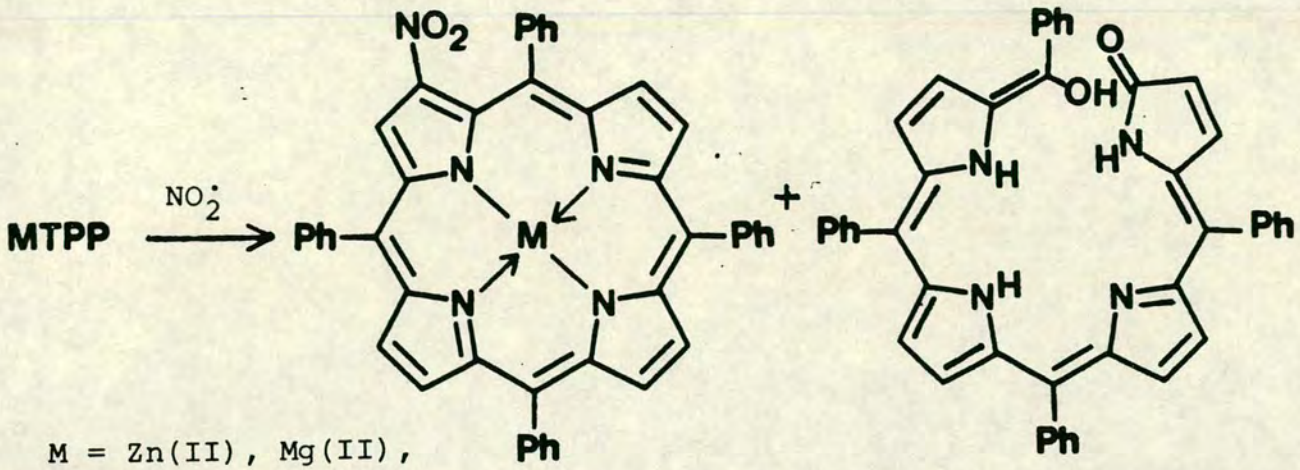

M = Zn(II), Mg(II), Cu(II), Ni(II), Pd(II)

(33) (34)

Direct attack of $NO_2^{\cdot}$ on the pyrrole carbon atoms would give (33), as was obtained exclusively for the Cu(II), Ni(II) and Pd(II) complexes, while direct attack on the meso carbon atoms was said to result in (34) which was obtained as a minor product (~30%) for the Zn(II) and Mg(II) complexes. It was stated that exclusive formation of (33) was caused by the electronic ground state of the π-radical-cation having a $^2A_{2u}$ ground state, which has large spin density on the pyrrole carbon atoms, while formation of (34) arose from the π-radical-cation having a $^2A_{1u}$ ground state. The latter ground state has most of its spin density residing on the meso carbon atoms. No spectroscopic evidence was presented to support this assertion.

The oxidative ring opening of zinc porphyrins to form bilinones has previously been observed. Smith, Cavaleiro and Evans[37,38] have reported the oxidation of Zn(II)TPP with Thallium(III) Trifluoroacetate. This reaction, followed by work-up with trifluoroacetic acid, resulted in the formation of (34) plus some of the α,γ-dihydroxyporphodimethene (36).

The proposed reaction mechanism shown, in simplied form, on Scheme C.8 involves formation of the π-dication, $ZnTPP^{2+}$, which then reacts with trifluoroacetyl anion to give the isoporphyrin (35). This is itself subject to further nucleophilic attack to give the final products (34) and (36) which were both identified by their ^1H n.m.r. spectra. Reinsertion of zinc was possible with (34), but attempted metallation of (36) resulted in a metalloisoporphyrin being formed through elimination of one of the two hydroxyl groups.

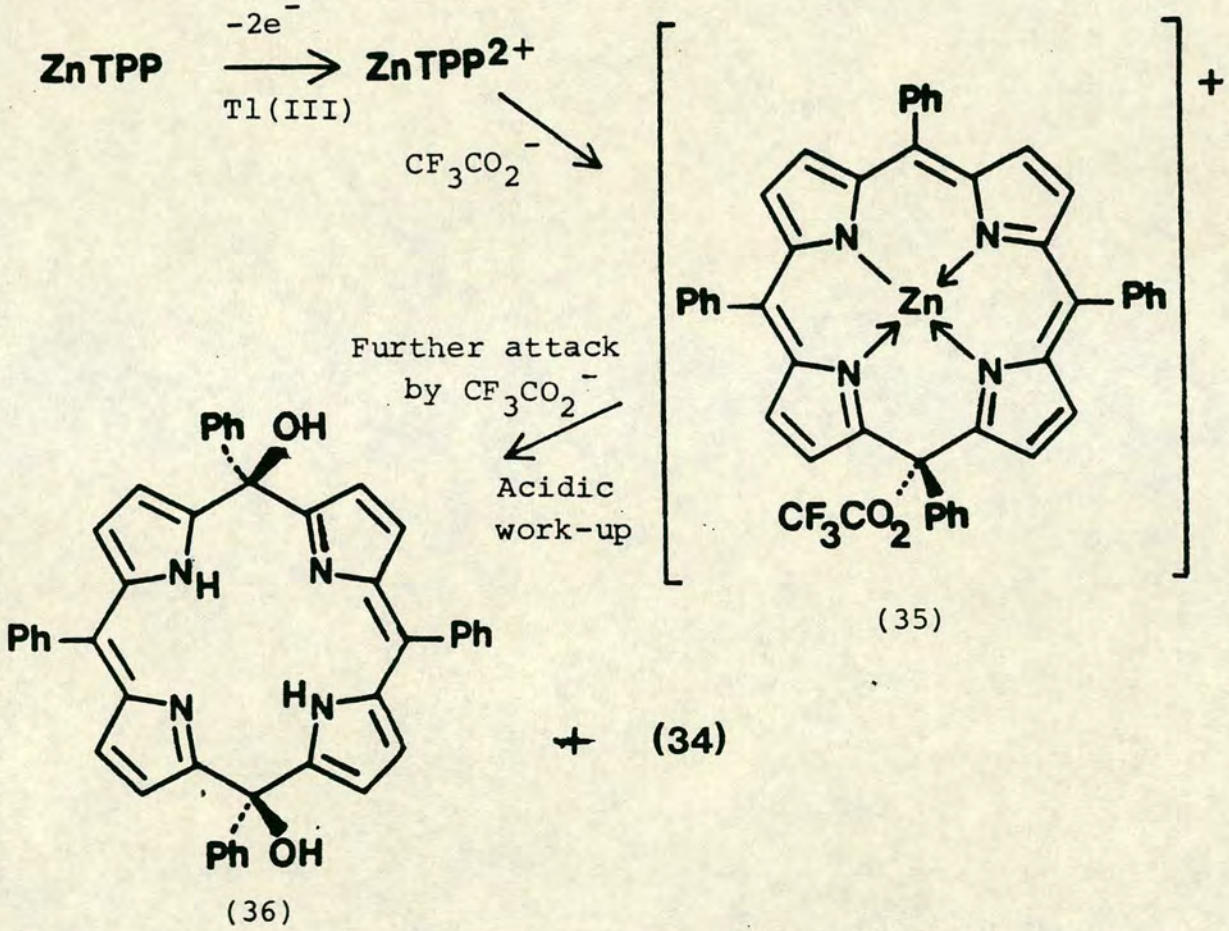

(35)

(36)

Scheme C.8: Oxidative Attack on Zn(II)TPP by $Tl(III)(CF_3CO_2)_3$

All the reactions of π-radical-cations of metalloporphyrins described so far have involved chemical oxidations. Bonnett and Martin[39] have reported analogous behaviour for the electrochemically generated π-radical-cation, $ZnOEP^{\cdot+}$, fully

in keeping with the reactivity reported earlier by Smith et al.[30-33] Callot, Louari and Gross[40,41] have successfully prepared mono , di, tri and tetra meso-cyano substituted Zn(II)OEP derivatives by electrooxidation of Zn(II)OEP in DMF/tetraethylammonium cyanide. Control of the level of addition of nitrile groups to the macrocyclic periphery was achieved by steadily increasing the potential, such that the oxidation potential selected was that of the particular π-radical-cation $ZnOEP(CN)_n^{+\cdot}$.

Photo-oxidation[42,43] of the water-soluble metallotetraaryl porphyrins (37) has resulted in the occurrence of peripherally altered macrocycles.

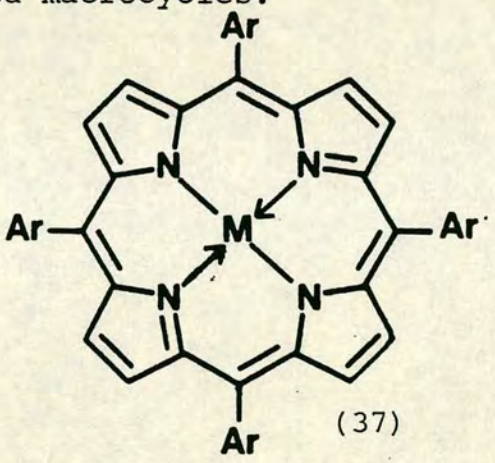

(37)

M = Zn(II), Pd(II), $Sn(IV)Cl_2$.

For zinc complexes of this type, photolysis of an aqueous solution of pH 1.6 results in the formation of the π-dication. At pH's greater than 8.0, however, the spectrum changes to that of an isoporphyrin, presumably due to the coordination of hydroxide to the macrocycle. In contrast, photolysis of the palladium complexes, at pH 5.0, resulted

in the formation of a species with a maximum in its electronic spectrum at 655 nm. This product which decomposed rapidly ($t_{\frac{1}{2}} \sim 3$ min.), was not observed at lower pH's, but had longer lifetimes at higher pH values. No assignment of the structure of this complex was made, although the possibility of a Pd(II)$\rightleftharpoons$Pd(IV) couple, as has previously been postulated[29] for palladium porphyrins, was inferred.

Photo-oxidation of Sn(IV)TMPPCl$_2$ was reported to follow a long mechanistic sequence ultimately forming a chlorin. This reaction at pH 2.6, which was subject to spectral monitoring, initially gave the π-dication which then reacted with hydroxide to form the isoporphyrin (38). Further attack of hydroxide was then observed and the isoporphyrin spectrum of (38) changed to one with maxima at ∿420 and 620 nm. On the basis of the electronic spectrum this product was assigned as the dihydroxychlorin (39). This itself was observed to slowly decompose to a colourless product which was thought to be the ketoporphyrin (40). The proposed mechanism is illustrated in Scheme C.9

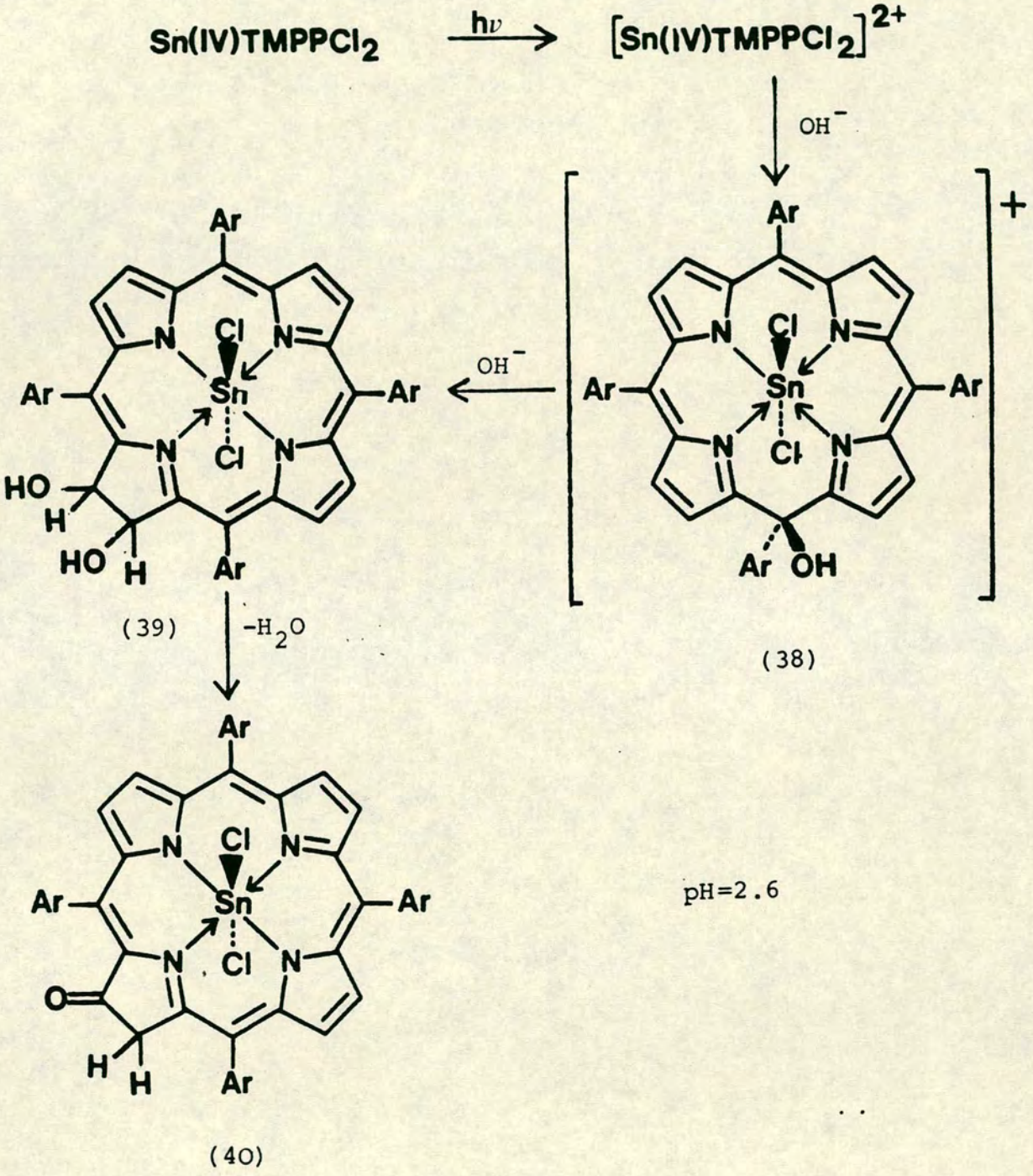

Scheme C.9: Photo-oxidation of Sn(IV)TMPPCl$_2$

C.2 Discussion

C.2-1 The Electrochemical Behaviour of the d^8 Metallo-Octaethylporphins and Tetraphenylporphins

Previous electrochemical studies on metalloporphyrins have focussed sometimes on those systems containing central metals of individual importance due to their occurrence in natural systems e.g. Fe, Co, and sometimes on broader series of complexes. Where wider ranges of metals have been examined, these studies have sought to explore general relationships encompassing the redox behaviour of different metalloporphyrins. These studies have emphasised metals of the first transition series and other light metals e.g. Zn, Al, while comparatively little is known about the electrochemical behaviour of complexes of the 2nd and 3rd transition series.

The present study examines systematically the electrochemistry of the nickel(II), palladium(II) and platinum(II) octaethylporphins and tetraphenylporphins for a number of reasons. Hitherto, comprehensive electrochemical measurements, particularly on the $4d^8$ and $5d^8$ systems have been either incomplete, missing altogether, or the subject of an inconsistency in the literature. (For example, separate studies,[44,45] over the same voltage range, on the reductive behaviour of Pt(II)TPP report four reductions in one case and only two in the other.) In addition, the comparative data for these, square-planar, $3d^8$, $4d^8$ and $5d^8$ systems should give new insight into the interactions occurring between the transition

metal and porphyrin macrocycle whereby the redox potentials for macrocycle-centred electron transfers are influenced by the nature of the central metal.

This is apparently the first study directed to the redox behaviour of an isostructural series of metalloporphyrins containing all three members of one transition metal triad. The $3d^8$, $4d^8$ and $5d^8$ metals under study form the most suitable triad for such internal comparisons. Aside from these, there is a general scarcity of isostructural metalloporphyrins containing all the members of one transition metal triad with the same ligands and in the same oxidation state.

Results

The nickel(II), palladium(II) and platinum(II) octaethylporphins and tetraphenylporphins were synthesised and purified by the methods detailed in C.3-1. Voltammetry of these complexes was carried out in a three-electrode cell, using a platinum mini-disc working electrode, in a dichloromethane/tetrabutylammonium fluoroborate solution. Half-wave potentials for these complexes, and the corresponding free-base and zinc compounds, were obtained using cyclic and A.C. voltammetry. The voltammograms of the zinc and free-base porphyrins were recorded, under similar conditions, so that the data for the transition metal species might be compared with that for the macrocycles binding Zn^{2+} (d^{10}) and $2H^+$.

The values obtained are listed in Table C.1. The cyclic and A.C. voltammograms of a typical member of this series, Pd(II)OEP, are presented in figure C.13. This illustrates

Table C.1: Redox potentials of MOEP and MTPP compounds studied

Complex	$E_{\frac{1}{2}}$				
	Ox			Red	
	3	2	1	1	2
H_2OEP		1.16	0.66	-1.54	-2.00
ZnOEP		0.74	0.44	-1.76	-2.22
NiOEP	1.50	1.08	0.56	-1.68	-2.28
PdOEP		1.31	0.63	-1.75	-2.40
PtOEP	1.78	1.40	0.68	-1.78	-2.44
H_2TPP		1.00	0.76	-1.41	-1.77
ZnTPP		0.86	0.60	-1.57	-1.94
NiTPP	1.49	1.01	0.77	-1.49	-2.06
PdTPP		1.27	0.84	-1.54	-1.98
PtTPP	1.54	1.31	0.82	-1.56	-2.04

$E_{\frac{1}{2}}$ vs Ag/AgCl reference electrode

$E_{\frac{1}{2}}$ values measured on platinum mini-disc working electrode in CH_2Cl_2/0.5M $TBABF_4$

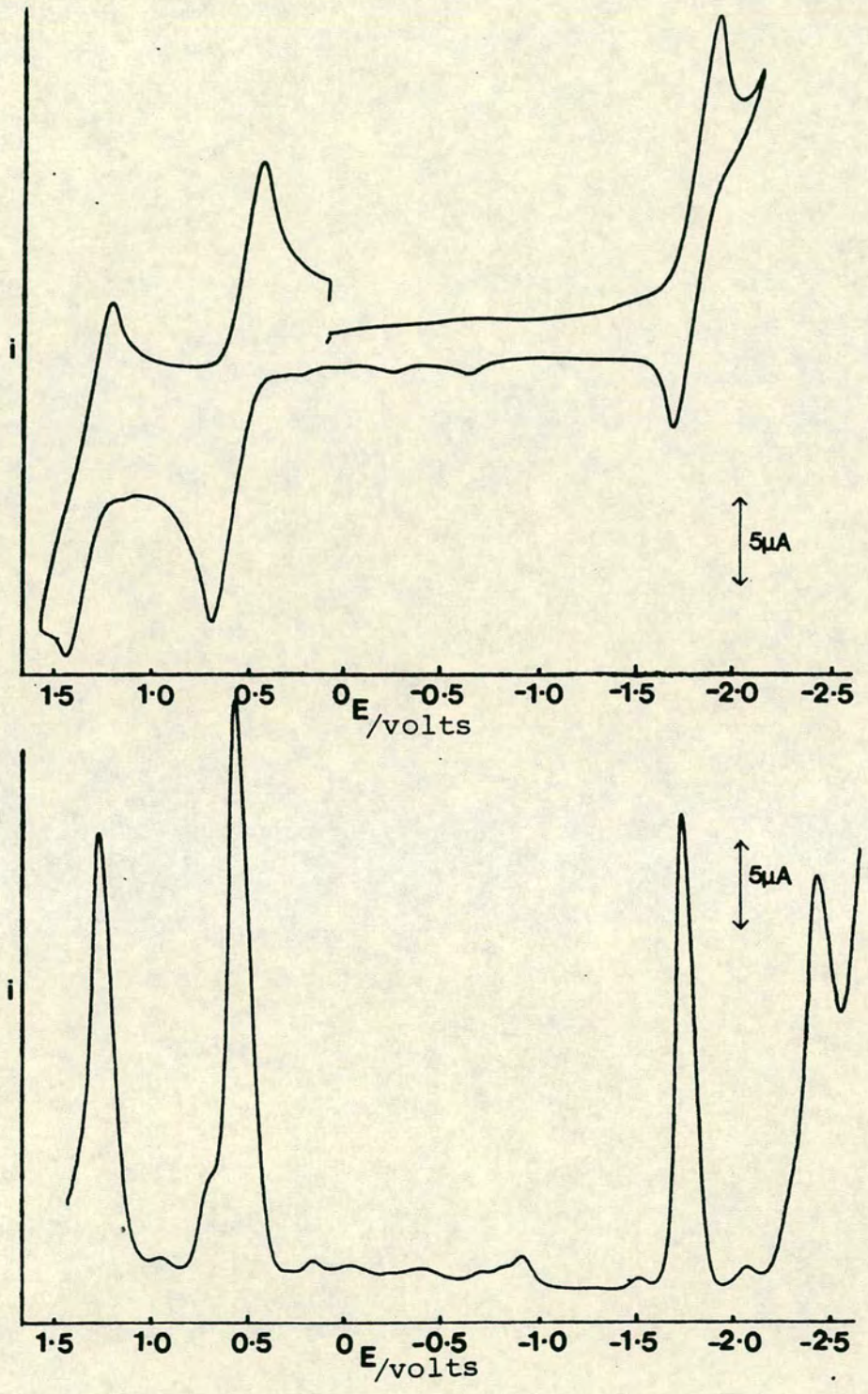

Figure C.13: Cyclic and A.C. Voltammograms of PdOEP

Potential vs Ag/AgCl reference electrode

CH_2Cl_2/0.5M $TBABF_4$

the usefulness of A.C. voltammetry for detecting electrode processes that occur at more extreme potentials than can be observed by cyclic voltammetry. This has resulted in many second oxidations and second reductions of the species in this study being observed for the first time.

Direct spectroscopic characterisation of electrogenerated products was used to assign the site of electron-transfer on the metalloporphyrin as either the metal or macrocycle. This entailed controlled potential electrolysis at an optically transparent electrode, accompanied by in situ monitoring of the electronic spectrum. Where necessary such assignments were supported by coulometry and/or e.s.r. spectroscopy. In fact, these assignments showed that simple, macrocycle-based, reversible electron-transfers forming π-radical-cations, π-dications, π-radical-anions and π-dianions generally prevail. The following important exceptions were found:-

(i) The first oxidation of Pt(II)TPP involves a metal-centred redox process. (Section C.2-2)

(ii) The second oxidation of Pd(II)TPP and third oxidation of Pt(II)TPP (i.e. its second macrocyclic ligand oxidation) result in the formation of the π-dication which rapidly undergoes an irreversible solvolysis reaction at 25°C. (Section C.2-3)

In addition to these, the third oxidation waves observed for NiTPP, NiOEP and PtOEP remain, as yet, unassigned. It is likely, however, that these electron-transfers involve new species formed by disproportionation or decomposition of the preceding π-radical-cation or π-dication.

Full characterisation of the electronic spectra of all these electrogenerated species has been made in a parallel complementary study[46] in our laboratory. This study also detected the thermally controlled valence isomerism of $[NiTPP]^+$ previously reported[16], where at low temperatures the cationic Ni(II)/π-radical complex transforms to a Ni(III)/unoxidised porphin complex.

The electronic spectra of the π-radical-cation, π-dication, and π-radical anion of PdOEP are illustrated in figure C.14.

The Influence of d^8 Transition Metals on Porphyrin Voltammetric Behaviour

The voltammetric results for correctly assigned and fully characterised electron transfer steps are graphically displayed in figure C.15. For illustrative purposes the redox potentials of the TPP series are systematically displaced by -0.21V, such that the first macrocyclic oxidations of the two nickel(II) porphyrins are made to coincide. This facilitates internal comparisons of the pattern of $3d^8/4d^8/5d^8$ metal influence.

This study set out to identify possible metal-macrocycle interactions which influence the porphyrin π and π* frontier orbital levels. It was hoped that study of trends in the redox potentials of a series of metalloporphyrins containing all the members of one transition metal triad would give further insight. Certainly it provided systematic data which was previously lacking and which runs counter to previous assumptions.

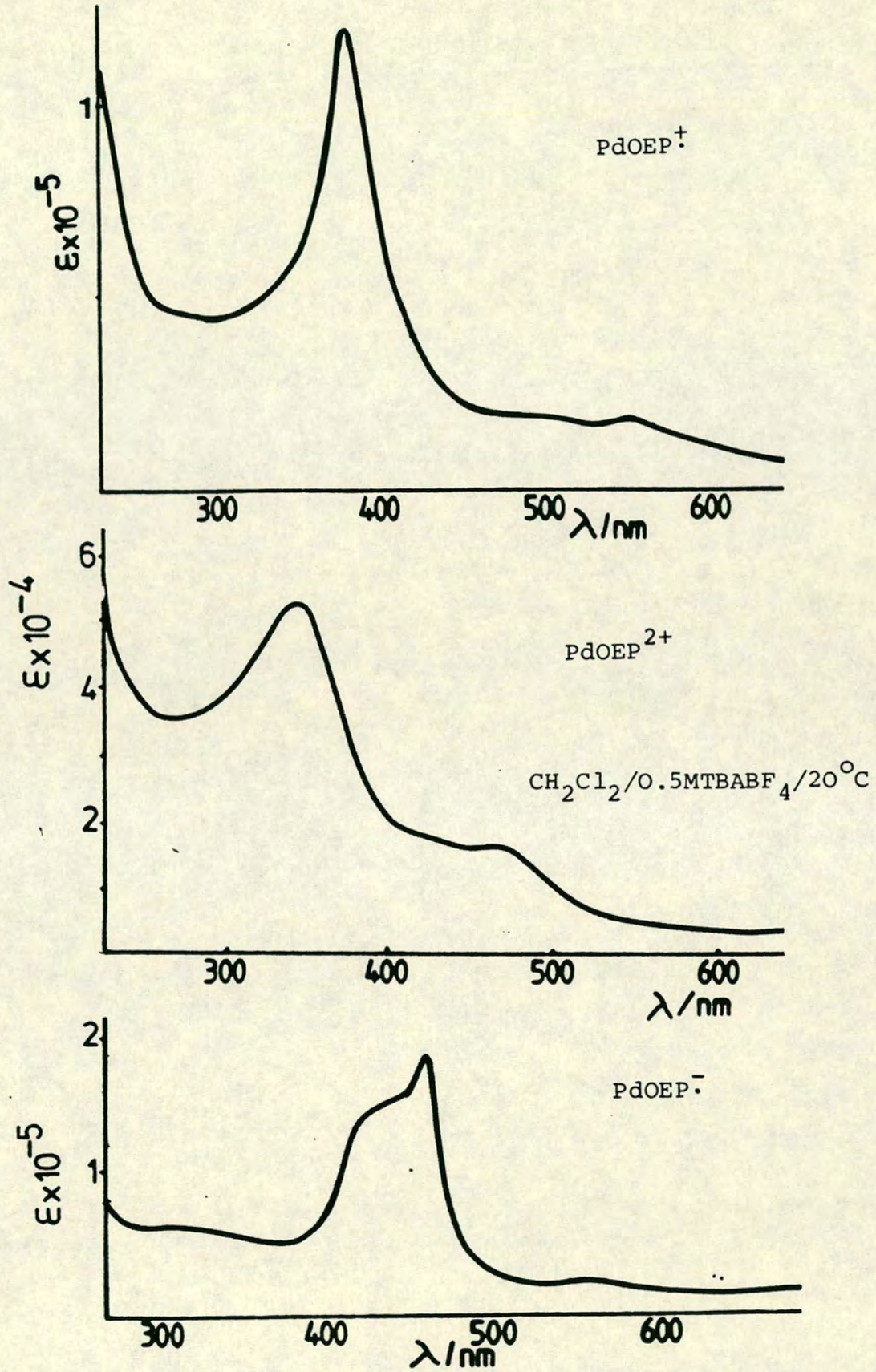

Figure C.14: Electronic Spectra of the π-radical-cation $PdOEP^{+\cdot}$, π-dication $PdOEP^{2+}$ and π-radical-anion $PdOEP^{-\cdot}$

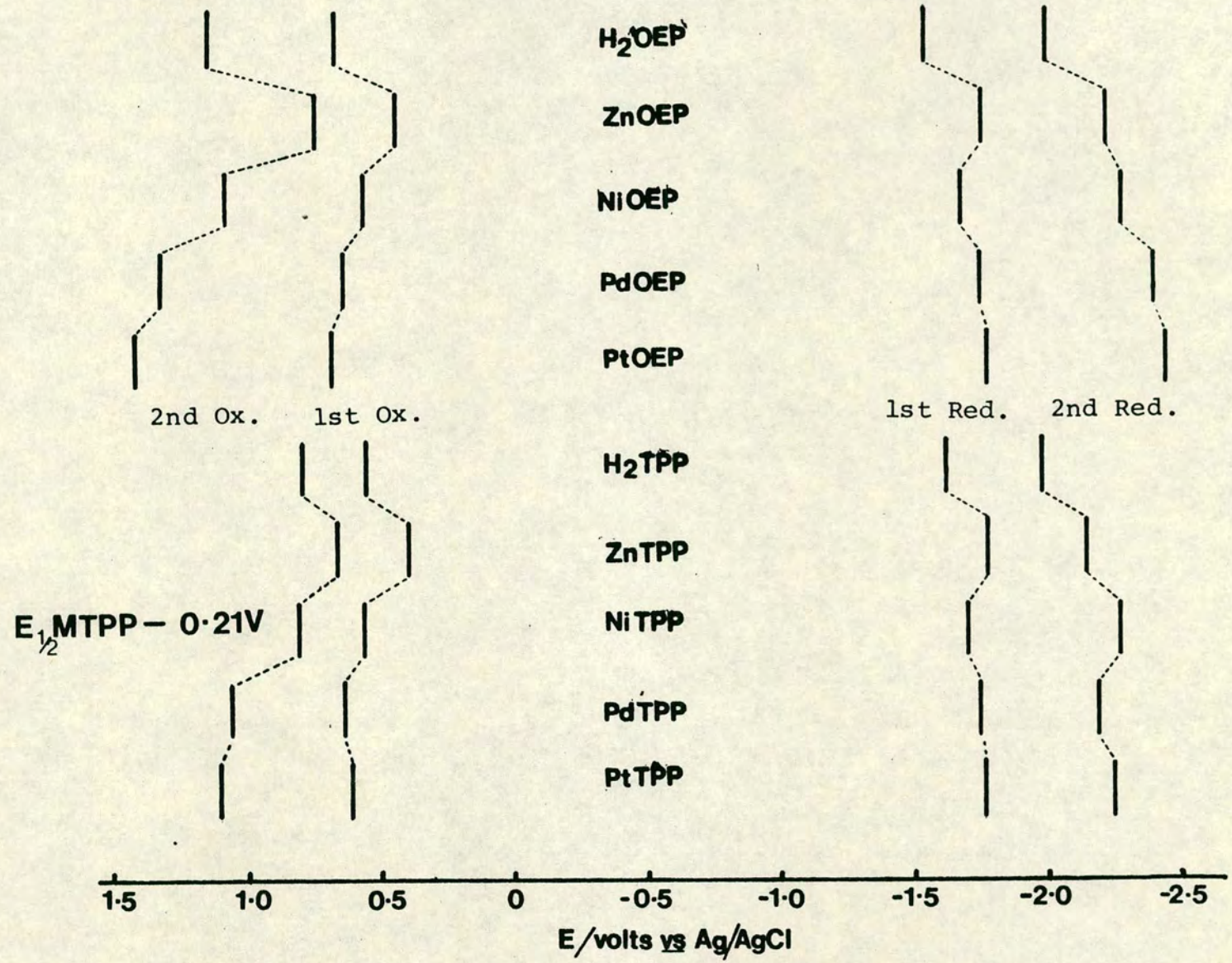

Figure C.15: Normalised Representation of MOEP and MTPP Redox Potentials

The most comprehensive study of this question, hitherto by Fuhrop, Kadish and Davies[11] proposed that the only influence that either main-group or transition metal ions have on porphyrin frontier orbital levels, as determined by macrocycle-centred redox potentials, is an inductive, essentially electrostatic, one. They proposed that the central metal, in a metalloporphyrin, acts as a point positive charge causing electrostatic interactions. This is reflected in the porphyrin πHOMO and π^* LUMO shifting in energies in the same direction by approximately equal amounts. For the subset of divalent metals, this postulate was backed up when linear plots were presented relating first macrocyclic based oxidation and reduction potentials to the electronegativity of the central metal.

Subjecting the $E_{\frac{1}{2}}$ *vs* electronegativity data of Fuhrop *et al* to least squares analysis, it is found that the gradients for the electronegativity/redox potential relationships are 0.21 ± 0.04 for the reductions, and 0.32 ± 0.04 for the oxidations of the OEP complexes studied. Thus, two, almost parallel lines are obtained giving some credence to the model postulated.

It is interesting to plot similar graphs for the comprehensive data collected for the restricted set of d^8 metalloporphyrins in this study to see if they roughly conform to the generalisations of Fuhrop *et al*. The graphs of first oxidation and first reduction potential against metal electronegativity are shown for both MOEP and MTPP series on figure C.16. Both the electronegativity values derived from the Gordy-Thomas

values[47], as selected by Fuhrop et al, and also the more common Pauling electronegativities[48] are tested. Data for the first oxidation of PtTPP are included, even though this is a metal-centred electron-transfer. The energy level of the porphyrin π HOMO for this complex must be more positive than this value ensuring that the gradient obtained for the oxidative behaviour of this complex must be considered as a minimum value.

The results show that for the oxidative behaviour of the d^8 MTPP's the relationship previously obtained is roughly mimicked, while for the d^8 MOEP's studied the scatter of the points is too great (in the case of the Gordy-Thomas values) for any meaningful interpretation. For the reductions of these complexes, however, the correlations show reasonably well fitting straight lines but with negative gradients.

This limited study on the complexes of one transition metal triad thus gives results somewhat in disagreement with those obtained by Fuhrop et al[11] for their studies on complexes containing 3d and 4d transition and lighter metals. The complexes studied, in fact, show an increase in the frontier orbital gap with increasing central metal electronegativity. This further adds to the evidence previously[12] assembled, that metal-macrocycle induction cannot be the determining influence upon the frontier orbital levels of metalloporphyrins.

The most fundamental experimental observation made in proposing the inductive effect for metalloporphyrins was the maintenance of an almost constant difference between the first

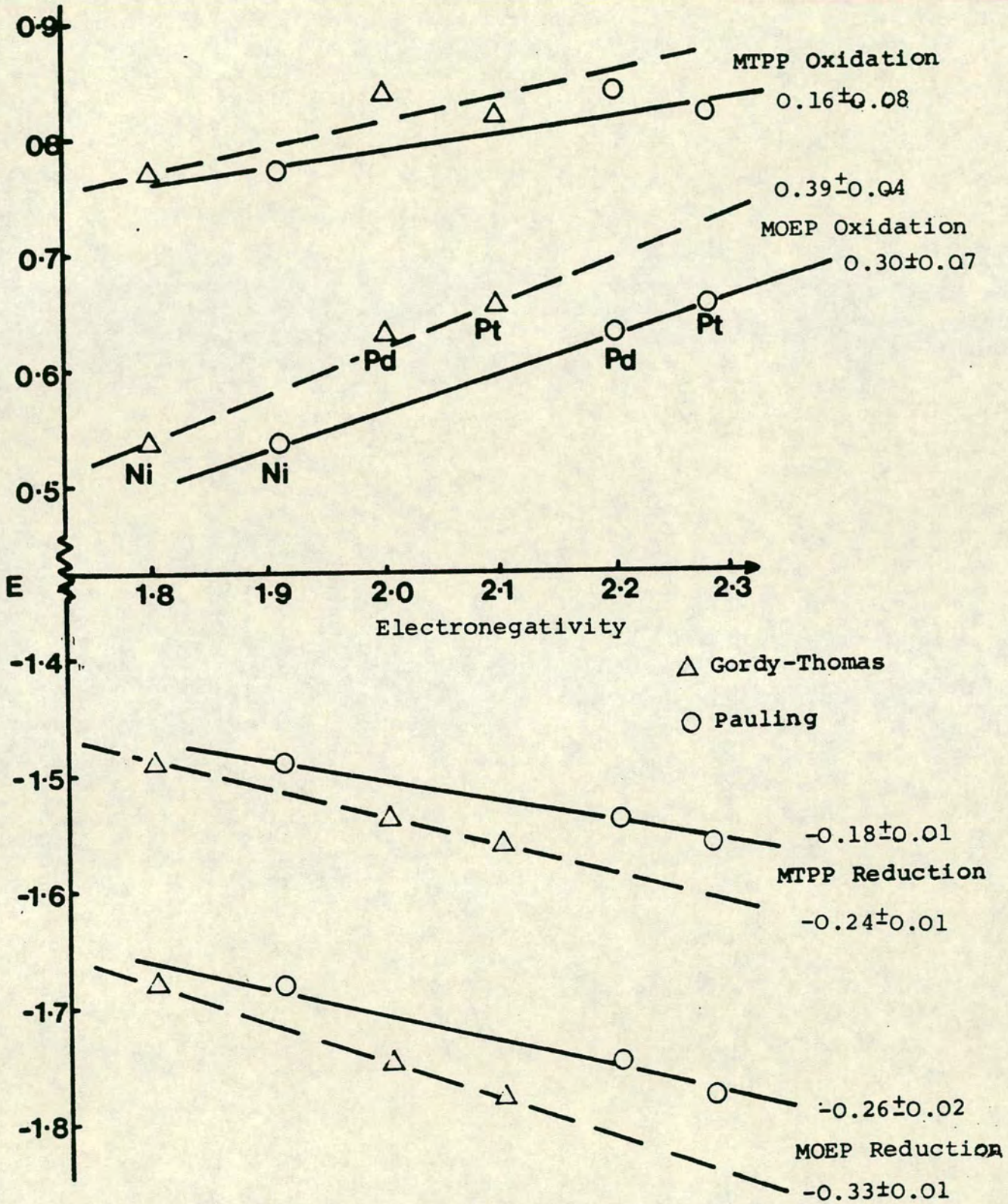

Figure C.16: Plot of Electronegativity vs 1st Oxidation and Reduction Potentials of d^8 Metalloporphyrins

macrocyclic oxidation and reduction potential, in the absence of metal-centred redox processes, in a wide variety of complexes. This was asserted to be effectively constant at 2.25 ± 0.15 V, indicating preservation of the π to π^* frontier orbital gap in these complexes. The values obtained for the differences between the first oxidation and first reduction potentials in the present work are listed in Table C.2. Once again the value for PtTPP is included, but can only indicate a minimum value since a PtII/III oxidation has intervened.

Generally speaking the transition metal complexes have values of ΔE greater than those of the corresponding zinc and free-base porphyrins. In particular, there is a small but significant increase in the ΔE values moving from $3d^8$ to $4d^8$ to $5d^8$ metals for each series. In an attempt to understand this noteworthy behaviour, the properties of the electronic spectra of these metalloporphyrins were examined.

Metalloporphyrins containing transition metals with between 6 and 9d electrons belong to a spectroscopic class known as hypsoporphyrins[3]. Their electronic spectra are characterised by being slightly blue-shifted compared to complexes containing metal ions with complete d-electron shells. This spectral shift to higher energy originates from interactions between the filled metal $d\pi$ orbitals and the porphyrin vacant π^* orbitals. This interaction is better known as $d\pi \rightarrow p\pi^*$ backbonding, a synergic bond-strengthening effect, common in transition metal organometallic complexes where the ligands have Lewis base and π-acid properties.

Table C.2: Electrochemically measured Frontier Orbital Gap for d^8 Metalloporphyrins

Complex	$\Delta E = E_{\frac{1}{2}}$ (1st ox.) - $E_{\frac{1}{2}}$ (1st red.)/V
H_2OEP	2.20
ZnOEP	2.20
NiOEP	2.24
PdOEP	2.38
PtOEP	2.46
H_2TPP	2.17
ZnTPP	2.17
NiTPP	2.26
PdTPP	2.38
PtTPP	>2.38

For the square-planar metalloporphyrins, the particular molecular orbitals involved in this interaction are the metal d_{xz} and d_{yz} orbitals, and the porphyrin π^* degenerate pair of LUMO's. Both these orbital sets are of e_g symmetry. The interaction taking place is illustrated in figure C.17.

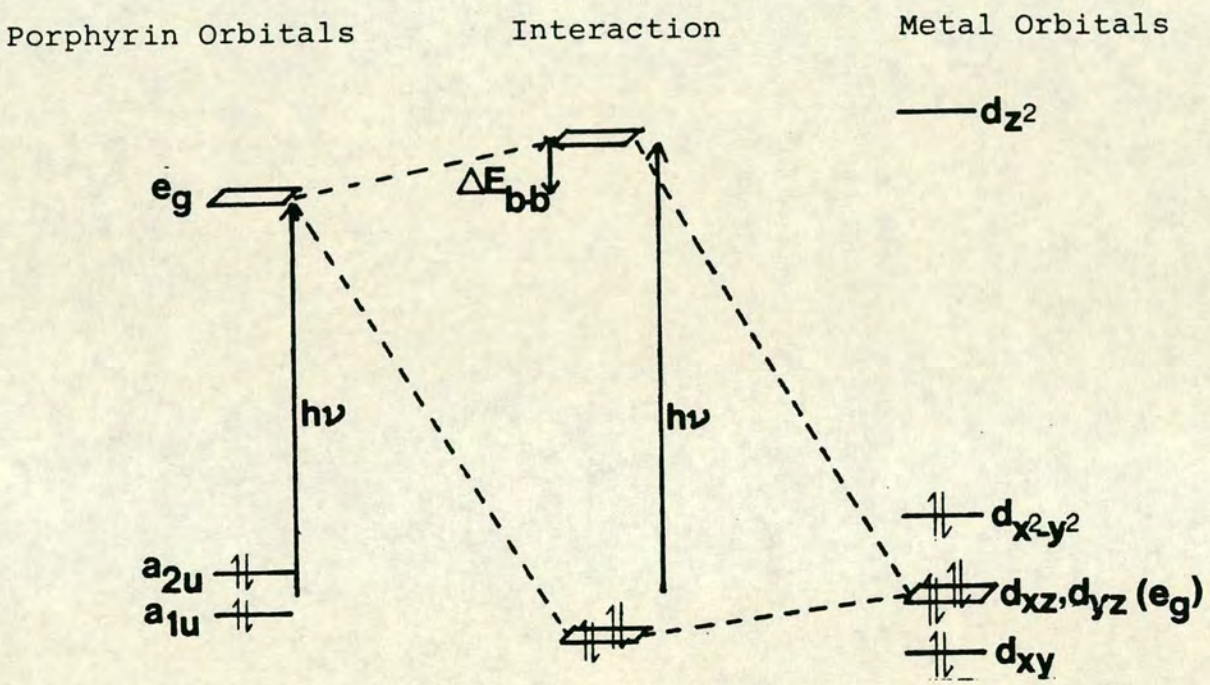

Figure C.17: Representation of the Molecular Orbital Interactions in d^8 Metalloporphyrins

Thus, it can be seen that the macrocyclic π^* LUMO's are raised in energy by this interaction with the symmetry-compatible $d\pi$ orbitals by an amount $\Delta E_{b\text{-}b}$. This results in the $\pi \rightarrow \pi^*$ spectral bands being shifted to higher energy by amounts related to $\Delta E_{b\text{-}b}$. Although the extent of this interaction has not been quantified for any metalloporphyrins the general qualitative trends can be understood. Moving along a transition series (i.e. increasing the atomic number), the

energies of the dπ orbitals will fall relative to the macrocyclic frontier orbitals. This ensures maximum backbonding for d^6 metals, rapidly decreasing to a minimum for d^9 and d^{10} metals in that series. In a transition metal triad molecular orbital overlap of the dπ orbitals with the π* orbitals will increase from 3d to 4d to 5d metals, ensuring maximum backbonding for the heavier complexes.

It would appear that the redox behaviour of the d^8 metalloporphyrins studied is also being influenced by backbonding, as the gap between first macrocyclic based oxidation and reduction potentials of these complexes is generally larger than that for the free-base and d^{10} analogues. In addition this gap increases steadily, for both metalloporphyrin series, on moving from the $3d^8$ to $4d^8$ to $5d^8$ metals. Thus we observe that trends in the $\pi \rightarrow \pi^*$ frontier orbital gap, previously seen only spectroscopically, have now also been observed in the voltammetry of the d^8 metalloporphyrins.

For aromatic systems in general comparison of frontier orbital energy gaps measured spectroscopically and electrochemically can never be exact. There are inherent differences in the parameters measured in each case. Electrochemistry determines the absolute energy levels for insertion or removal of electrons from the π-orbital manifold, whilst spectroscopy measures the energy required to raise an electron from the ground state of the neutral complex. The difference between these processes is illustrated in figure C.18.

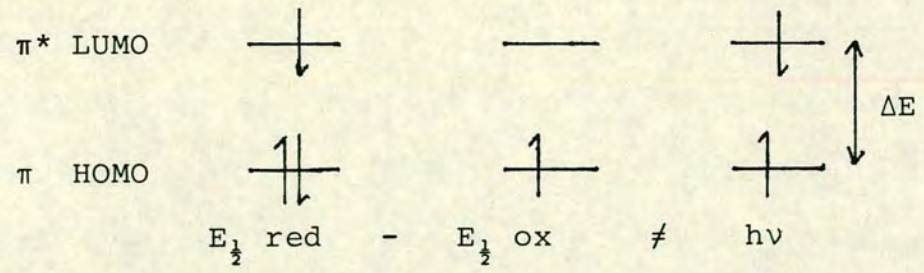

Figure C.18: Comparisons of the Electrochemical and Spectroscopic Determinations of the Frontier Orbital Energy Gap in Aromatic Systems

The electrochemically and spectroscopically determined values of ΔE differ in the extent of the contribution to each from long range electron-electron repulsions. These, themselves, are dependent on the magnitude of ΔE, being large for small ΔE values.

Stanienda and Biebl [10,49] have examined the differences between the electrochemically and spectroscopically determined values of ΔE for a number of aromatic polyenes, including some free-base porphyrins. It was found experimentally, for the systems studied, that the energy of the longest wavelength $\pi \rightarrow \pi^*$ absorbance, and the gap between first oxidation and reduction potentials agreed within 0.1 eV (800 cm^{-1}). In the porphyrin systems studied the longest wavelength band measured was the Q(0,0) band. The corresponding values for the d^8 metalloporphyrins in this study are listed in Table C.3.

Thus, while the electrochemical determinations of the metalloporphyrin $\pi \rightarrow \pi^*$ frontier orbital gap will never correspond exactly with the spectroscopically obtained values, trends in one series of determinations should also be present in the other. This is what in fact is observed for the studied

Table C.3: Electrochemically and Spectroscopically determined values of the d^8 Metalloporphyrin Frontier Orbital Gap

Complex	ΔE		
	$E_{\frac{1}{2}}$ ox - $E_{\frac{1}{2}}$ red/cm^{-1}	hν	
		nm	cm^{-1}
NiOEP	18,100	551	18,150
PdOEP	19,200	545	18,350
PtOEP	19,900	534	18,700
NiTPP	18,300	562	17,800
PdTPP	19,200	555	18,000
PtTPP	>19,200	537	18,600

d^8 metalloporphyrins, with increases in ΔE on moving down the d^8 triad for both series of complexes. This trend strongly suggests that the redox behaviour of d^8 metalloporphyrins is influenced by the presence of metal to porphyrin π-backbonding.

Conclusions

This examination of the voltammetry of the d^8 metallooctaethylporphins and tetraphenylporphins, in addition to detecting new processes, and clarifying previously observed redox potentials, has found a hitherto unrecognised pattern of metalloporphyrin redox behaviour. The values obtained for the first macrocyclic based oxidation and reduction potentials of these species have not fitted the, previously accepted, inductive model of metal-porphyrin interactions, where the metal raises or lowers the energies of the HOMO and LUMO of the aromatic porphyrin ring equally in direction and magnitude. A small, but progressive, increase in the difference between the first macrocyclic oxidation and reduction potentials has been found, moving down the d^8 triad for each metalloporphyrin series.

This last effect is attributed to the occurrence of metal to porphyrin $d\pi \rightarrow p\pi^*$ backbonding, which raises the energy of the macrocyclic π^* LUMO, leaving the energy of the π HOMO unaffected. This necessarily increases the frontier orbital gap in these systems. This effect has previously been observed in the electronic spectra of these species, and is here, for the first time detected electrochemically. The general trends

in the $\pi \rightarrow \pi^*$ energies of the electronic spectra of these compounds are reflected in their voltammetry.

It can be concluded, therefore, that the metal ions present in metalloporphyrins can affect the redox properties of the π and π^* frontier orbitals by interactions along the metal to nitrogen π-bonds. This secondary, "conjugative" effect, in addition to the known inductive effect, which acts along the metal to nitrogen σ bonds, will be present in all transition metal metalloporphyrins with metal ions containing between 6 and 9 d electrons. The d^8 metals studied here form the most suitable triad for detecting this effect as the electrochemistry of these species involves only minimal intervention of metal-based valency changes.

C.2-2 Characterisation of the Metal-Centred Oxidation of Platinum(II) Tetraphenylporphrin

The anodic voltammetry of Pt(II)TPP previously described in this thesis (Section C.2-1) and in a separate[44], earlier study reveals three discrete oxidations. Our recorded cyclic and a.c. voltammograms are illustrated in Figure C.19. The presence of three oxidations sharply contrasts with the typical voltammetry of metalloporphyrins containing redox-inert central metals, which usually reveal only two reversible oxidations both involving one-electron abstraction from the porphyrin macrocyclic π-orbital manifold. The species formed under these circumstances are the metalloporphyrin π-radical-cation and π-dication previously described. The presence of a third oxidation in metalloporphyrin electrochemistry is normally indicative of the occurrence at some stage of a metal-centred redox process (e.g. Fe^{2+}/Fe^{3+} or Co^{2+}/Co^{3+}), which was not anticipated for Pt(II)TPP.

In order that this unusual behaviour could be characterised, the electro-oxidations of Pt(II)TPP were closely followed by *in situ* monitoring of the compound's electronic spectrum during bulk electro-oxidation. Three successive electro-generations were carried out, just beyond each half-wave oxidation potential.

For the first oxidation the spectral changes observed are illustrated in figure C.20. The spectrum formed is similar in shape and intensity to that of the unoxidised neutral species, but has been red-shifted by approximately 20nm. It was confirmed that reverse electrolysis quantitatively

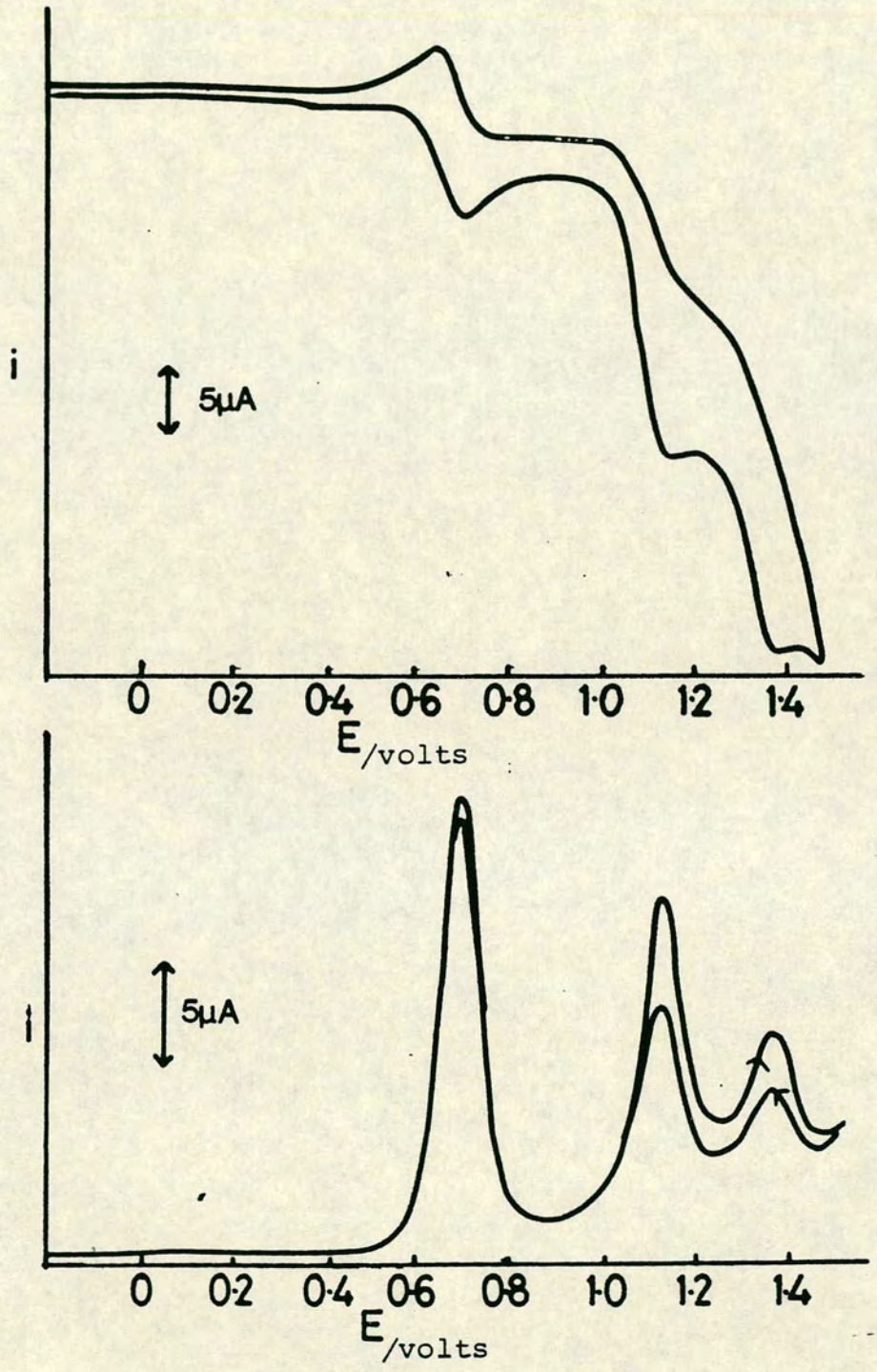

Figure C.19: Cyclic and A.C. Voltammograms of the Anodic Electrochemistry of Pt(II)TPP

E vs Ag/AgCl reference electrode.

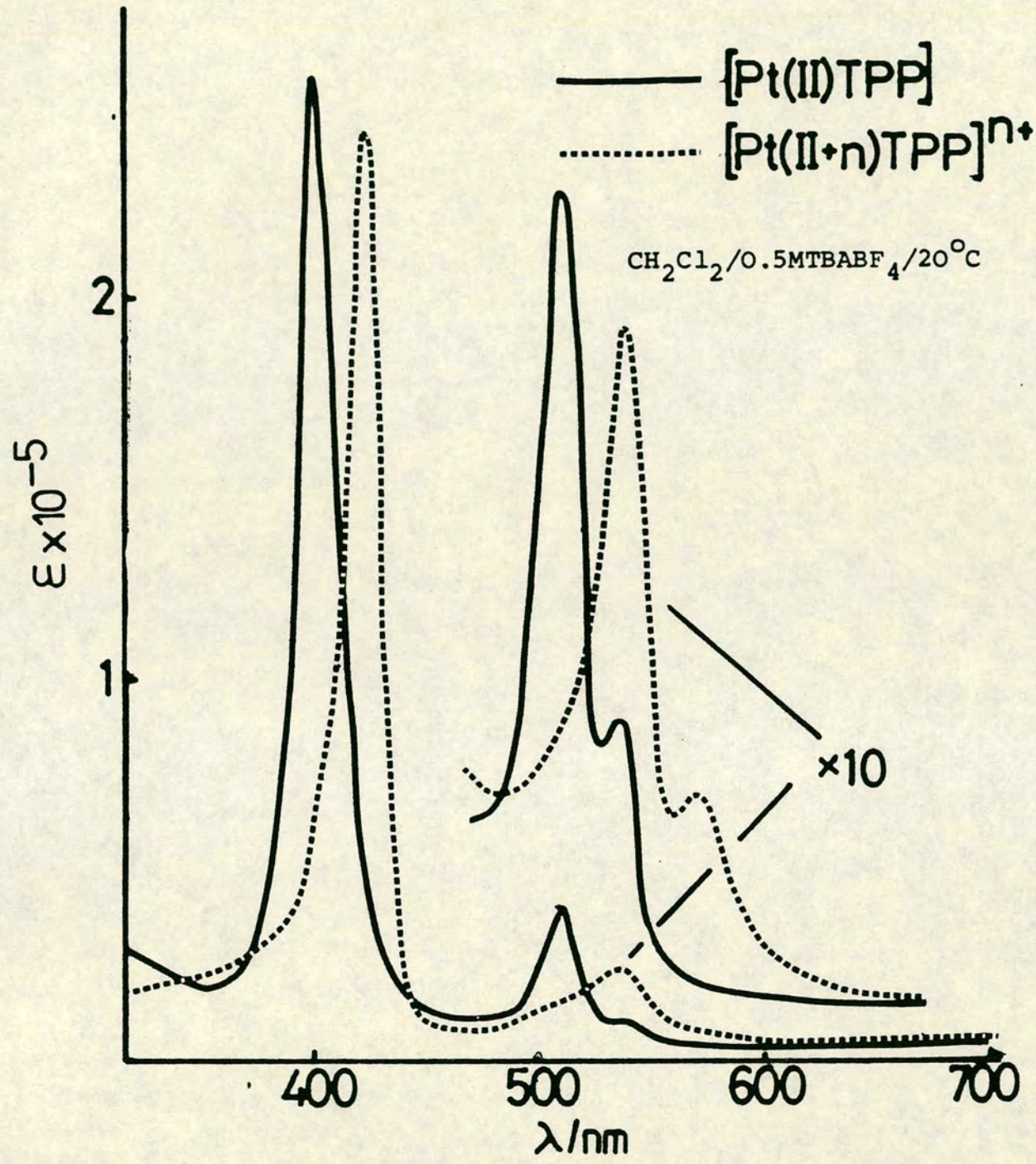

Figure C.20: The change in the electronic spectrum of Pt(II)TPP upon its first oxidation

recovered the starting spectrum. The electrolysis product is stable when the oxidation-potential is maintained, but open-circuit conditions result in rapid reformation of Pt(II)TPP at ambient temperature.

The similarity in the spectra of the product and starting complex implies that essentially no alteration in the electronic configuration of the macrocyclic π-orbital system takes place with this oxidation. This points toward electron-abstraction occurring directly from the metal centre. However, the number of electrons removed and the resulting oxidation state of platinum cannot be determined from this experiment.

In order that the number of electrons transferred during the first electro-oxidation of Pt(II)TPP could be accurately determined, coulometry was carried out. This established that the number of Faradays transferred was 0.98 ± 0.05 per mole, i.e. that the process is a one-electron oxidation as shown below.

$$\text{Pt(II)TPP} \underset{+e}{\overset{-e}{\rightleftharpoons}} [\text{Pt(III)TPP}]^{+}$$

The proposed formation of a Pt(III) species, rather than the more common Pt(IV) oxidation state, presented the possibility that the electro-oxidised product could be characterised further by e.s.r. spectroscopy (see later).

Electrolysis just beyond the second oxidation potential results in the spectral changes shown on figure C.21. Both the Soret and the visible regions of the spectrum have broadened

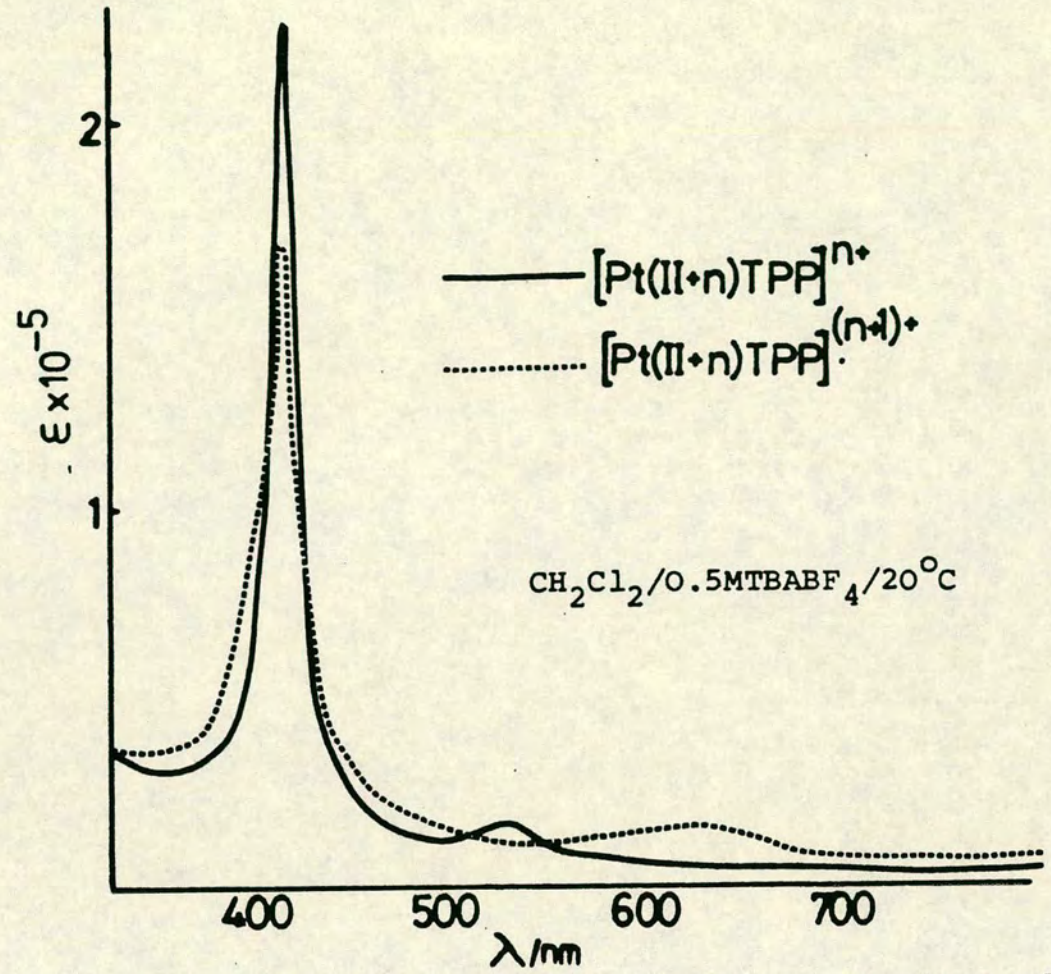

Figure C.21: The changes in the electronic spectrum of Pt(II)TPP during its second oxidation

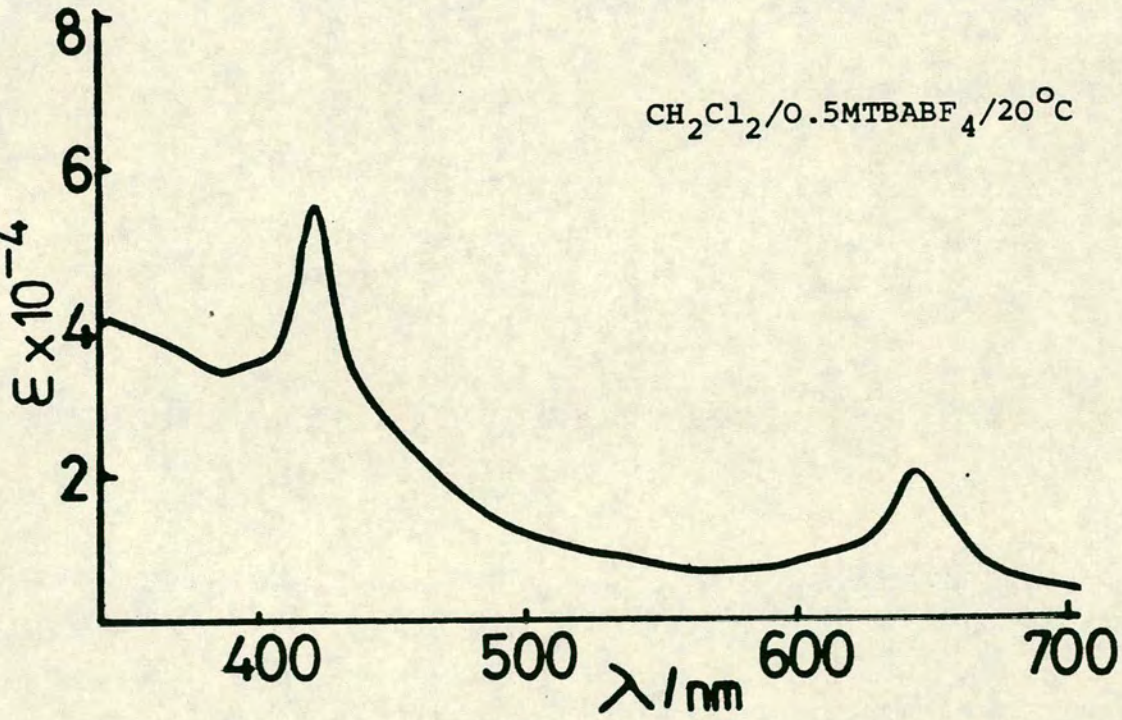

Figure C.22: Electronic Spectrum of the product of the third oxidation of Pt(II)TPP

and decreased in intensity. The spectrum formed is of the type typically associated with a metalloporphyrin π-radical-cation, as was outlined in Section C.1-1. Reverse electrolysis results in the quantitative regeneration of the spectrum of the starting complex i.e. $[Pt(III)TPP]^+$, while open-circuit conditions lead to rapid reformation of Pt(II)TPP.

This particular experiment implies that the second oxidation of Pt(II)TPP involves abstraction of a single electron from the porphyrin π-orbital manifold, forming the recognizable π-radical oxidized ligand. This species contains the metal centre in its redox-altered oxidation state, formed during the first oxidation, and a macrocyclic π-orbital system with 17 π-electrons. The overall process is summarised below.

$$[Pt(III)TPP]^+ \underset{+e^-}{\overset{-e^-}{\rightleftharpoons}} [Pt(III)TPP]^{\cdot 2+}$$

Electrolysis just beyond the third oxidation potential resulted in formation of the species with the unfamiliar electronic spectrum shown on Figure C.22. This spectrum is not of the expected metalloporphryin π-dication type, but is, however, similar to the spectrum obtained for the product of the second electro-oxidation of Pd(II)TPP at ambient temperature. The platinum(III) complex of this type is in fact unstable, decomposing rapidly to an unidentifiable product mixture. The corresponding Pd(II) species is, however, stable indefinitely. Characterisation of the latter complex and consequent identification of its platinum analogue are outlined in Section C.2-3.

E.s.r. studies on $[Pt(III)(TPP)]^+$

E.s.r. spectroscopy is an important method for characterising paramagnetic species. It has been widely employed in organometallic and coordination chemistry, and in particular many paramagnetic metalloporphyrin species have been examined by this technique.

The e.s.r. spectra of metalloporphyrin π-radical-cations consist, under normal resolution, of a narrow isotropic signal with a g-value close to that of a freely spinning electron. Under higher resolution, and in the frozen-glass state some narrow hyperfine coupling (1.4 to 1.7G) to the aza nitrogen atoms is observed. An example of this spectral type, that of $[Ni(II)OEP]\cdot^+$ is illustrated in Figure C.23.

In contrast, metalloporphyrins containing paramagnetic metal centres embedded in a spin-paired macrocycle exhibit e.s.r. spectra typical of the particular metal oxidation state and coordination environment. The most striking difference between this spectral type and those of the π-radical-cations is that the signal in the frozen-glass state becomes anisotropic and splits into two components. The splitting of the signal is due to a loss of degeneracy between the xy (parallel) tensor and the xz and yz (perpendicular) spectral tensors; this loss of degeneracy occurs because the metal ion is held rigidly in a square-planar ligand field. An example of this type of spectrum, that of $[Ni(III)TPP]^+$, is illustrated in Figure C.24 with the two spectral components being labelled $g_{\parallel}$ (parallel) and $g_{\perp}$ (perpendicular).

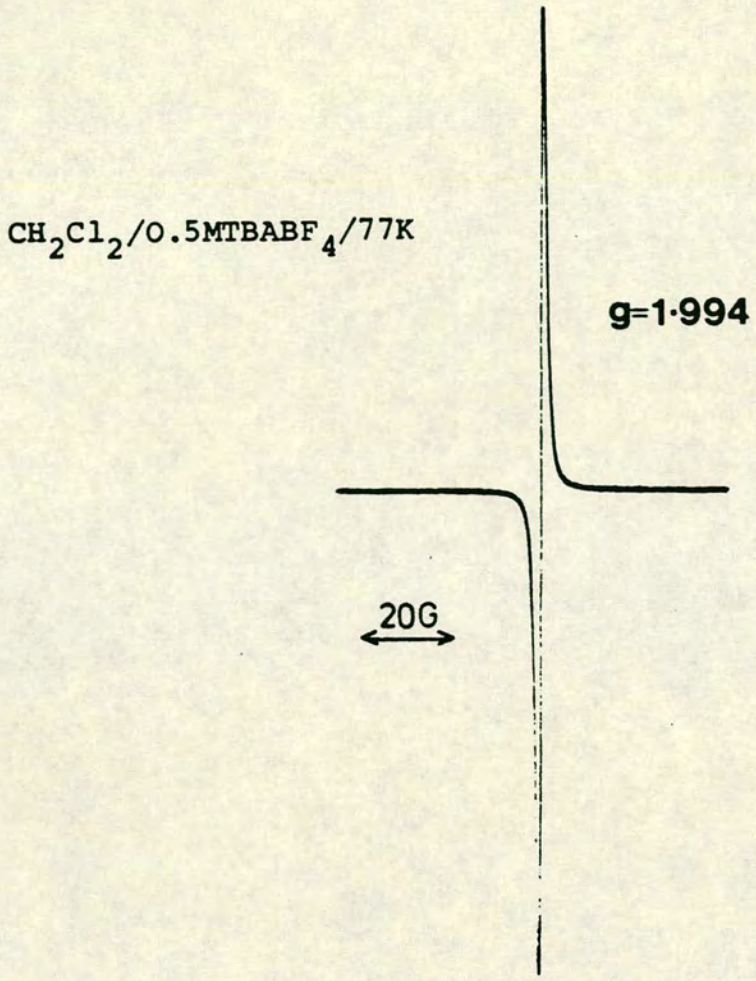

Figure C.23: E.s.r. spectrum (frozen-glass) of $[Ni(II)OEP]^+$

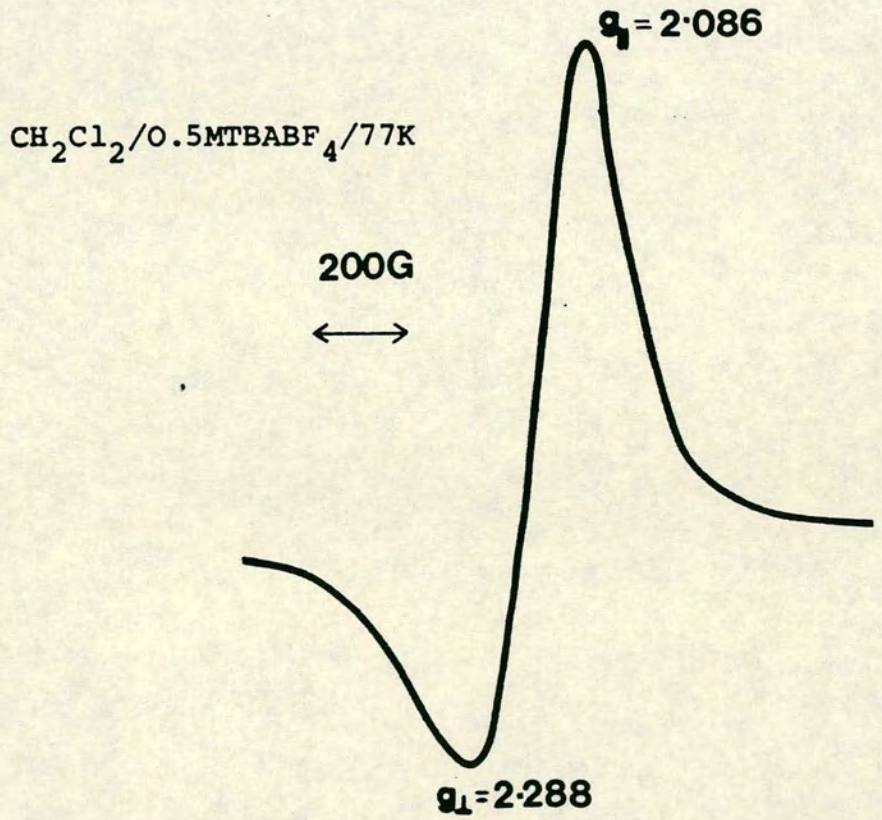

Figure C.24: E.s.r. spectrum (frozen-glass) of $[Ni(III)TPP]^+$

In the present work the e.s.r. spectrum of electrogenerated $[Pt(III)TPP]^+$ recorded at 198K consists of a single line, but cooling the solution to 77 K (frozen-glass state) results in the two-component anisotropic signal illustrated in figure C.25. The measured g-values are $g_{\parallel} = 1.982$ and $g_{\perp} = 2.012$, and the peak to peak separation is 50G.

Monomeric Pt(III) species are rare, complexes of this type having only recently been established. In contrast, binuclear Pt(III)-Pt(III) complexes are well documented[50,51] but these species are intrinsically diamagnetic and hence e.s.r. silent. Crystalline $\{[Pt(III)(diphenyl\ glyoximate)_2]ClO_4\}_2$ provides an interesting example of this type[52].

Only three truly mononuclear Pt(III) complexes have been recognised hitherto: $[Pt(III)(C_6Cl_5)_4]^-$(41)[53,54], $[Pt(III)$-$(diamsar)]^{3+}$(42)[55], and $[Pt(III)(S_3)_2]^{3+}$(43)[56]. In addition to these recent examples an earlier report exists[57,58] where the product of one-electron oxidation of [Pt(II)(o-phenylenedi-imine)$_2$](44) was characterised by virtue of its two-component e.s.r. spectrum as having significant unpaired electron density on the metal; i.e. the monomeric cation may be formulated to contain Pt(III).

Unfortunately, no e.s.r. data are available for the crystallographically defined square-planar complex $^nBu_4N^+[Pt(C_6Cl_5)_4]^-$, although magnetic susceptibility measurements are fully consistent with its Pt(III) d^7 ($S=\frac{1}{2}$) formulation[54]. The e.s.r. spectra which have been reported for the

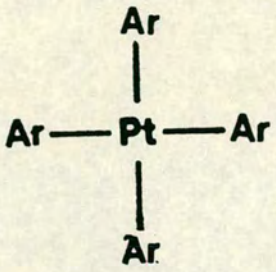

$Ar = C_6Cl_5^-$

(41)

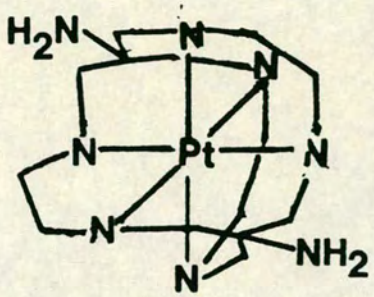

diamsar= 1,8-diamino-hexaazabicyclo[6.6.6] icosane

(42)

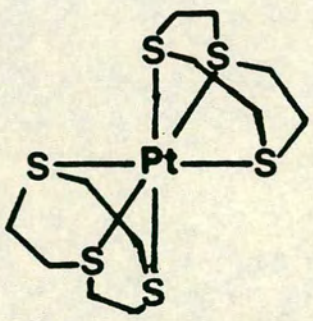

S_3= 1,4,7-trithiacyclononane

(43)

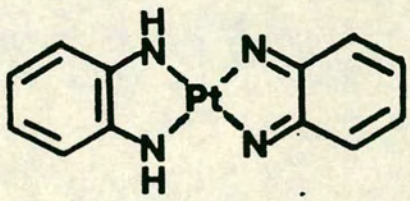

(44)

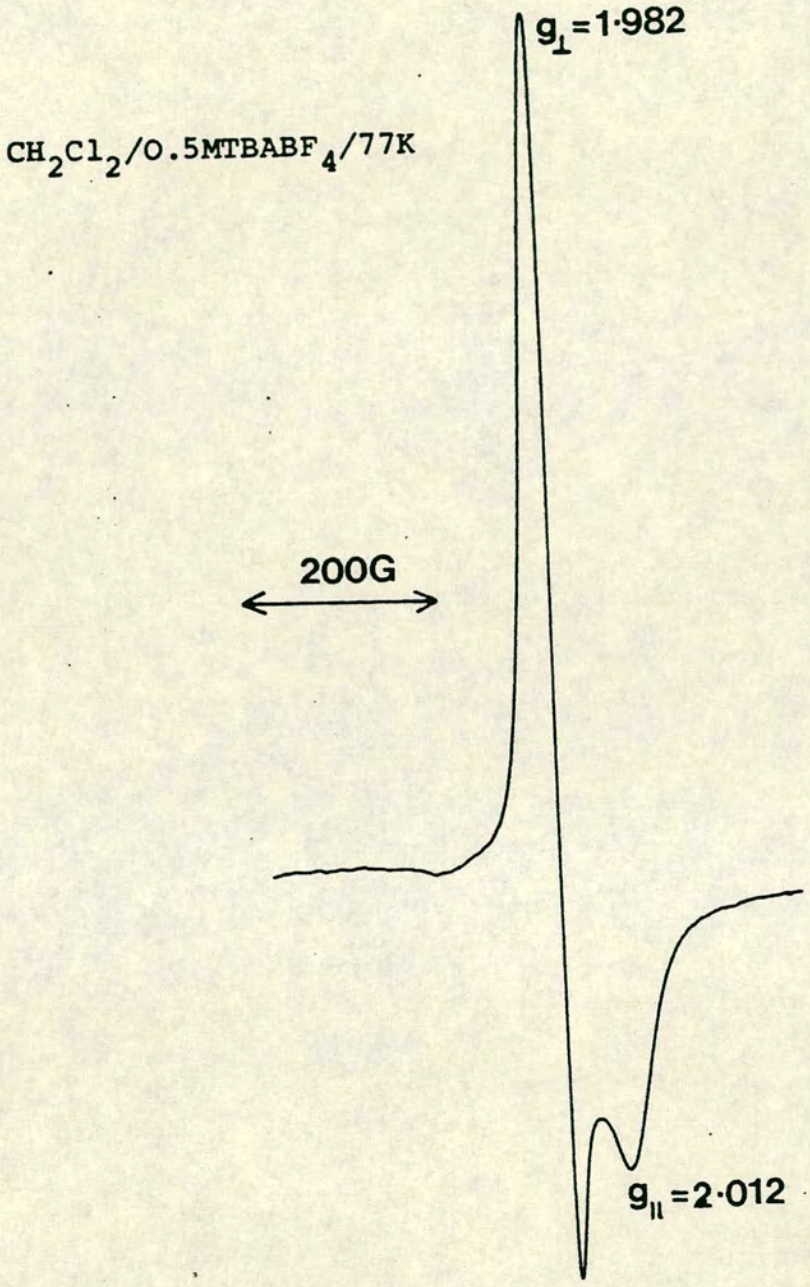

Figure C.25: E.s.r. spectrum (frozen-glass) of $[Pt(III)TPP]^+$

other monomeric Pt(III) complexes are all anisotropic. At 4K, the spectrum of $[Pt(III)(diamsar)]^{3+}$, an octahedral cage complex generated transiently by γ-radiolysis of its Pt(IV) parent compound, is broad, centred at g = 2.0 and additionally exhibiting hyperfine coupling to ^{195}Pt(I = ½, natural abundance = 37.7%), the coupling constant being 50G. The complex $[PT(III)(S_3)_2]^{3+}$, generated by electro-oxidation of its Pt(II) parent, reveals an e.s.r. spectrum which, at 77K, splits into two components. The lines recorded are at $g_{||}$ = 1.982 and $g_{\perp}$ = 2.044; each spectral component exhibits ^{195}Pt hyperfine coupling, the coupling constants being $A_{||} \sim 85G$ and $A_{\perp} \sim 30G$. The complex is likely to have a distorted octahedral coordination geometry[56].

The reported e.s.r. spectrum of planar, tetra-aza dentate $[Pt(o\text{-}HNC_6H_4NH)_2]^+$ (44) which presumably has the coordination environment most similar to $[Pt(III)TPP]^+$, has components at $g_{||}$ = 1.940 and $g_{\perp}$ = 2.009, compared to 1.968 and 2.012 respectively for the porphyrin. No ^{195}Pt hyperfine coupling was observed in this case either.

The reported data reveal a significant anomaly in the e.s.r. spectrum of $[Pt(III)TPP]^+$ in the unexpected absence of any resolvable ^{195}Pt hyperfine coupling. This discrepancy cannot be explained at this stage although the coupling is likewise unobserved in the spectrum of $[Pt(o\text{-}HNC_6H_4NH)_2]^+$, which probably has the greatest chemical similarity to $[Pt(III)TPP]^+$. Notably, even isostructural $[Pt(o\text{-}HNC_6H_4NH)_2]^-$, formally Pt(I) d^9, does display strong hyperfine coupling; evidently an interplay of donor atom identity, coordination

geometry, and metal oxidation state must influence the detection of hyperfine coupling.

Conclusions

The first electro-oxidation of Pt(II)TPP has been shown to be a reversible one-electron metal-centred oxidation to form the Pt(III) species as shown below.

$$\text{Pt(II)TPP} \underset{+e}{\overset{-e}{\rightleftharpoons}} [\text{Pt(III)TPP}]^{+}$$

This assignment is made on the basis of uv/visible spectroscopy, coulometry and e.s.r. spectroscopy. The electronic spectrum of the electrogenerated product clearly shows that no alteration in the macrocyclic π-orbital electronic configuration has taken place. Additionally, the observed 20nm red-shift of the spectral bands is similar to that observed on one-electron oxidation of Co(II)TPP. (This has been established in previous studies[59] to be a one-electron oxidation to the Co(III) porphyrin.)

Coulometry confirms the assignment of a one-electron oxidation, and e.s.r. spectroscopy enhances the evidence for a metal-centred (anisotropic) paramagnetic complex. The lack of resolvable hyperfine coupling in the e.s.r. spectrum presents an apparent anomaly, but it does have a close precedent amongst one of the few known Pt(III) e.s.r. spectra. It is only when e.s.r. spectra of Pt(III) species are more generally available that this discrepancy will be satisfactorily explained.

It is interesting to note that the original study by Bard et al[44] on the electrochemistry of Pt(II)TPP showed rather indirect evidence, not commented upon at the time, for the formation of a Pt(III) species. This study involved cycling the cell potential between that of the first oxidation and first reduction in the hope of observing chemi-luminescence from the reaction below.

$$PtTPP^{+\cdot} + PtTPP^{-\cdot} \rightarrow PtTPP^{*} + PtTPP$$

$$PtTPP^{*} \downarrow -h\nu$$

$$PtTPP$$

However the study found that no chemi-luminescence was observed unless the cell potential was cycled between the first reduction and the second oxidation. This fits in with our discovery that electron-removal from the macrocyclic π-orbitals does not occur until the second oxidation, since the first oxidation involves electron abstraction from the metal. Implicit in this remark is the notion that perhaps the 'orbital matching' of the π-cation-radical $[Pt(III)TPP]^{2+\cdot}$ and π-anion-radical $[Pt(II)TPP]^{-\cdot}$ facilitates the generation of the long-lived emitting state. Thus [Zn(TPP)] provides a straightforward example of electrogenerated chemi-luminescence.

$$[Zn(II)TPP]^{+\cdot} + [Zn(II)TPP]^{-\cdot} \rightarrow [Zn(II)TPP]^{*} + [Zn(II)TPP]$$

This result opens up an exciting new area of chemistry whereby manipulation of the electron donating/withdrawing nature of the peripheral substituents on the porphyrin macrocycle can dictate whether Pt(II/III) or macrocycle oxidation occurs. Complexes of the type M(II)OEP generally have their

first macrocyclic oxidations 300mv more cathodic than their M(II)TPP analogues. This difference is such that the Pt(II) complexes of this type undergo macrocyclic oxidation for Pt(II)OEP but metal oxidation for Pt(II)TPP. The use of porphyrin macrocycles containing peripheral substituents that are more electron-withdrawing than the four meso-phenyl groups in the TPP macrocycle should lead to further Pt(III) species being formed upon first oxidation. This would add new members to thelimited family of monometallic Pt(III) species. In addition, by careful manipulation of the substituent pattern it should be possible to establish a cross-over situation where $E_{\frac{1}{2}}$ for Pt(II)/Pt(III) and for ring oxidation are matched.

It would also be of interest to examine alternative but related macrocycles such as the phthalocyanines and tetra-aza-porphyrins to examine the effects of varied macrocyclic structure on this phenomenon. Both the latter systems are more resistant to oxidation than porphyrins themselves.[60]

C.2-3 Nucleophilic Addition to the π-dications of Palladium and Platinum Tetraphenylporphin

Study of the oxidative voltammetry of Pd(II)TPP (Section C.2-1) revealed the presence of two discrete electron-transfer processes. Examination of the cyclic voltammogram of this species (figure C.26) led to the tentative assignment that the electron transfer processes involve successive removal of electrons from the 18 π-electron aromatic core of the porphyrin. This will result in the formation of the well-documented metalloporphyrin π-radical-cation and π-dication.

Characterisation of the oxidation products was carried out by exhaustive electrolysis at the necessary potentials, accompanied by *in situ* determination of the uv/visible spectrum of the redox-altered species. The visible spectrum of Pd(II)TPP changed, during the first oxidation, from the narrow, two-banded, metalloporphyrin spectrum to a much broader and diffuse spectrum as illustrated in figure C.27. The visible spectrum of the electrogenerated product has a major peak at ∿620nm with a high-energy shoulder. This visible spectrum is characteristic of a metalloporphyrin π-radical-cation with a $^2A_{2u}$ electronic ground state[13].

In contrast, electrolysis just beyond the potential of the second oxidation did not result in the appearance of the expected featureless visible spectrum known for metalloporphyrin π-dications. The visible spectrum, in fact, changed to one with a narrow band at ∿660 nm as illustrated in figure C.28. The species generated was found to be stable on reversal of the oxidation potential, i.e. resistant to reduction, and also stable on setting the cell potential to 0V.

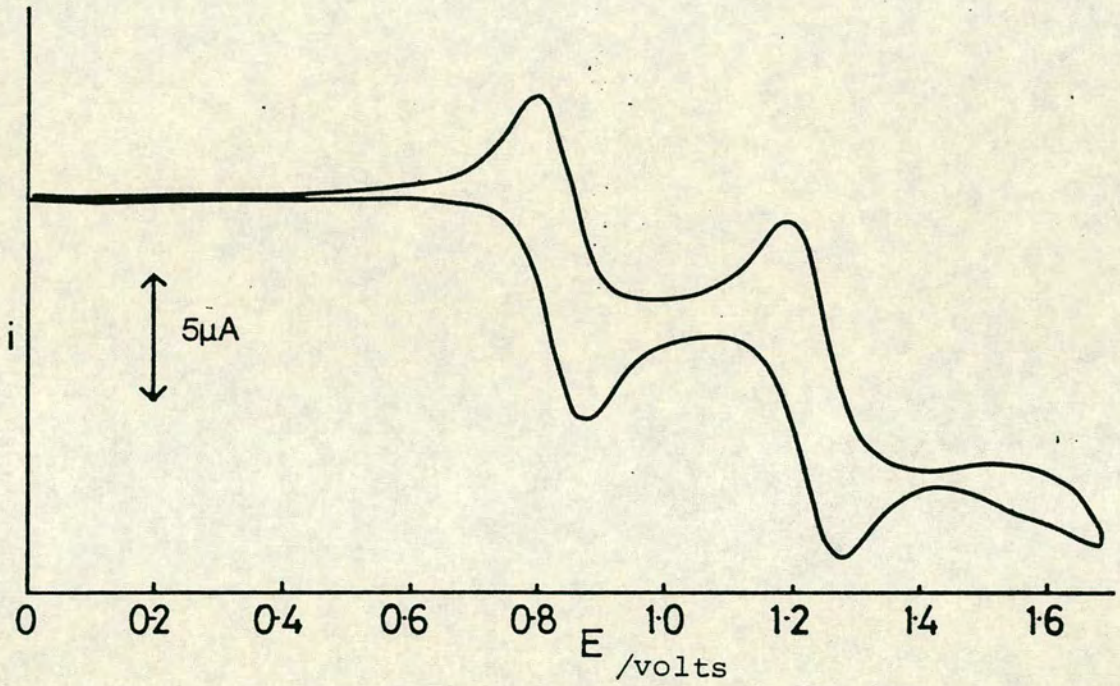

Figure C.26: Anodic cyclic voltammogram of Pd(II)TPP
E vs Ag/AgCl reference electrode
CH_2Cl_2/0.5MTBABF_4

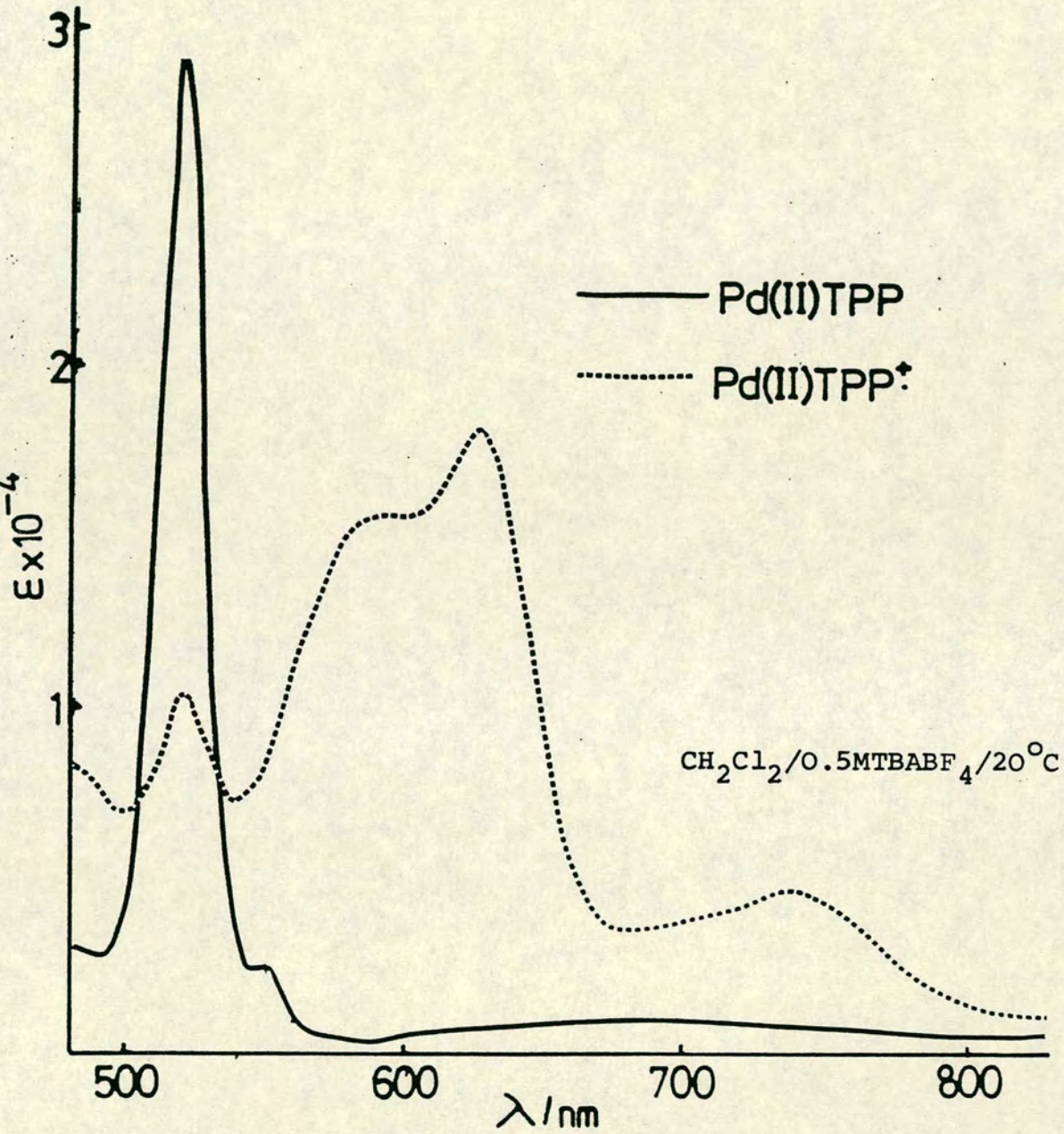

Figure C.27: Changes in the Visible Spectrum of Pd(II)TPP on its first oxidation

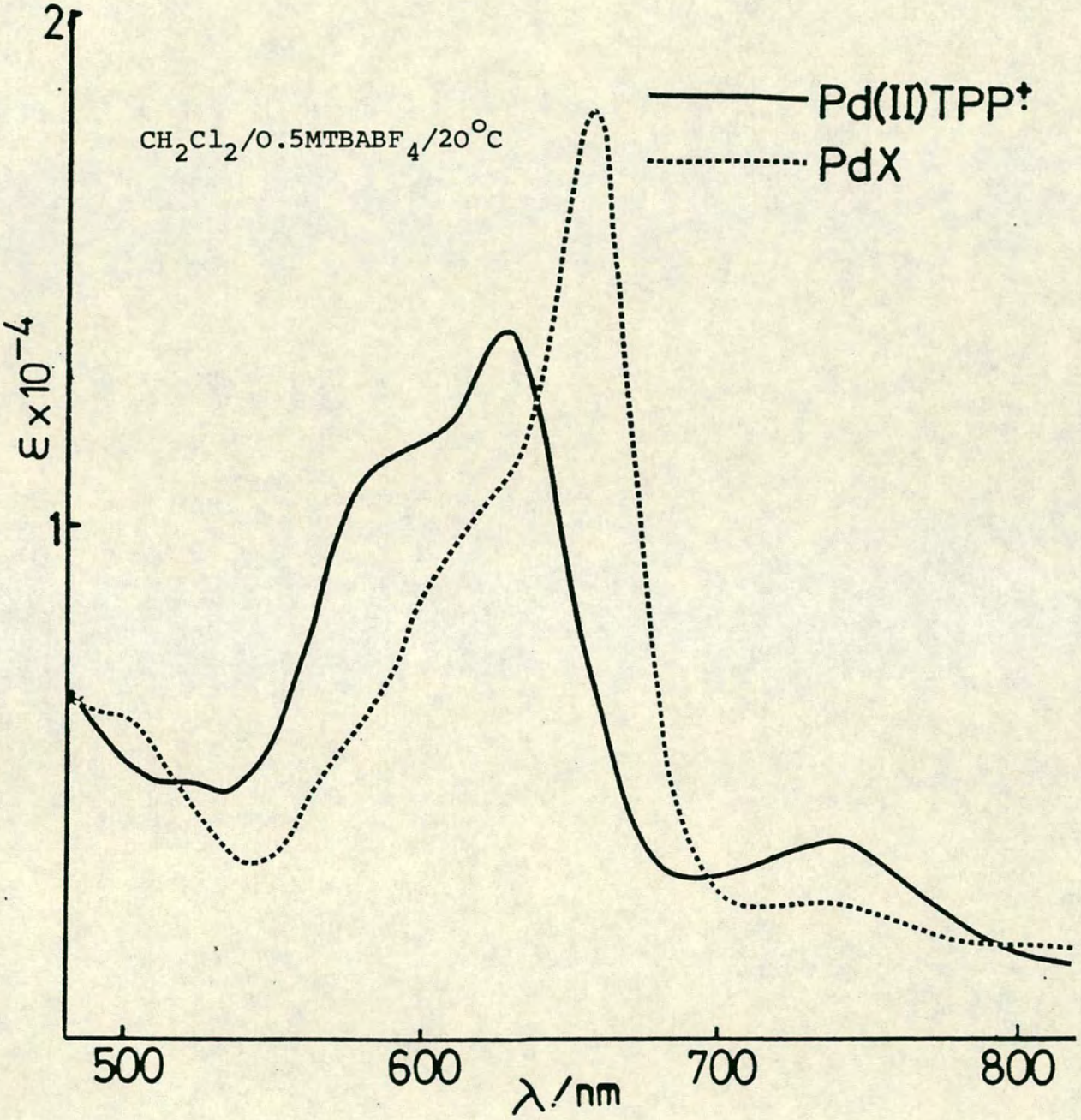

Figure C.28: Changes in the Visible Spectrum of Pd(II)TPP during its second oxidation

Bulk electrooxidation of PdTPP in a conventional electrolysis cell resulted in generation of the same product. The complete uv/visible spectrum of the unidentified complex is illustrated in figure C.29. This shows major peaks at 660nm (ε = 12,000 $M^{-1}cm^{-1}$) and 418nm (28,000 $M^{-1}cm^{-1}$), in contrast to the starting complex Pd(II)TPP which has a much more intense spectrum with major peaks at 524nm (29,300 $M^{-1}cm^{-1}$) and 418nm (332,000 $M^{-1}cm^{-1}$). The green solution of the unidentified species was stable in air, over a period of seven days, and also on addition of glacial acetic acid.

Similar spectral changes were observed for the second macrocyclic oxidation of Pt(II)TPP as illustrated previously in figure C.22. The species generated in this case, which is coordinated to a Pt(III) centre, is however very unstable, decomposing over a period of two to three minutes apparently to a mixture of products.

Therefore, for both PdTPP and PtTPP, we have observed that their second macrocyclic oxidations, in bulk and at room temperature, eventually result not in their π-dications, as detected voltammetrically, but in hitherto unknown species. The drastic changes in the electronic spectra, common to both palladium and platinum systems imply an alteration of the 18 π-electron aromatic core. This can occur possibly by addition of some nucleophile, or nucleophiles, toward a presumably very reactive $MTPP^{2+}$ π-dication, or possibly via an intramolecular rearrangement. In any case, our limited knowledge, at this stage of the investigation, could be summarised as in Scheme C.10.

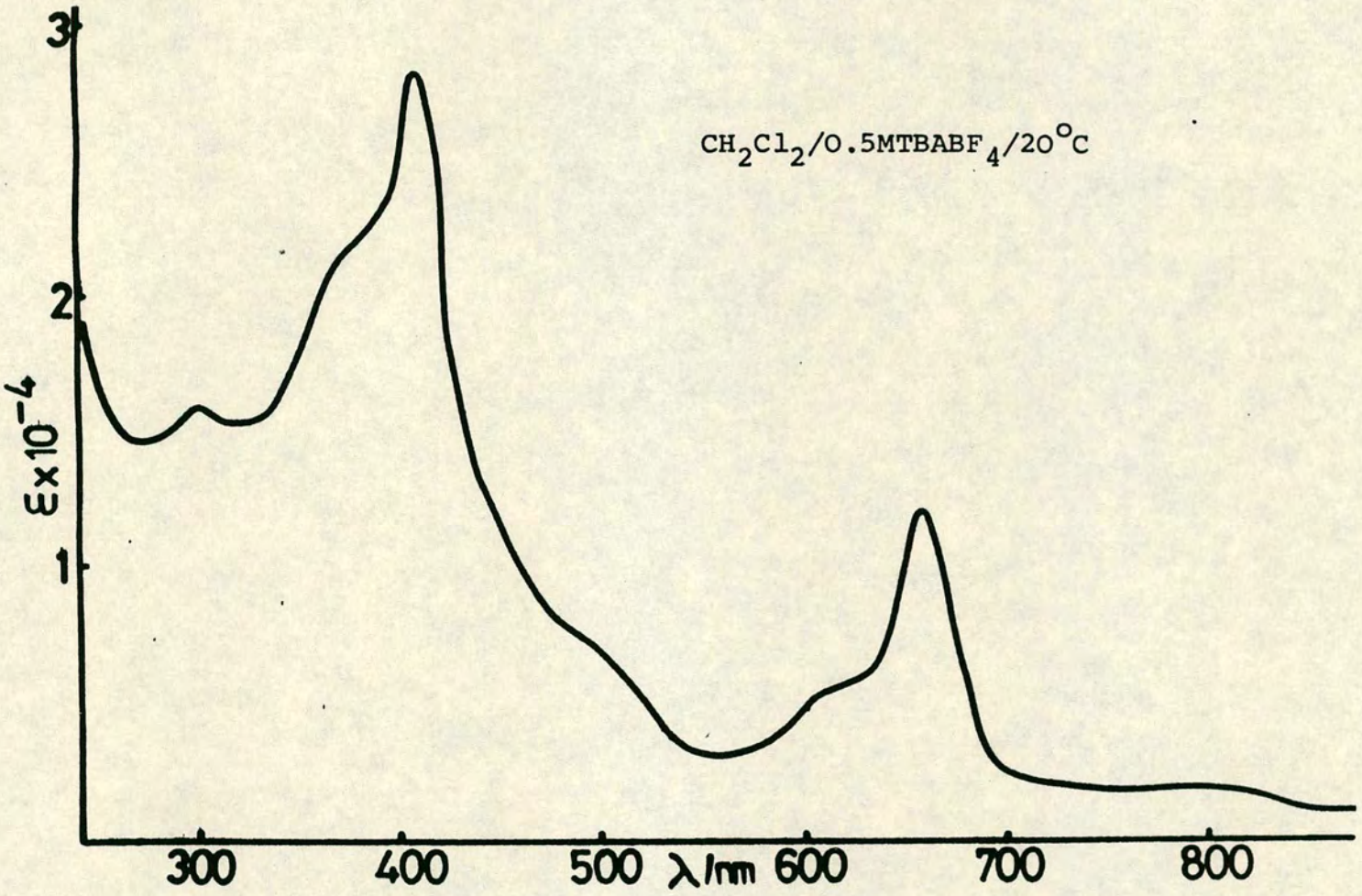

Figure C.29: Complete uv-visible spectrum of unidentified species generated by the second electro-oxidation of Pd(II)TPP

$$\text{MTPP} \underset{+e^-}{\overset{-e^-}{\rightleftharpoons}} \text{MTPP}^{+\cdot} \xrightarrow[L]{-ne} \text{MX}$$

M = Pd(II) or Pt(III) $\qquad n \geqslant 1$

X = Unidentified tetrapyrrolic macrocycle

L = Possible Attacking Nucleophile

Scheme C.10: Oxidative Rearrangements of PdTPP and PtTPP

This section details the electrochemical and spectroscopic characterisation of the important, new, stable palladium(II) complex, which will hereafter be abbreviated as PdX.

Electrochemical Studies on PdX and some related Metalloporphyrin Oxidation Products

Coulometry established precisely that only one electron is transferred from $PdTPP^{+\cdot}$ during its oxidation to the unidentified complex PdX. Accordingly, it is presumed that the π-dication, $PdTPP^{2+}$, is formed initially in this reaction but is too reactive to be observed at room temperature. In an attempt to stabilise the π-dication and observe its electronic spectrum, *in situ* electrolysis was carried out at -45°C, the lowest possible operating temperature for the optically transparent cell. Electrolysis at this temperature resulted, once again, in formation of the unknown product. However, when the electrolysis was repeated at -75°C, in a conventional cell, the product of the second oxidation of PdTPP was found, by stirred cyclic voltammetry, to be the same as that observed on the much shorter time-scale of voltammetry. As this series of experiments conclusively showed that the new product, PdX, was formed by rapid irreversible reaction of the, initially

formed, two-electron oxidation product of PdTPP, then this precursor is most likely the π-dication, $PdTPP^{2+}$, as detected voltammetrically. Metalloporphyrin π-dications are understandably very reactive, the most well-known products derived from them are the metalloisoporphyrins described in Section C.1-2, which have the general structure (45).

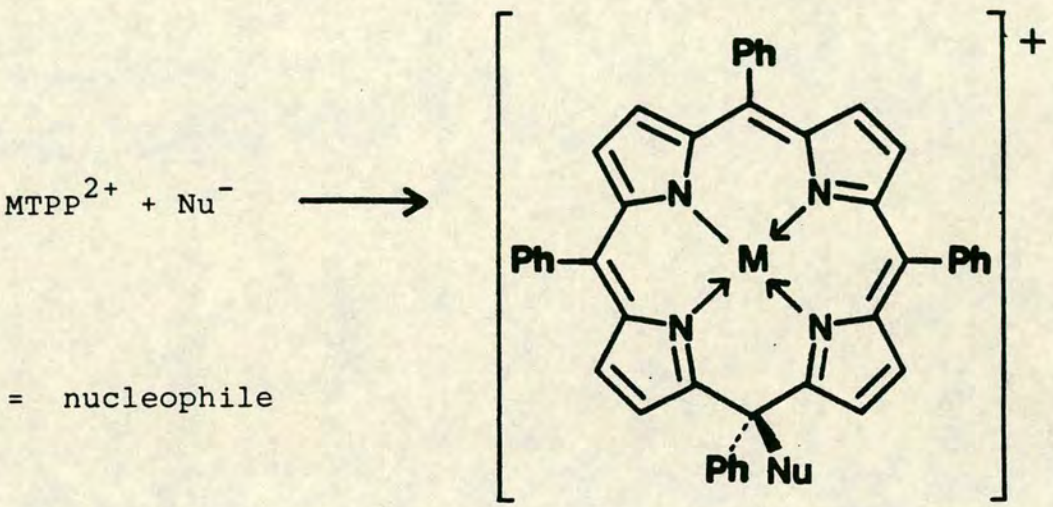

(45) Metallotetraphenyl-isoporphyrin cation

In order to see whether PdX was an isoporphyrin it was thought that valuable comparative information could be obtained from preparing some of these known complexes. Consideration of the potential nucleophiles present led to the identification of hydroxide as a likely anion available to attack $PdTPP^{2+}$. The presence of trace water in conventionally dried solvent/electrolyte media has been discussed in Part B. As the π-dication, $PdTPP^{2+}$, has been found to be much more reactive than e.g. $NiTPP^{2+}$, $ZnTPP^{2+}$, then as a first hypothesis, it was supposed that hydroxide ion is attacking $PdTPP^{2+}$ to form a hydroxy isoporphyrin. To date, the electronic spectrum of a hydroxy-isoporphyrin has not been reported, so the hydroxy isoporphyrin of Zn(II)TPP was prepared, along with

its, known, methoxy analogue. These species were prepared by electrolysis in dichloromethane/tetrabutylammonium fluoroborate containing 1%(v:v) water and methanol respectively. The electronic spectra of these isoporphyrins, illustrated in figures C.30 and C.31, show that both species possess the absorptions at ∿850 nm and ∿760nm that have previously been stated to be characteristic of the isoporphyrin macrocycle.[23]

Further comparisons were made between the voltammetry of the zinc isoporphyrins and PdX. The first oxidation and reduction potentials of these species are listed in Table C.4. While further reductions are observed for all of these species, they are not listed due to the probability of their arising from products formed by the breakdown, on the first reduction, of the parent complexes.

Table C.4: Voltammetric data for PdX and Zinc Isoporphyrins

E vs Ag/AgCl reference electrode

Complex	$E_{\frac{1}{2}}$ ox	$E_{\frac{1}{2}}$ red
PdX	1.50	-0.38
Zn-iso-HO-TPP	1.01	-0.44
Zn-iso-MeO-TPP	1.03	-0.36

The voltammetry of the isoporphyrins, like their electronic spectra, is very similar. The reduction of both complexes is irreversible, in the protic media used for their electrogeneration, in both cases leading to the reformation of ZnTPP.

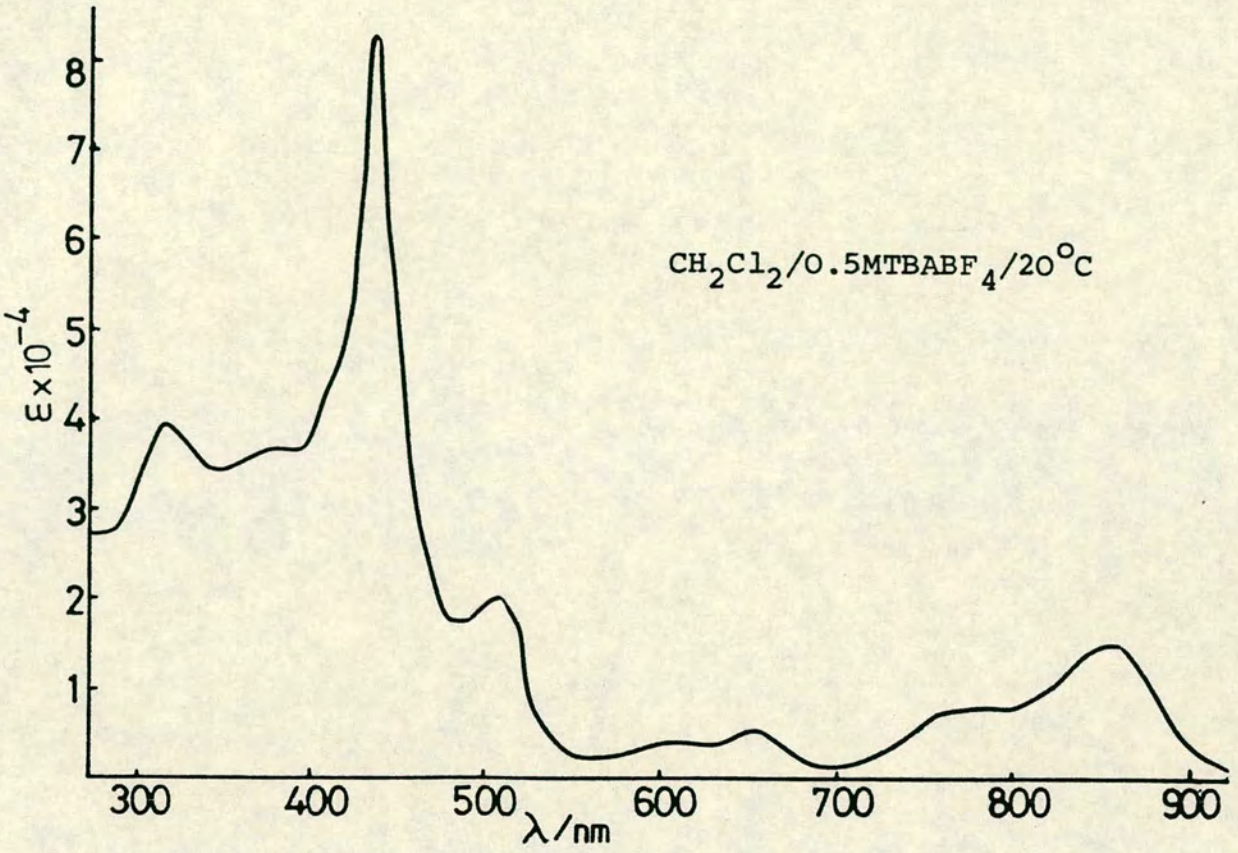

Figure C.30: Electronic Spectrum of Zinc-iso-hydroxy-tetraphenylporphin $(Zn\text{-}iso\text{-}HO\text{-}TPP)^+$

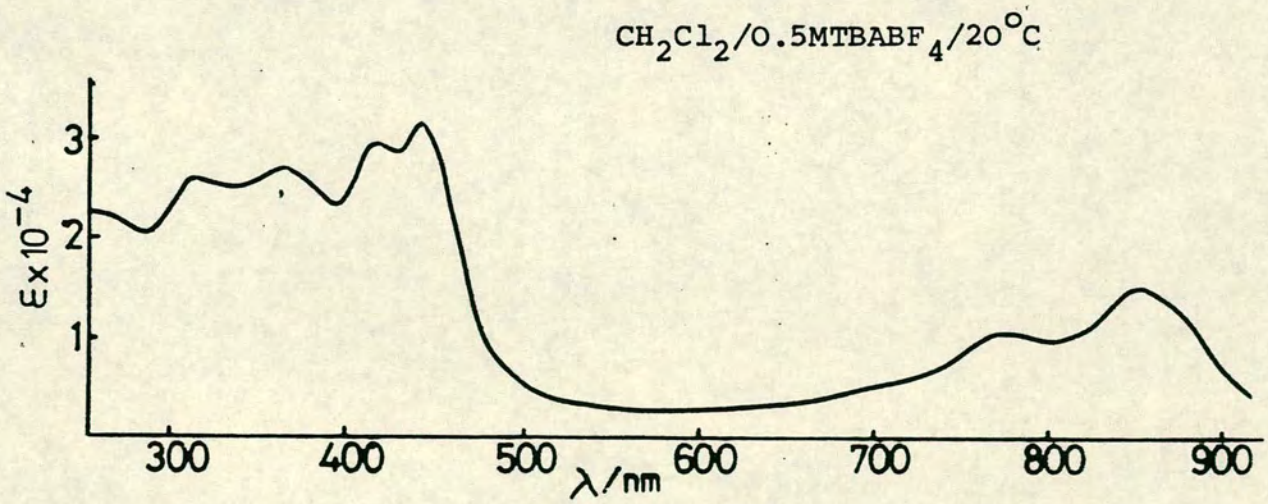

Figure C.31: Electronic Spectrum of Zinc-iso-methoxy-tetraphenylporphin $(Zn\text{-}iso\text{-}MeO\text{-}TPP)^+$

The cyclic voltammetric wave for the oxidation of each isoporphyrin shows 100% reversibility. The oxidative process occurring is most likely to be abstraction of an electron from the π electron manifold of the isoporphyrin, forming a π-radical species.

The electrochemistry of PdX, like its electronic spectrum, shows significant differences from that of the isoporphyrins. An attempt to generate the π-dication, $PdTPP^{2+}$, in the presence of methanol failed due to the oxidative range of dichloromethane/methanol (1%) being insufficient to allow the second oxidation of PdTPP to take place. In fact, the only area of similarity between the spectral and electrochemical behaviour of PdX and the zinc isoporphyrins is in the magnitude of the extinction coefficients of their electronic spectra. These are approximately 10% of the size of the Soret bands of the parent metalloporphyrins. A lowering of this magnitude in the spectral intensity of a tetrapyrrolic complex points toward disruption having taken place of the 18 π electron aromatic ring system found in metalloporphyrins.

Thus, further electrochemical study of PdX showed that this species is probably formed by reaction of its π-dication, $PdTPP^{2+}$, either intramolecularly or intermolecularly with a nucleophile. If nucleophilic attack is occurring, though, the final product is <u>not</u> an isoporphyrin. Thus, the revised mechanistic sequence is as outlined in Scheme C.11.

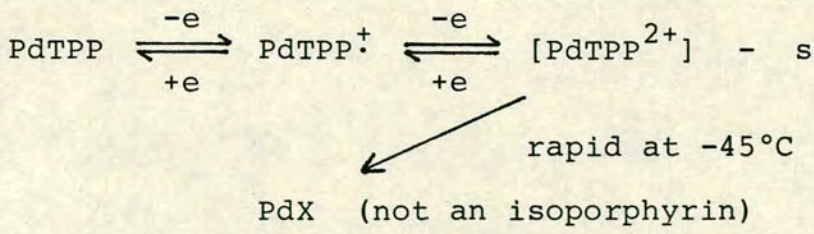

Scheme C.11: Revised Mechanistic Sequence for Pd(II)TPP Oxidation

Spectroelectrochemistry of PdX

It was hoped that useful structural information about PdX would emerge studying its electrochemical processes spectroscopically.

Oxidation of PdX results in the loss of the peaks at 418nm and 660nm, and the growth of an electronic spectrum with broad absorptions at 820nm (10,000 $M^{-1}cm^{-1}$) and 420nm (8,500 $M^{-1}cm^{-1}$). This process was found to be reversible, leading to its assignment as a new π-radical species $PdX^{+\cdot}$: the electronic spectrum of this product is illustrated in figure C.32.

Reduction of PdX was found to be a two-electron process and results in the collapse of the visible band of PdX at 660nm. This was replaced, in the visible region, by peaks of approximately equivalent intensity at 520 and 735nm. These were accompanied by the dramatic reemergence at ∿420nm of an intense band in the same position as the Soret band of PdTPP. The final electronic spectrum obtained is illustrated in figure C.33. This spectrum can either represent formation of one novel species or, more likely, because of the remarkable coincidence of the positions of the near-uv and high-energy

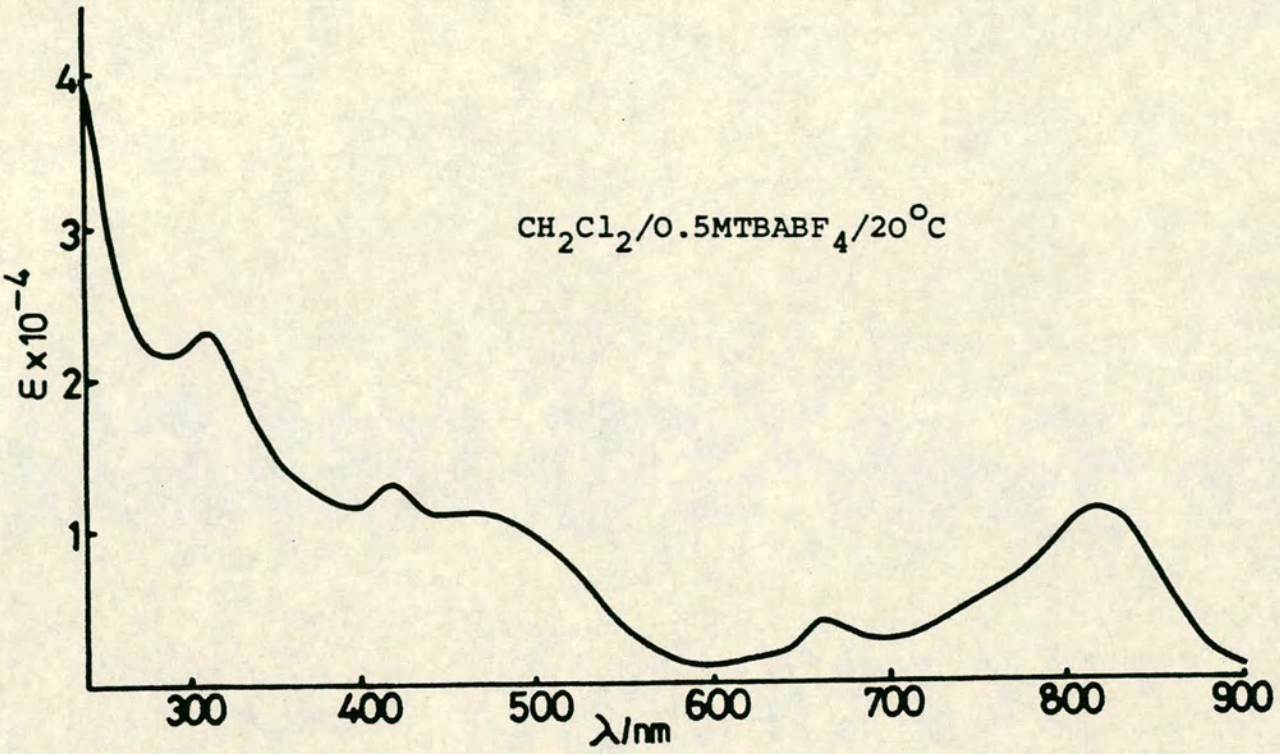

Figure C.32: Electronic Spectrum of the Oxidation Product of PdX

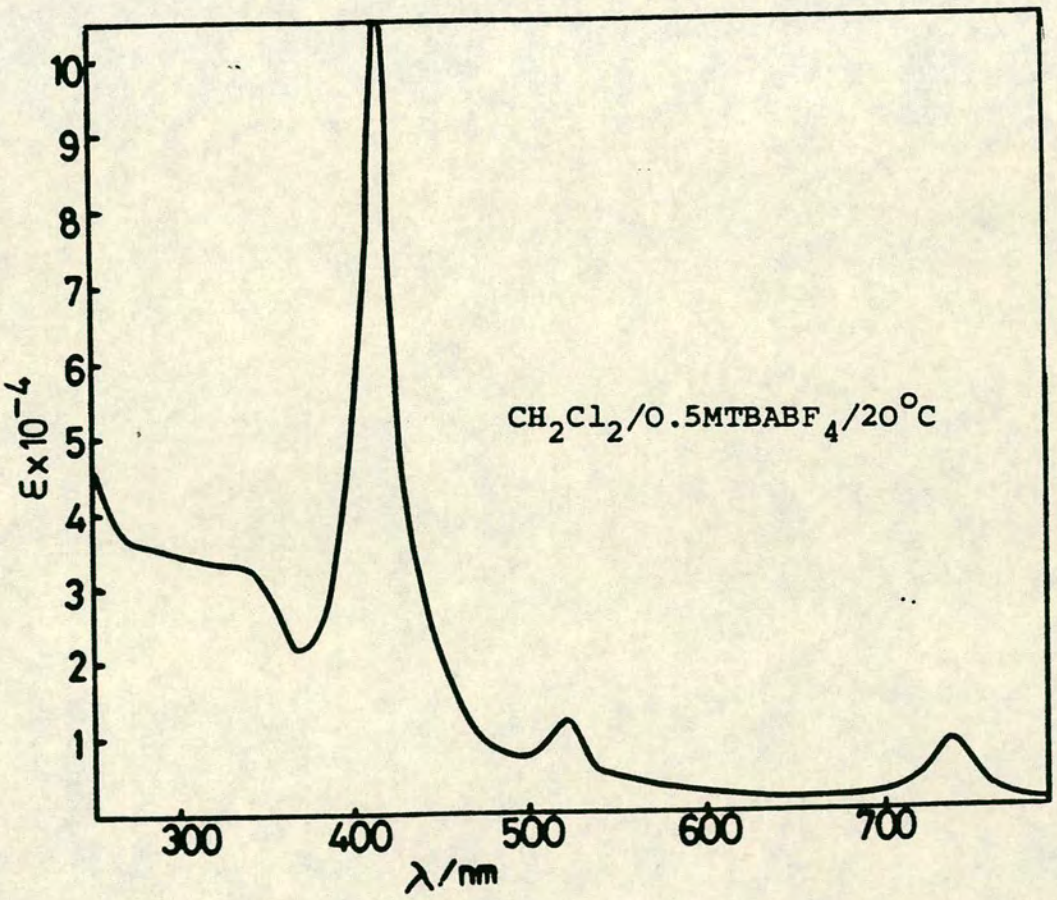

Figure C.33: Electronic Spectrum of the Reduction Product(s) of PdX

visible bands with the wavelengths of the Soret and visible bands of Pd(II)TPP, is caused by a mixture of products containing at least 50% PdTPP. Attempted study of the electrochemistry of the products of reduction of PdX proved to be impossible due to the general loss in electrochemical cleanliness of the electrolyte solution.

The regeneration of Pd(II)TPP from PdX has shown, however, that the structural alterations to the porphyrin macrocycle brought about by rapid reaction of its π-dication, $PdTPP^{2+}$, are reversible under drastic conditions. This implies, for the first time, the continued presence of the metal in the altered complex. It has also been recognised that the 18 π-electron aromatic ring system, found in metalloporphyrins and related species can be generated by reduction of PdX. This suggests that the tetrapyrrolic unit in PdX is a metallated macrocycle, as opposed to a possible ring-opened structure.

The mechanistic sequence, including the information obtained from the spectroelectrochemistry of PdX, is outlined in Scheme C.12.

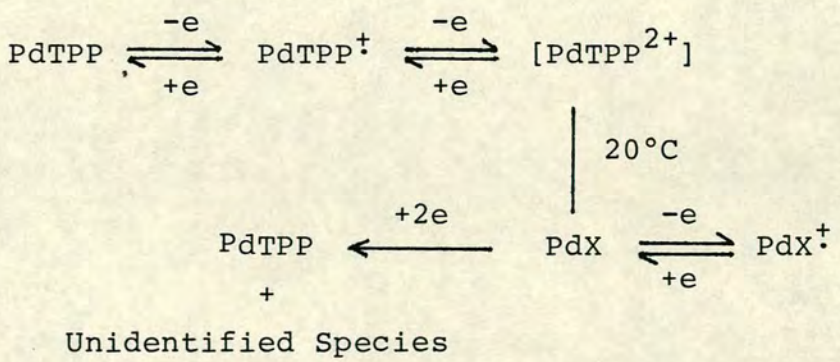

Scheme C.12: Revised Mechanism for the electrochemical behaviour of PdTPP Oxidation Products

Chemical Synthesis and Further Spectral Examination of PdX

As the structure of PdX could not be readily assigned to any known metallotetrapyrrollic complex on the evidence collected so far, it was important that sufficient quantities of the pure complex be prepared to enable further spectroscopic examination. It was found that chemical oxidation of PdTPP with an equivalent amount of ceric ammonium sulphate led to formation of a solution with the electronic spectrum of PdX. Chromatographic purification of this material led to isolation of a solid with extinction coefficients the same as those previously reported for PdX. This technique enabled preparation of ca. 50 mg of pure material at a time.

The mass spectrum of PdX is unobtainable using conventional electron-impact ionisation techniques due to the complexes involatility. Fast Atom Bombardment (F.A.B.) mass spectroscopy[61] of this compound in a thioglycerol/oxalic acid matrix showed, in addition to peaks caused by matrix aggregation, the presence of a major peak with M/E 752. The spectrum obtained is illustrated in figure C.34 with the area around M/E 752 expanded in figure C.35. It should be noted that the spectra obtained are the cationic $(M + H)^+$ spectra. The figures illustrated, though, list the molecular weights corrected for addition of one proton.

A molecular weight of 752 corresponds to the addition of 34 a.m.u. to PdTPP. This is the molecular weight obtained by addition of two hydroxyl groups to the parent complex. This result was then used to assign PdX as being a dihydroxy

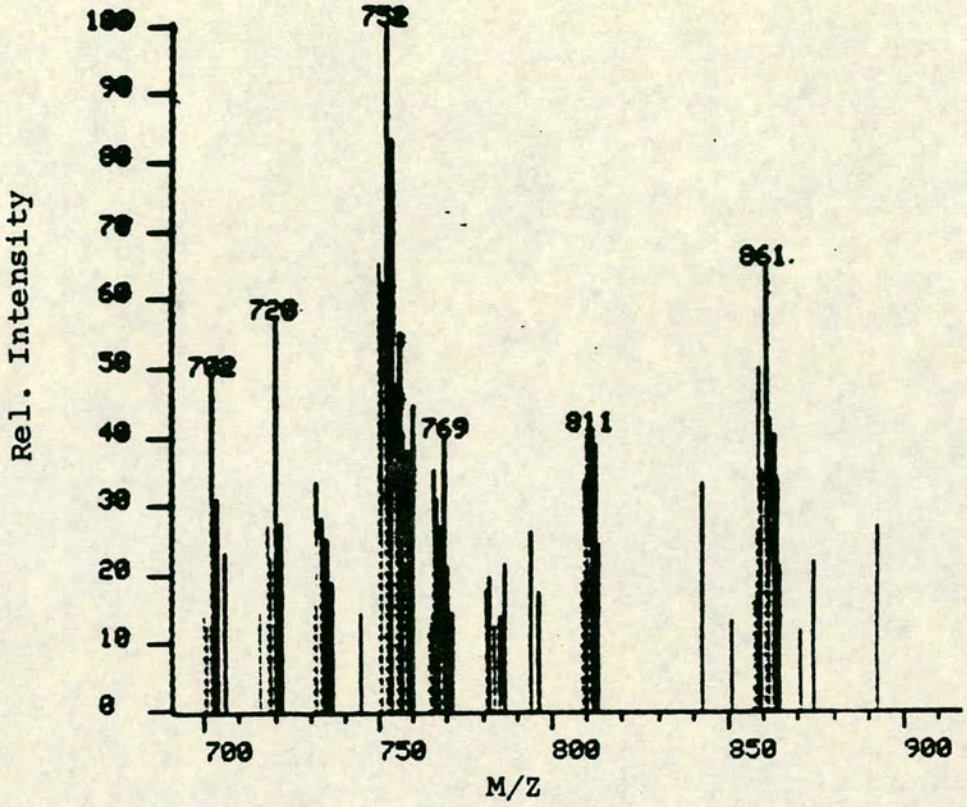

Figure C.34: F.A.B. Mass Spectrum (Thioglycerol/Oxalic Acid matrix) of PdX

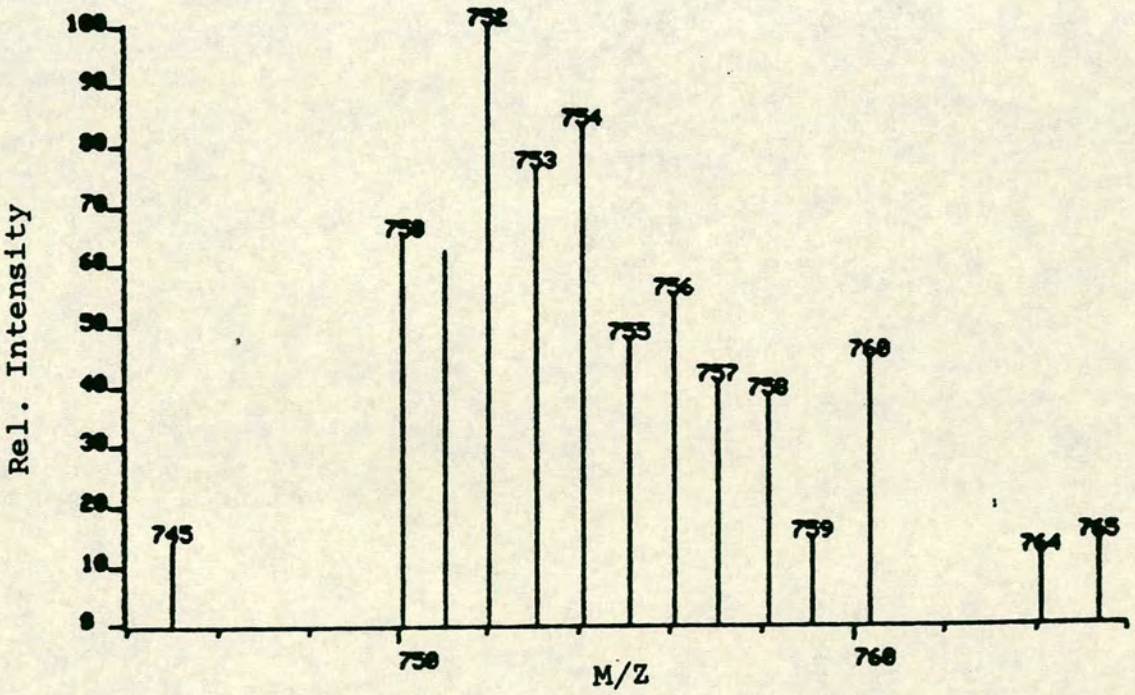

Figure C.35: F.A.B. Mass Spectrum of PdX with area around M/E 752 expanded

derivative of PdTPP. Crucially, the F.A.B. mass spectrum of PdTPP, in the same matrix solution, has its molecular ion peak at M/E 718.

Having established that two hydroxyl groups become bonded to PdTPP upon oxidation to its π-dication, it is necessary to determine the location of these groups in PdX. A possible formulation is represented by the dihydroxychlorin (46). A similar complex was proposed as being the product of photo-oxidation of tin(IV) tetra-arylporphyrins by Harriman et al.[43] (Section C.1-2).

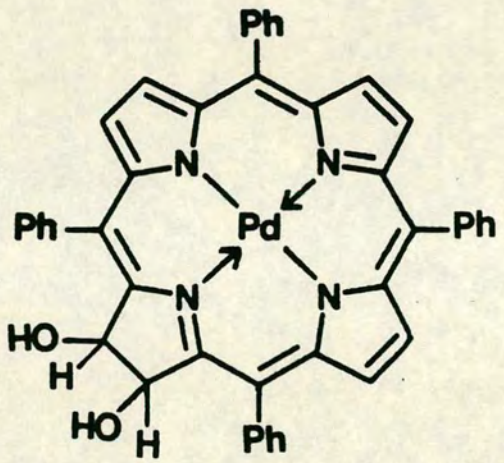

(46)

The electronic spectrum of PdX has a qualitatively similar shape to that of a metallochlorin[62], in that each has a band between 600 and 700 nm of about one-third the intensity of the accompanying Soret band. The PdX spectrum has, however, radically lower extinction coefficients throughout than would be expected for (46), which contains the full 18 π-electron aromatic ring known for tetrapyrrolic macrocycles. In addition, the electronic spectrum of the π-radical species, $PdX^{\ddagger}$ (figure

C.32), is unlike those reported for the π-radical-cations of metallochlorins[46]. Metallochlorin π-radical-cations exhibit electronic spectra characterised with overlapping bands in the visible region similar to those of metalloporphyrin π-radical-cations.

With (46) eliminated as a plausible structure of PdX, a wider consideration was prompted of any possible products formed by nucleophilic attack on a, presumably, reactive palladium hydroxy-isoporphyrin. In order for a product of this type to form, the isoporphyrin, as well as the preceding π-dication, must react rapidly as shown below.

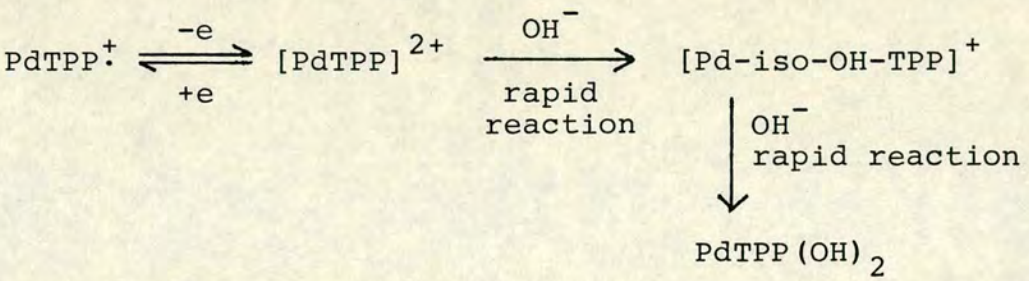

The major canonical forms of metalloisoporphyrin cations have been described previously[37]. The forms of a palladium hydroxy-isoporphyrin are shown in Scheme C.13, with the positive charge situated on either the meso carbon atom opposite to the hydroxylated meso position, the metal centre, or the inner pyrrolic carbon atom immediately adjacent to the hydroxylated meso carbon.

Substitution of hydroxide on the metal centre would have no major effect on the relative energy levels, within the π-orbital manifold, from those of the isoporphyrin. Thus, a hydroxy-palladium centre, bound to a hydroxy isoporphyrin, can

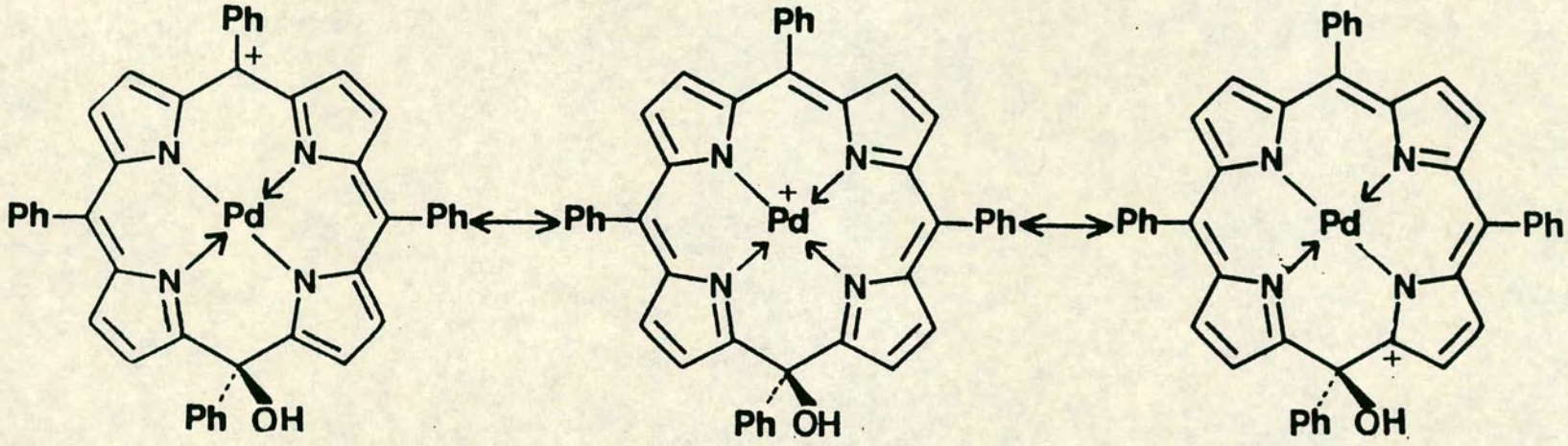

Scheme C.13: Major Canonical Forms of a Palladium Hydroxy-Isoporphyrin

be discounted as the structure of PdX due to the large differences in the electronic spectrum of the latter and those reported for isoporphyrins.

Attack of hydroxide ion at the meso carbon atom opposite to the substituted meso position would result in the 5,15-dihydroxyporphodimethene complex (47)

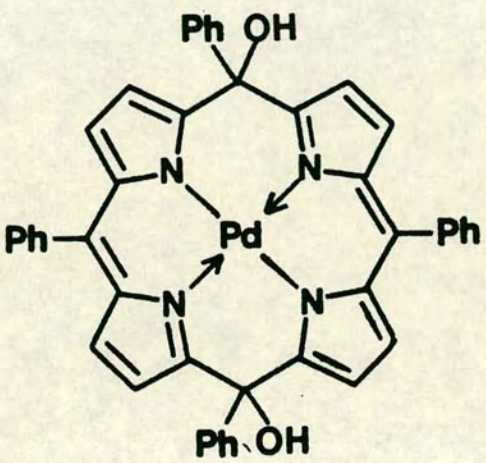

(47)

Porphodimethene complexes like (47) are well known, though without hydroxy group substitution on the methene carbons, and their electronic spectra have been recorded[21]. Such metalloporphodimethene electronic spectra are characterised by the presence of a single main absorption between 440 and 480nm, while there are often less intense bands observed between 550 and 590nm. As the electronic spectrum of PdX is wholly unlike this, then it was thought extremely unlikely that PdX is a metallo-porphodimethene.

Attack of hydroxide ion at the inner pyrrolic carbon atom, adjacent to the methene-meso carbon atom will produce

the species (48). This structural type has, as yet, not been reported.

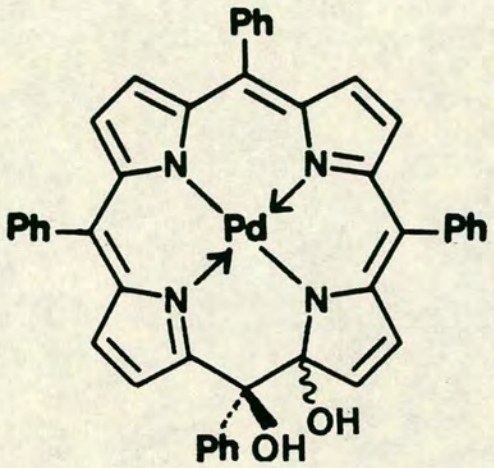

(48)

Although species like (48) have not been isolated, these complexes have been proposed as intermediates in the ring-opening of ZnTPP to form bilinones[37,38]. In these reports thallium(III) trifluoroacetate oxidised ZnTPP to its π-dication. This was followed by nucleophilic attack of trifluoroacetyl groups, firstly to form an isoporphyrin, and then to form the zinc di-trifluoroacetyl complex like (48). Protic work-up, however, demetallated the complex and formed the free-base dihydroxy complex, which undergoes ring-opening under protic conditions as outlined in Scheme C.8.

The ^{1}H n.m.r. spectra of PdTPP and PdX are shown in figures C.36 and C.37. The spectrum of PdTPP shows a sharp singlet at 8.85δ, which corresponds to its eight equivalent pyrrolic protons, while the two multiplets in the aromatic region between 7.6 and 7.8δ, and 8.1 and 8.2δ arise from the protons on the meso-phenyl groups. In contrast, the spectrum

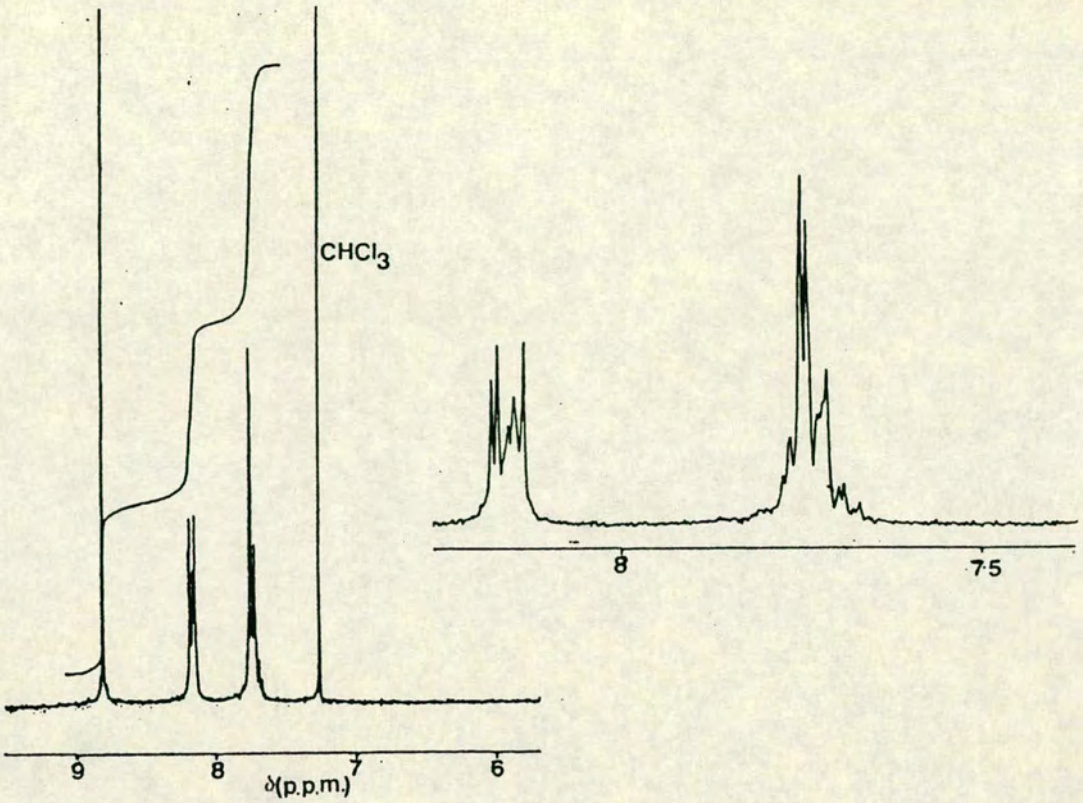

Figure C.36: ^{1}H n.m.r. spectrum (200 MHz) of PdTPP

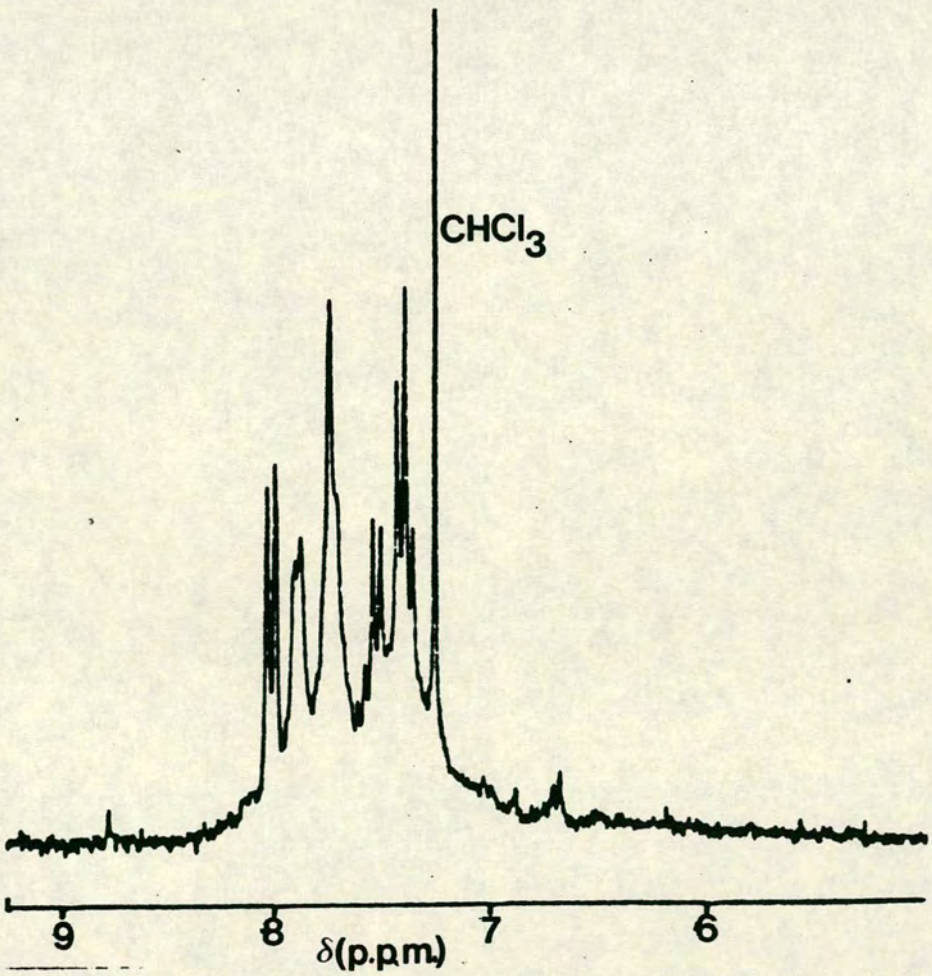

Figure C.37: ^{1}H n.m.r. spectrum (200 MHz) of PdX

of PdX is much less well-defined, with the main spectral region being dispersed between 6.5 and 8.2δ. This does however demonstrate the loss of the sharp singlet caused by the pyrrolic protons in the parent complex. The absence of this singlet anywhere in the spectrum indicates the loss of equivalence of these protons, and by inference of the four pyrrole rings themselves.

Treatment of the n.m.r. solution of PdX with D_2O resulted in the ^1H n.m.r. spectrum shown in figure C.38. In this spectrum there are no singlets at 7.74δ and 8.87δ as were observed in the spectrum of the untreated solution. This result implies that two types of non-equivalent hydroxyl protons are present in PdX. This spectrum also shows what is apparently a series of small doublets between 6 and 7.5δ. These peaks are all split by 4.7 Hz, a coupling constant consistent with those recorded between adjacent protons on pyrroles[63]. This observation led to the postulate that all eight pyrrolic protons on PdX are non-equivalent, causing the observed doublet structure. In addition, the considerable upfield shift of these resonances, from those of the parent complex, is indicative of a significant reduction in the aromaticity of the entire macrocycle.

The ^{13}C n.m.r. DEPT spectrum of PdX, shown in figure C.39, which illustrates only the ^{13}C resonances of the CH carbon atoms, also implies a highly unsymmetrical structure for PdX.

The i.r. spectrum of PdX exhibits a broad OH stretching frequency at ∿3550 cm^{-1}. The regions of the i.r. spectra of

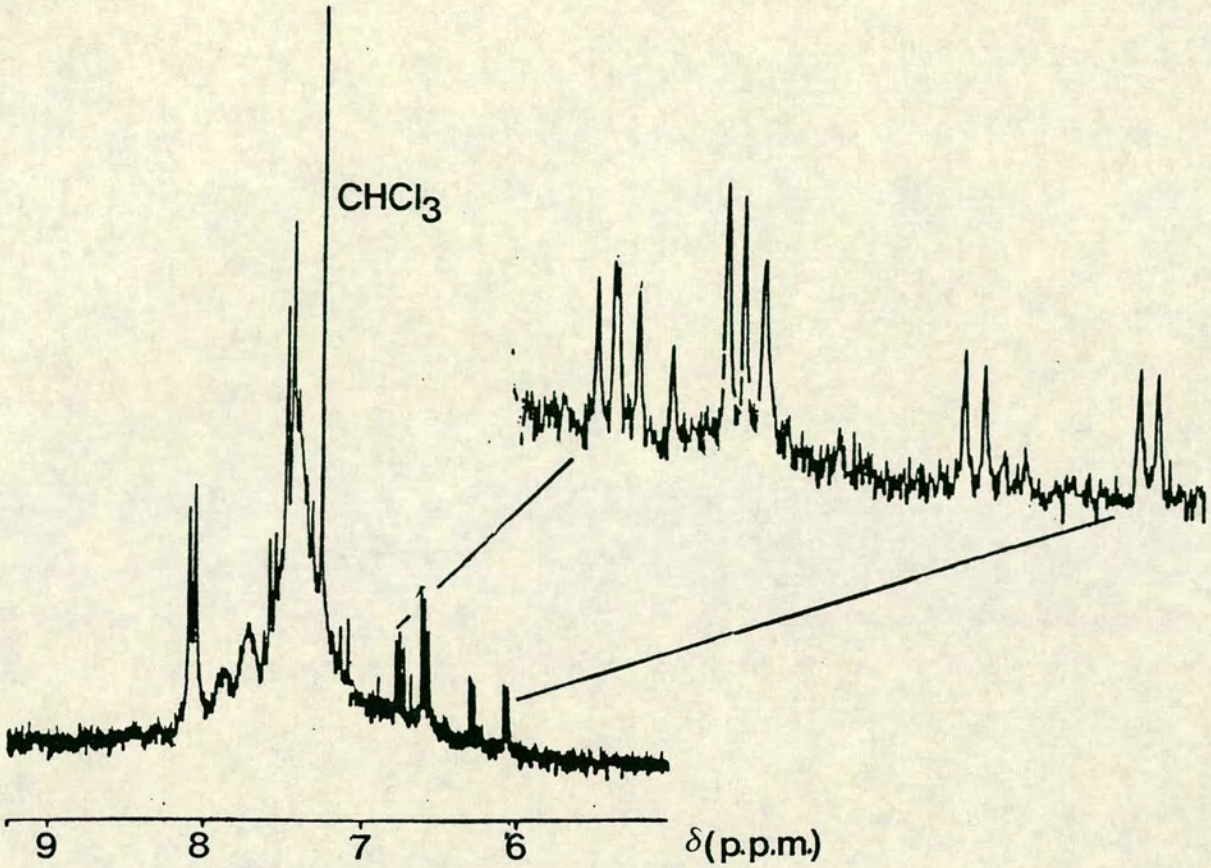

Figure C.38: ^{1}H n.m.r. spectrum (200 MHz) of PdX after $CDCl_3$ solution has been treated with D_2O

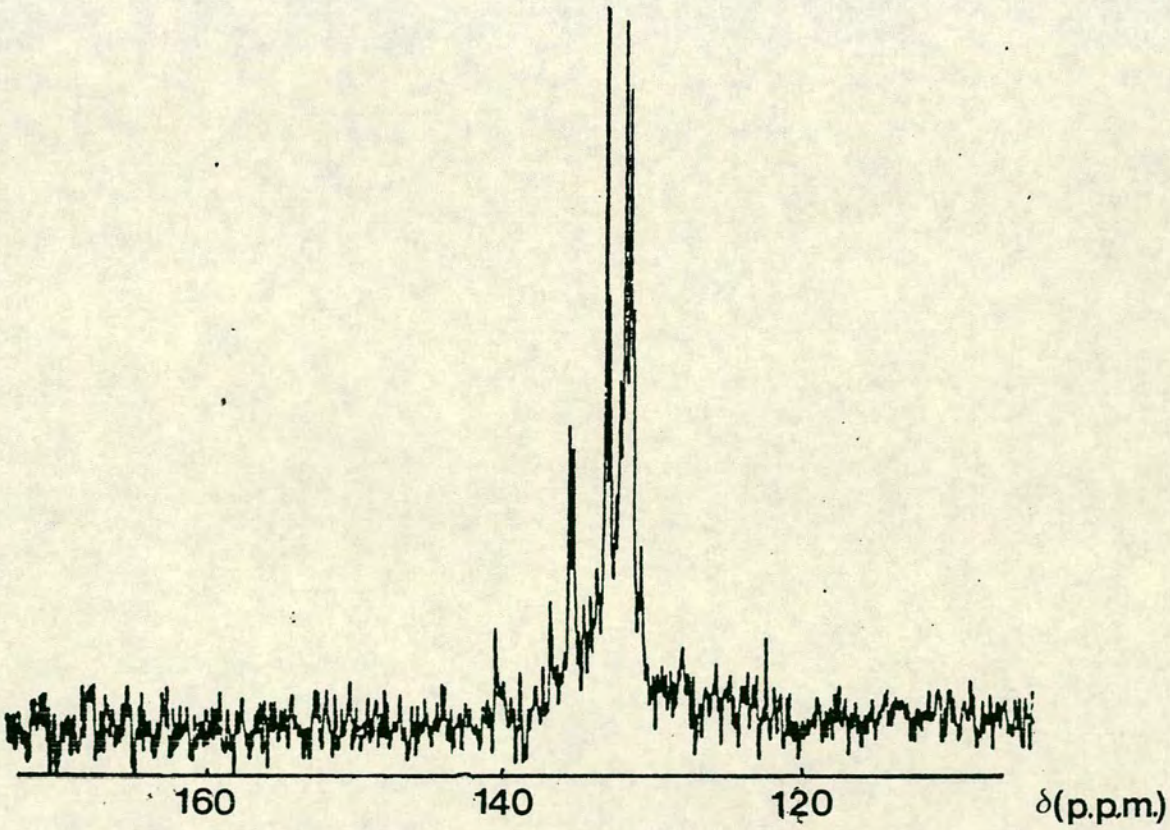

Figure C.39: ^{13}C n.m.r. (DEPT) spectrum of PdX (50·6 MHz) showing C-H resonances only

PdX and PdTPP between 1800 and 600 cm^{-1}, showing the skeletal vibrations of the different macrocycles are illustrated in figures C.40 and C.41 respectively.

Thus the spectral evidence gathered strongly suggests that (48) is the structure of PdX. The conformation of the adjacent hydroxy groups in the final structure is, as yet, unassigned, though steric considerations would suggest that a syn conformation would be favoured.

Therefore, the product of oxidation of PdTPP to its π-dication, $PdTPP^{2+}$, in a conventionally dried solvent system (i.e. solvent distilled over drying agent but thereafter handled in the atmosphere), is deduced to be (48) which can be named systematically; Palladium-14,15-dihydroxy-14,15-dihydrotetraphenylporphin.

Structural Implications

There are many questions that are posed by the assignment of (48) as the structure of PdX. These questions concern firstly the structural aspects of the final product and the reactivity patterns of the cationic intermediates during the synthesis.

Although (48) is the first reported example of a stable complex of a metalloporphyrin-like macrocycle containing a substituent on an inner pyrrolic carbon atom, there are examples of this substitution pattern known throughout the chemistry of tetrapyrroles. The photo-oxygenation of Mg(II)OEP[64] in benzene has been found to produce (49), a complex with an oxygen bridge, and an aldehyde group attached

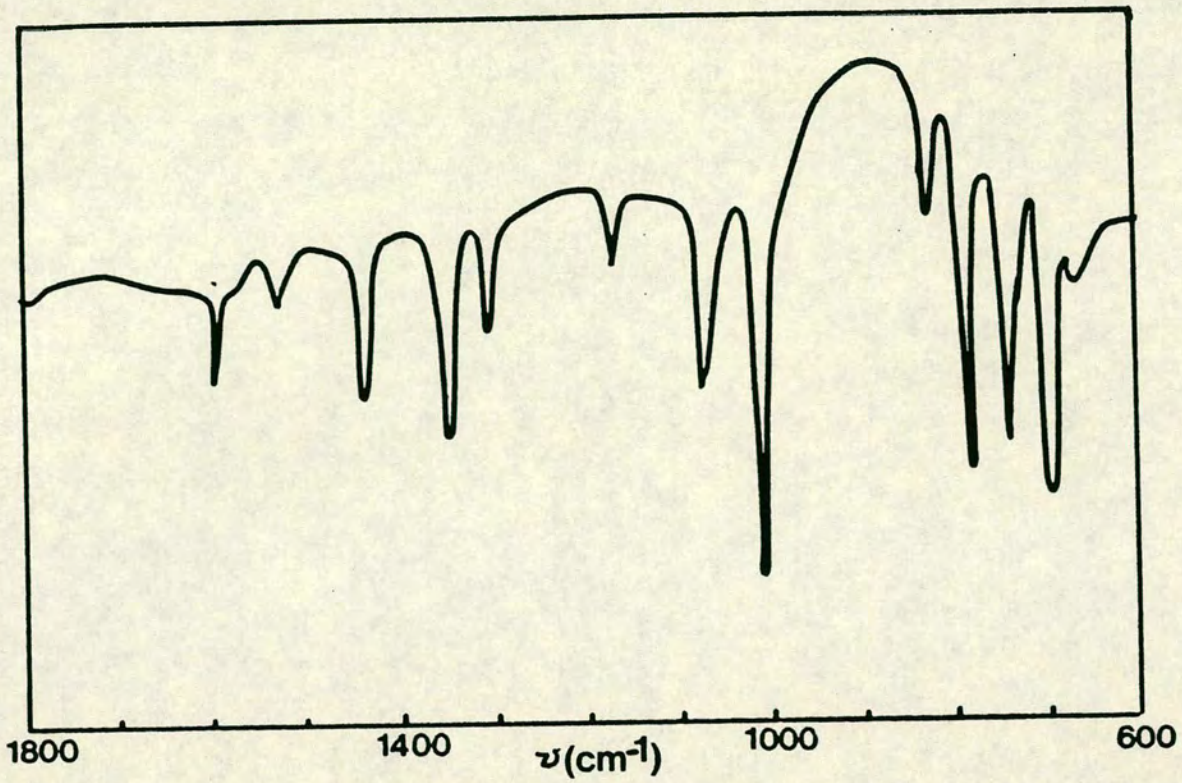

Figure C.40: Infra-red Spectrum (KBr disc) of Pd(II)TPP

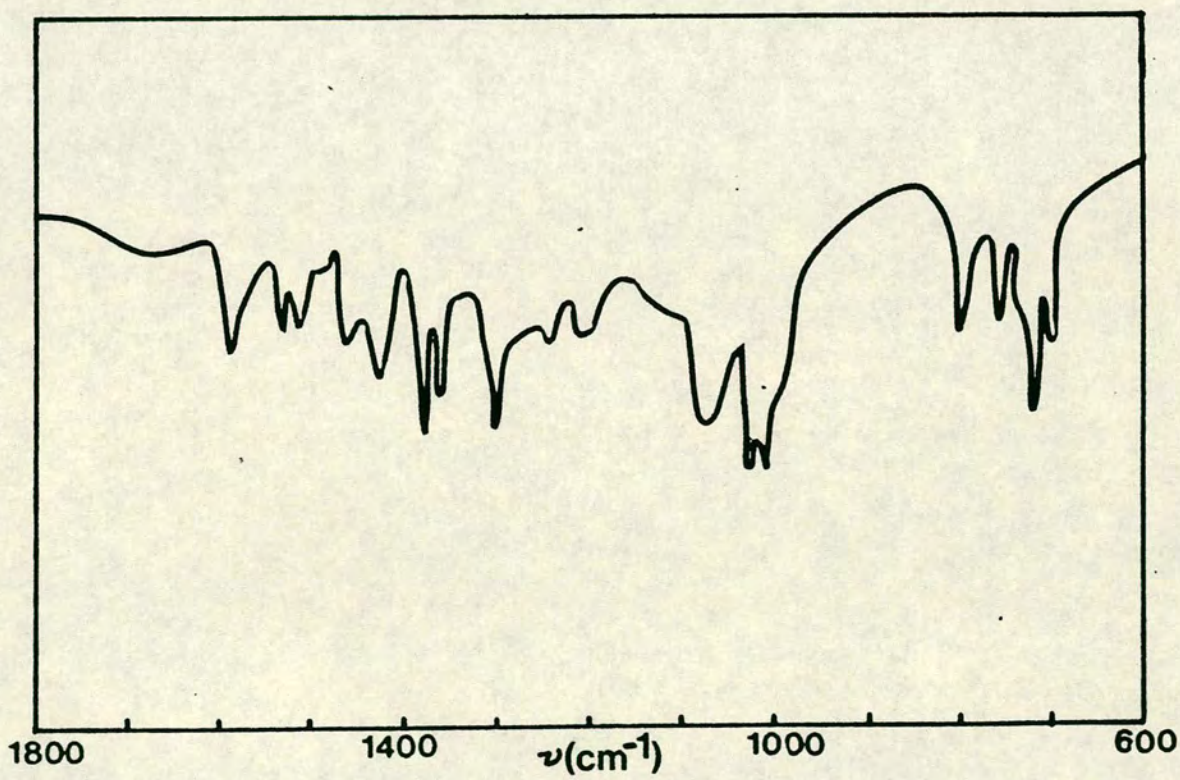

Figure C.41: Infra-red Spectrum (KBr disc) of PdX

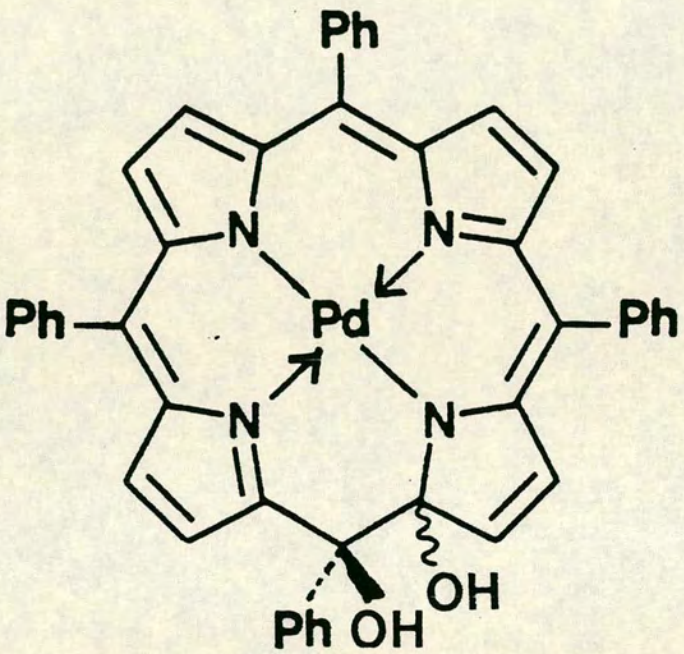

Palladium-14,15-dihydroxy-14,15-dihydrotetraphenylporphin

[Pd-14,15-$(OH)_2$TPP]

to the inner pyrrolic carbon atom adjacent to this bridge.

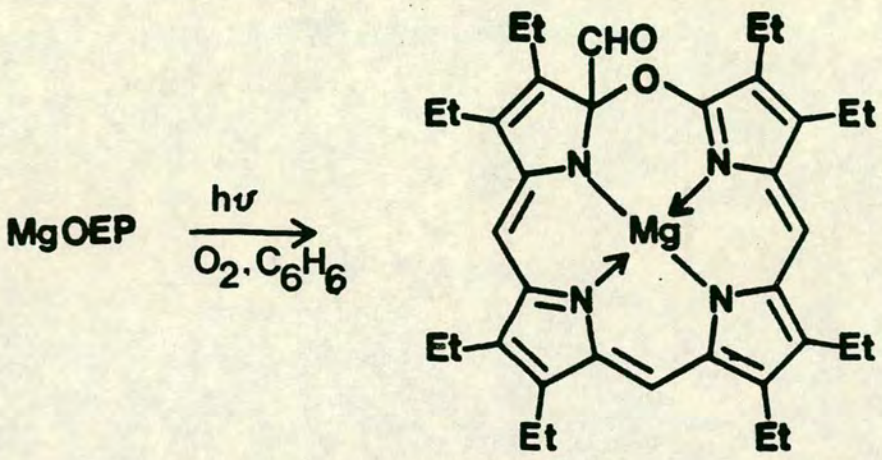

(49)

Interestingly, in accord with the close structural and electronic analogy, the electronic spectrum of (49) is of the same disposition as that of Pd-14,15-$(OH)_2$TPP, i.e. has its largest absorption at 408nm (ε = 30,000 $M^{-1}cm^{-1}$) with another main absorption with a shoulder at 825nm (14,000 $M^{-1}cm^{-1}$). Thus, although the positions of the secondary bands in (48) and (49) differ by 150nm, the extinction coefficients and spectral patterns for both species are similar.

Another example of a tetrapyrrolic system with this substitution type is that of the metallocorrins. These compounds have direct bonding between the inner pyrrolic carbon atoms of two pyrrolic units, as opposed to a bridging methine group. There are many examples where complexes of this type have inner pyrrolic substituents between the two directly bound pyrrole groups. An example of this structural type is (50), known as nickel(II)-1,19-dimethyltetradehydrocorrin[65].

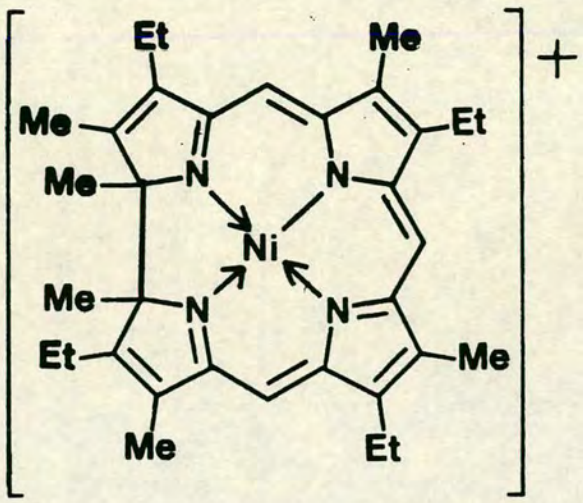

(50)

Thus, the presence of inner-pyrrole substituted complexes is well established in tetrapyrrolic chemistry. For metalloporphyrins, hitherto, no complexes of this type have been reported, although they have been postulated as being present in reaction sequences that have gone further to form ring-opened products.

A question also concerns the apparently enhanced reactivity of π-dications incorporating metals of the second and third transition series, $MTPP^{2+}$ where M = Pd, Pt. These appear to be much more reactive in comparison with first transition series and main-group analogues. These latter π-dications can normally be prepared, at room temperature, using conventionally dried solvent/electrolyte media, and are stable over a period of five to ten minutes. The much greater reactivity of the second and third transition series π-cations is also observed for the π-radical-cations of these species. First transition series and main group metalloporphyrin π-radical-cations of the type, $MTPP^{+\cdot}$, can be electrogenerated

in a conventional bulk cell, and their electronic spectra recorded after solution transfer, through air, to the spectroscopic cell. In contrast, the palladium π-radical species, $PdTPP^{+\cdot}$, decomposes to PdTPP under these conditions, even using rigorously degassed apparatus. This ensures that the authentic electronic spectrum of this species can only be recorded by using in situ spectroelectrochemical techniques. The reasons for the difference in reactivity between the first transition series and main-group metallo-π-cations, and their second and third transition series analogues have not been explained, although the differing tendency to axial ligation of counter-ions would appear to be an important consideration, with both electrostatic and mechanistic implications.

Similar criteria appear to apply for the stability of the first transition series cationic isoporphyrin complexes compared to those of the second and third transition series, since the palladium and platinum systems proceed to react further. Literature reports of the isolation of isoporphyrins have concerned only those containing the first transition series metal ions: Ni(II), Fe(III) and Zn(II) (Section C.1-2).

Having established that second and third row transition metal π-dications, $MTPP^{2+}$, and their hydroxyisoporphyrins are too reactive towards nucleophiles to be observed under normal conditions at room temperature, then the proposed site of attack by a further hydroxide anion on the isoporphyrin assumes further significance. There is one report[66] on the reactions of $[Zn(II)\text{-iso-MeO-TPP}]^{+}$ (21) toward methoxide and hydroxide. Reaction of (21) with sodium methoxide led to the

formation of the zinc-5,15-dimethoxyporphodimethene (51).

(21) $\xrightarrow{\text{NaOMe}}$

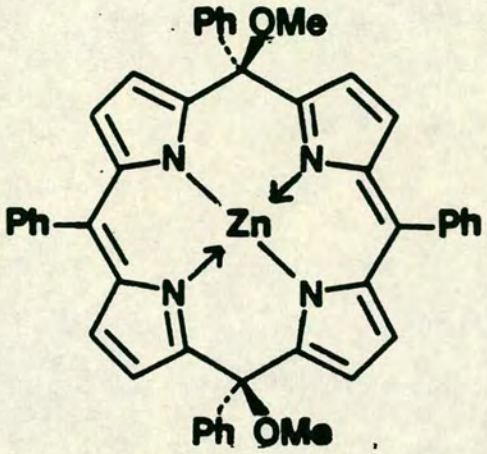

(51)

A similar reaction of (21) with 2N NaOH however did not produce the analogous 5,15-dihydroxyporphodimethene. Instead, reaction occurred at the adjacent inner pyrrolic carbon atom to the hydroxylated meso position. This forms a zinc dihydroxy complex, similar to (48), but further reaction with hydroxide leads to the overall ring-opening reaction outlined in Scheme C.14. In this reaction it was proposed that exposure of the methoxyisoporphyrin to hydroxide results in formation of the hydroxy isoporphyrin.

Thus, this reaction sequence suggests that formation of metallo-5,15-dihydroxyporphodimethenes does not readily occur. There are also two separate reports[66,67] on the preparation of the free-base 5,15-dihydroxyporphodimethenes which have found that metallation of these species with zinc results in loss of one hydroxyl anion leaving the hydroxy isoporphyrin as the only product.

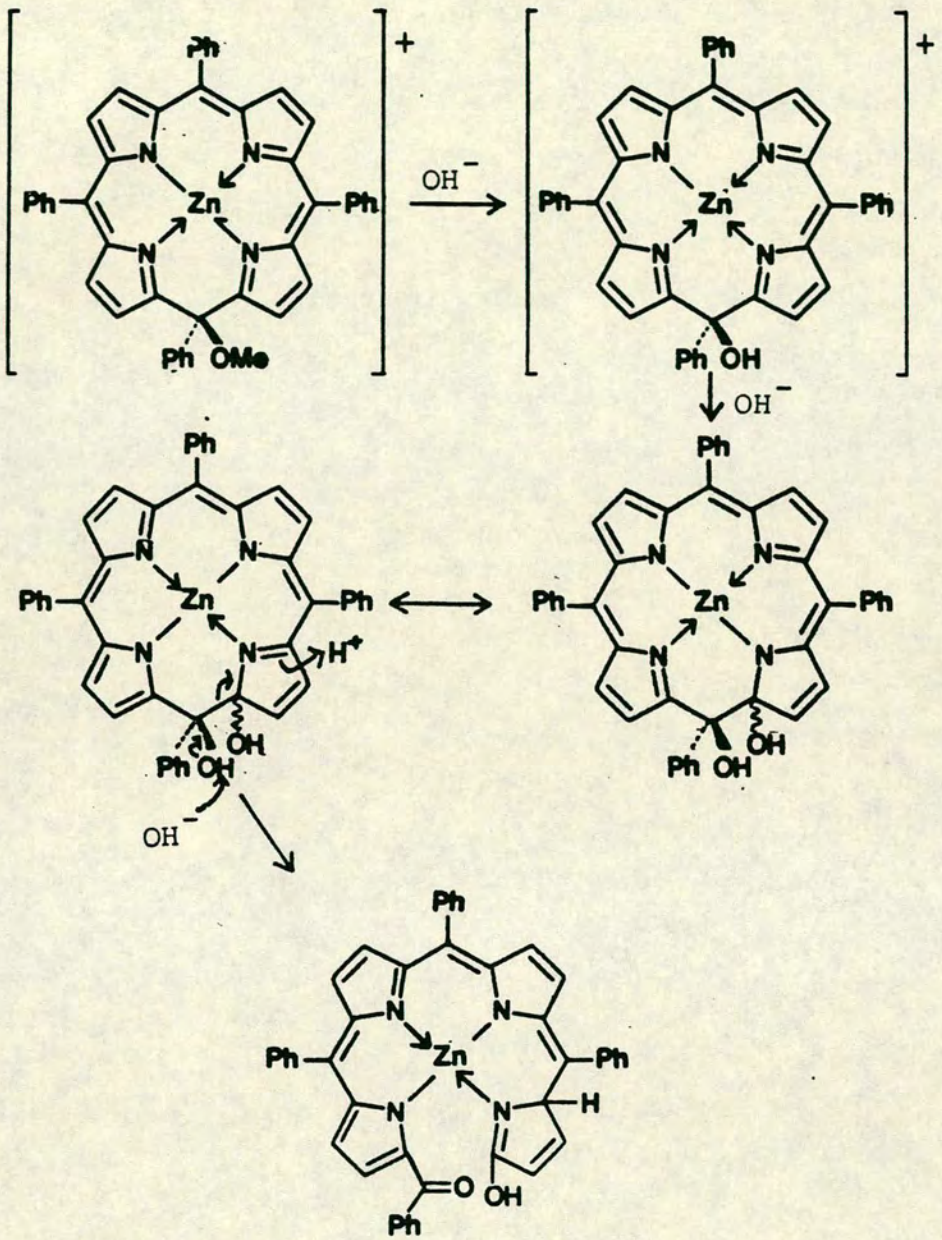

Scheme C.14: Reaction of zinc-methoxy-isoporphyrin cation with excess hydroxide

It is therefore probable that in the reaction taking place with PdTPP, that since there is no excess hydroxide present, reaction ceases with the dihydroxy derivative (48). Attempted reaction of 2N NaOH with a solution of (48) produced some changes in the electronic spectrum, which are illustrated in figure C.42, with the growth of a broad peak at ∿320nm, and a distinct gap appearing between the two visible peaks. This spectrum shows some of the same characteristics as the spectrum of the ring-opened zinc bilinone in Scheme C.14. However, this spectrum was achieved only after reaction for seven days, indicating that ring-opening occurs more slowly for the palladium dihydroxy species than the zinc complex.

Conclusions and Further Work

From the experiments described in this section, it is apparent that oxidation of Pd(II)TPP to its π-dication, even in conventionally "dry" media, results in rapid reaction with trace water to form palladium-14,15-dihydroxy-14,15-dihydrotetraphenylporphin. This reaction occurs because of the high reactivities toward nucleophiles of the π-dication and intermediate isoporphyrin cation. The actual final isomeric form of the dihydroxy product is determined by the difference in stability between (50) and the alternative 5,15-dihydroxyporphodimethene. The latter type of complex is known to be unstable to metallation, reverting to the isoporphyrin cation when a metal ion is inserted in the free-base.

Similar reactivity is observed for the oxidation to the π-dication of Pt(II)TPP, but as the dihydroxy complex is

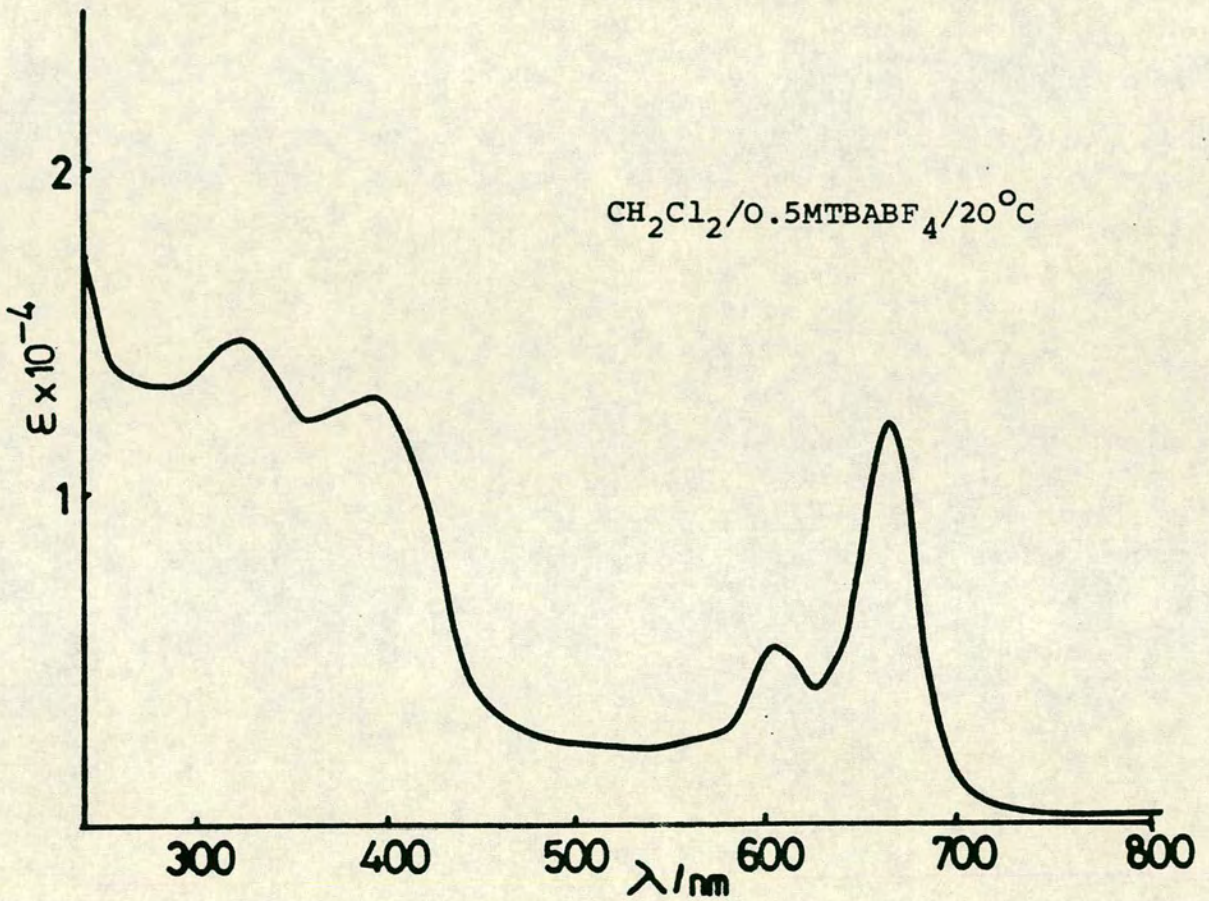

Figure C.42: Electronic Spectrum of the Product of Reaction between [Pd-14,15$(OH)_2$TPP] and 2N NaOH

coordinated to an unstable Pt(III) centre, the final product rapidly decomposes.

The overall reaction pathway, outlined in this section, for Pd(II)TPP is shown in Scheme C.15.

Further study of (48) is possible by many electrochemical and chemical means. It would be of interest to carry out the electro-oxidation of Pd(II)TPP in an electrolysis cell that is directly connected to a vacuum line, thereby ensuring that solvents and supporting electrolyses are as "dry" as is attainable. This could possibly permit the stabilisation of the π-dication, $PdTPP^{2+}$, at higher temperatures than have been possible to date.

It would also be of interest to find a strong nucleophile whose presence in an electrolysis solution does not restrict the anodic range of dichloromethane/$TBABF_4$. It would then be of interest to observe whether this nucleophile reacts preferentially over hydroxide with the π-dication, and what the isomeric forms of any disubstituted products are.

From a chemical viewpoint it would be particularly valuable to convert the hydroxide groups of [Pd-14,15-$(OH)_2$TPP] to methoxide. This would simplify the ^1H n.m.r. spectrum of the product, and also improve the volatility of the complex, thereby possibly enabling a conventional electron-impact mass spectrum to be recorded. This form of mass spectroscopy avails itself to greater analysis of the breakdown products of the molecular ion, as opposed to the limited information revealed using F.A.B. ionisation techniques.

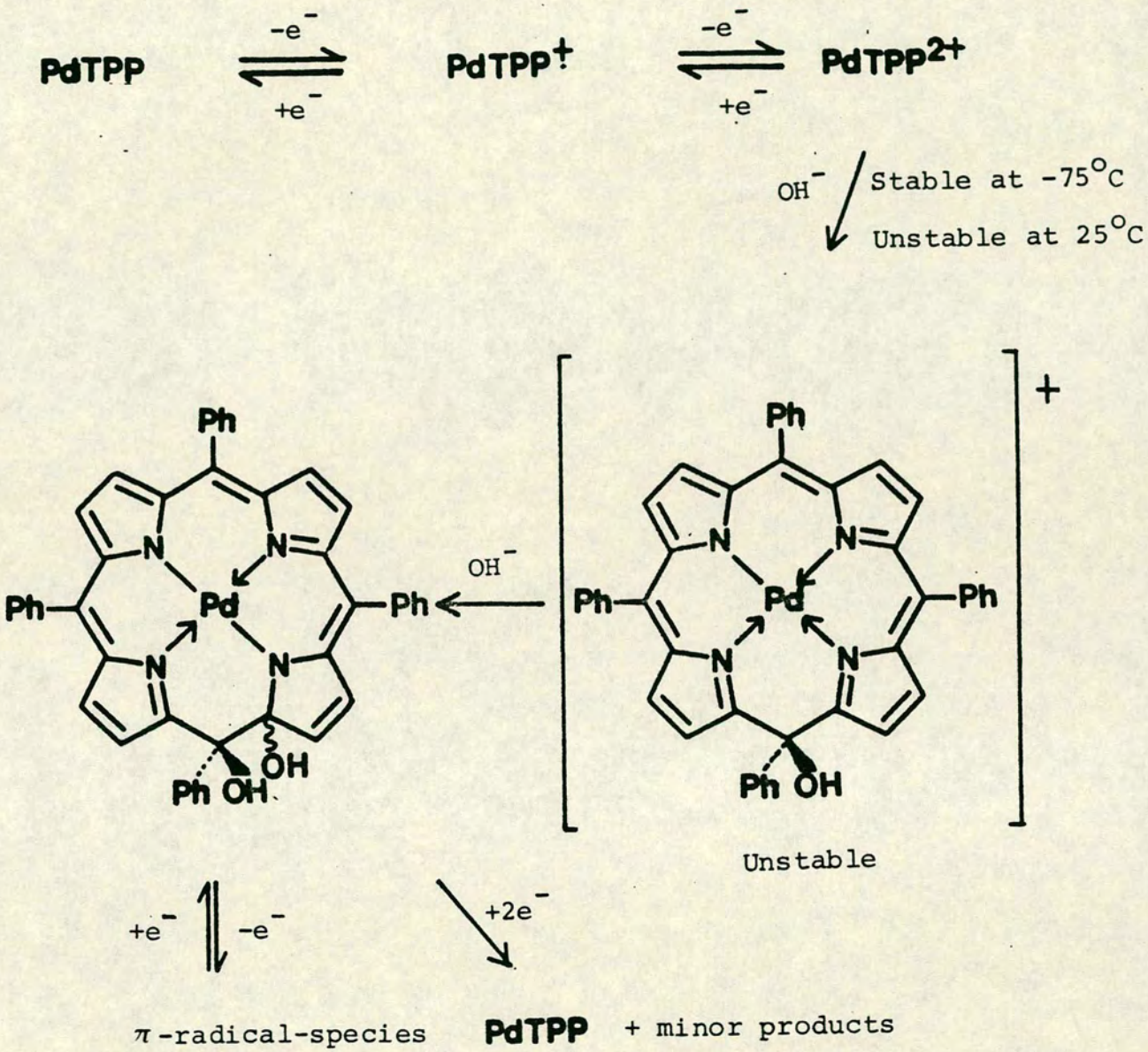

Scheme C.15: Overall Mechanistic Sequence for the Oxidative Electrochemistry of Pd(II)TPP

C.3 Experimental

C.3-1 Preparation of Metalloporphyrin Complexes

(a) Porphyrin Free-Bases

(i) Octaethylporphin (H_2OEP) [68]

Diethylpropionylmalonate:- A solution of diethyl malonate (320 g, 2 mol) in dry ethanol was prepared. 50 ml of this solution was added to magnesium turnings (50 g, 2.2 mol) covered in dry ethanol (50 ml), and the mixture maintained under a nitrogen atmosphere. Carbon tetrachloride (1 ml) was added to the mixture, which was stirred and refluxed gently until a vigorous exothermic reaction commenced. The remaining diethyl malonate solution was added to the mixture over a period of 30 minutes, during which time the vigour of the reaction was maintained. The mixture was then cooled, dry ether (500 ml) added, and the mixture refluxed for 1 h, thus removing any remaining undissolved metal. Freshly distilled propionyl chloride (235 g, 2 mol) was added dropwise to the stirred mixture, which was then left to stand for 12 h at room temperature. A cooled sulphuric acid solution was prepared by pouring concentrated sulphuric acid (98 g, 1 mol) onto crushed ice (200 g), followed by dilution to 600 ml with distilled water. The cooled acid solution was added dropwise to the stirred ethereal solution, which was then separated. The organic layer was washed with water, dried ($MgSO_4$), and concentrated by rotary evaporation. The residual oil was distilled under vacuum, and the fraction boiling at 115-135°C (18 mm Hg) collected. This fraction contained diethyl-propionylmalonate (253 g, 1.18 mol, 59%).

δ^1H(CCl_4) was in agreement with the literature.

Ethyl propionylacetate:- Diethylpropionylmalonate (250 g, 1.17 mol) was dissolved in water (500 ml) and the stirred mixture hydrolysed by slow distillation. The volume of the pot-still was maintained by the addition of water every hour during the 5 h distillation. At the end of the hydrolysis the pot-still residue and distillate were combined and the organic layer separated. The aqueous layer was extracted with ether (2 x 500 ml) and the organic extracts were combined, dried ($MgSO_4$) and concentrated by rotary evaporation. The residual oil was distilled under vacuum and the fraction boiling at 75-85°C (19 mm Hg) collected. The total yield of product was 128.5 g, this being a mixture of ethylpropionylacetate and diethylmalonate.

$\delta^1H(CCl_4)$ was in agreement with the literature, and showed that in this case the product consisted of 83% ethylpropionylacetate and 17% diethylmalonate.

4-acetyl-2-ethoxycarbonyl-3-ethyl-5-methylpyrrole:- Ethyl oximinopropionylacetate was prepared by the dropwise addition of sodium nitrite (62 g, 0.9 mol) in water (100 ml) to a solution of crude ethylpropionylacetate (125 g) in glacial acetic acid (200 ml), with the temperature held below 45°C throughout addition. The resulting solution was added dropwise to a solution of acetylacetone (138 ml, 134.5 g, 1.34 mol) in glacial acetic acid (185 ml). The temperature of the reaction mixture was raised to 100°C by the addition of a thick aqueous slurry containing zinc dust (240 g, 3.7 mol). Midway through the addition, extra acetylacetone (46 ml, 45 g) in glacial acetic acid was added to the

mixture. On completion of addition the hot solution was decanted from any residual zinc which was itself washed with hot glacial acetic acid. The combined acetic acid extracts were diluted to 4 l with distilled water. This caused the product to oil out and precipitate. The solid was filtered off, washed with water, and dissolved in dichloromethane (200 ml), whereupon the solution separated into aqueous and organic phases. Both phases were filtered to remove any residual zinc, and the organic layer separated and washed with water (150 ml). The dichloromethane solution was then slowly distilled, with the volume of the pot-still maintained by frequent additions of hot n-hexane. As distillation proceeded the product commenced to precipitate. The distillation was ceased when the solid was only barely covered with liquid. The solid was filtered off, washed with n-hexane and dried, giving crude 4-acetyl-2-ethoxycarbonyl-3-ethyl-5-methylpyrrole (104.1 g).

$\delta^1H(CDCl_3)$ was in agreement with the literature, showing that the product consisted of 81% 4-acetyl-2-ethoxycarbonyl-3-ethyl-5-methylpyrrole, and 19% 2-ethoxycarbonyl-3,5-dimethylpyrrole.

2-ethoxycarbonyl-3,4-diethyl-5-methylpyrrole:- Freshly distilled boron trifluoride diethyl etherate (160 g, 1.20 mol) was added dropwise to a stirred ice-cold solution of the crude preceding pyrrole (100 g) in THF (1l). Sodium borohydride (31.2 g, 0.8 mol) was added to the mixture at a rate that maintained the reaction temperature at 100°C. On completion of addition the mixture was stirred for a further 1 h, then glacial acetic acid was added to the solution until gas

evolution ceased. An equal volume of water was then added to the mixture and the organic layer was separated, filtered and concentrated by rotary evaporation. The residue was dissolved in the minimum volume of aqueous ethanol (95%), then diethylamine (25 ml, 17.7 g), aqueous formaldehyde (37%, 25 ml) and concentrated hydrochloric acid (0.5 ml) added. The mixture was heated under reflux for 12 h, then concentrated by rotary evaporation. The resulting residue was then dissolved in ether (400 ml). The Mannich base formed from the unwanted pyrrole was removed by extraction, firstly with water (400 ml), and then repeatedly with aqueous hydrochloric acid (5%, 400 ml) until the aqueous washings remained acidic. The ethereal solution was then washed with water, concentrated to 100 ml by rotary evaporation and diluted with aqueous methanol (70%, 600 ml). The resulting slurry was filtered off, washed with aqueous methanol (70%), and dried leaving pure 2-ethoxycarbonyl-3,4-diethyl-5-methylpyrrole (68.1 g, 0.33 mol).

$\delta^1H(CDCl_3)$ was in agreement with the literature.

5-N,N-diethylaminomethyl-2-ethoxycarbonyl-3,4-diethylpyrrole:- A solution of bromine (62 g, 0.4 mol) in dichloromethane (200 ml) was added to a stirred, nitrogen blanketed, solution of the preceding pyrrole (65 g, 0.31 mol) in dry ether (1l). On completion of addition the mixture was stirred for a further 20 minutes, followed by the rapid addition of a solution of diethylamine (130 ml, 92 g) in dry ether (350 ml). Water (750 ml) was added to the mixture which was then separated. The organic layer was washed with water and excess crushed ice added. The organic layer was then washed with a solution of

aqueous (10% v:v) hydrochloric acid (750 ml). The aqueous acid was then separated, washed with ether (500 ml) and added to a mixture of aqueous ammonia (37%, 75 ml) and water (75 ml). The product which oiled out was extracted with light petroleum (b.p. 30-40°C, 500 ml). The organic extract was washed with water, dried ($MgSO_4$) and concentrated by rotary evaporation. The resulting oil was distilled, and the fraction boiling at 160-165°C (2 mm Hg) collected, this being pure 5-N,N-diethylaminomethyl-2-ethoxycarbonyl-3,4-diethylpyrrole (39.1 g, 0.14 mol, 50% yield).

$\delta^1H(CDCl_3)$ was in agreement with the literature.

Octaethylporphin:- A solution of potassium hydroxide (19.3 g, 0.3 mol) in water (30 ml) was added to a solution of the preceding pyrrole (39.0 g, 0.14 mol) in aqueous ethanol (95%, 150 ml). The mixture was heated at 100°C for 3 h, then diluted by the addition of water (300 ml). The cooled mixture had glacial acetic acid (300 ml) added to it. The resultant mixture was slowly distilled, while a steady stream of air passed through the pot-still solution. After the pot-still volume was reduced by one half (1 h), methanol (200 ml) was added to the mixture which was then cooled. The crude porphyrin precipitated, and was filtered off and washed with methanol. The crude product was purified by recrystallisation, from a Soxhlet, with toluene. Violet crystals of pure octaethylporphin (9.75 g, 0.018 mol, 51.5%) were filtered off and dried.

$C_{36}H_{46}N_4$ requires: C 80.90% H 8.61% N 10.49%

observed: C 80.84% H 8.39% N 10.34%

$\lambda_{max}(C_6H_6)$: 400 (ε = 150,000), 499(14,200), 532(10,800), 568(7,000), 622(5,700).

(ii) Tetraphenylporphin (H_2TPP) [69]

Benzaldehyde (40 ml, 42 g, 0.4 mol) and pyrrole (28 ml, 27 g, 0.4 mol) were dissolved in propionic acid (1.5 l). The solution was heated under reflux for 30 minutes, then allowed to cool whereupon the precipitated solid was filtered off and washed firstly with hot methanol then hot water. A solution of 2,3-dichloro-5,6-dicyanobenzoquinone (2.5 g) in dry benzene was added to a solution of the crude prophyrin in ethanol-free chloroform (1.25 l). The mixture was heated under reflux for 3 h, then the hot solution filtered under suction through an alumina column (5 x 20 cm). The alumina was washed with dichloromethane (200 ml), and the combined filtrate concentrated to 200 ml by rotary evaporation. Methanol (200 ml) was added to the solution, and the resulting precipitate filtered off, washed in methanol, and dried to give pure tetraphenylporphin (8.96 g, 0.015 mol, 15%).

$C_{44}H_{30}N_4$ requires: C 85.99% H 4.89% N 9.12%

observed: C 85.80% H 4.88% N 9.04%

$\lambda_{max}(C_6H_6)$: 419(ε = 450,000), 515(19,000), 546(7,900) 592(5,300), 647(3,400)

(b) Metalloporphyrins

(i) Zinc porphyrins

The porphyrin (250 mg) was dissolved in chloroform (150 ml), and a saturated solution of zinc(II) acetate in methanol (1 ml) added. The mixture was heated under reflux for 30 minutes, then the solution volume reduced to 30 ml by rotary evaporation. Methanol (50 ml) was added to the solution, and the precipitated solid was filtered off, dried and recrystal-

lised from chloroform. The following pure zinc porphyrins were prepared by this method:-

Zn(II)OEP (230 mg, 82%), $\lambda_{max}(C_6H_6)$: 400(ε = 323,000), 530(14,100), 570(20,400)

Zn(II)TPP (252 mg, 91%), $\lambda_{max}(C_6H_6)$: 417(ε = 550,000), 557(19,100), 594(5,200)

(ii) Nickel porphyrins

The porphyrin (250 mg) and nickel(II) acetate (200 mg) were dissolved in glacial acetic acid (100 ml), and the mixture heated under reflux for 6 h. On cooling, the precipitated solid was filtered off and purified by column chromatography (alumina, 5% (v:v) methanol/chloroform eluant). The following pure nickel porphyrins were prepared by this method:-

Ni(II)OEP (170 mg, 68%), $\lambda_{max}(C_6H_6)$; 389 nm(ε = 205,000), 518(7,800), 551(44,700)

Ni(II)TPP (150 mg, 60%), $\lambda_{max}(C_6H_6)$; 416(ε = 233,000), 490(3,400), 529(17,500), 562(shoulder).

(iii) Palladium and Platinum porphyrins [22]

The porphyrin (0.5 mmol) and the metal(II) chloride (0.5 mmol) were dissolved in benzonitrile (150 ml). The mixture was heated under reflux for 4 h while a stream of dry nitrogen was passed through the solution. On completion of heating the mixture was concentrated by rotary evaporation, and purified by dry-column chromatography (silica, dichloromethane eluant). The following pure palladium and platinum porphyrins were prepared by this method:-

Pd(II)TPP (280 mg, 79%), $\lambda_{max}(C_6H_6)$; 418(ε = 330,000), 486(2,500), 524(29,300), 555(2,500).

Pt(II)TPP (230 mg, 58%), $\lambda_{max}(C_6H_6)$; 403(ε = 266,000), 510(24,500), 537(6,000)

Pd(II)OEP (230 mg, 72%), $\lambda_{max}(C_6H_6)$; 395(ε = 198,000), 515(12,700), 534(49,700).

Pt(II)OEP (190 mg, 52%), $\lambda_{max}(C_6H_6)$; 382(ε = 220,000), 503(10,500), 534(54,000)

C.3-2 Electrochemical Experiments

(a) General

All electrochemical experiments were carried out in a dichloromethane/0.5M tetra-n-butylammonium fluoroborate solution. The concentration of substrate used was 10^{-4}M except where solubility constraints existed, or in spectro-electrochemical experiments where the necessary concentrations were individually selected.

(i) Solvent Purification

Reagent grade dichloromethane was stored over potassium hydroxide pellets for 48 h, then distilled over phosphorous pentoxide for at least 4 h prior to its use as an electro-chemical solvent.

(ii) Preparation of Supporting Electrolyte

A 40% aqueous solution of tetra-n-butylammonium hydroxide (160 ml, 0.25 mol) was neutralised by the slow addition of 40% aqueous fluoroboric acid (∿37.5 ml). The resulting precipitate was filtered off, dried, then dissolved in the minimum volume of hot 'Analar' methanol. The hot solution was

filtered, and the solid that formed on cooling filtered off and further recrystallised from 'Analar' methanol. This produced white needles of pure tetra-n-butylammonium fluoroborate ($TBABF_4$).m.p.>300°C.

Prior to its use, the supporting electrolyte was dried at 100°C (0.5 mm Hg) for 24 h.

(b) Voltammetry

Voltammetric experiments were carried out in a glass cell which accommodated 5 ml of cell solution. During operation the cell was clipped on an air-tight plastic cell top. This contained five SQ14 socket joints, into which the following cell components were placed.

(i) Working Electrode:- This consisted of a polished platinum disc (diameter = 1 mm), sealed in a glass tube. Electrical contact was made via a copper wire.

(ii) Secondary Electrode:- This consisted of a platinum coated stainless steel rod (diameter = 2 mm).

(iii) Reference Electrode:- The reference electrode used was a commercial Ag/AgCl electrode immersed in an electrolyte solution containing 0.45M $TBABF_4$ and 0.05M TBACl in dichloromethane. To prevent possible contamination of the cell solution the reference electrode compartment was separated from the cell by a salt bridge containing dichloromethane/ 0.5M $TBABF_4$.

(iv) Gas Inlet:- Dry, dichloromethane saturated nitrogen was passed through this inlet which terminated in two

teflon tubes, one of which was immersed in the cell solution. An adaptor enabled gas either to be bubbled through, or passed over the cell solution. Prior to electrochemical measurements the cell solution was thoroughly degassed.

(v) Sample Inlet:- This compartment was stoppered during cell operation, but could be opened in order to facilitate addition of dry substrate.

(c) Electrolysis Experiments

Large scale electrogenerations were carried out in the three-compartment cell illustrated in figure C.43. This had a total cell volume of 25 ml, with the volume of the working electrode compartment being 10 ml. This cell was used for coulometry and also the preparation of the following products:-

Zinc-iso-methoxytetraphenylporphin fluoroborate:- 2-electron oxidation of Zn(II)TPP in a 1% (v:v) methanol/dichloromethane 0.5M $TBABF_4$ solution resulted in the formation of $[Zn\text{-}iso\text{-}MeO\text{-}TPP]^+BF_4^-$. $\lambda_{max}(CH_2Cl_2)$; 442(ε = 31,000), 770(12,000), 855(17,000).

Zinc-iso-hydroxytetraphenylporphin fluoroborate:- 2-electron oxidation of Zn(II)TPP in a 1% (v:v) water/dichloromethane 0.5M $TBABF_4$ solution resulted in the formation of $[Zn\text{-}iso\text{-}HO\text{-}TPP]^+BF_4^-$. $\lambda_{max}(CH_2Cl_2)$; 437(ε = 83,000), 505(21,500), 765(11,000), 850(16,400).

(d) Spectroelectrochemical Experiments

In situ spectroelectrochemical experiments were carried out in the cell illustrated in figure C.44. (Designed by

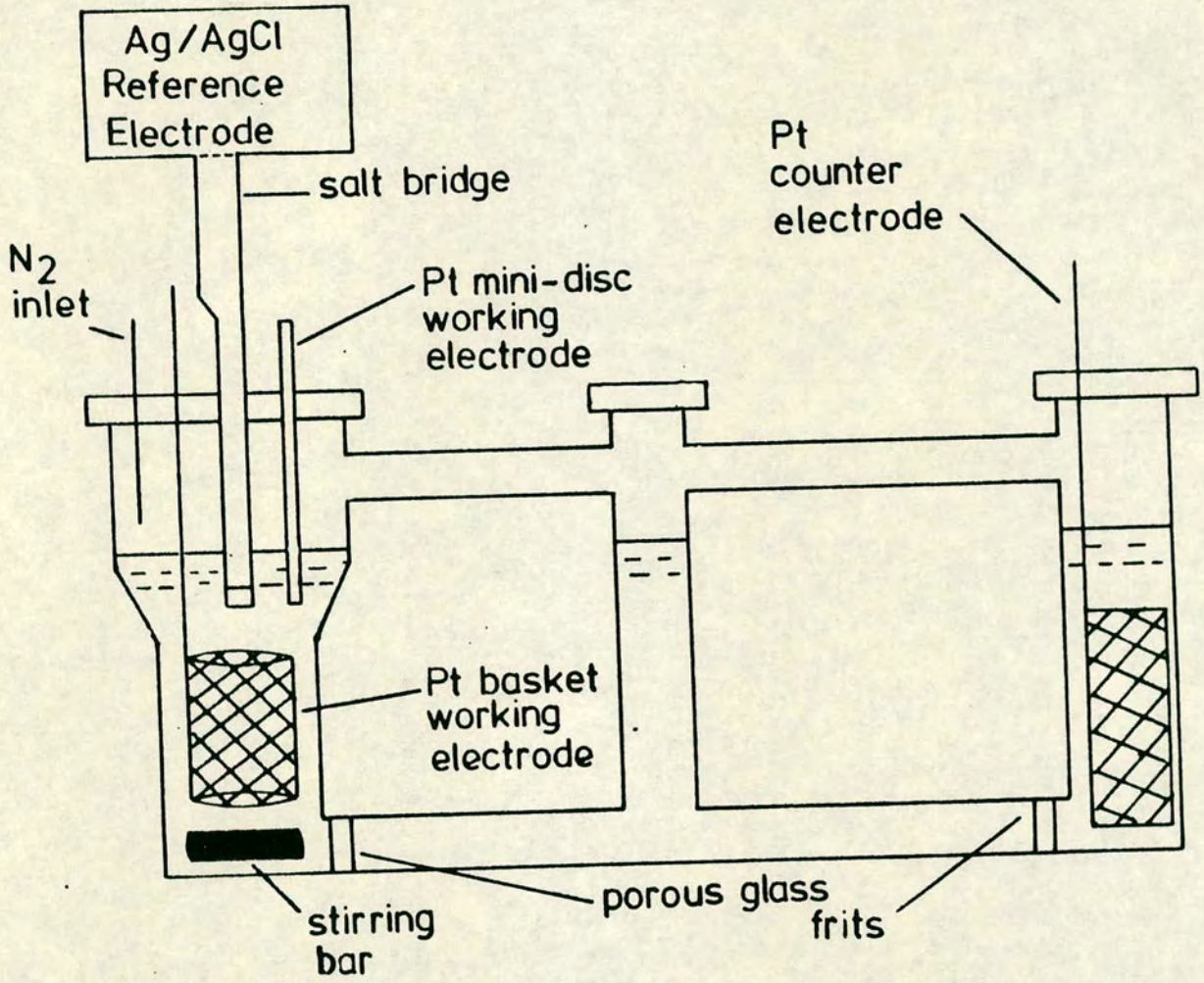

Figure C.43: Three Compartment Electrolysis Cell

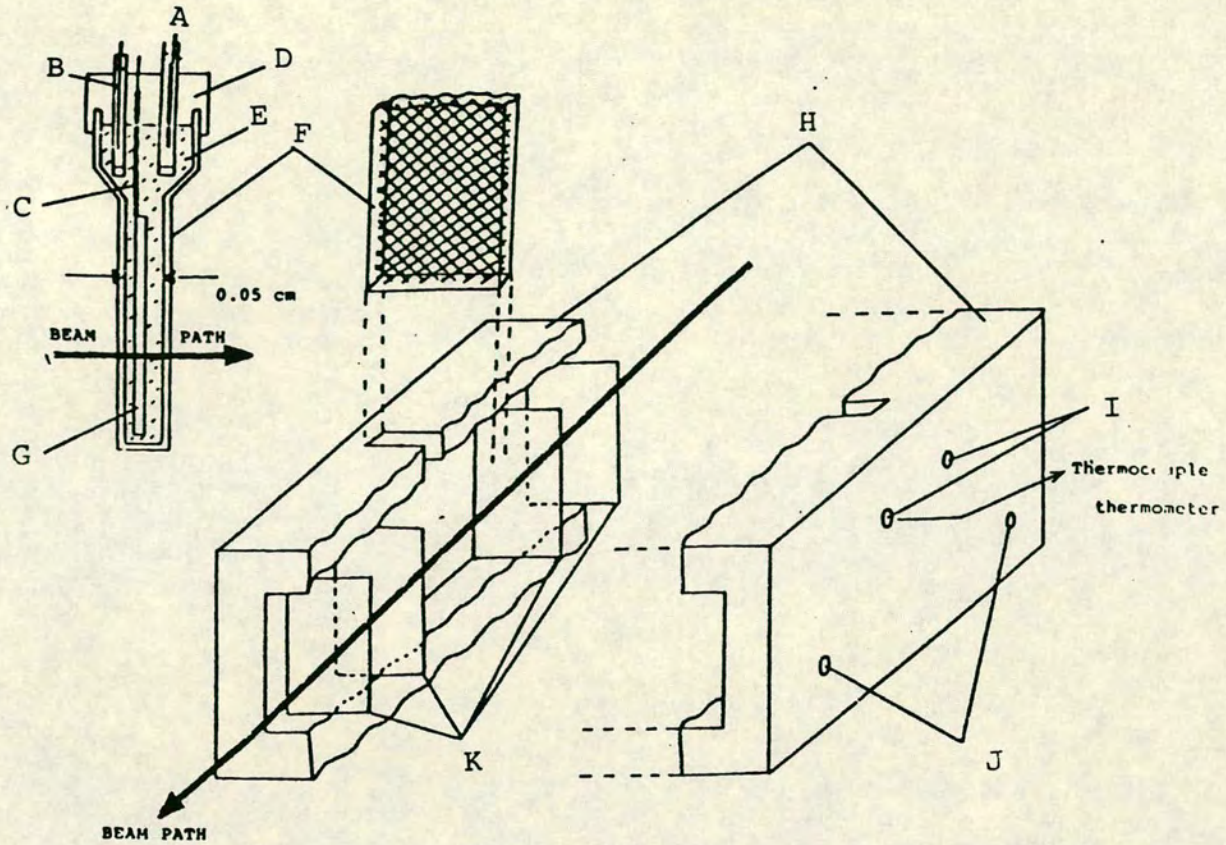

A Counter Electrode

B Reference Electrode

C Working Electrode connection protected from bulk solution by PTFE sleeve

D PTFE cell cap

E Test solution, deoxygenated with Ar or N_2

F 0.1cm Infrasil Quartz cell containing platinum grid working electrode

G Platinum grid working electrode

H PTFE cell block

I Variable Temperature nitrogen inlet ports

J Dry nitrogen inlet ports (to prevent fogging of inner quartz windows)

K Infrasil Quartz cell block windows

Figure C.44: Optically Transparent Cell used for Spectroelectrochemical Experiments

Yellowlees, Heath and Braterman[70].) The path length of the optical cell was 1 mm, and the optically transparent working electrode consisted of a layer of fine platinum gauze.

Control of cell temperature was possible by passing a stream of cooled nitrogen gas around the cell. It was possible, using this apparatus to carry out experiments at temperatures as low as -45°C.

(e) E.s.r. Measurements

Where the e.s.r. spectra of air-sensitive species was to be recorded, special apparatus and handling techniques were required.

An e.s.r. tube (diameter = 4 mm) had a rubber tube connected to the top of it. On the other end of the air-tight rubber tube a glass adaptor containing a ground glass tap and a SQ18 socket joint was placed. Prior to its use the apparatus was sealed with a suba-seal over the socket joint, evacuated and flushed with nitrogen. This process was repeated a further two times when the assembly was ready for use.

Once the observed species had been electrogenerated, 1.5 ml of the cell solution were rapidly transferred to the e.s.r. tube, using a nitrogen-flushed syringe. The e.s.r. tube was then immediately immersed in liquid nitrogen until required.

C.3-3 Related Chemical Syntheses

Palladium-14,15-dihydroxy-14,15-dihydrotetraphenylporphin:- Ceric ammonium sulphate (1.5 g) was added to a solution of Pd(II)TPP (250 mg) in dichloromethane (500 ml). The mixture was shaken for 4 h, then filtered to remove any solid cerium salts. The solution was concentrated to 10 ml by rotary evaporation, then purified by chromatography (silica, 5% (v:v) methanol/chloroform eluant). The second, deep-green, fraction was collected and concentrated to give pure Pd-14,15-$(OH)_2$-TPP (60 mg, 22%).

$\lambda_{max}(CH_2Cl_2)$; 418(ε = 28,000), 605(shoulder), 660(12,000)

$\delta^1H(CDCl_3)$ 200 MHz, 8.03(s), 7.99(s), 7.87(s), 7.74(s), 7.54(s), 7.51(s), 7.43(s), 7.39(s), 7.35(s), as well as a complex series of overlapping peaks. A D_2O shake results in the singlets at 7.87 and 7.74δ disappearing.

$\delta^{13}C(CDCl_3)$ 50.6 MHz, DEPT($P\phi = \frac{3\pi}{2}$) spectrum showing CH peaks only shows a complex series of singlets in the range 127 to 134 ppm indicating the unsymmetrical nature of the product.

M/E (F.A.B. thioglycerol/oxalic acid) shows major peaks at 753 $(M + H)^+$ and 861 $(M + \text{thioglycerol} + H)^+$.

References

1. C.K. Chang and T.E. Traylor, J.Am.Chem.Soc., 1973, 95, 5810.
2. J.L. Soret, Compt.Rend., 1883, 97, 1267.
3. M. Gouterman in "The Porphyrins", ed. D. Dolphin, Academic, New York, 1978, vol. III, Chapter 1.
4. J.R. Platt in "Radiation Biology", ed. A. Hollaender, McGraw-Hill, New York, 1956, vol. III.
5. D.W. Clack and N.S. Hush, J.Am.Chem.Soc., 1965, 87, 4238.
6. E. Rabinowitch and J. Weiss, Proc.R.Soc.London, Ser.A, 1937, 162, 251.
7. J.F. Gibson and D.J.E. Ingram, Nature (London), 1956, 178, 871.
8. G.L. Closs and L.E. Closs, J.Am.Chem.Soc., 1963, 85, 818.
9. R.H. Felton and H. Linschitz, J.Am.Chem.Soc., 1966, 88, 1113.
10. A. Stanienda and R. Biebl, Z.Phys.Chem.Neue Folge, 1967, 52, 254.
11. J.H. Fuhrop, K.M. Kadish and D.G. Davis, J.Am.Chem.Soc., 1973, 95, 5140.
12. R.C.S. McQueen, Ph.D. Thesis, University of Edinburgh, 1982.
13. J. Fajer, D.C. Borg, A. Forman, D. Dolphin and R.M. Felton, J.Am.Chem.Soc., 1970, 92, 3451.
14. A.J. Fajer and M.S. Davis in "The Porphyrins", ed. D. Dolphin, Academic, New York, 1978, vol. IV, Chapter 4.
15. A. Wolberg and J. Manassen, Inorg.Chem., 1970, 9, 2365.

16. D. Dolphin, T. Niem, R.H. Felton and I. Fujita, J.Am.Chem.Soc., 1975, 97, 5288.

17. J.W. Buchler in "The Porphyrins", ed. D. Dolphin, Academic, New York, 1978, vol. I, chapter 10.

18. R. Grigg, A. Sweeney and A.H. Johnson, J.Chem.Soc., Chem. Commun., 1970, 1237.

19. R. Bonnett and G.F. Stephenson, J.Org.Chem., 1965, 30, 2791.

20. J.W. Buchler and H.H. Schneehage, Tetrahedron Lett., 1972, 3803.

21. J.W. Buchler and L.H. Puppe, Justus Liebigs Ann.Chem., 1970, 740, 142.

22. J.W. Buchler and L.H. Puppe, Justus Liebigs Ann.Chem., 1974, 1046.

23. J.W. Buchler, Ann.N.Y.Acad.Sci., 1973, 206, 219.

24. G.R. Gurinovich and S. Sinyakov, Dokl.Akad.Nauk Beluross S.S.R., 1973, 17, 660.

25. D. Dolphin, R.H. Felton, D.C. Borg and J. Fajer, J.Am.Chem.Soc., 1970, 92, 943.

26. J.A. Guzinski and R.H. Felton, J.Chem.Soc., Chem.Commun., 1973, 715.

27. A. Gold, W. Ivey, G.E. Toney and R. Sangaiah, Inorg.Chem., 1984, 23, 2932.

28. G.H. Barnett, M.F. Hudson, S.W. McCombie and K.M. Smith, J.Chem.Soc., Perkin Trans.1, 1973, 691.

29. D. Dolphin and R.H. Felton, Acc.Chem.Res., 1974, 7, 26.

30. G.H. Barnett and K.M. Smith, J.Chem.Soc., Chem.Commun., 1974, 772.

31. G.H. Barnett, B. Evans and K.M. Smith, Tetrahedron Lett., 1976, 4009.

32. B. Evans and K.M. Smith, Tetrahedron Lett., 1977, 3079.

33. G.H. Barnett, B. Evans, Z. Martynenko and K.M. Smith, J.Am.Chem.Soc., 1979, 101, 5953.

34. A.G. Padillo, H.J. Shine and S.M. Wu, J.Chem.Soc., Chem. Commun., 1976, 236.

35. J.E. Baldwin, M.J. Crossley and J. DeBernhardis, Tetrahedron, 1982, 38, 685.

36. M.M. Catalano, M.J. Crossley, M.M. Harding and L.G. King, J.Chem.Soc., Chem.Commun., 1984, 1535.

37. J.A.S. Cavaleiro, B. Evans and K.M. Smith, Tetrahedron Lett., 1976, 4863.

38. J.A.S. Cavaleiro, B. Evans and K.M. Smith, J.Chem.Soc., Perkin Trans.1, 1978, 768.

39. R. Bonnett, A.A. Charalambides and R.A. Martin, J.Chem.Soc., Perkin Trans.1, 1978, 974.

40. H.J. Callot, A. Louari and M. Gross, Tetrahedron Lett., 1980, 3281.

41. H.J. Callot, A. Louari and M. Gross, Bull.Soc.Chim.Fr., 1983, 317.

42. A. Harriman, G. Porter and J. Waites, J.Chem.Soc., Faraday Trans. 1, 1983, 79, 1335.

43. A. Harriman, Inorg.Chim.Acta, 1984, 83, 151.

44. N.E. Tokel-Takvoryan and A.J. Bard, Chem.Phys.Lett., 1974, 25, 235.

45. H. Kageyma, M. Hidan and Y. Uchida, Bull.Chem.Soc.Jpn., 1972, 45, 2898.

46. M.R. Low, Ph.D. Thesis, University of Edinburgh, 1987.

47. J.R. Gordy-Thomas, J.Chem.Phys., 1956, 24, 439.

48. A.L. Allred, J.Inorg.Nucl.Chem., 1961, 17, 215.

49. A. Stanienda, Z.Naturforsch., Teil B, 1968, 23, 1285.

50. J.D. Woolins and P.F. Kelly, Coord.Chem.Rev., 1985, 65, 115.

51. T.V. O'Halloran and S.J. Lippard, Isr.J.Chem., 1985, 25, 130.

52. H. Endres, H.J. Kener, H. Van De Saud and V. Doug, Z.Naturforsch., Teil B, 1978, 33, 843.

53. R. Usòn, J. Forniés, M. Tomás, B. Menjón, K. Sunker and R. Bau, J.Chem.Soc., Chem.Commun., 1984, 731.

54. R. Usòn, J. Forniérs, M. Tomás, K. Sunker, R. Bau and E. Kuwabara, Organometallics, 1986, 5, 1576.

55. H.A. Boucher, G.A. Lawrence, R.A. Lay, A.M. Sargeson, A.M. Bond, D.F. Sangster and J.C. Sullivan, J.Am.Chem. Soc., 1983, 105, 4652.

56. A.J. Blake, R.O. Gould, A.J. Holder, T.I. Hyde, A.J. Lavery, M.O. Odulate and M. Schröder, J.Chem.Soc., Chem.Commun., 1987, 118.

57. A.L. Balch and R.H. Holm, J.Am.Chem.Soc., 1966, 88, 5201.

58. J.A. McCleverty, Prog.Inorg.Chem., 1968, 10, 49.

59. K.S.M. Docherty, Chemistry Honours Project, University of Edinburgh, 1984.

60. R.H. Campbell, G.A. Heath, G.T. Heffer and R.C.S. McQueen, J.Chem.Soc., Chem.Commun., 1983, 113.

61. J.M. Miller, J.Organomet.Chem., 1983, 249, 299.

62. C. Weiss Jr., J.Mol.Spectrosc., 1972, 44, 37.

63. S. Gronowitz, A. Hornfeldt, B. Gestblom and R.A. Hoffmann, Arkiv.Kemi., 1961, 18, 133.

64. J.H. Fuhrop and D. Mauzerall, Photochem.Photobiol., 1971, 13, 453.

65. D.A. Clarke, R. Grigg, R.L.N. Harris, A.W. Johnson, I.T. Kay and K.W. Shelton, J.Chem.Soc.C, 1967, 1648.

66. D. Dolphin, D.J. Halko, E.C. Johnson and K. Rousseau in "Porphyrin Chemistry Advances", ed. R.F. Longo, Ann Arbor Science, Ann Arbor, 1979, p. 119.

67. J.A. Cavaleiro, B. Evans and K.M. Smith in "Porphyrin Chemistry Advances", ed. F.R. Longo, Ann Arbor Science, Ann Arbor, 1979, p. 335.

68. J.B. Paine, W.B. Kirshner, D.W. Moskowitz and D. Dolphin, J.Org.Chem., 1976, 41, 3857.

69. G.H. Barnett, M.F. Hudson and K.M. Smith, Tetrahedron Lett., 1973, 2887.

70. G.A. Heath, L.J. Yellowlees and P.S. Braterman, J.Chem.Soc., Chem.Commun., 1981, 287.